ISSN 2663-1407
Volume 9, Isuue 1, March 2019

Libyan Journal of Science & Technology

Special Issue

The 2nd International Conference on Geosciences of Libya-GeoLibya 2 (2017)

14-16 October 2017, Benghazi-Libya

An online refereed scientific journal issued by Faculty of Science, University of Benghazi

Benghazi, Libya

Editorial Board

 ISSN 2663-1407; National Library of Libya, Legal number: 390/2018

Libyan Journal of Science and Technology

Contents

Volume 9, Number 1, March 2019

Special issue

The 2nd International Conference on Geosciences of Libya-GeoLibya 2 (2017), 14-16 October 2017, Benghazi-Libya

Libyan Journal of Science & Technology 9:1 (2019) 01–10
The 2nd International Conference on Geosciences of Libya-GeoLibya 2 (2017), 14-16 October 2017, Benghazi-Libya

Faculty of Science - University of Benghazi
Libyan Journal of Science & Technology
journal home page: www.sc.uob.edu.ly/pages/page/77

Geochemical and mineralogical studies of the celestite bearing formations and associated sediments in Benghazi Formation, Ar Rajmah Group (Middle Miocene), Al Jabal Al Akhdar, NE Libya

Saad K. El Ebaidi

Department of Earth Sciences, Faculty of Science, University of Benghazi, Benghazi-Libya

E-mail address: saad.elebaidi@uob.edu.ly

Highlights

- **This paper has an excellent contribution to the geology of Cyrenaica.**
- **In this paper find out geochemically and mineralogically the source of strontium element. Also the distribution of strontium in allochems, matrix and cement in the Benghazi Formation of the Ar Rajmah Group.**

ARTICLE INFO

Article history:
Received 01 February 2018
Revised 02 March 2018
Accepted 10 March 2018
Available online 31 March 2019

Keywords:
Celestite, Ar Rajmah Group, Benghazi, Benghazi Cement Quarry, Wadi Al Qattarah, Al Jabal Al Akhdar.

ABSTRACT

The study area is located in the northeast of Libya, in the areas of Benghazi city and Ar Rajmah village. The purpose of this study is to find out geochemically and mineralogically the source of strontium element. Also the distribution of strontium in allochems, matrix and cement in the Benghazi Formation of the Ar Rajmah Group. Celestite grade 88.3 % ($SrSO_4$) occurs only in the Benghazi Formation at Benghazi Cement Quarry as geodic nodules in the Middle Miocene rocks. Detailed mineralogical and chemical data have been collected on the celestite and associated sediments using XRF, XRD, EPMA, SEM and DSC techniques. Authigenic celestite and strontianite minerals occur both as a cement and as a replaced by other fracture filling minerals such as anhydrite. However, carbonate skeletal grains have quite high $MgCO_3$ contents, reflecting sometimes the presence of dolomite and brucite minerals. The average Sr/Ca ratio of coralline algae is 0.65. Echinoderm fragments have the highest value 1.31 of Sr/Ca and containing 0.47 to 1.8 mole percent of $MgCO_3$ in the Benghazi Formation. Echinoid spines contain higher strontium contents than other echinoderm fragments. Some bivalves are replaced totally by apatite and had a very high absolute concentration of strontium. The high strontium- low magnesium contents and vice versa are related to the diagenesis, mineralogical nature of the sediments and organic remains. Celestite occurs mainly in sedimentary beds of the Benghazi Formation, adjacent to the evaporitic environment (gypsum/anhydrite) and near sites of intense dolomitization.

Introduction

The geology of Libya is dominated by sedimentary rocks, occurring in distinct sedimentary basins. The basins of southern Libya are filled with Palaeozoic and continental Mesozoic strata. In northern Libya, the Precambrian and Palaeozoic strata are covered by marine Mesozoic and Tertiary sediments, which consist principally of carbonates and marl (Klitzch, 1968). Many general investigations have been carried out on the geology of Libya including the geology of Cyrenaica region. Most of these studies have concentrated on the surface outcrops of Al Jabal Al Akhdar, providing a general description of the lithofacies and some detailed work on the micropalaeontology. The sedimentary sequence exposed at the surface of Al Jabal Al Akhdar ranges in age from Cenomanian to Quaternary (Kleinsmiedi and Van Den Berg, 1968; Klen, 1974; Zert, 1974; Rohlich, 1974; El Hawat and Shelmani, 1993). The locations of the study area; Benghazi Cement Quarry and Ar Rajmah Quarry are illustrated in Fig. 1.

Objectives

The celestite in the study area has not yet been mentioned in the previous studies and has been considered in this work to determine geochemically the source of strontium element in Benghazi Formation. The study is also included the distribution of strontium in allochems, matrix and cement in the Benghazi Formation of the Ar Rajmah Group.

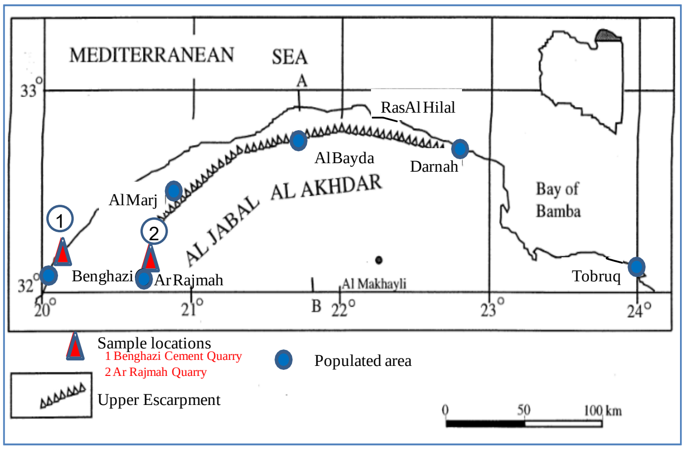

Fig. 1. Location map of the studied area, Benghazi Cement Quarry and Ar Rajmah Quarry

 ISSN 2663-1407; National Library of Libya, Legal number: 390/2018

Methodology

Strategic evaluations of the limestones in Benghazi Formation, the work in this paper need to involve far more than a basic geological appraisal and it was included laboratory determinations of the chemical and mineralogical properties of this rock types. A variety of techniques were used in this study included; X-Ray Fluorescence (XRF), Scanning Electron Microscopy (SEM), Electron Probe Microanalysis (EPMA), X-Ray Diffraction (XRD) and Differential Scanning Calorimetry (DSC).

Stratigraphy of Ar Rajmah Group, Benghazi Formation (Middle Miocene)

Ar Rajmah Group is the youngest unit in Al Jabal Al Akhdar area (Fig. 2). It comprises of two formations; from the oldest to the youngest are Benghazi and Wadi Al Qattarah formations. This division is based on the differences in lithology and faunal content (Klen, 1974; Rohich, 1974).

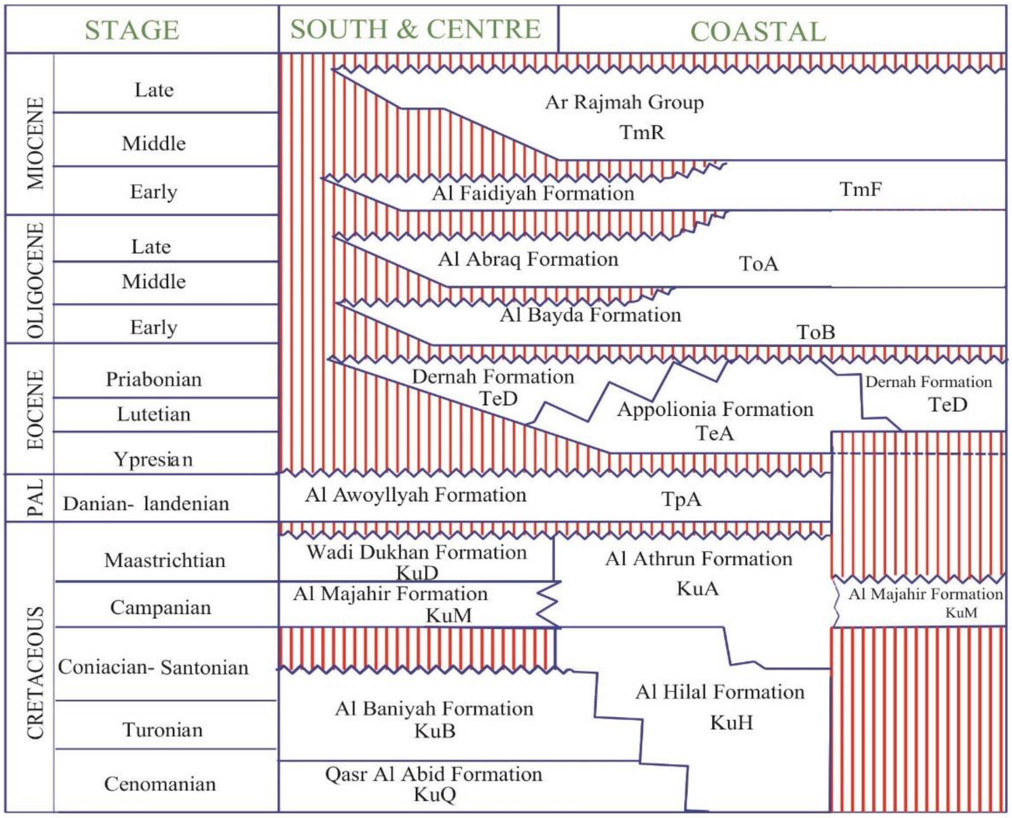

Fig. 2. Surface and Stratigraphic chart of Al Jabal Al Akhdar, NE Libya (modified after Muftah *et al*., In press)

Benghazi Formation

The formation consists chiefly of fossiliferous limestone, white to yellowish, thick-bedded to massive (< 10 % dolomite), hard to medium hard (Fig. 3). With an abundance of fossils including large echinoids, sometimes bored (Fig. 4), bivalves e.g. Pectinids and gastropods. There is an abundance of coralline algae and one species of coral *Tarbellastraea* sp. in the lower part of the formation, was noticed in Benghazi Cement Quarry. It also contains brachiopods and echinoid spines, bryozoans and foraminifers. Celestite is also observed in the Benghazi Formation of the Ar Rajmah Group. Celestite of brownish colour and it is formed of friable prismatic crystals aggregates infilling vuggy pores (Figs. 5 and 6). XRD of a powdered specimen showed the presence of impurities such as relics of anhydrite, gypsum, calcite and dolomite. The presence of anhydrite within the celestite crystals indicates that the origin might be anhydrite nodules later replaced to celestite, as described by Wood and Shaw (1976). Authigenic celestite and strontianite minerals occur both as a cement and as a replaced by other fracture filling minerals such as anhydrite (Fig. 7).

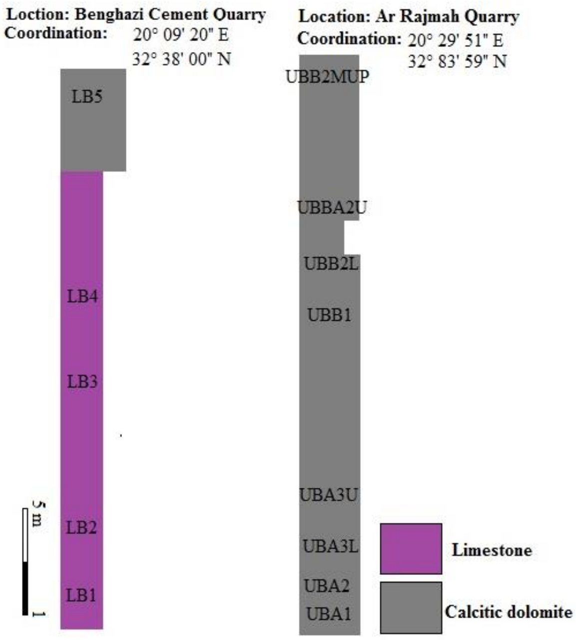

Fig. 3. Two logs of the Benghazi Cement Quarry (Lower Part), and Ar Rajmah Quarry (Upper part) of the Benghazi Formation (Middle Miocene).

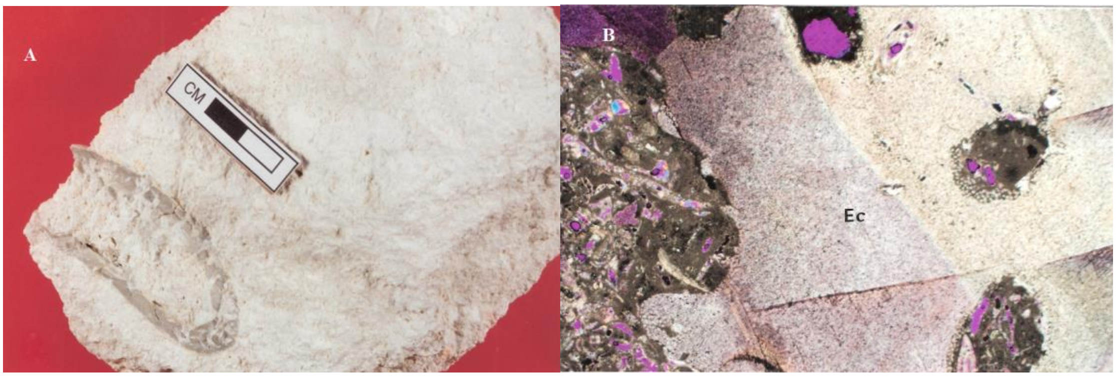

Fig. 4. A) Echinoid; B) Large echinoderm fragment (Ec), with borings filled with carbonate and bioclasts, Benghazi Cement Quarry. Field of view= 6 mm, (XPL, with gypsum accessory plate).

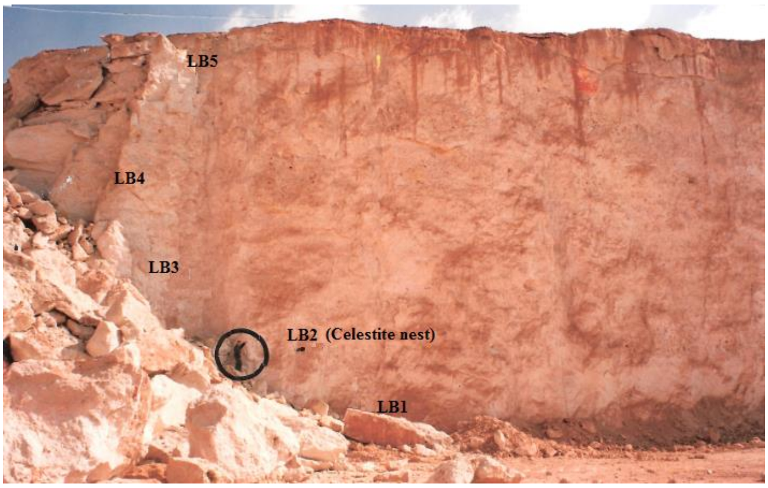

Fig. 5. A massive limestone bed of Benghazi Formation, Benghazi Cement Quarry. Displays; LB1, LB2, LB3, LB4 and LB5.

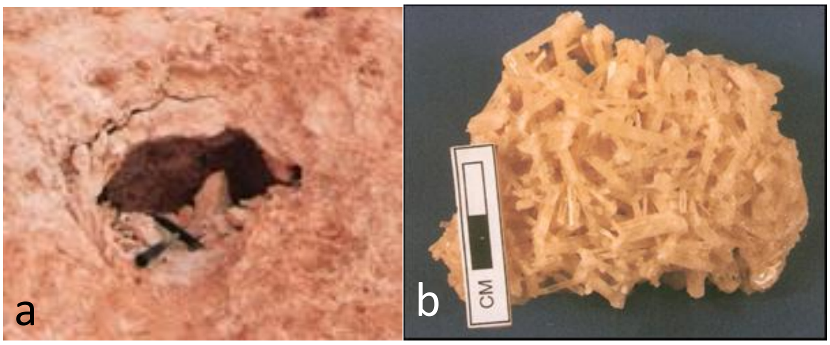

Fig. 6. a) Celestite nest at height of 4.5 m; and b) Celestite mineral sample was taken from the nest (4.5 m) and as geodic nodules, Benghazi Formation, Ar Rajmah Group, in Benghazi Cement Quarry.

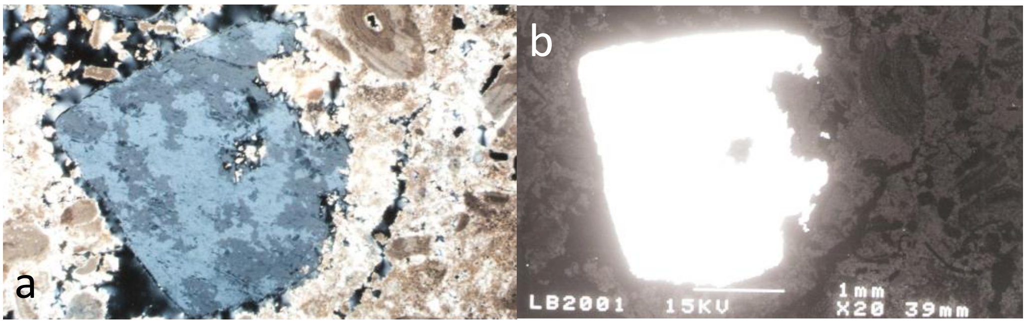

Fig. 7. a) A photomicrograph of a Strontianite mineral is etched by dolomite crystals, Field of view = 6 mm; and b) SEM (BSE) of the strontianite mineral, the brightness is due to the highest in atomic number, Benghazi Formation.

Dolomite in Benghazi Formation

Dolomite mineral is common in the Benghazi Formation in varying amounts. The lower part of the formation contains about 2 - 8 % dolomite whereas in the upper part (Ar Rajmah Quarry), consists of 10 - 80 dolomite (Table 1). Generally, dolomite crystals were present as limpid euhedral crystals with a planar (idiotopic), inequicrystalline (micron to decimicron in size) fabric (Fig. 8). It occurs both as fabric selective replacement of the carbonate mud matrix and as a cement. Grains of primary high-Mg calcite (HMC), such as red algae (Fig. 9), foraminifers, and echinoderm fragments are often more susceptible to dolomitization than low-Mg calcite (LMC); (Buchbinder, 1979; Armstrong *et al*., 1980; Sibley, 1980; Tucker, 1991). Some dolomite crystals have a hollow centre and that may result of the complete removal of metastable dolomite and/or soluble calcite zones (Sibley, 1982; Ward and Halley, 1985; Theriault and Hutcheon, 1987). Overall, the Benghazi Formation is quite porous and point-counter estimates of porosity range from 4 to 38 %.

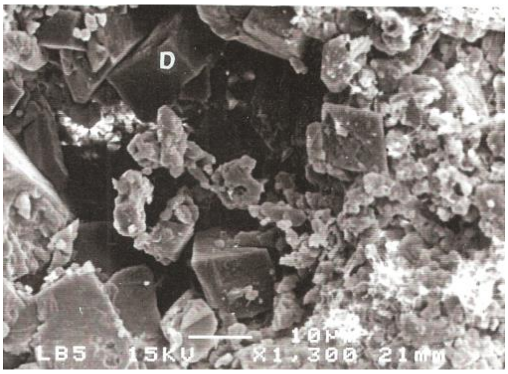

Fig. 8. SEM of the void-filling dolomite (D), Benghazi Formation (LB5), Benghazi Cement Quarry.

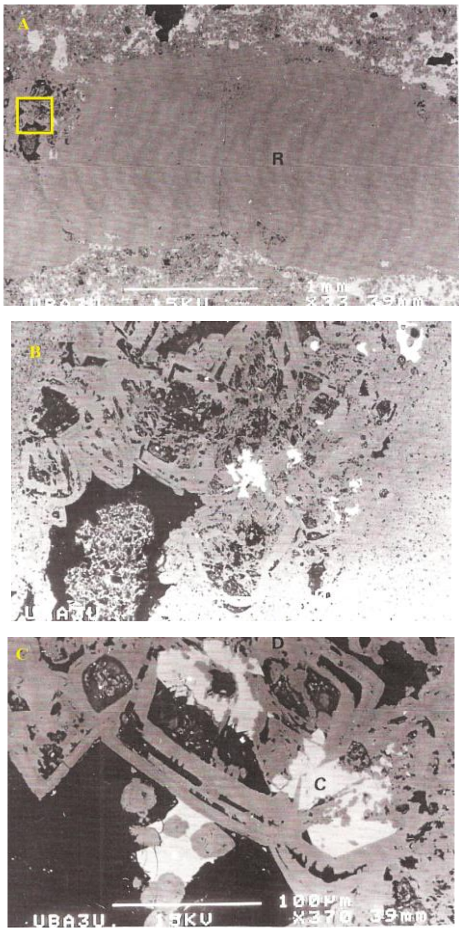

Fig. 9. SEM-BSE; A) Red algae (R); B & C) Close up view showing some euhedral dolomite (D) crystals cores filled with calcite (C).

Table 1

Chemical analysis for major and trace elements of the lower part of the Benghazi Formation (M. Miocene), Benghazi Cement Quarry.

Sample no.	LB1	LB2	LB3	LB4	LB5	UBA1	UBA2	UBA3L	UBA3U	UBB1	UBB2L	UBB2U	UBB2MUP
Oxides (wt. %)	Benghazi Cement Quarry (Lower part of the Benghazi Formation)					Ar Rajmah Quarry (Upper part of the Benghazi Formation)							
SiO_2	0.87	0.00	0.11	0.00	0.67	0.07	0.57	0.63	0.00	0.00	0.00	0.00	0.01
Al_2O_3	0.25	0.00	0.01	0.00	0.24	0.03	0.24	0.33	0.01	0.00	0.00	0.00	0.05
Fe_2O_3	0.09	0.00	0.00	0.00	0.06	0.03	0.03	0.05	0.00	0.00	0.00	0.00	0.04
$MgCO_3$	5.97	2.61	3.52	2.44	6.30	30.38	25.21	22.88	28.85	24.81	28.01	19.89	29.70
$CaCO_3$	92.78	97.7	96.65	98.11	92.66	67.21	72.03	74.25	68.95	73.81	70.22	78.98	67.78
S	0.00	0.02	0.00	0.00	0.00	0.03	0.03	0.02	0.04	0.02	0.04	0.02	0.07
K_2O	0.04	0.00	0.00	0.00	0.04	0.00	0.01	0.01	0.00	0.00	0.00	0.00	0.00
TiO_2	0.01	0.00	0.00	0.00	0.01	0.00	0.01	0.01	0.00	0.00	0.00	0.00	0.00
MnO	0.00	0.09	0.02	0.01	0.03	0.00	0.00	0.00	0.00	0.00	0.00	0.03	0.00
P_2O_5	0.03	0.00	0.03	0.01	0.03	0.12	0.18	0.30	0.20	0.24	0.17	0.17	0.31
Total	100.04	100.42	100.34	100.57	100.04	97.87	98.31	98.48	98.05	98.88	98.44	99.09	97.96
CaO	51.90	54.70	54.10	54.90	51.89	37.60	40.34	41.60	38.61	41.34	39.32	44.23	37.96
MgO	3.52	1.54	2.10	1.44	3.72	17.92	14.87	13.50	17.02	14.64	16.53	11.74	17.52
Limestone Quality	***LP**	***HP**	***MP**	***HP**	***LP**	**Impure**							
Trace elements (ppm)													
Nb	0	0	0	0	0	0	3	0	2	0	3	0	0
Zr	127	719	111	98	666	27	34	34	30	21	29	28	39
Y	40	34	41	42	31	42	43	46	43	44	42	40	45
Sr	1306	8042	1226	1082	7761	279	274	261	310	226	291	265	373
Rb	44	41	42	47	38	44	45	43	43	41	45	45	45
Zn	0	0	0	2	0	0	6	0	0	0	0	0	0
Cu	12	6	16	11	2	12	19	11	9	18	29	31	12

Table 2, continued

Ni	0	0	0	0	0	0	0	0	0	0	0	0	0
Cr	18	0	0	11	1	17	17	14	24	21	13	18	32
Ce	0	26	0	26	14	0	14	30	36	1	0	18	0
Nd	0	0	0	0	0	0	0	18	8	0	0	7	0
V	18	14	11	11	9	16	18	16	7	11	1	18	25
La	12	4	0	18	8	21	11	0	13	0	9	0	0
Ti	321	188	204	250	186	255	322	316	226	169	188	173	223
Ba	1	0	0	0	25	0	0	0	0	8	0	0	0
Sc	87	79	77	100	87	46	62	48	67	67	70	71	45

* LP = Low Purity, MP = Medium Purity and HP = High Purity; Based on Harris, 1979 Classification

Wadi Al Qattarah Formation

This formation occurs close to the main road to Deryanah Al Abyar. It is composed of hard, white, porous, oolitic limestone, with massive gypsum in the upper part. Thin section showed grainstone texture with ooid and superficial ooids, Isopachous cement is also observed (Fig. 10a). This circumgranular calcite crust cement is characteristic of phreatic precipitation. Gypsum occurs in the upper part of the formation (Fig. 10b) together with quartz grains and minor amounts of scattered micron-sized dolomite crystals filling fractures.

Results and Discussions

DSC curve of celestite:

In air, the DSC curve shows two steps resulting from weight losses. The first weight loss of 3.7 % is associated with peaks 785 °C and 801 °C. The second peak showed a 0.37 % loss at about 1060 °C. The last endothermic peak is very sharp at about 1155 °C (Fig. 11). The first and second peaks represent traces of dolomite and that's confirmed by XRD analysis. The small peak at 1060 °C and very sharp peak at 1155 °C are probably due to the presence of some foreign material such as impure strontianite. Celestite was heated at a range of temperatures (800°C, 1000°C, 1150°C, and 1500 °C; Fig. 12). The only effects to be detected using XRD (approx. 0.5 mg) include a change in the sequence of peak intensities (Table 2). There is no change in mineralogical composition, but the degree of order changes, reducing at a higher temperature.

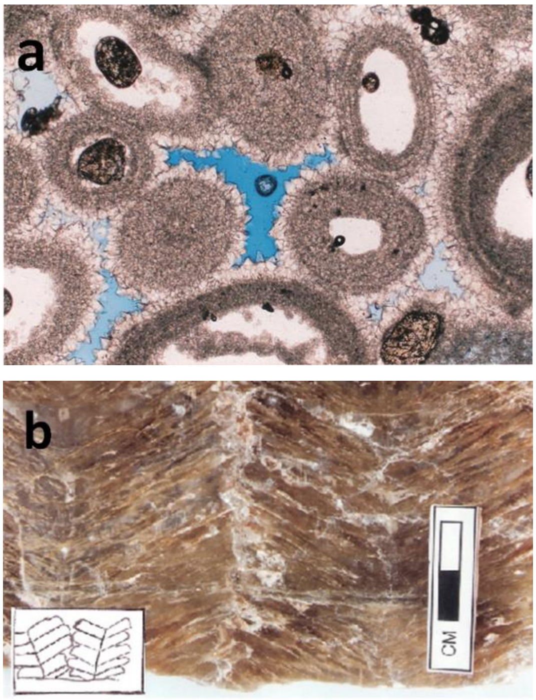

Fig. 10. a) Ooid grainstone with isopachous cement (vacuum impregnated with blue-dye resin), Field of view = 1.3 mm, (PPL); b) Coarsely crystalline swallow-tailed gypsum from a quarry NE Ar Rajmah village, Wadi Qattarah Formation.

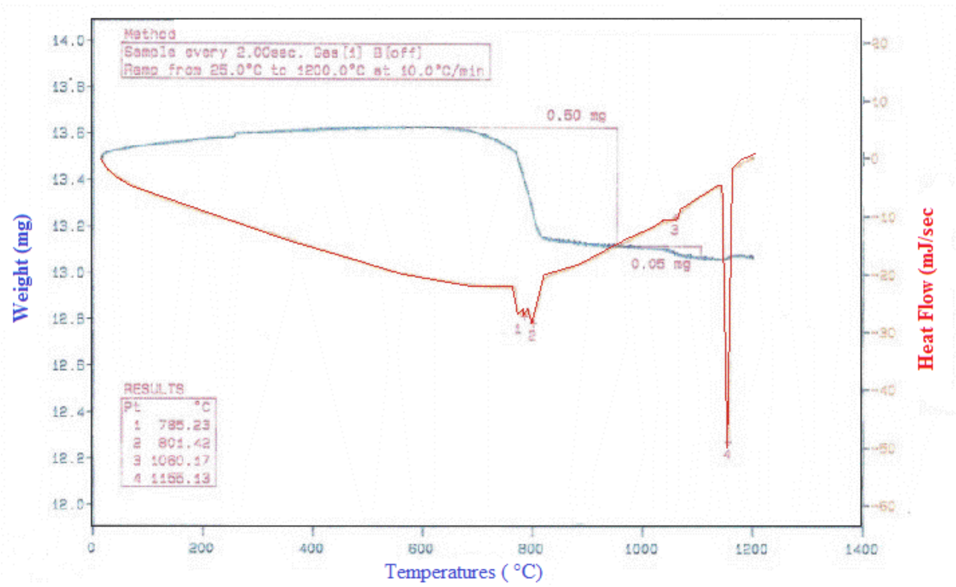

Fig. 11. TG-DSC curves of celestite of the Benghazi Formation, in the air (sample size = 13.5 mg) and CO_2 (sample size = 18.82 mg) at Benghazi Cement Quarry.

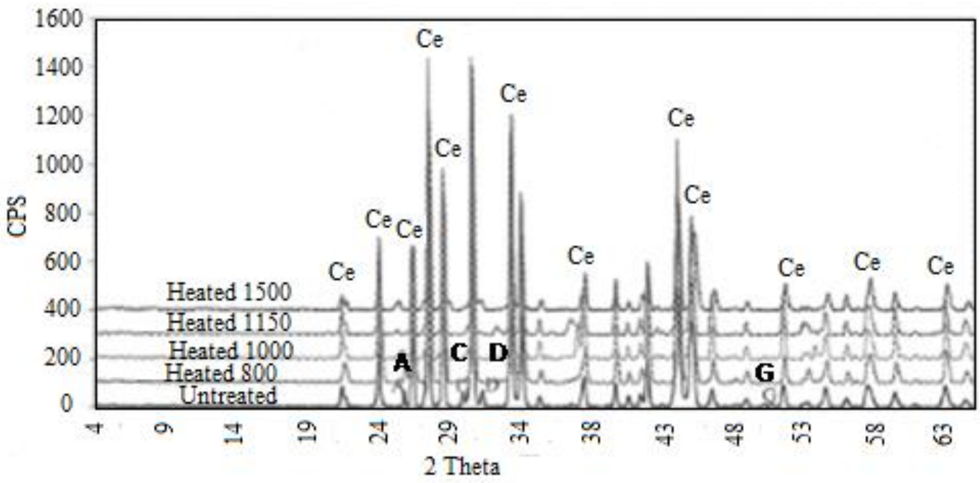

Fig. 12. XRD pattern of celestite mineral of the Benghazi Formation showing; (Ce) Celestite; (A) Anhydrite; (G) Gypsum; (D) Dolomite; (C) Calcite. Untreated (Air treated) and treated (heated to 800°C, 1000°C, 1150°C, 1500°C.

Table 2

Dominant X-ray diffraction peaks of celestite, in the Benghazi Formation

Age	Formation	Temperature (°C)	2 Theta	d-spacing d (Å)	Int. (%)	hkl
Middle Miocene	Benghazi	untreated	30.095	2.967	100	211
			27.077	3.291	98.80	210
			28.093	3.174	77.27	102
			32.793	2.729	67.02	112
			44.321	2.042	62.38	113
		800	27.210	3.275	100	210
			30.217	2.995	93.08	211
			44.431	2.037	68.49	113
			32.908	2.720	65.56	112
			28.216	3.160	59.56	102
		1000	27.104	3.287	100	210
			30.121	2.965	98.99	211
			32.805	2.728	60.89	112
			28.103	3.173	58.16	102
			44.337	2.041	52.89	113
		1150	27.094	3.289	100	210
			30.107	2.966	97.57	211
			32.807	2.728	74.07	112
			28.107	3.172	60.83	102
			44.317	2.042	54.16	113
		1500	30.178	2.959	100	211
			27.147	3.282	82.88	210
			32.837	2.725	80.79	112
			33.485	2.674	53.89	020
			28.165	3.166	50.55	102
			44.358	2.041	39.33	113

Occurrence and distribution of Sr in Benghazi Formation

Most the limestones in the study area contain skeletal materials such as shells and coral skeletons. Coralline algae contain a large amount of an $MgCO_3$, sometimes more than 35 $MgCO_3$ mole percent. The distribution of high Mg-Calcite (HMC) and low Mg-Calcite (LMC) in coralline algae and the other components were discovered and illustrated in Fig. 13.

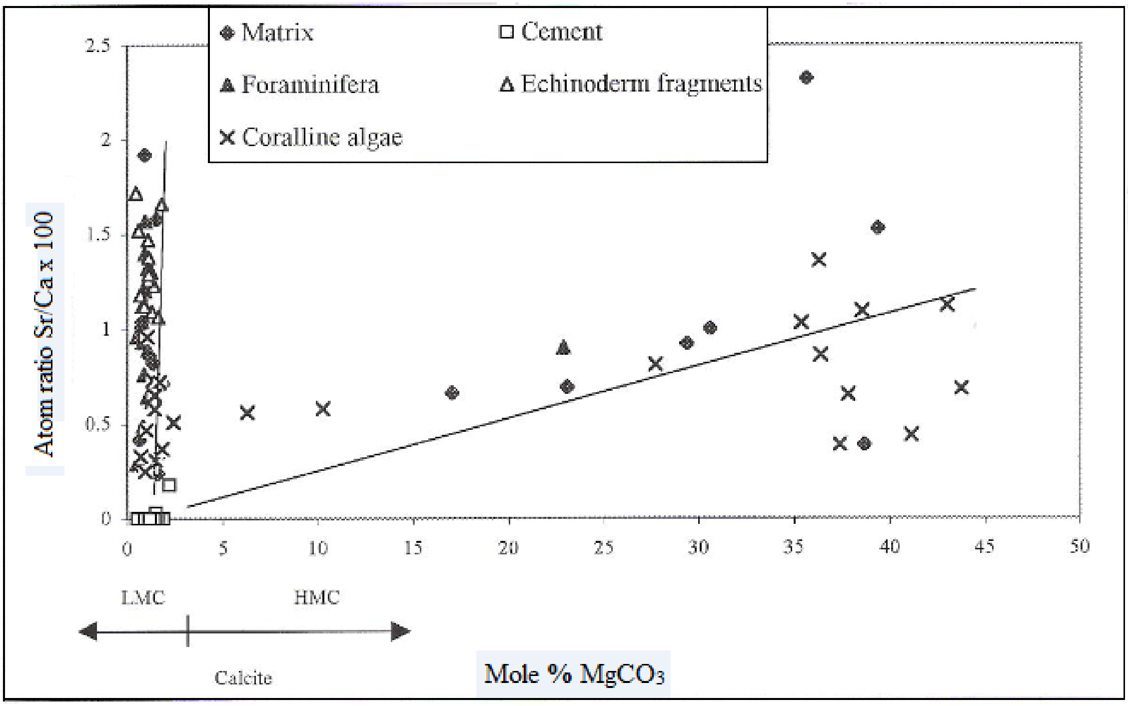

Fig. 13. Scatter diagram of Sr/Ca x 100 atom ratios vs Mole % $MgCO_3$ concentrations of the major components (coralline algae, echinoderm fragments, foraminifera, matrix and cement) in Ar Rajmah Group, Benghazi Formation.

Low magnesium calcite has less than 4 mole percent $MgCO_3$ and high magnesium calcite greater than 4 mole percent (Chave *et al.*, 1964; Blatt *et al.*, 1980; Carter, 1990; Tucker, 1991). Because of their lower stability, carbonate skeletal materials with high magnesium calcite, such as coralline algae are most likely to be replaced with metastable phases (e.g brucite). However, carbonate skeletal grains have quite high $MgCO_3$ contents, reflecting sometimes the presence of dolomite and brucite minerals. The average Sr/Ca ratio of coralline algae is 0.65. Echinoderm fragments have the highest value 1.31 of Sr/Ca and containing 0.47 to 1.8 mole percent of $MgCO_3$ in the Benghazi Formation. Echinoid spines contain higher strontium contents than other echinoderm fragments. Some bivalves are replaced totally by apatite and had a very high absolute concentration of strontium (Fig. 14; Table 3).

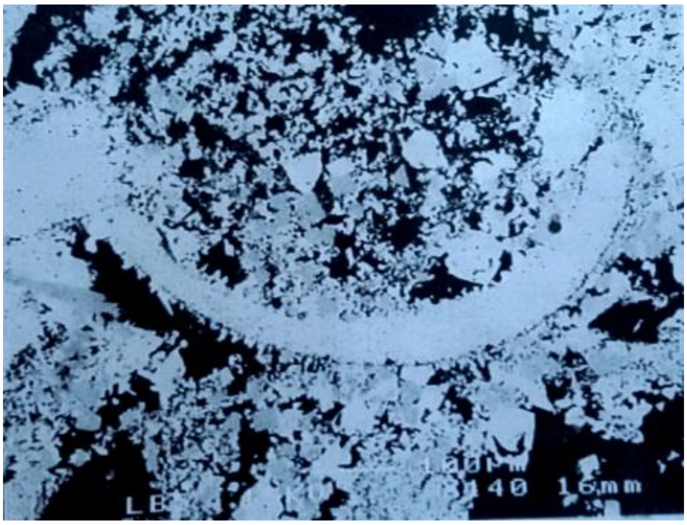

Fig. 14. BSE-SEM image of bivalve, totally replaced by apatite in Benghazi Formation

Table 3

High-resolution EPMA analyses of the bivalve shell fragment in (Sample no. LB5) Benghazi Formation

Oxides (wt. %)	Sample no. LB5 (Benghazi Cement Quarry)		
P_2O_5	36.495	39.047	36.456
SO_2	1.061	0.327	1.041
TiO_2	0.002	0.016	0.016
MgO	0.149	0.140	0.154
CaO	50.470	50.305	50.105
MnO	0.000	0.000	0.004
FeO	0.185	0.321	0.195
NiO	0.000	0.007	0.000
CuO	0.000	0.000	0.002
SrO	0.226	0.161	0.299
BaO	0.000	0.000	0.034
Na_2O	1.120	1.024	1.100
K_2O	0.021	0.017	0.015
Total	89.729	91.365	89.421

Magnesium and strontium relationship

The amount of strontium in the lower Benghazi Formation (Benghazi Cement Quarry) increases due to contamination of the limestone rocks with celestite and dolomite as well. The magnesium content decrease as strontium content increases and reaches a maximum where the strontium content reaches a minimum (Table 4). The high strontium- low magnesium contents and vice versa are related to the diagenesis, mineralogical nature of the sediments and organic remains. The loss of Sr is connected with observed high dolomitization, Sr % vs Mg % (Fig. 15) showed a decrease in Sr content with increasing dolomitization and showed also the Sr distribution and its relation to facies types.

Table 4

Strontium, magnesium and calcium analyses (XRF) of sediments of the traverse LB1 to LB5 of the Benghazi Formation (Benghazi Cement Quarry).

Location	Ca Wt. %	Mg Wt. %	Sr Wt. %	Atom ratio Sr/Ca x 1000 (Siegel, 1961)	Celestite & strontianite + Facies
Benghazi Cement Quarry					
LB1	37.09	2.12	0.13	1.61	Present + Dolomitic limestone
LB2	39.09	0.93	0.13	1.54	
LB3	38.66	1.27	0.12	1.45	
LB4	39.24	0.87	0.11	1.26	
LB5	37.09	2.24	0.11	1.39	

In other places such as Ar Rajmah the facies becomes calcitic dolomite to dolomite with absent of celestite minerals and diminishes in Sr content.

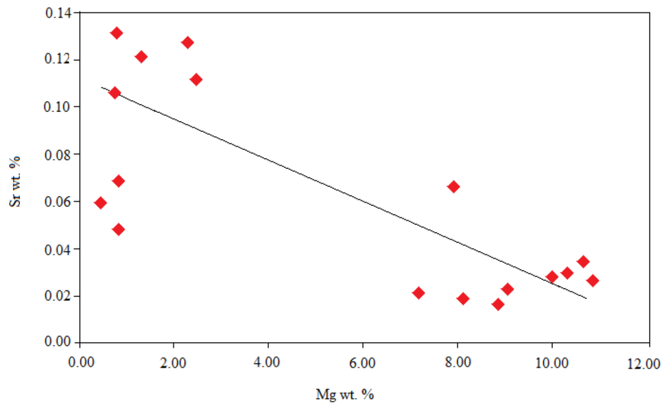

Fig. 15. Sr (wt. %) vs Mg (wt. %) of the Benghazi Formation, Ar Rajmah Group

Dolomite, anhydrite, celestite and replacement

Celestite ($SrSO_4$) is a member of the barite group and the principal source of strontium in many respects but it has a considerably lower density. Celestite occurs mainly in sedimentary rocks, by the interaction of gypsum or anhydrite with Sr-rich (Harben and Bates, 1990; Ober, 1994; Chang *et al.*, 1996). Celestite in the study area contains the strontium that was released from limestone in the formation of dolomite (such dolomites are extremely low in strontium content). Dolomite and celestite are often associated with the presence of evaporate deposits such as gypsum and/or anhydrite and the percolation within limestone by waters containing high sulphate. Generally, the composition of celestite depends on three main factors; 1) the nature and intensity of diagenesis such as the chemical composition of interstitial waters on their movement and renewal; 2) dolomitization; 3) recrystallization as described by West (1964), Lloyd and Murry (1965), Jorgensen (1994), Purser (1998) and Rosell *et al.*, (1998). The celestite in the lower part of Benghazi Formation occurs mostly as clear prismatic or tabular euhedral crystals and is coarse to extremely coarsely crystalline. Most of the replacement celestite occurs in nodular anhydrite; a complete replacement of isolated anhydrite nodules was occasionally observed. XRD analysis of the central portion of celestite nodules showed numerous relicts of anhydrite (Fig. 16).

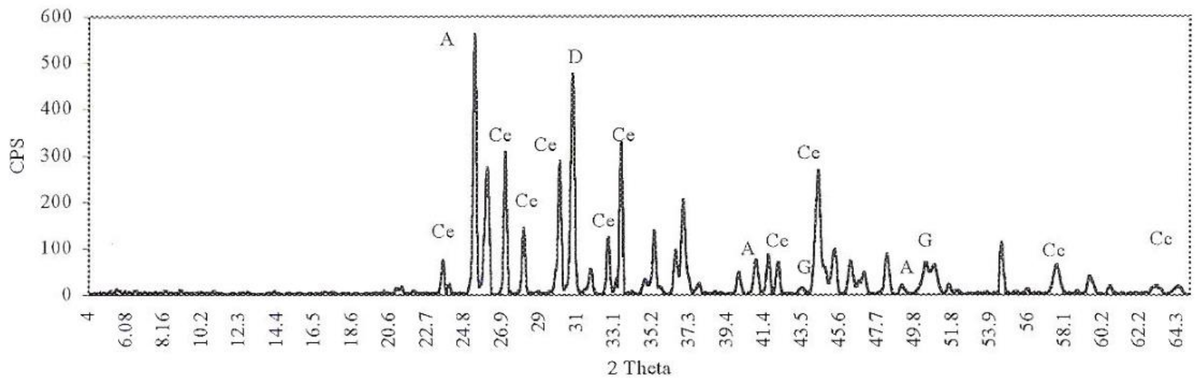

Fig. 16. XRD pattern of sediment taken from celestite nest of the Benghazi Formation (Benghazi Cement Quarry). Showing Celestite (Ce), Anhydrite (A), Dolomite (D) and Gypsum (G).

In Rhaetia limestones of southern England, gypsum veins originating from underlying Triassic strata have similarly been converted to celestite (West, 1964). Because of its low solubility in water, celestite of Ar Rajmah Group could be also precipitated previously in association with dolomite (in high porosity) and after removal took place, celestite re-deposited in the lower part of Benghazi Formation (Benghazi Cement Quarry).

Formation of Celestite

Celestite has been formed from pore water enriched in both SO_4 and Sr contents. A possible mechanism for concentration of strontium ions may be related to the loss of strontium by; 1) aragonite to calcite transformation (Dodd, 1967; Bathurst, 1975; Nicholas, 1978); and 2) intense dolomitization of aragonite mud. The Sr released during the replacement of aragonite (7000 - 8000 ppm Sr) by dolomite (600 - 700 Sr) is added to interstitial water and form celestite (Kinsman, 1969; Garea and Baitwaite, 1996). Nickless et al., (1976), concluded that sulphate is derived from anhydrite and gypsum, suggested that the strontium became available when aragonite converted to calcite. Celestite is much less soluble than gypsum and anhydrite and in most cases, celestite is formed by the replacement of those two minerals (West, 1973). Gypsum or anhydrite both contain small amounts of strontium, more strontium can be accommodated in solid solution in anhydrite (up to 0.74 % = 7400 ppm) than gypsum (up to 0.1 %; Dean and Tung (1974)). Therefore, in the transformation from anhydrite to gypsum, Sr can be released to form celestite (de Brodtkorb, 1989). Olaussen (1981) presented three models to explain the formation of celestite in a subtidal to supratidal facies in the Wenlock of Norway; 1) early diagenetic dolomitization of aragonite mud release Sr, which may react with the brine to form celestite; 2) Sr enrichment of the interstitial fluid produced by transformation of aragonite to calcite; and 3) late diagenetic dolomitization in which Sr released may precipitate as late-stage authigenic celestite in geodes and veins.

Conclusion

- Celestite occurs mainly in sedimentary beds of the Benghazi Formation, adjacent to the evaporitic environment (gypsum/anhydrite) and near sites of intense dolomitization.
- The high strontium content of the bulk sample (LB2) examined by XRF (see Table 1) is due to contamination by celestite relicts.
- The significant variations in their strontium contents commonly accompany the transition from one facies to another, influenced mainly by diagenetic processes such as inversion of aragonite to calcite and replacement of calcite by dolomite dolomitization as well as part of the strontium content of the originally aragonitic bioclasts have been mobilized during late diagenesis. All these factors have provided considerable amounts of strontium.
- Fossils from low permeability/porosity sediments such as shale or claystone (closed system) may better indicators of the amount of strontium present originally within the fossils than highly porous and permeable limestones (open system). The fossil echinoderm fragments reported in the literature are low in strontium content, but in fact, have commonly the highest Sr/Ca values of all allochems in the Benghazi Formation of the Ar Rajmah Group (Table 5).

Table 5

EPMA analyses (average of about 20 readings each) of strontium contents of the main components in the Benghazi Formation.

Group	Formation	Bioclasts					
			Red algae	Echinoderm fragments	Foraminifers	Matrix	Cement
Ar Rajmah	Benghazi	Mg (wt. %)	7.08	0.32	0.62	3.67	0.33
		Ca (wt. %)	28.70	39.94	38.68	35.28	40.56
		Sr (wt. %)	0.20	0.10	0.06	0.05	0.001
		$MgCO_3$ (Mol.%)	24.45	1.08	2.14	12.68	1.13
		Atom ratio Sr/Ca ×1000	0.72	0.94	0.69	0.63	0.01

In the study area, Wadi Al Qattarah Formation, the upper part of Ar Rajmah Group is consists of white, porous oolitic limestone with gypsum. Freshwater infiltrating through the gypsum of this formation and may have dissolved calcium sulphates, resulting in the groundwater being enriched with SO_4. The Benghazi Formation has high porosity (secondary porosity), and due to dolomitization and dissolving aragonite fossils, and these are giving a high Sr content in the interstitial water. However, Sr reacted with SO_4 within and formed celestite in pore structures of the lower part of the Benghazi Formation (Fig. 17).

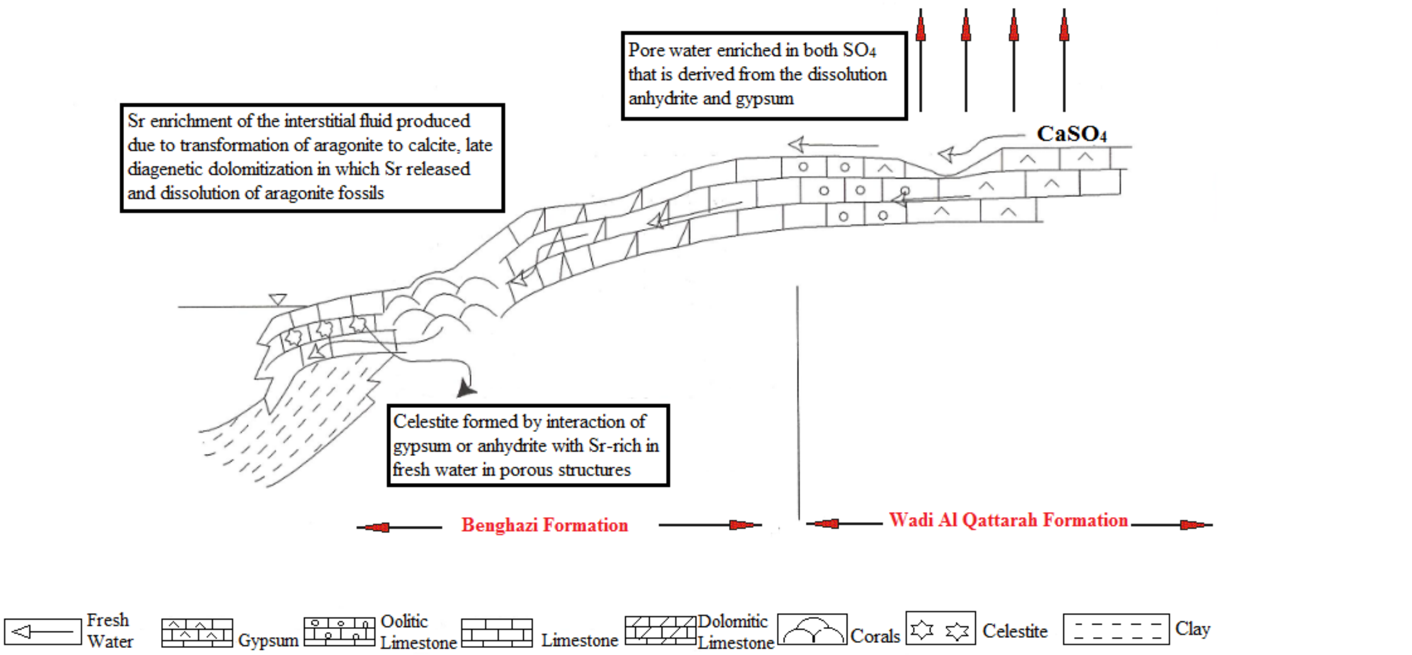

Fig. 17. A schematic model for the formation of celestite in the lower part of the Benghazi Formation of Ar Rajmah Group.

Acknowledgments

The author is thankful and acknowledges to Prof. D. A. C. Manning from Newcastle University, School of Civil Engineering and Geosciences, Newcastle upon Tyne, UK, Prof. A. E. Adams and Prof. J. Zussman from the University of Manchester for their valuable help, guidance and encouragement throughout this study. I am so grateful to Jowfe Company for Oil Technology and all technical and staff members of the Earth Sciences Department at the University of Manchester all for their help and support.

References

Armstrong, A. K., Shavely, P. D. Addicot, W. O. (1980) 'Porosity evaluation of Upper Miocene reefs, Almeria Province, southern Spain', *Am. Assoc. Petroleum Geologists Bull.*, 64, pp. 188-208.

Bathurst, R. G. C. (1975) *Carbonate sediments and their diagenesis*. Developments in sedimentology 12. (Second edition), Elsevier Publishing Co., Amsterdam, 658 pp.

Blatt, H. Middleton, G. and Murray, R. (1980) *Origin of sedimentary rocks*. (Second edition), New Jersey, 782 pp.

Buchbinder, B. (1979) 'Facies and environments of Miocene reef limestones', *Jour. Sed. Petrology*, 49, pp. 1323-1344.

Carter, J. G. (1990) Skeletal biomineralization: pattern, processes and evolutionary trends. Van Nostrand Reinhold, New York, 1, pp. 832

Chang, L. L. P., Howie, R. A., and Zussman, J. (1996) Rock Forming Minerals. Non-silicate: sulphates, carbonates, phosphates, halides. 5B, (second edition), pp. 383

Chave, K. E., Deffeyes, K. S., Weyl, P. K., Garrels, R. M. and Thompson, M. E. (1964) 'Observations on the solubility of skeletal carbonates in aqueous solutions', *Science,* 137, pp. 33-34.

Dean, W. E. and Tung, A. L. (1974) Trace and minor elements in anhydrite and halite. Supai Formation (Permian), east central Arizona. In: *4th symposium on salt* (ed. Coogan, A. H.), *North Ohio* Geological Society. pp. 287-301.

de Brodtkorb milka, K. (1989) *Non-metalliferous strata bound ore fields*. Van Reinhold, pp. 332

Dodd, J. R. (1967) 'Magnesium and strontium in calcareous skeletons: A review', *J. Paleontol*., 41, pp. 1313-1331.

El Hawat, A. S. and Shelmani, M. A., (1993) *Short notes and guidebook on the geology of Al Jabal al Akhdar, Cyrenaica, NE Libya*. Inter-print Limited Malta, 70p.

Garea, B. B. , and Baitwaite, C. J. R. (1996) 'Geochemistry, isotopic composition and origin of the bed dolomites, Block NC 74 F, SW Sirte Basin, Libya', *Jour. Sed. Petrology*, 19 (3), pp. 289-304.

Harben, P. W., and Bates, R. L. (1990) Industrial minerals, geology and world deposits. Industrial mineral division, London, 312pp.

Harris, P. M. (1979) *Limestone and dolomite*. Mineral Resources Consultative Committee. Minerals Strategy and Economics Research Unit. Institute of Geological Sciences. Mineral Dossier, 23, pp. 111

Jorgensen, D. B. (1994) Gypsum and anhydrite. In: *Industrial minerals and rocks*. 6th edition, (ed. Donald, D. C.), Society for mining, Metallurgy and Exploration, Inc. Littleton, Colorado, 571-581.

Kinsman, D. J. (1969) Interpretation of Sr^{2+} concentrations in carbonate minerals and rocks. *Jour. Sed. Petrology*, 39, 486-508.

Kleinsmiedi W. F. J. and Van Den Berg, N. J. (1968) Surface geology of the Jabal Al Akhdar, northern Cyrenaica, Libya. In: *Geology and archaeology of northern Cyrenaica, Libya* (ed. Barr, F. T.), *Explor. Soc. Libya*, Tripoli, 115-123.

Klen, I. (1974) *Geological map of Libya 1:250000. Sheet*. NI 34-14, Benghazi Explanatory Booklet. Indust. Resear. Cent. Tripoli, pp. 56

Klizsch, E. (1968) Outline of geology of Libya. In: *Geology and archaeology of northern Cyrenaica, Libya* (ed. Barr, F. T.) 10th Annual Field Conf., pp. 71-78.

Lloyd, C. P. and Murry, R.C. (1965) Dolomitization and limestone diagenesis. Society of Economic Paleontologists and Mineralogists, 180pp.

Nicholas, E. (1978) 'The behavior of Zn^{2+} and Mn^{2+} during carbonate diagenesis: theory and applications', *Jour. Sed. Petrology*, 48, 3, pp. 799-814.

Nickless, E. F. P., Booth, S. J., and Mosley, P. N. (1976) *The celestite resources of the area north-east of Bristol*: 1st Geol. Sci., Miner. Assessment Rept. No. 25, 83pp.

Ober, J. A. (1994) Strontium minerals. In: *Industrial minerals and rocks*. 6th edition (ed. Donald, D. C.), Society for Mining, Metallurgy and Exploration, Inc., Littleton, Colorado, 1003-1009.

Olaussen, S. (1981) 'Formation of celestite in Wenlock, Oslo region Norway evidence for evaporitic depositional environments', *Jour. Sed. Petrology*, 51, pp. 37-45.

Purser, B. H. (1998) Syn-rift diagenesis of Middle Miocene carbonate platforms on the north-western Red Sea coast, Egypt. In: *Sedimentation and tectonics of Rift Basins*: Red *Sea-Gulf of Aden* (ed. Purser, B. H. and Bosence D. W. J.), Chapman and Hall, London, pp. 369-389.

Rohlich, P. (1974) *Geological map of Libya 1:250 000. Sheet. Al Bayda: NI 34-15, Explanatory Booklet*. Indust. Resear. Cent. Tripoli. Pp. 70

Rosell, L., Orti, F., Kasprzyk, A., Playa, E. and Peryt, T. M. (1998) 'Strontium geochemistry of Miocene primary gypsum: Messinian of Southern-eastern Spain and Sicily and Badenian of Poland', *Journal of Sedimentary Research*, 68, 1, pp. 63-79.

Sibley, D. F. (1980) Climatic control of dolomitization Sero Domi Formation (Pliocene). In: *Concepts and models of dolomitization* (eds. Zenger, D. H., Dunham, J. B. and Ethington, R. L.). Soc. Econ. *Palaeontologists Mineralogists Spec*. Pub. 28, pp. 247-258.

Sibley, D. F. (1982) 'The origin of common dolomite fabrics: clues from the Pliocene', *Jour. Sed. Petrology*, 52, pp. 1087-1100.

Siegel, F. R. (1961) 'Variations of Sr/Ca ratios and Mg contents in recent carbonate sediments of northern Florida Keys area', *Jour. Sed. Petrology*, 31, 3, pp. 336-342.

Theriault, F. and Hutcheon, I. (1987) 'Dolomitization and calcitization of the Devonian Grosmont Formation, northern Alberta', *Jour. Sed. Petrology*, 57, pp. 955-966.

Tucker, M. (1991) *Sedimentary petrology, an introduction to the origin of sedimentary rocks*. (Second edition), Blackwell Science, pp. 260

Ward, W. C. and Halley, R. B. (1985) 'Dolomitization in a mixing zone of near sea water composition, Late Pleistocene, Northeastern Yucatan Peninsula', *Jour. Sed. Petrology*, 55, pp. 407-420.

West, I. M. (1964) Evaporite diagenesis in the lower Purbeck beds of Dorset. *Proc. Yorkshire Geol. Soc*., 34, pp. 315-330.

West, I. M. (1973) 'Vanished evaporites - significance of strontium minerals', *Jour. Sed. Petrology*, 43, pp. 278-279.

Wood, M. W. and Shaw, H. F. (1976) 'The geochemistry of celestites from the Yate area near Bristol (U.K)', *Chemical Geology*, 17, 1pp. 79-193.

Zert, B. (1974) *Geological map of Libya*. Scale 1:250,000, Sheet NH 34-16. Darnah Sheet, Explanatory booklet, Industrial Research Center. Libya, Tripoli, 83pp.

Libyan Journal of Science & Technology 9:1 (2019) 11–20
The 2nd International Conference on Geosciences of Libya-GeoLibya 2 (2017), 14-16 October 2017, Benghazi-Libya

Faculty of Science - University of Benghazi
Libyan Journal of Science & Technology
journal home page: www.sc.uob.edu.ly/pages/page/77

The hydrocarbon source potential of the Paleozoic rocks of Ghadamis Basin Northwestern Libya.

Moftah Ahmed Dieb

Libyan Petroleum Institute, Tripoli, Libya

E-mail address: dieb63@yahoo.com

Highlights

- **This paper provides comprehensive synthesis of the geochemical analysis of the source rocks and thermal maturity regime for Paleozoic strata in Ghadamis Basin, Northwest of Libya.**
- **This paper also provides a new geochemical knowledge about the characteristics of the main effective source rocks in Ghadamis Basin, Northwest Libya .**
- **A new source rock and thermal maturity maps were constructed based on total organic carbon content and spore color index that can be used to investigate a new petroleum prospective regions in Ghadamis Basin, Northwest Libya .**

ARTICLE INFO

Article history:
Received 01 February 2018
Revised 10 March 2018
Accepted 17 March 2018
Available online 31 March 2019

Keywords:
Source rock, maturity, kerogen type, organic facies, optical; lower 'hot' Tanezzuft Formation, Ghadamis Basin, Libya.

ABSTRACT

Ghadamis Basin is an intracratonic sag basin and is considered as an important hydrocarbon province in the North African continent. In Libya, the Ghadamis Basin is located in the western part of the country and filled by Palaeozoic sediments and overlying thin Mesozoic-Tertiary sequences. The Palaeozoic rocks range from Cambrian to Carboniferous with a maximum thickness of about 12, 000 feet. They consist of alternating transgressive and regressive marine sandstones, shales, siltstones and, locally limestones. The present study, based on the ditch cuttings shale samples, investigate the bulk organic geochemistry, kerogen microscopy and thermal maturity. The geochemical results demonstrated the presence of various organic-rich zones within the Palaeozoic sequences. The Mamuniyat, the lower 'hot' Tanezzuft and the Awaynat Wanin formations are considered to have a good to excellent potential source and are particularly prospective hydrocarbon generation in the study area. The Tanezzuft formation is divided into an upper 'cool' shale and lower 'hot' shale based on the basis of high gamma-ray response in wireline logs and high organic carbon content (TOC). Generally, the Palaeozoic sequence has TOC values ranging from 0.5 to 21.4 wt%. Maturity data indicate that the Devonian shale samples are immature to marginally mature and that the Silurian and the Ordovician shale samples are mostly middle to late mature. Visual Kerogen examination showed that organic matter is comprised mainly of amorphous and palynomorphs components (Type II Kerogen) oil prone with some phytoclasts materials (Type III), gas prone.

1. Introduction

Organic matter-rich sediments in modern and ancient depositional environments are the result of a complex interaction between several factors, such as primary productivity in the water column, supply of nutrients, redox–oxidation processes and sediment accumulation rates (Demaison & Moore 1980). An extraordinary geological test site to unravel the significance of these single factors, which may have controlled organic matter richness, is the marine calstic shale in the Ghadamis Basin (Fig. 3). The Ghadamis Basin of northwestern Libya encompasses an area of about, 200,000 Km². It is situated in the northwestern part of Libya. It is delimited in the north by Nufusa Uplift and to the east Hun Graben, Gargaf Uplift to the south and to the west the basin extends to Tunisia and Algeria (Fig. 1). It is considered one of the largest basins in North Africa, which is filled by Paleozoic sediments, which are overlain by thin Mesozoic–Tertiary sequence (Fig. 2). Cambrian, Ordovician, Silurian, Devonian and Carboniferous rocks represent the Paleozoic sequence. Ghadamis Basin holds approximately the one-third of discovered hydrocarbons in Libya. The Paleozoic sequences consist of thick Cambro-Ordovician sandstone and shale. It is overlain by Silurian section consisting of Tanezzuft and Acacus formations. When new sea invasion started during the early Devonian, the sedimentary sequence was highly deformed by the effect of Caledonian tectonics. The Devonian section is represented by Tadrat sandstone, grading upwards into middle and upper Devonian sandstone and shale Awaynat Wanin Formation. The Carboniferous sections consist of shale and carbonate Mrar and Assedjefar formations. It terminates the Paleozoic sequence. During the late Carboniferous to early Permian, the Hercynian tectonics occurred and changes the tectonic framework causing a general regression of the sea over most Libya (Hamyouni *et al*. 1984).

In this work, we present detailed geochemical investigations of the source rock potential of the Paleozoic sequences in the Ghadamis Basin and the possibility of oil generation from this strata. The purpose of the study is to investigate the aerial extent, thickness, productivity, lateral and vertical variation of potential source rocks and to reconstruct the maturity history of the areas and present the evidence of it's bearing on generation, migration and trapping petroleum. Our investigations focus on selected wells located in the western and central part of the basin.

2-Geological setting

a) Structural framework

Libya, southern Tunisia and Algeria south of Atlas Mountain are part of the stable Saharan platform that was intensively folded in

 ISSN 2663-1407; National Library of Libya, Legal number: 390/2018

the Precambrian. Since then it has been effected only by epeirogenic movements, which produced wide, shallow basins and uplifts. In Ghadamis Basin the sedimentary sequence was affected by the Caledonian orogeny which produced the Edjeleah anticline and Al Gargaf Arch (Fig. 1), respectively. The northern part of the basin was uplifted during Hercynian orogeny (Burollet 1963b) but subsided again during the early Mesozoic. It was uplifted again towards the end of Cretaceous time, the uplift being accompanied by northwest trending faults. The old high, Jifarah to the north and Al Gargaf to the south, were reactivated in Late Cretaceous or Early Paleocene time, (Jordi and Ionfat 1963; Gouderzi, 1991).

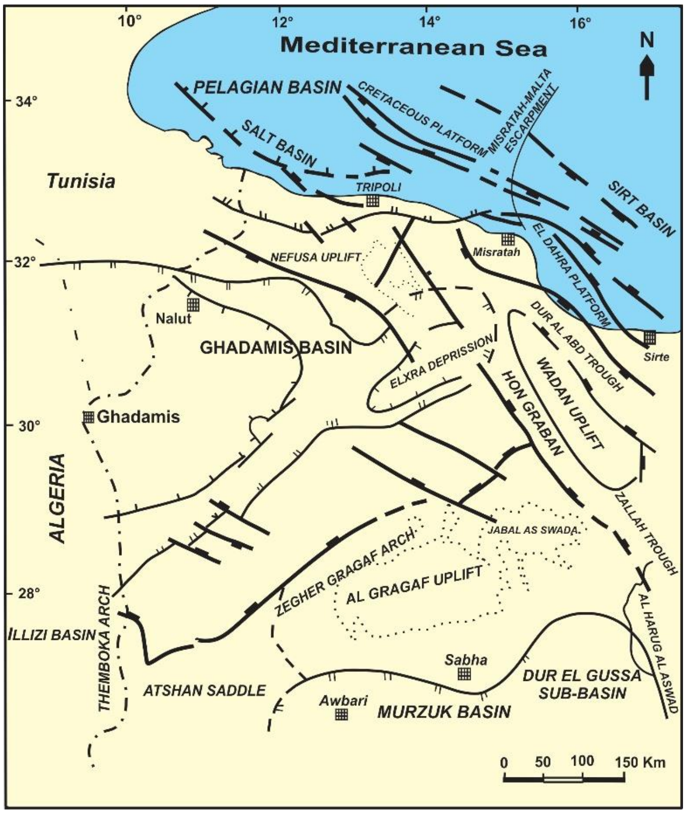

Fig. 1. Tectonic structure map of the Ghadamis Basin Libya.

b) Stratigraphic framework

In Ghadamis Basin, the thickness of the Paleozoic sequence is about 11,000 feet. It is composed of Cambro–Ordovician sandstone and shale. It is overlain by Silurian section consisting Tanezzuft Shale and Acacus Sandstone. The Silurian sections are generally conformable with the Ordovician Memoniate Formation. This sedimentary sequence was highly deformed by the effect of Caledonian tectonics, where a new sea invasion started during the early Devonian (Hamyouni *et al*., 1984). The Devonian section is disconformable with Silurian sediments. The Devonian section represented by Tadrat Sandstone and Ouan Kasa Sandstone with Shale, grading upward into middle and upper Devonian Awaynat Wanin sandstone and shale. The Devonian section is disconformable overlain Carboniferous section. The Carboniferous section is represented by Mrar and Assed Jefar formations and consists of shale and carbonate sediments (Fig. 2) (Hamyouni *et al*., 1984).

The Early Silurian of Lower Tanezzuft Formation is composed of dark gray to black graptolitic shale with rhythmical alterations. It usually shows high gamma-ray response on wireline logs. The true thickness of Lower Tanezzuft Formation that was determined is about 150 to 300 feet. It represents the broad marine transgression of the Silurian Sea over the North African carton.

c) 3-Methods of the study

The main method applied in this study was the analysis of 52 shale samples of well ditch cutting and cores. Samples were analyzed by conventional geochemical and microscopic techniques (Rogers 1979, Demaison *et al*., 1983 and Jones 1984) to evaluate the prospective source rocks and thermal maturation of organic matters in the Paleozoic strata within Ghadamis Basin. Whole samples were washed out, picked, and lithologically described. Rock–Eval II Pyrolysis plus TOC was used for determination of free hydrocarbons (S1), residual potential hydrocarbons (S2), maximum temperature Pyrolysis degradation (T max), Hydrogen index (HI), oxygen index (OI), production index (PI) and total organic carbon content (TOC), Espitalie *et al.* (1977). Selected shale samples were subjected to extract in a Soxhlet apparatus with chloroform and concentrated for determination of soluble organic matter (bitumen). Asphaltene was precipitated from this extract and the remaining filtrate was fractionated on an alumni silica–gel column and separated into the following hydrocarbon fractions. Saturated hydrocarbon, aromatic hydrocarbon and Polar resin (NSOs). Gas chromatography (GC) analysis of the Paraffin–Naphthene were carried out by means of Karlo Erba 4000 instrument equipped with a 25 m * 0.32 mm Cp-sil –5- CB column.

In addition, selected shale samples were subjected to kerogen isolation and visual kerogen assessment for microscopy by treatment with HCl and HF followed by flotation in heavy liquid ($ZnCl_2$ solution, density 2 g/ cm^3). Kerogen composition and spore color index (SCI) scale 1.0 to 10.0 was performed using transmitted and blue fluorescence light on Leica Microscope.

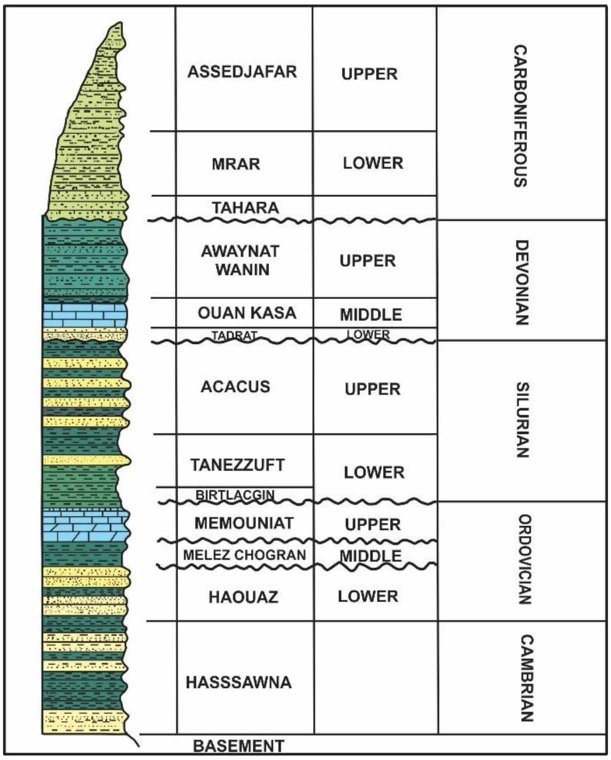

Fig. 2. Stratigraphic column section of the Ghadamis Basin, Libya

4-Results and interpretation

d) Source richness and maturity

The source potential and productivity are related to source rock thickness, maturity and to kerogen facies and therefore to depositional environment and type of organic matter input. Source rock quality is best in the central and west-central part of the basin where a stratified water column and suboxic-anoxic bottom condition, combined with high productivity in the photic zone, favored the preservation of liptinic, oil generative kerogen. The shale generally contains mixed kerogen of marine algal sapropelic (Type II) and land plant (Type III) facies, and proximity to the paleo-shoreline controls source rock quality, with greater amounts of terrestrially derived humic kerogen and consequently poorer oil source rock quality nearer the paleo-shoreline. In the southern flank of the basin close to the Gargaf uplift, the formation contains oxidized organic matter with poor oil source potential; these organic sediments are probably deposited in shallow, to sometimes deep, oceanic water. The marine succession in the studied wells at the southern part of the basin presents evidence for these criteria. In the west-central part of the basin where the Tanezzuft Formation reaches the late maturity stage, they have generated significant volumes of light oil, gas and condensate. The dark shale within the upper Awaynat Wanin Formation of the upper Devonian age is commonly organically rich and contain sapropelic kerogen, with oil and gas source potential. Shales in the Assed Jefar and Mrar Formations of the Carboniferous age are commonly have above average total organic carbon content but contain humic kerogen of mainly vitrinite and inertinite components. Therefore, there are no significant hydrocarbons could be anticipated from these formations.

a) Central and west-central part of the basin

In the central and west-central part of the Ghadamis Basin, the geochemical results of the studied wells showed that the Lower Tanezzuft Formation (Hot shale), has a dark gray to black shale and usually shows high gamma-ray response on wireline logs, and high resistivity with low density and sonic values, is rich in organic matter. It has TOC values range from 1.07% to 19.93 % concentrations with an average value of 8.50% (Fig. 3). These geochemical data confirmed that shale unit has good characteristics to be source rock for generating oil and gas. The genetic potential varied from 1.61 to 58.18 mg HC/g rock, indicating fair to excellent quality source rock (Dow, 1977; Espitalie *et al.*, 1977).

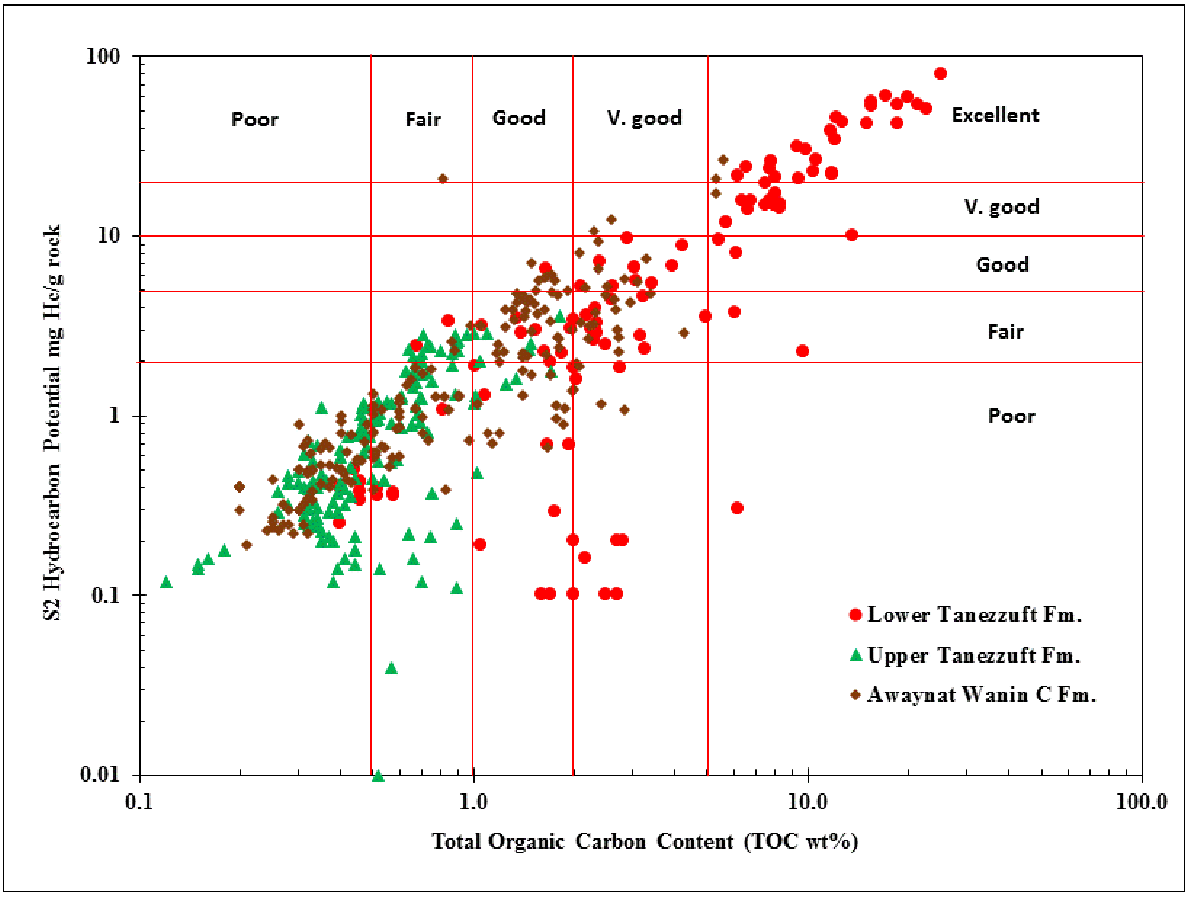

Fig. 3. Total organic carbon content (TOC) versus hydrocarbon potential (S2), showing the hydrocarbon potentiality of the source rocks in the Ghadamis Basin.

The geochemical logs (Fig. 4) show variation in organic matter content and hydrocarbon potential of Paleozoic sequence and its increase with increasing depth of the Tanezzuft Formation. The Lower Tanezzuft Formation in the central and west-central part of the basin has hydrogen index HI ranges from 108 to 393 mg HC/ g TOC. The good total organic carbon (TOC) and a high hydrogen index indicated that the amorphous organic matter probably preserved in an anoxic deep marine condition and good source rock for hydrocarbon generation. The measured T_{max} values indicates that the shale samples from Lower Tanezzuft Formation are immature, and middle to late mature, which are ranged from 423 to 460 °C. This is also in agreement with spore color index SCI, which indicate that the maturity level ranges from middle mature to late mature 6 to 8 SCI, respectively. The gas chromatography C15+ of the Paraffin–Naphtheane hydrocarbon fractions (Fig. 5) indicates that the samples are mature and farther more by the shape of normal Paraffin (envelope) and by the carbon preference index (CPI) values 1 to 1.17. The samples show evidence of a significant contribution from algae amorphous organic matter as suggested by *nC17* and *nC19* dominance. For all analyzed samples, the pristine to phytane ratio indicates that the shale of the Lower Tanezzuft Formation is deposited under reducing marine conditions. The ratio of pristine/phytane ranges from 0.80 to 1, represents the characteristic of normal transgressive anoxic marine shale source rocks (Jones, 1984).

The hydrogen index HI and oxygen index OI cross–plot (Fig. 6) indicates that the organic matter classified as type II kerogen with hydrogen index ranging from 160 to 393 mg HC/ g TOC, these indicated that hydrogen is good to rich and typical for oil-prone (Tissot, 1984). The Pyrolysis maturation index T_{max} gradually increases with depth (Fig. 4). Most of the analysis samples are in the mature petroleum generating range 430 to 451 °C. Fig. 7 shows the hydrogen index HI versus T_{max} of Tanezzuft and Awaynat Wanin formations, most of the samples are in the mature range (430–460 °C) and the rest, including some immature samples, are (less than 430 °C). Kerogen is a mixture between type II and type III, which indicates that source rock will produce oil and gas if its reach enough maturity.

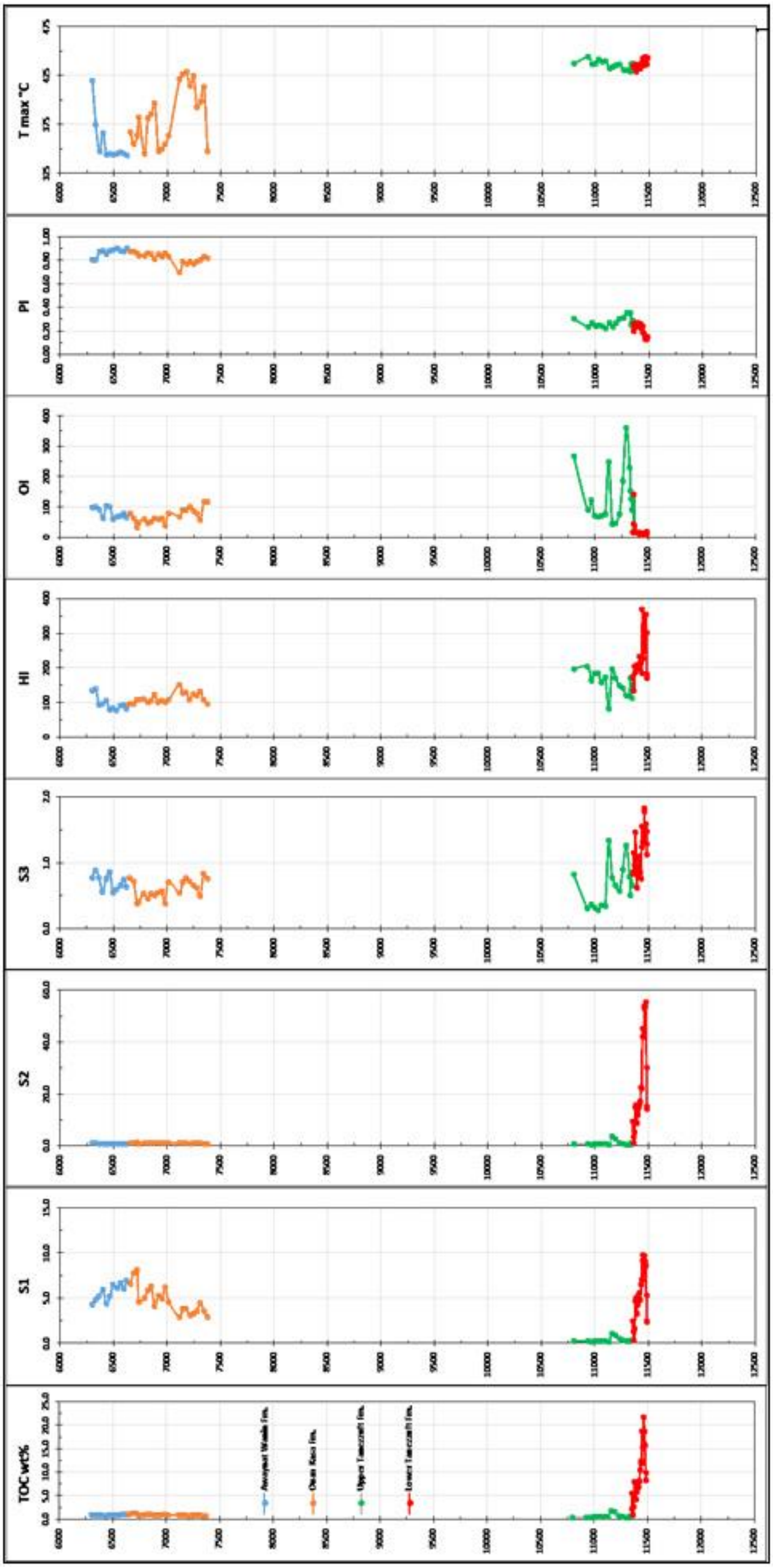

Fig. 4. Geochemical log for the Paleozoic Sequences of the studied well located in the central part of the Ghadamis Basin.

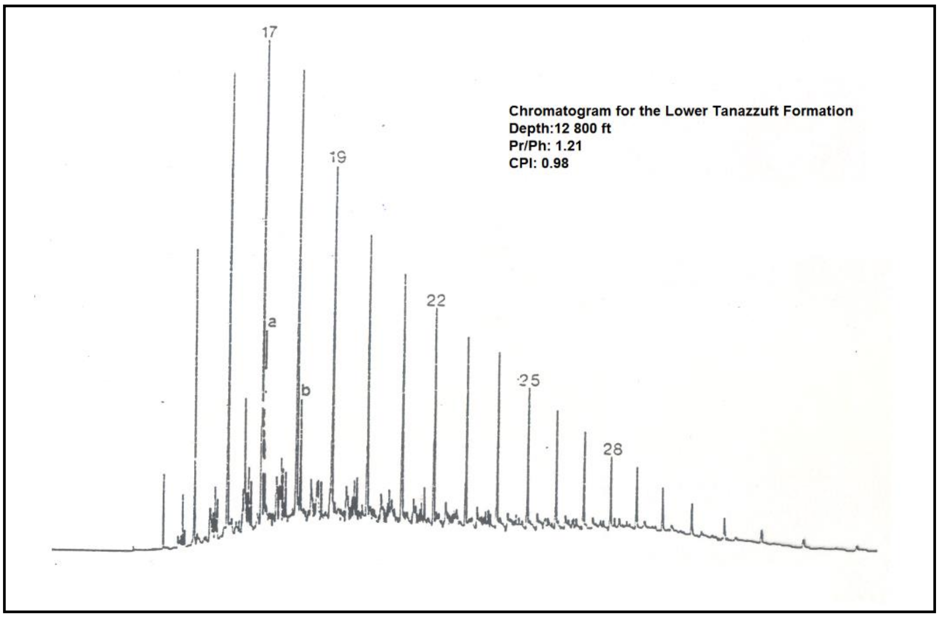

Fig. 5. Gas Chromatogram chart of the hydrocarbon fractions for the Lower Tanezzuft Formation.

Analyzed samples from the Upper Ordovician, Memoniate Formation are consisted mainly of siltstone and shale with some contaminated materials which caved from the overlying formations, their total organic carbon are generally low, and S2 potential hydrocarbon yield are also similarly low, therefore no significant source rock potential can be anticipated from sediments of the Memoniate Formation. The Bir Tlacsin Formation of the Upper Ordovician age consists mainly of limestone, shale and siltstone, the analyzed samples show, a fair to good TOC values that are ranged from 0.7 to 1.7%. Cuttings samples of the Middle Ordovician age, Melaz Shuqran Formation have been analyzed in some wells. The samples consist mainly of shales, black to dark grey, brownish grey with minor siltstone. It has a good TOC values, ranging from 1.2 to 1.85%. Therefore, the Bir Tlacsin shale and Melaz Shuqran formations could be also recognized as additional source rocks potential in Ghadamis Basin.

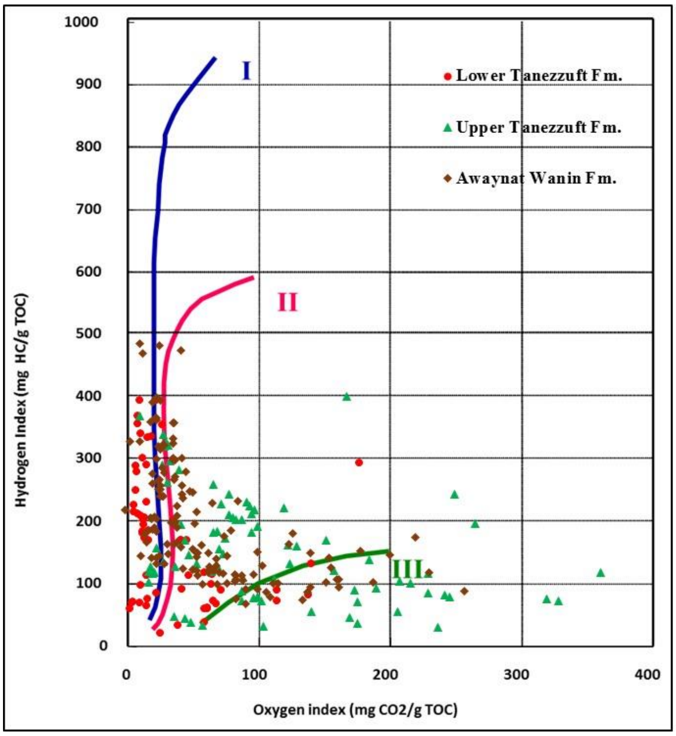

Fig. 6. Hydrogen Index versus Oxygen Index for the Paleozoic Rock, Ghadamis Basin

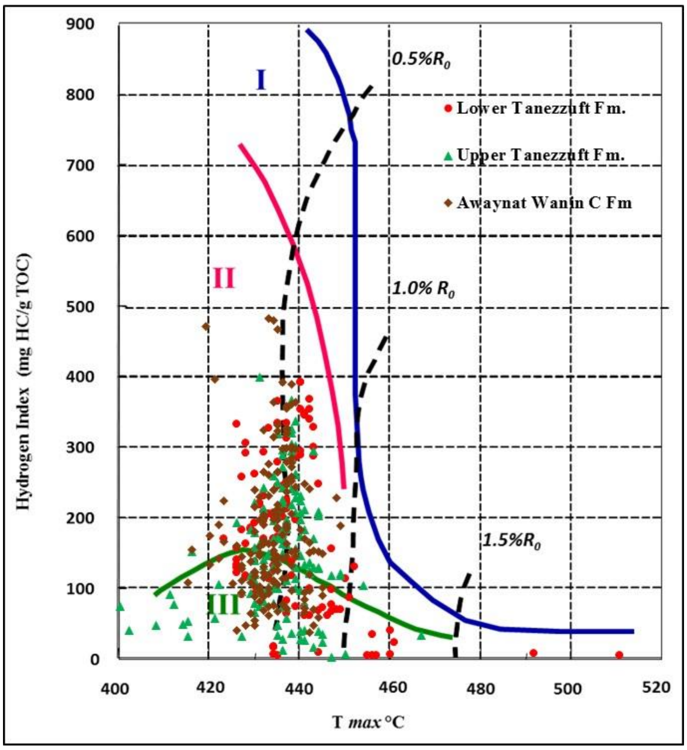

Fig. 7. Hydrogen index versus T max of the Tanezzuft and Awaynat Wanin formations.

Visual examination of kerogen type and maturity

Visual examination of kerogen type and thermal maturity have been assessed by means of spore color analysis supplemented by qualitative fluorescence of planomorphous in UV blue light. Spore color data are presented in terms of spore color index (SCI) assigned values from 1.0 to 10.0 in order to increase color from transparent to orange and finally black. The spore color index data for Lower Tanezzuft Formation in the central and west-central part of the basin are shown in Figure 8. The Lower Tanezzuft Formation is interpreted as mature to late mature for hydrocarbon generation and evidenced by measurement of spore color index SCI 6 to 8, and vitrinite reflectance measurements 0.7 to 1.3 Ro%, respectively.

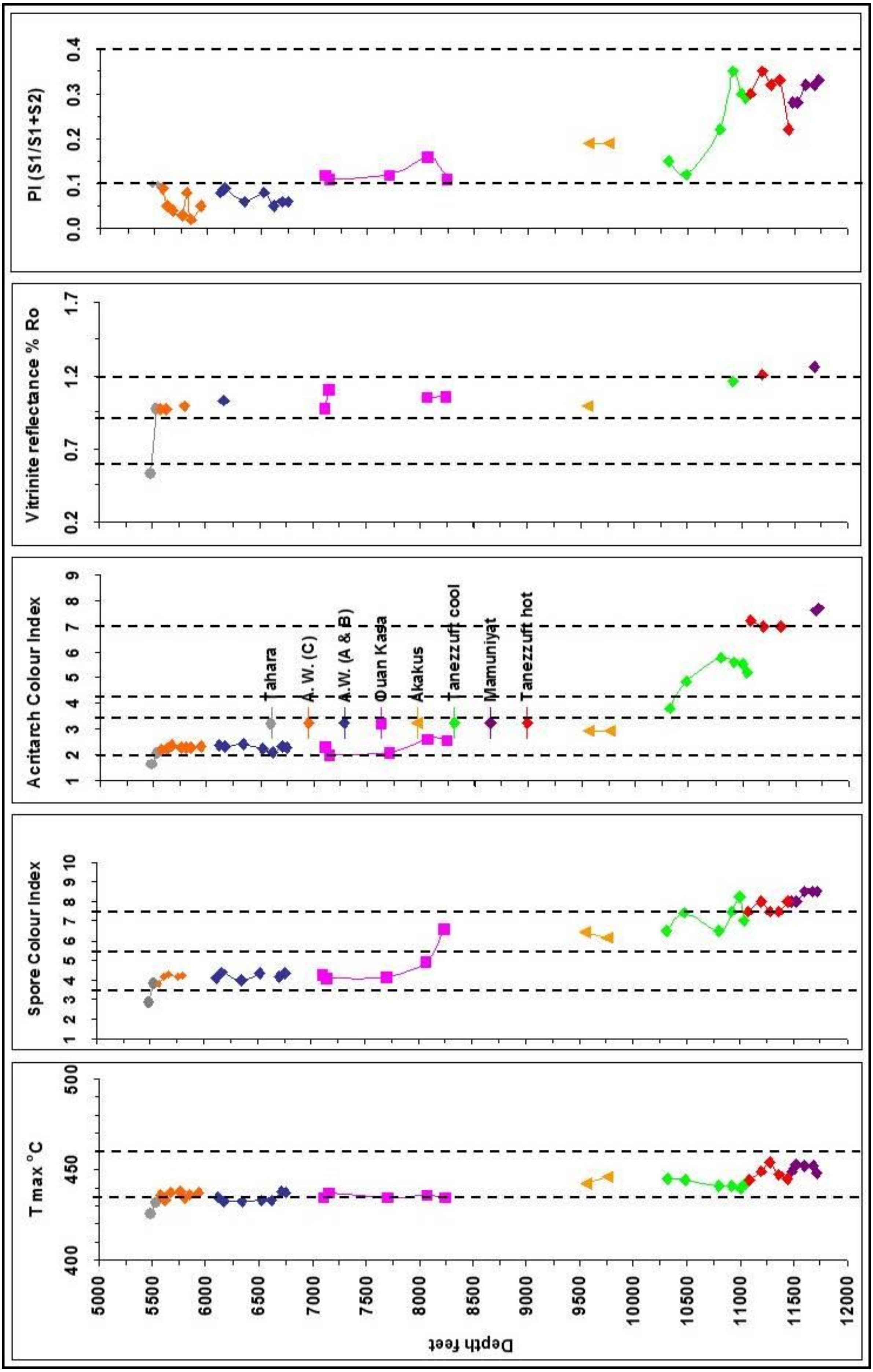

Fig. 8. Geochemical maturity log for the Paleozoic source rocks at the western part of the Ghadamis Basin

The visual kerogen composition analysis was carried out at the same time as spore coloration. Most of the kerogen comprises an amorphous sapropelic material with acritarch, and cuticle and actinozoan with minor inertinite debris Fig. 9. The predominance of the sapropelic amorphous material indicates that the kerogen will generate a significant amount of oil. Most of the samples are organically rich and have significant characteristics to be source potential for hydrocarbon generation.

An isopach map (Fig. 10) of the basal radioactive zone indicates that the Ghadamis Basin has the thickest radioactive zone (Hot Shale) interval in the deepest part of the basin, where thicknesses reach more than 200 feet (Echikh and Sola, 2000). However, the radioactive zone is missing over some palaeohighs area, for instance in the Al Gargaf Uplift, where Ghadamis Basin is separated from Murzuq Basin, suggesting that this area was a positive feature and a site of shallow water depositional environments (Echikh and Sola, 2000). Fig. 11 illustrates the contour map of thermal maturity (SCI) on top of Tanezzuft Formation. The map exhibits that Tanezzuft Formation has enough maturity to be generating hydrocarbon. It also showed that thermal maturity level increase toward the west, the central part of the basin, compared with the southern flank of the basin.

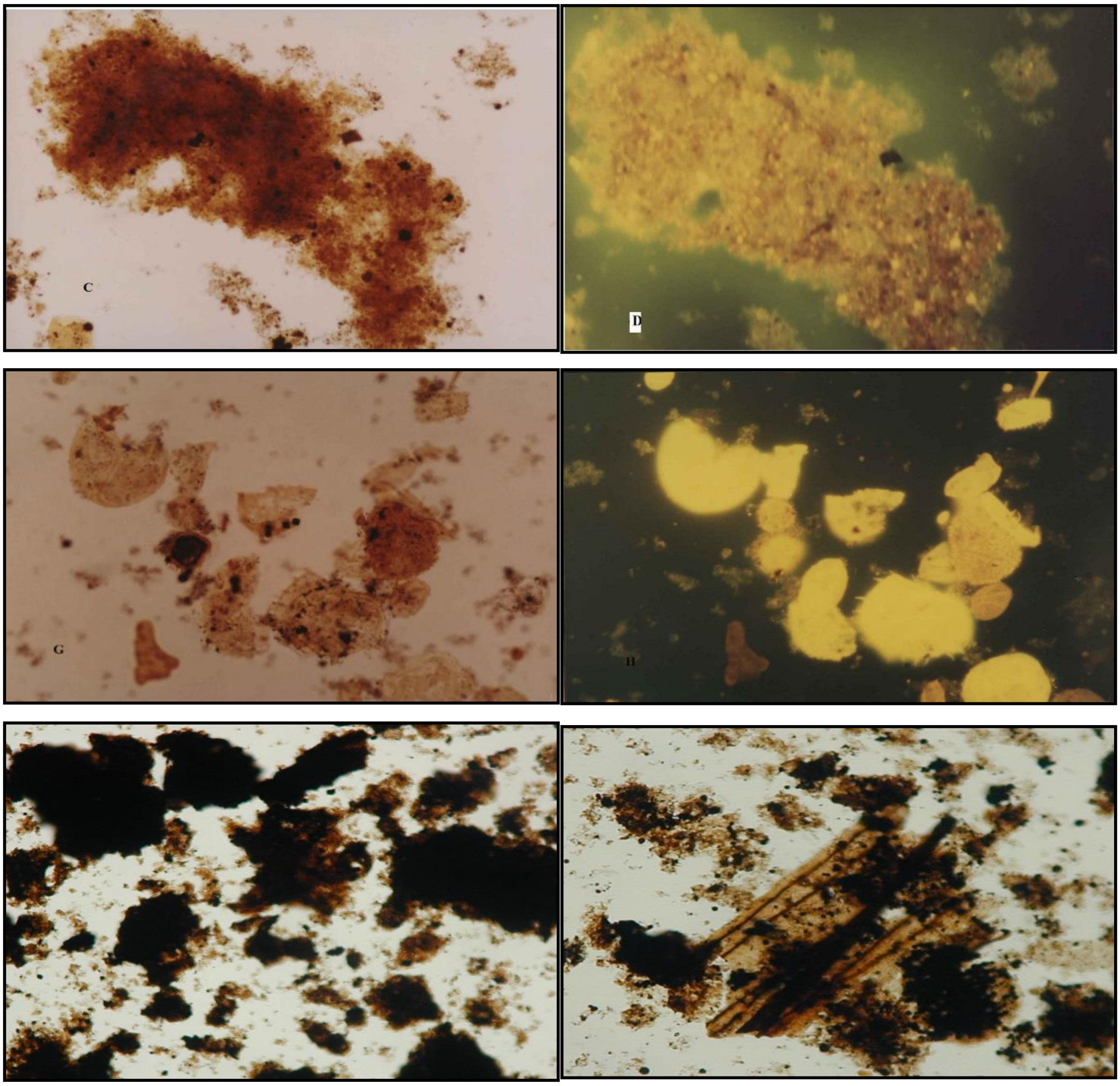

Fig. 9. Amorphous sapropelic material and acritarch, with minor inertinite debris.

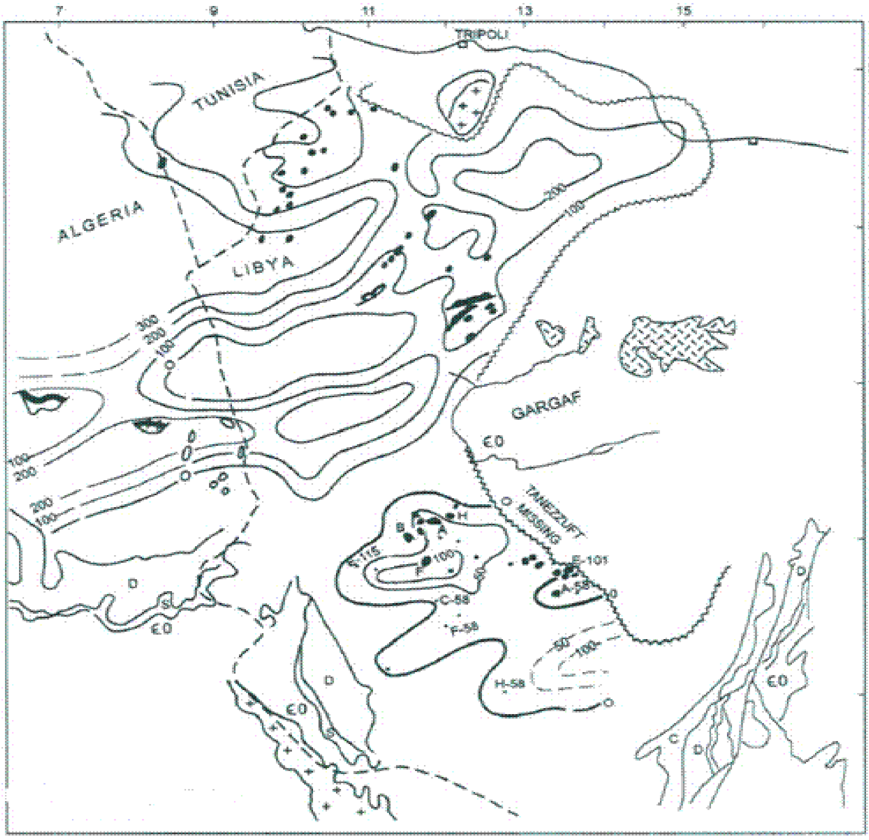

Fig. 10. Tanezzuft Formation "hot shale" radioactive zone map for the Ghadamis Basin and Murzuq Basin Libya, (After, Echikh and Soloa, 2000).

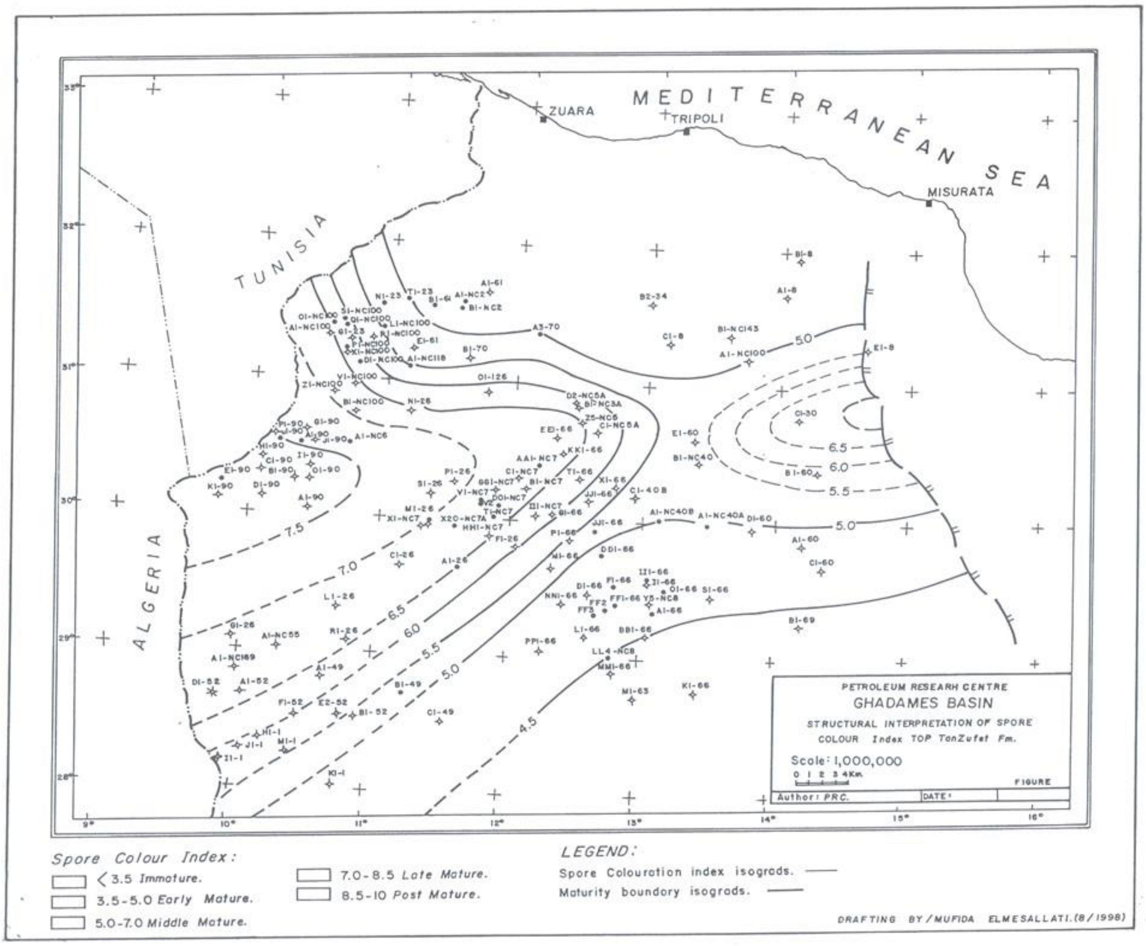

Fig. 11. Maturity map (SCI) for the Tanezzuft Formation, Ghadamis Basin.

b) Southern flank of the basin (close to Gargaf uplift along the paleo-shoreline)

In the southern flank of the Ghadamis Basin close to Gargaf Uplift along the Paleo shoreline, the geochemical data of the selected wells observed that, the lower Tanezzuft Formation consists of gray to dark gray or black shale and has an organic carbon content (TOC) ranges from 0.85% to 3.37% with an average 2.01%. Generally, the low values of pyrolysis potential yield (S2) 0.23 to 4.45 mg HC/ g rock with an average 3.10 mg HC/g rock indicate that the dark gray to black shale of the Lower Tanezzuft Formation at the best will be a gas source potential, which would be generated at higher levels of maturity (Fig. 12).

The pyrolysis maturation index (T_{max}) 439 °C indicates that the shale samples are mature. The low pyrolysis hydrogen index (HI) 6 to 195 mg HC/g TOC with an average of 92 mg HC/g TOC indicated that organic matter is capable to generate gas. The good total organic carbon (TOC) and low hydrogen index (HI) indicates that amorphous organic matter and inertinite probably neither well preserved (on suboxic to oxic condition), or probably post mature source rocks or rocks that probably never had much generation potential. A cross–plot of hydrogen index (HI) and oxygen index (OI) on modified Van Krevelen diagram (Fig. 6) indicates that the organic matter is a mixture of type II and type III organic matter; it is capable to generate oil and gas.
Fig. 7 shows the hydrogen index (HI) versus (T_{max}) of Lower Tanezzuft Formation. The shale samples are mature ranged from 430 to 451 °C and the rest, including some immature samples, (are less than 430 °C). Kerogen is a mixture between type II and type III, which fits with a predominance of oil and gas on the source.

The gas chromatography C15 + of Paraffin–Naphtheane hydrocarbon fractions (Fig. 5) indicates that samples of Lower Tanezzuft Formation are mature, this indicated by the shape of normal Parafins (envelope) and carbon preference index (CPI) values 1.0 – 1.40. All samples show evidence of a significant contribution from amorphous organic matter as suggested by nC17 to nC19 abundance. The pristine to phytane ratio for most samples indicates that the shale of Lower Tanezzuft Formation deposited under marine conditions. Pristine/Phytane ratio between 0.8 and 1 are characteristics of normal transgressive marine shale source rocks.

Visual examination of kerogen type and maturity

The kerogen examined of the Lower Tanezzuft Formation was noted to compose mainly of amorphous with a herbaceous and woody material. The lower part of the formation is interpreted to be mature to post mature for hydrocarbon generation indicated by SCI measurement 6 to 9.5 respectively. The predominance of an amorphous material indicates that the kerogen will generate oil but the higher maturity of that organic matter 9.5 SCI indicates that organic matter will generate gas instead of oil or both.

5-Source rock to reservoirs relationship in Ghadamis Basin

Approximately all of the hydrocarbons accumulations so far discovered in the Ghadamis Basin seem to be generated primarily from Lower Silurian, Tanezzuft hot shale and less degree from Devonian strata, Awaynat Wanin C Formation and was reservoired within the Silurian and Devonian sandstone. According to Echikh (1998), all known commercial oil accumulations are within the porous sandstones of the Upper Silurian, Lower Acacus Formation, and the Lower Devonian Tadrat, and Oan Kasa formations, with only small accumulations in the Upper Tanezzuft, Bir Tlacsin, Awaynat Wanin B and A, Tahara, Marar and Triassic Ras Hamia formations (Echickh, 1998 and 2000). Moreover, communication between these strata (sources and reservoirs) seems to be necessary for any successful hydrocarbons accumulation in the basin. In the Ghadamis Basin, the significant of the direct contact between source and reservoirs rocks is improved with dominate of the reservoirs lithofacies, which has generally a relatively tight clean quartz sandstones that is not inductive to long-distance migration, such as in the Acacus Formation (Echikh and Soloa, 2000).

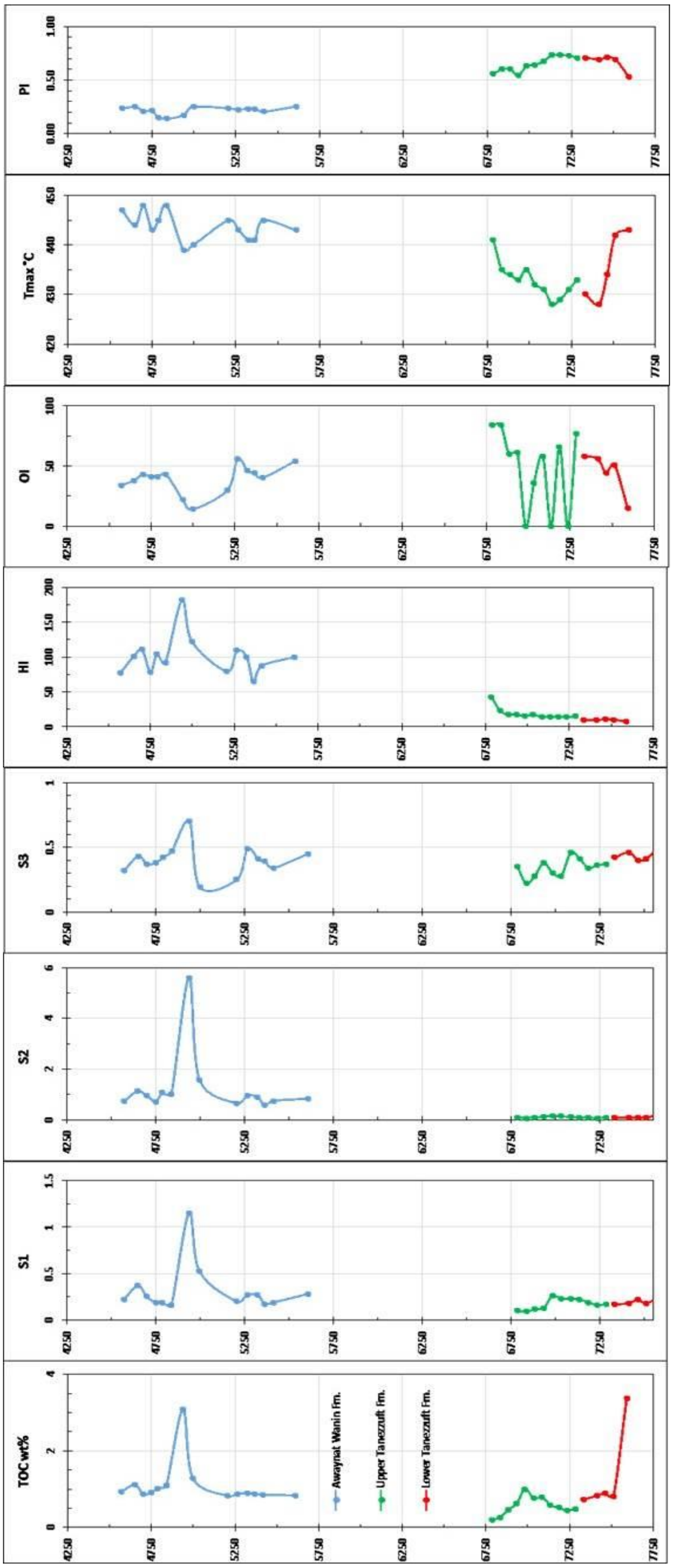

Fig.12. Geochemical log for the Paleozoic Sequences of the studied well located in the southern flank of the Ghadamis Basin.

However, most of the oil fields are gathered in the three discrete areas, which are in the northwest, central and southern parts of the Ghadamis Basin, each has different trap style, charge history and principal reservoir beds (Dardour *et al*,. 2004). Reservoirs occurred in the northwest part characterized by both low-displacement fault and unconformity sub-crop traps such as Acacus Formation. While in the southern part of the basin, three-way dip fault traps characterized the Tadrat reservoir (Dardour *et al*., 2004). In the central part of the basin, traps characterized with more typical of the elongated low-relief anticline structure with reservoirs occurred at several horizons (Dardour *et al*., 2004).

In the Ghadamis Basin, the structural feature is characterized by depocenter migration with a time that was controlling the lateral changes in the depositional environments, in the maturity of the source rocks, and also in migration pathways distributions and directions. However, several factors could be controlled the migration pathways such as source to reservoirs communication, nature of the seal, lateral changes in the reservoir quality and the influences of the folding and faulting.

The migration and accumulation of hydrocarbon are highly depended on the structural morphology of the seal, which is also the surface under which the hydrocarbon generally migrate from the source rocks (kitchen) to the structural highest part in the basin. Echikh and Soloa (2000) illustrated that the distribution areas for any hydrocarbon accumulations are highly affected by the structure of the sealing surface. Therefore, if the highest part of the basin is regional high, folded as anticline in form, hydrocarbon will normally gather on or around this high. Whereas, if the highest part of the basin has a syncline form, the hydrocarbon accumulation may be following a curved distribution trend. The shales of the Upper Tanezzuft and Mrar formations are representing the regional seal for most hydrocarbon accumulations in the Ghadamis Basin.

6-Conclusion

The Lower Tanezzuft Formation consists of gray, dark gray or black shale and usually show high gamma-ray response on wireline logs (radioactive shale). It's age of Early Silurian (Llandovery). The Lower Tanezzuft Formation in the greater part of the Ghadamis Basin appears to have been deposited in deep marine reducing environments. The thickness of Lower Tanezzuft Formation is about 150 – 300 feet and generally considered the main oil source rock unit in the Ghadamis Basin. At the central and west-central parts of the basin, the Lower Tanezzuft Formation is a good source rock unit with high potential for hydrocarbon generation. Toward the southern flank of the basin, close to Gargaf Uplift and along the Paleo shoreline the Lower Tanezzuft Formation is a good source rock unit with low potential for hydrocarbon generation. This is caused either by poor preservation of organic matter or by the high level of thermal maturity. In the central and west-central part of the basin from the analyzed wells, the maturity level rnges from mature to late mature (SCI 6 to 8) and it will generate significant oil. In analyses wells the maturity level range from mature to post mature (SCI 6 to 9.5) and it will generate significant oil and gas in the southern flank of the basin closed to Gargaf Uplift along the Paleo shoreline. The organic facies of the source rock are generally oil prone with type II kerogen and content amorphous, herbaceous with acritarch, cuticle and actinozoan and sometimes algal matter in the central and west-central part of the basin. Southern flanks of the basin closed to Gargaf Uplift along the Paleo shoreline the organic facies of the source rock are generally, oil to gas prone with mixture type II and III kerogen. The marine organic matter contents are amorphous, herbaceous and coaly material. In the northwest part of the basin, oils reservoired within thinly interbedded sandstones of shelf-dominated facies and are characterized by lateral migration with less leakage into an overlain Devonian reservoir. Sub-unconformity traps and low displacement fault represents the main traps in this area. Both traps style influenced by late tilting and fault reactivation with an increased chance of post-charge dispersal. While, in the central part of the basin, most of oils and gases were reservoired within Upper Silurian, Upper Devonian and Carboniferous Strata. Oil fields and gas fields that located in this part of the basin are charged from the west by short distance migration. Structurally, this part of the basin was affected by less late uplift and regional tilting than the west and south. Most of the traps are of low relief structures. The Upper Silurian strata, Acacus Formation and Upper Devonian strata and Tadrart Formation represent the main reservoirs in the south part of the basin, where vertical hydrocarbon short distance migration is dominant in this part. All the hydrocarbon accumulations occurred are structural traps. However, a huge high thick and continuity of the sand intervals that represents Acacus and Tadrat formations make a little chance to form stratigraphic traps in this part.

Acknowledgement

We would like to thank the secretary of the people's committee of Libyan Petroleum Institute Dr. Mansur Imatir and Salam El Akther, and exploration manager Dr. Khalifa Abdulnaser for their support and permission to publish this study. And also thank all member staff of the exploration department for their discussion and helping to conduct this work.

Reference

Burollet, P. F. (1960) 'Lexique Stratigraphic International, 4, Afrique, Pt. 4a, Libya', *Comm. Strat., Cent. Nat. Rech. Sci*., 62p.

Dardour, A. M, Boote, D. R., and Barid, A. W. (2004) 'Stratigraphic controls on Palaeozoic petroleum system, Ghadamis Basin, Libya', *Journal of Petroleum Geology*, 72(20, pp. 141-162.

Demasion, G. J., Holck, A. J. J., Jones, R. W. and Moore, G. T. (1983) Predictive source bed stratigraphy: a guide to regional petroleum occurrence. In: *Proc. 11th Worled Perol. Congr*., London, 2, 17-19.

Dow, W. G. (1977) 'Kerogen studies and geological interpretations', *J. Geochem. Explor*., 7, pp. 79 – 99.

Echikh, K. (1998) Geology and hydrocarbon occurrence in the Ghadamis Basin, Algeria, Tunisia and Libya. In: MACGREGOR, D. S., MOODY, R. J. and CLARK-LOWES, D. D. (Eds), Petroleum geology of North Africa, Geol. Soc. Land, Spec. Publ, 132, pp. 109-129.

Echikh, K. and Sola, M. A. (2000) Geology and hydrocarbon occurrence in the Murzuq Basin, SW Libya. In: SOLA, M. A., and WORSLEY, D. (Eds), Geological Exploration in Murzuq Basin. Elsevier, London, pp. 175-222.

Espitalie, J., Laporte, J. L., Madec, M., Marquis, F., Leplat, P., Paulet, J. and Boutefeu, A. (1977) Methode rapide de characterisation des rocks meres de leur potential petrolier et leur degre d، evolution. Rev. Inst. Fr. Petrole, 32, pp. 23-42.

Gouderize, G. H. 1991. The Geology of Libya, Volume III, Structure of Libya. Elsevire Science Publishers B V. Burgerhartstraat, 25 Amsterdam, the Netherlands, p 883.

Hamyouni, E. A., I. A.Amr, M. A. Riani, A. B. El-Ghull, and S. A. Rahoma (1984) Source and habitat of oil in Libyan basins: Presented at seminar on source and habitat of *Petroleum in the Arab countries*, Kuwait, p. 125–178.

Jones, R. W. (1984) Organic facies. In: Advance in petroleum geochemistry (eds J. Brooks and D. Welet). Academic Press, London, 2, pp. 1-90.

Jordi, H. A. and Lonfat, F. (1963) Stratigraphic subdivision and problems in Upper Cretaceous–Lower Tertiary deposits in north- western Libya. Rev. Inst. Fr. Petrole, 18, pp. 1428–1436.

Rogers, M. A. (1979) Application of organic facies concepts to hydrocarbon source rock evaluation. In: Proc. 10th World petrol. Congr. Bucharest.

Tissot, B. and Wellet, D. H. (1984) Petroleum formation and occurrence, 2nd edition Berlin, springer–verlog, P- 503.

Libyan Journal of Science & Technology 9:1 (2019) 21–25
The 2nd International Conference on Geosciences of Libya-GeoLibya 2 (2017), 14-16 October 2017, Benghazi-Libya

Faculty of Science - University of Benghazi
Libyan Journal of Science & Technology
journal home page: www.sc.uob.edu.ly/pages/page/77

Gas detection technique in low resistivity pays of Lower Acacus reservoir, concession NC7A, Ghadames Basin, NW Libya

Abraheem A. Elmasli * and Ismaeil I. Mohamed

Department of Geology Department, Exploration Division, Arabian Gulf Oil Company, Benghazi.

Highlights

- **Low Resistivity Pay represents the main challenge in the shaly-sand Lower Acacus reservoir in Ghadames Basin. Up to date, no real procedure has been found to define the hydrocarbon in this type of reservoir.**
- **In this study, we were able to define gas reservoir by applying a specific feature in Techlog software named ''Pallete-Spectrum'' of the sonic log. However, this is not applicable on oil reservoir.**
- **The advantage of this procedure is that, it does not need any extra measurement or calculation. In addition, it has been applied on different gas wells in Ghadames Basin, which shows a good result.**

ARTICLE INFO

Article history:
Received 01 February 2018
Revised 10 March 2018
Accepted 17 March 2018
Available online 31 March 2019

Keywords:
Ghadames Basin, Lower Acacus, low resistivity pay, gas reservoir, sonic log, Palette

*Corresponding Author:
E-mail address: i.elmasli@agoco.com.ly
A. A. Elamsli

ABSTRACT

Lower Acacus Member is one of the main reservoirs in the Ghadames Basin and it is composed of alternation sandstone and shale facies. It is characterized by low resistivity multiple stacked pays, making the hydrocarbon detection task difficult. To date, no real procedure has been found to correctly define the hydrocarbon in low resistivity intervals. Gas layers as an example could be defined using density and neutron cross-over, but in shaly sand reservoirs as in this case, the shale effect on the neutron log measurement is opposite to the gas effect making the detection of the gas zone by cross-over not valid. On the other hand, the sonic log is affected by the gas by decreasing the rock density, which leads to overestimation of porosity. This phenomenon shall help diagnose the gas presence in low resistivity reservoir. Using color editor of petrophysical software enables the subdivision of log curves into horizontal intervals with specific color or shade based on certain values. Intervals with DT (90-100 msec/ft), which corresponding to 25-36% porosity unit, are shaded red. Comparing production test results with high porosity zones (red shaded on logs) proved that they are gas producers. The advantage of this procedure is that it does not need any extra measurement or calculation; it is only a way of displaying the logs. It has been applied to different gas wells in Ghadames Basin, and it shows a good result. However, this procedure is not applicable to oil pays.

1. Introduction

The present study is based on the need for generating a new approach aimed to delineate gas intervals within Lower Acacus reservoir, which characterized by Low Resistivity Pay (LRP) phenomena.

1.1 Location of the Study Area

The study area (Fig. 1) (Arabian Gulf Oil Company, 2007) is located in the south-central part of Ghadames Basin, with three wells (Well-1, Well-2, and Well-3) under the supervision of Arabian Gulf Oil Company (AGOCO). The study area (Concession NC7A) is located about 100 km to the East of Dirj City.

1.2 Regional Tectonic Setting

The Ghadames Basin is a large intracratonic basin on the North African platform. Formed during the early Paleozoic era, it covers an area of 350,000 km^2 and straddles the borders of Libya, Tunisia, and Algeria. The Libyan portion represents the eastern flank of the basin and covers an area of about 183,000 km^2. It is an important hydrocarbon province since the 1950s (Echikh, 1998). The main tectonic elements bounding the Ghadames Basin are the Dahar–Nafusa uplift to the north, the Qarqaf arch to the south, partially bounded by the extension of Tihemboka uplift to the west, and the western flank of the younger Sirt Basin to the east (Fig. 2).

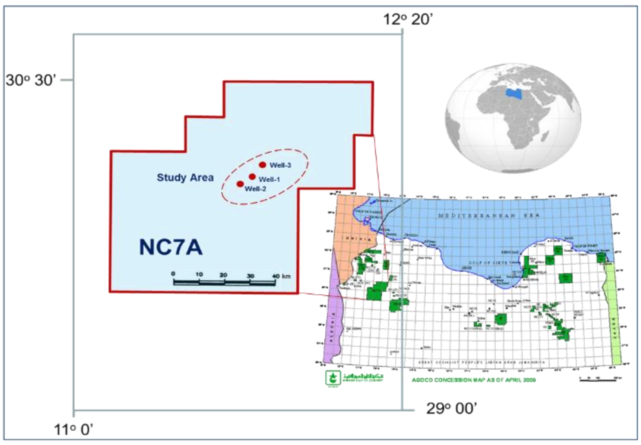

Fig. 1. Location of the study area in Ghadames Basin (Arabian Gulf Oil Company, 2007)

Many of these structural features were initiated in the late Precambrian Pan-African orogeny, with repeated reactivation of older structures occurring throughout the Phanerozoic. The basin contains up to 5,200 m [~17,000 ft] of Paleozoic and Mesozoic sediments, the Paleozoic section being separated from the Mesozoic deposits by a major regional unconformity of the Hercynian(Devonian-Carboniferous) age (Figs. 2&3).

 ISSN 2663-1407; National Library of Libya, Legal number: 390/2018

This Hercynian unconformity is represented as the most conspicuous feature of the basin as Paleozoic sequence is overlain by Mesozoic succession with a markedly different basin configuration. Erosion patterns and the topography that developed on the surface of this regional unconformity have had a direct influence on the petroleum systems within the basin. (Hallett, 2002).

1.3 Regional Geological Setting

The Ghadames Basin comprises four major tectonic cycles. The oldest one, that represents the Cambro-Ordovician cycle, ended by the Early Caledonian tectonism; the second one of Silurian age ended by the Late Caledonian epeirogeny and the third one of Devonian–Carboniferous age terminated by the Hercynian epeirogeny. The Alpine Orogeny, represented by Mesozoic sedimentary cycle, has increased the northern extension of the basin and changed it into a marginal sag basin (Hallett, 2002). Paleozoic deposits are dominated by non-marine and marine clastics: conglomerates, sands, silts and shales that comprise more than 95% of the total section. There are much more carbonates and evaporates in Mesozoic deposits, while the Cenozoic deposits consist of limestone and shale. The depositional setting in Paleozoic is an interior, cratonic regime of subsidence characterized by shallow marine and non-marine environments. The depositional setting of marginal platform regime dominates during Mesozoic time.

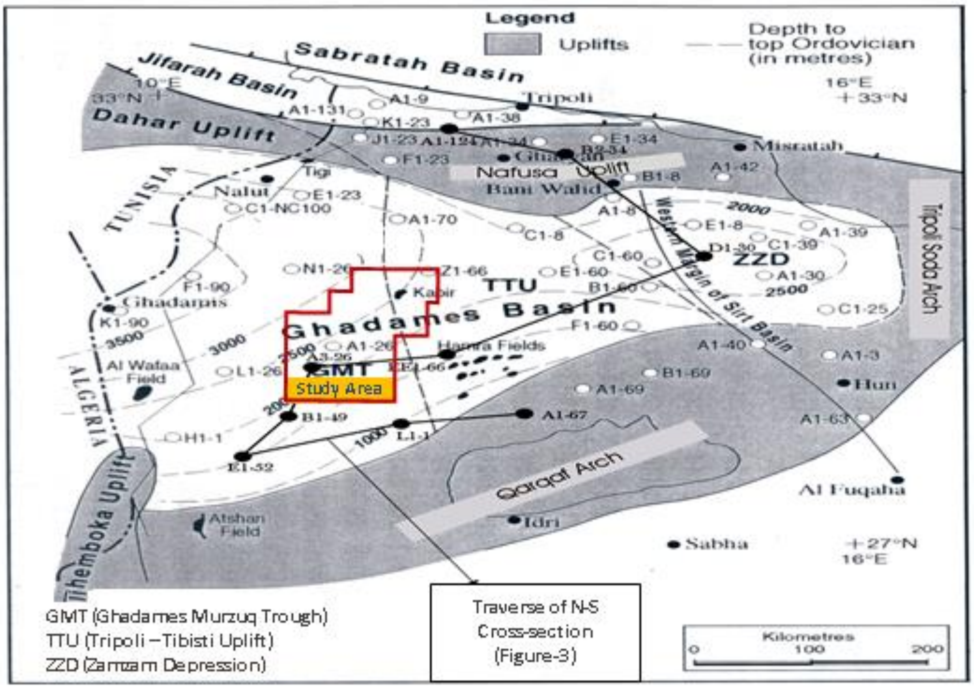

Fig. 2. Tectonic elements of Ghadames Basin (Hallett, 2002)

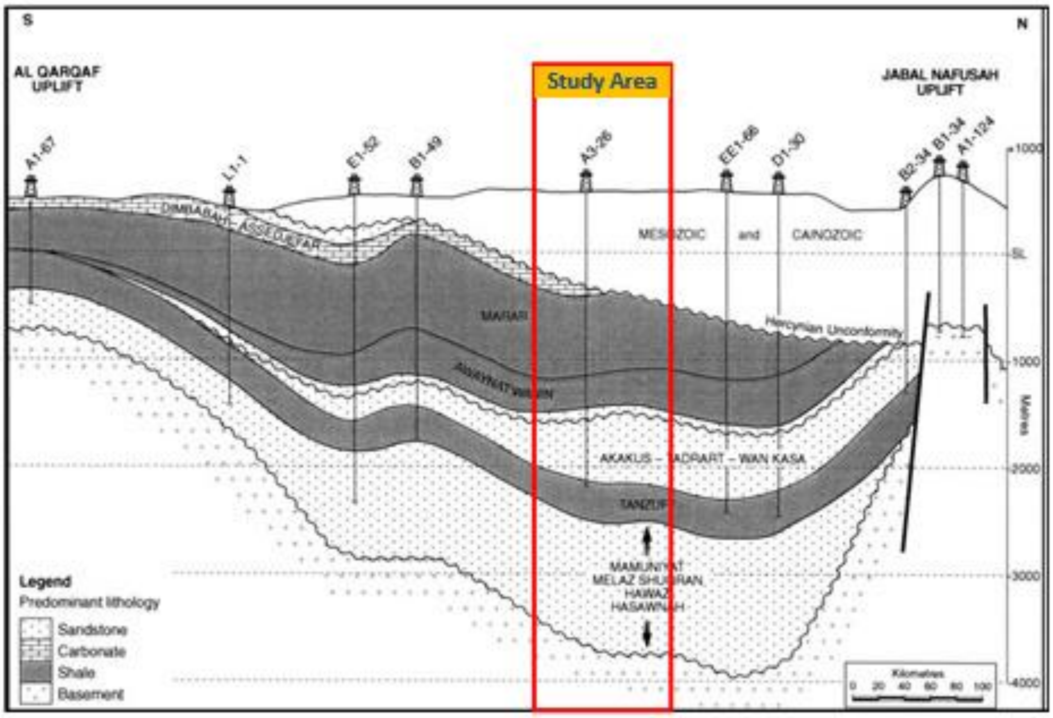

Fig. 3. N-S cross-section line of Ghadames Basin (Hallet, 2002).

In general, development of the Lower Acacus reservoir coincides with a high stand system tract during Late Silurian time, which leads to the development of prograding delta complex. The inter-fingering of the delta front sandstones with adjacent prodelta mudstone provides the multi-pay reservoirs. This reservoir represents the main targets for oil exploration and production and it is characterized by the low resistivity phenomena, making the hydrocarbon detection from well logs a very difficult task.

1.4 Objectives

The main aim of this study is to introduce a new, best-fit reservoir determination approach between sonic log analysis and production tests data on three wells with multi-pay intervals. It could also indicate additional reservoir intervals as bypassed pays.

2. Methodology

The method is based on the best display of sonic log in order to indicate the gas-bearing reservoir. In Techlog (Schlumberger software), they develop a type of color-fill known as (Palette) instead of using only vertical base-line to separate between the log measurements. In the Palette editor, you can divide any type of logs to the number of intervals horizontally and define the intervals by a specific type of lithology (shale or sand). In order to indicate the gas zone, sonic log was divided into six intervals from 40 up to 100 msec/ft (Fig. 4). Every interval is represented by a specific color, for example, green color (value ranges 60-80 msec/ft) represents normal sandstone units with no gas presence, while the values between (90-100 msec/ft) shaded red to indicate gas-bearing reservoir in the study area.

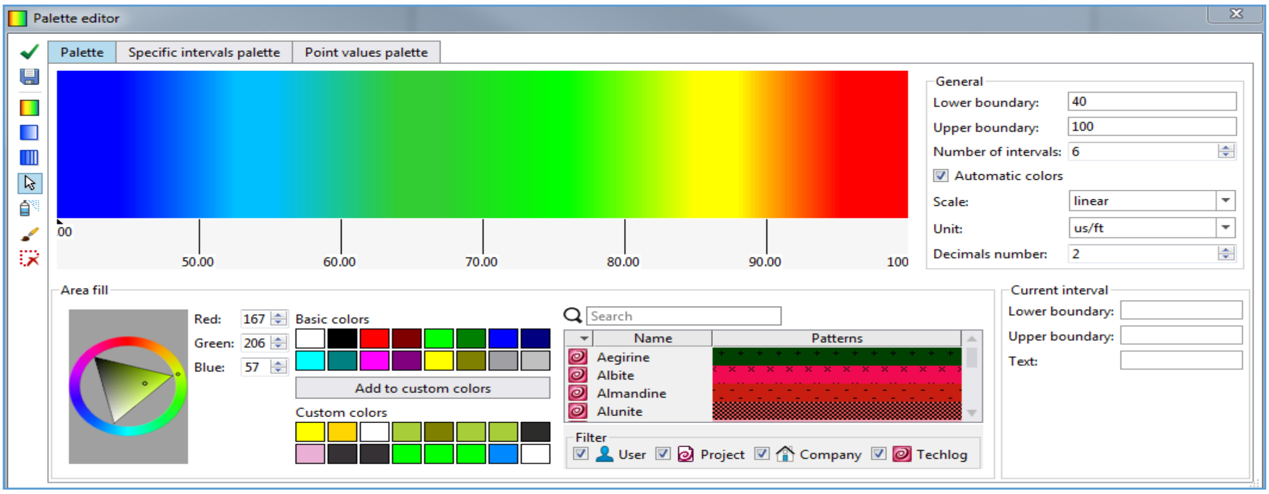

Fig. 4. The Palette editor in Techlog Software shows the six intervals used in this study with the selected colors, in which red color indicates values of gas formation.

The red color should be corresponding to a high concentration of gas molecules illustrating high sonic log reading. This range is actually equal to (26-33 %) porosity unit, which is not common to develop in sandstone reservoirs at deeper sections unless unconsolidated sand is detected. The loose sand could be detected when a wash-out zone occurs in sand layers and it could be excluded by applying the (bad hole flag) between bit size and caliper log giving a value equal to 0.3 inch. As a result, every time caliper log reads 0.3 inch higher than bit size in the sandstone intervals will indicate the unconsolidated aspects and hence, the interval should be further tested to confirm the gas accumulation in the sandstone reservoir intervals.

3. Results and discussions

In order to see the impact of this technique on the gas bearing intervals, two gas wells (Well-1, and Well-3) and one dry well (Well-2) are used in this study. Table 1 represents the top and bottom of Lower Acacus reservoir and the total gross thickness of the formation.

Table 1

Lower Acacus Formation tops and gross thickness among the studied wells.

	Well-1	Well-2	Well-3
Top	9025	9126	9046
Bottom	9730	9820	9786
Thickness	705	694	740

Presentation Summary Track:

Table 2 represents the well-log plot summary tracks (from left to right).

Table 2

Well-log plot summary tracks

Track#1	GR log with lithology Pallete of Sandstone (0-75 API), Silt (75-100 API), and Shale (100-200 API)
Track#2	Measured depth with vertical scale in feet (1:200)
Track#3	Density and Neutron logs with Sand-Shale zone shaded
Track#4	Deep Resistivity
Track#5	Sonic log with gas indication Pallete, and Bad Hole Flag indicated red color

Well-1:

The test results of the well indicate a tremendous amount of gas, and accordingly additional well (Well-2) was drilled to appraise the discovered structure. In the normal reservoir, gas zones could be defined when high resistivity values come across low neutron log reading and low-density log measurement (known as density-neutron crossover). Nevertheless, it can be seen that density-neutron crossover is not pointing to the gas bearing intervals in Lower Acacus shaly-sand reservoir due to the shale effect on the log measurement. Moreover, deep resistivity measurement should read high at gas intervals but this is not the case in the low resistivity pay of Lower Acacus reservoir. Comparing that to the sonic log analysis, in which the log response in the gas zone is more reliable. An increase in the sonic log porosity is clearly seen in gas reservoir interval, which actually was confirmed by production test intervals. In this procedure, gas intervals appear as red color while other sandstone units look green in color. Fig. 5 and Fig. 6 show the result of DT_Facies_Pallete and how correlatable to the production test data. Furthermore, a new zone was identified as bypassed zone (Fig. 7) which might express the advantage of this technique.

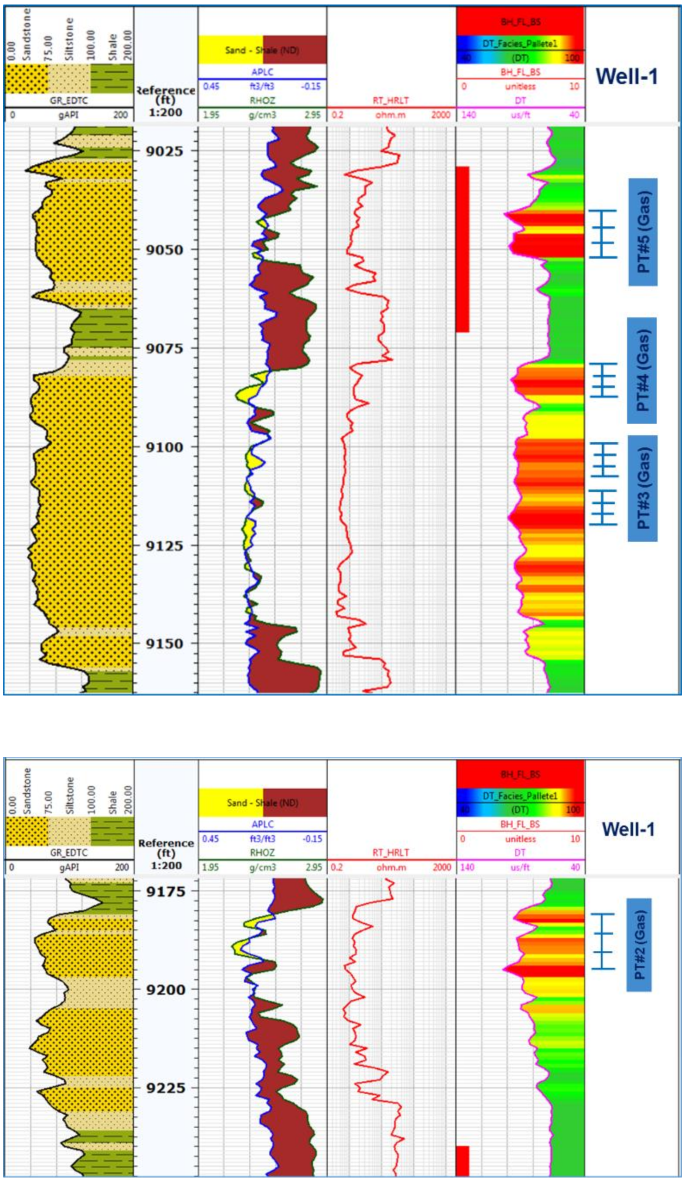

Fig. 5. **(A)** and **(B)** production test near the top part of Lower Acacus reservoir shows a good fit between gas intervals and DT_Facies_Palette.

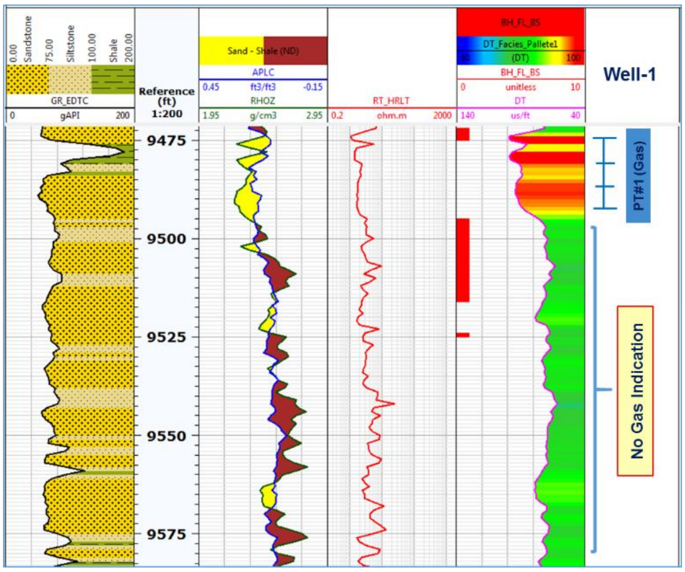

Fig. 6. Thick sandstone unit with gas accumulation at the top of the unit.

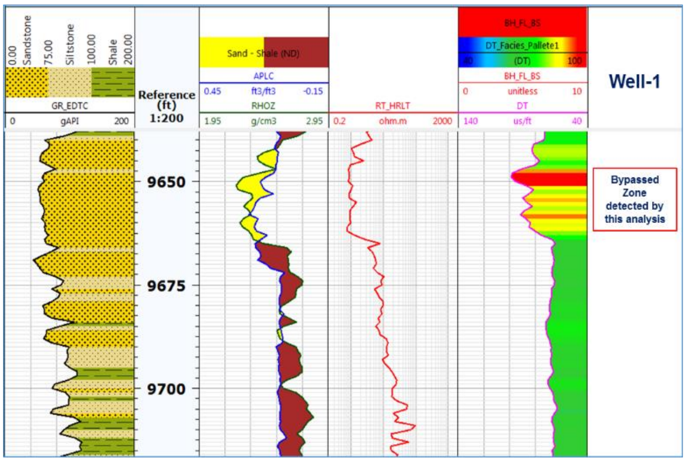

Fig. 7. A new zone was defined at the deeper part of Lower Acacus reservoir, which actually was not tested previously.

Well-2:

The well is aimed to appraise the discovery that was made by Well-1. Regarding the structural status of the well, the DT analysis shows that no gas zones could be defined in the reservoir intervals and the production tests confirm the DT evaluation on the well. Fig. 8 shows that water-producing intervals shall appear in different colors corresponding to values less than that of gas bearing formation.

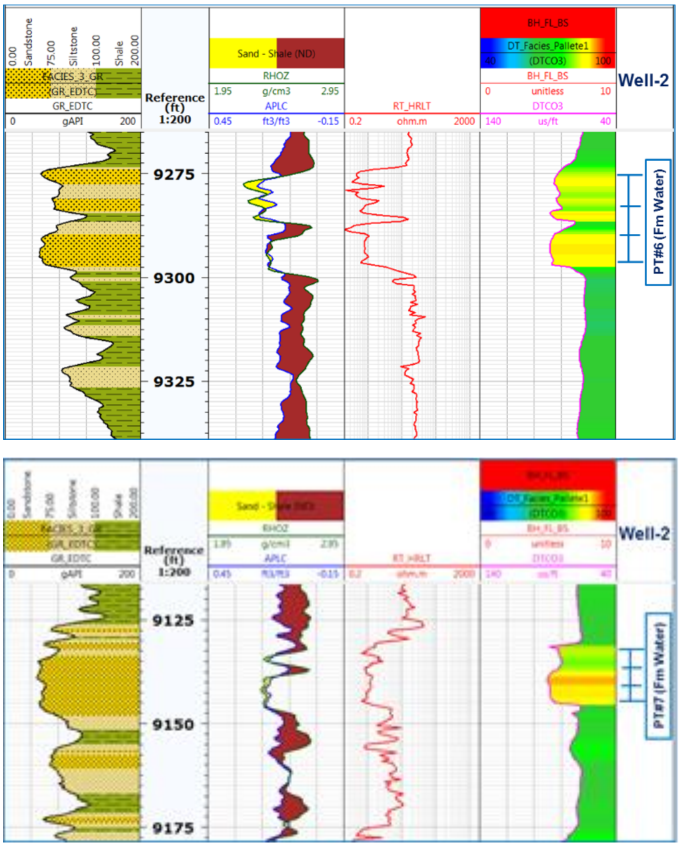

Fig. 8. (A) and (B) production test near the top part of Lower Accus reservoir shows a good fit between water intervals and DT_Facies_Pallete.

Well-3:

In order to confirm the gas presence in the area another well was drilled NE of Well-1 targeting the Lower Acacus shaley-sand reservoir. In a similar way of evaluation of Well-1, different reservoir intervals were recommended for production tests and only one test is contradictory to flowed gas. This gas interval is clearly defined by DT-Pallete analysis confirming the formation production test and delineating the gas-bearing interval (Fig. 9).

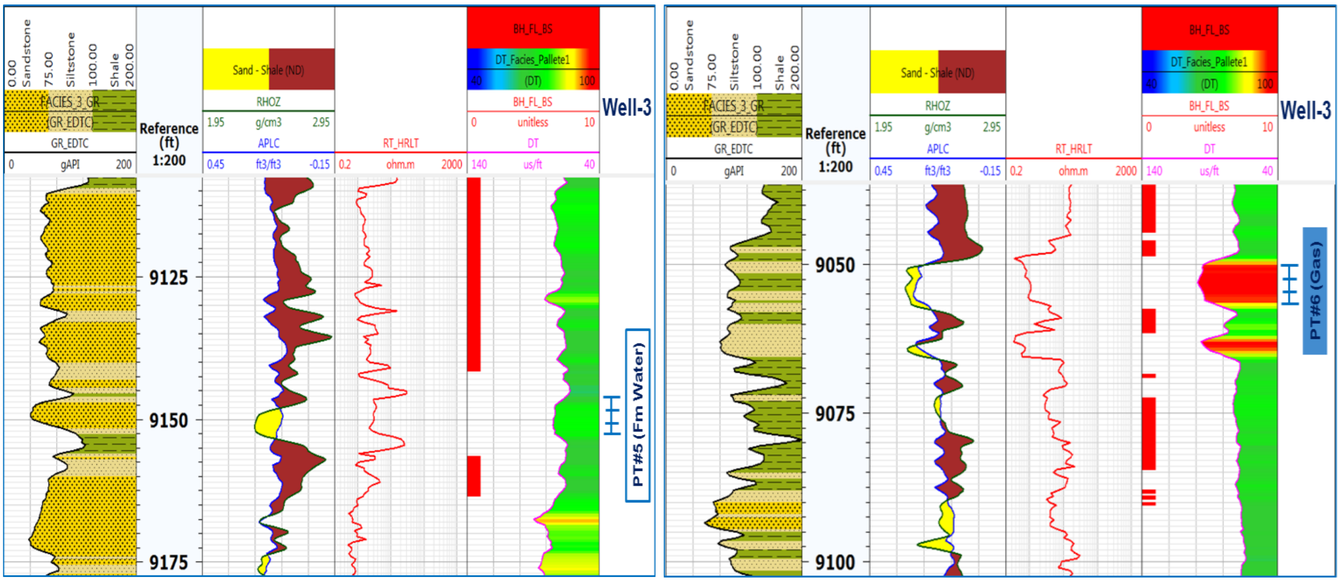

Fig. 9. (A) Production test near the top part of Lower Acacus reservoir shows a good fit between water interval in PT#5 and **(B)** Gas interval in PT#6 with DT_Facies_Palette.

4. Cross Section:

In order to better display the result of the studied well horizontally, a stratigraphic cross section was generated among the area of interest to the upper part of Lower Acacus reservoir in order see the reservoir lateral continuity as well as to simply observe the gas intervals (Fig. 10). Flattening the top of Lower Acacus reservoir, Well-1 comprise of the thickest sandstone intervals with lateral continuity in both directions. However, it is seen that neither density-neutron crossover nor resistivity log is a good indicator to the gas presence in Lower Acacus reservoir. On the other hand, sonic log supported by the DT-Pallete analysis is more reliable to detect gas intervals in the targeted reservoir.

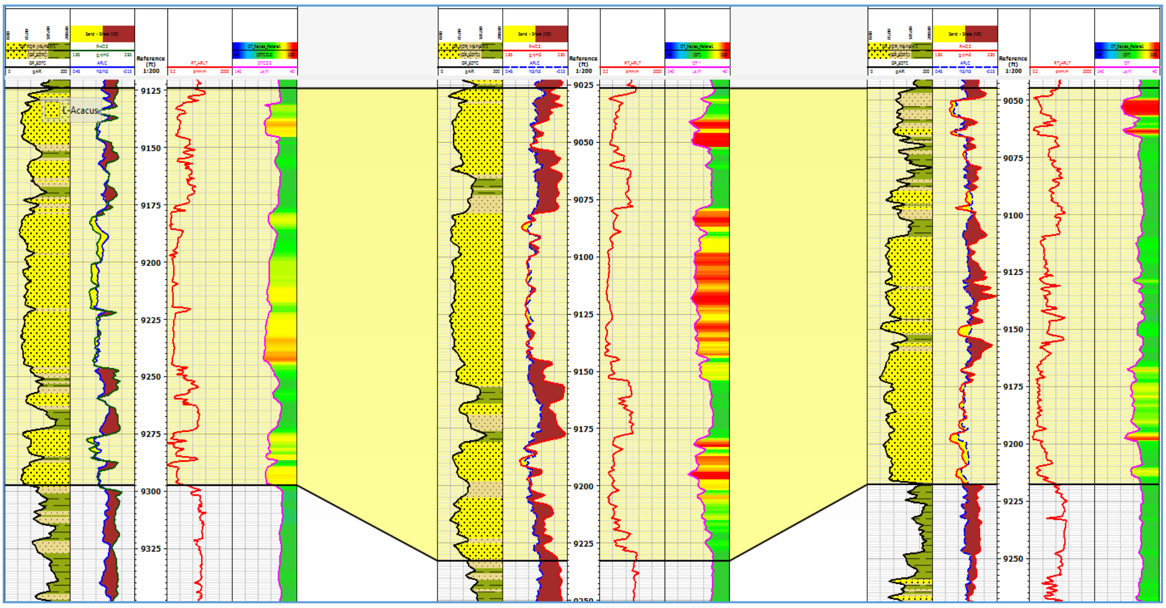

Fig. 10. Stratigraphic cross section of the upper part of Lower Acacus reservoir among the studied wells.

5. Conclusions

In the shaley-sand reservoir, neither density-neutron crossover, nor resistivity log is a good indicator of the gas bearing formation as in the case of Lower Acacus reservoir. On the contrary, Pallete-spectrum of the sonic log could be used to support other analysis (for example; gas measurement in the field, and/or petrophysical analysis) to delineate gas intervals in Lower Acacus reservoir. In DT-Palletegas zones appear red colored indicating a high concentration of gas molecules, while other sandstone units appear green showing no presence of gas in the sandstone reservoirs. Therefore, the DT values need to be calibrated in other fields to be set in the samerange of color. These calibrations allow DT-Pallete to be correctly displayed and acceptably indicate gas-bearing reservoir.

References:

Arabian Gulf Oil Company (2007) Intent To Drill (ITD) of Well1-NC7A, (AGOCO Internal Report).

Echikh, K. (1998) Geology and hydrocarbon occurrences in the Ghadames Basin, Algeria, Tunisia, and Libya, in Macgregor, D.S., Moody, R.T.J., and Clark-Lowes, D.D., eds., Petroleum geology of North Africa: Geological Society, London, Special Publication 132, pp. 109–129.

Hallett, Don, (2002) Petroleum geology of Libya: Amsterdam, Elsevier Inc., p. 503

Libyan Journal of Science & Technology 9:1 (2019) 26–30
The 2nd International Conference on Geosciences of Libya-GeoLibya 2 (2017), 14-16 October 2017, Benghazi-Libya

Faculty of Science - University of Benghazi
Libyan Journal of Science & Technology
journal home page: www.sc.uob.edu.ly/pages/page/77

Possible carbonate buildups in the Palaeocene sequence at the North-eastern margin of Ajdabia trough

Saad M. El-Shari

Department of Earth Sciences, Faculty of Science, University of Benghazi, Benghazi-Libya

E-mail address: smbelshari@yahoo.com

Highlights

- **The platform-basin relation-ship in a carbonate setting in the north-eastern shelf margin of Ajdabia Trough have been studied.**
- **The observed mounds in the seismic stratigraphic analysis of the Palaeocene sequence are interpreted as carbonate build-ups.**
- **Hydrocarbon reserves may be stored in the Palaeocene carbonate build-ups where potential seals over this platform would be expected because the section mainly consists of lime mudstone and shale.**

ARTICLE INFO

Article history:
Received 01 February 2018
Revised 20 March 2018
Accepted 28 March 2018
Available online 31 March 2019

Keywords:
Reef, carbonates Buildups, Carbonate platform, Palaeocene, Ajdabia Trough

ABSTRACT

Analysis of the seismic section from the eastern margin of Ajdabia Trough has resulted in a detailed study of carbonate buildups in the Palaeocene sequence. The main significant features identified in the seismic stratigraphic analysis are isolated mound features within the sequence in the northern shelf area. However, occasional discrete mounds of more diffuse seismic character have been seen in the extreme north-eastern part of the area, in an SW-NE trending feature. Large mounded structure of more than 200 ms thick and is composed of discontinuous, chaotic reflectors has been identified. Evidence for similar mound characters exists at the north-eastern part of the study area. The isolated mounds are draped and onlapped by later Palaeocene sediments.

The observed mounds in the Palaeocene sequence are interpreted as carbonate build-ups, which are usually mound-shaped biogenic deposits that display marginal onlapping reflections, whereas the overlying reflections drape the reefs, and the underlying reflections exhibit pull-down effect. This pattern may indicate growth of carbonate build up during the early Palaeocene time. From an exploration point of view, these features within the Palaeocene sequence probably contain the potential for stratigraphic hydrocarbon plays in the area.

1. Introduction

The results presented in this study are based mainly on the geological and geophysical investigation of the Paleocene sequence in north-eastern Ajdabia Trough and presents the approach used to explore possible carbonate build-ups in this sequence. The area of study is located at the hinge-zone between Cyrenaica Platform and Sirte Basin (Fig. 1). The main objective of this research is to identify and recognise occasional discrete mound features of more diffuse seismic character, seen within the Palaeocene sequence in the north-eastern shelf of Ajdabia Trough. These mound features may point to discrete organic carbonate build-ups.

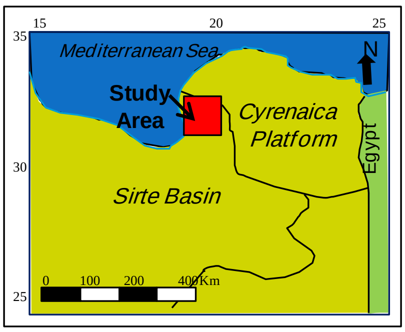

Fig. 1. Location map of the study area

Many studies have been published on the geology and geophysics of Sirte Basin, and Cyrenaica Platform. Berggren, (1974), studied and described the Tertiary rocks in the Sirte Basin and divided the sequence into a number of stratigraphic units. Subsidence and sedimentation rates have been analysed in the Sirte Basin to determine their relation to facies distribution Gumati & Kanes (1985) and Gumati & Narin (1991). El-Shari (2005) used the backstripping technique in the area to separate the subsidence of the sedimentary basin caused by sediment and water loading, from that caused by the tectonic driving force. The relationship between the stratigraphy and structural setting across the hinge-line in passive continental margins has been studied by El-Shari (2008). Elwerfalli & Stowe, (1998) through surface and subsurface petrographic investigations in NE-Libya, subdivide the lower Tertiary section into three main associations: slope facies association, shallow marine facies association and lagoonal facies association. In general, the Palaeocene facies distribution in the Sirte Basin and Cyrenica Platform has been described by Conley (1971), Brady *at el.* (1980), Bezan (1996), and Elshari (2017).

The availability of seismic and well data in this research provided the opportunity for the study of the platform-basin relationship in a carbonate setting, and testing occurrence of carbonates build-ups in the Palaeocene sequences. Seismic and well data from north-eastern margin of Ajdabia Trough enables seismic facies analysis, and interpretation Palaeocene depositional sequences in the area. Two and three-dimensions seismic reflection data tied to

 ISSN 2663-1407; National Library of Libya, Legal number: 390/2018

nineteen wells have been used. Generally, data quality decreases in faulted areas, and in the deeper sequences toward the southwest. Wire-line logs of sonic and gamma-ray types in a number of wells are used in this study.

3. Regional tectonic and depositional setting

During the late Cretaceous and Tertiary, the area of study was located on a broad carbonate platform that bordered the northern margin of the African continent (Del Ben & Finetti, 1991; Buxton & Pedley, 1989). During these times, there was a major marine transgression in the area coincident with the general eustatic high stand of sea-level (Pitman, 1978). This widespread marine transgression was associated with intense rift-related subsidence throughout the late Cretaceous in the western Cyrenaica. The first phase of extension and initial subsidence was followed by widespread thermally driven subsidence through the Tertiary period (El-Shari, 2005).

A widespread marine transgression, following basin subsidence, during the early Tertiary period. Carbonate depositional systems demonstrate distinctive patterns that often develop as a result of erosion and deposition in carbonate environments. Along horsts, carbonate banks and reefs under open marine conditions may be developed (Fig. 2). After this transgression, a shallow-marine environment was established across the area, and thick intervals of carbonate with a minor amount of siliciclastic and evaporite sediments were deposited on a carbonate ramp. During Palaeocene and Eocene time, normal faulting occurred, mainly as reactivation along a hinge-line between the Sirte Basin and Cyrenaica Platform (El-Shari, 2008). Generally, rapid thickening of the syn-rift section is noticed at the hinge-line. The post-rift sequence formed a relatively simple sedimentation model in which the section shows an overall thickening towards the southwest.

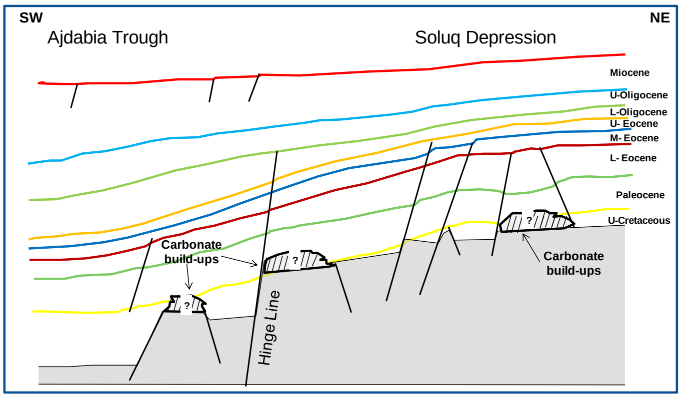

Fig. 2. SW-NE geo-seismic cross section showing the possible development of carbonate build-ups on structural blocks.

The carbonate platform on the north-eastern margin of the Ajdabia Trough contains a record of interactions between the factors that controlled carbonate platform deposition during the Palaeocene time. Development of this carbonate platform is an excellent example of interaction between regional effects and governed by thermal subsidence following extension (El-Shari, 2008). The shelf edge is the most sediment-starved part of the margin and given suitable climatic conditions, carbonate deposition can occur at rates equal to subsidence thus maintaining and building the platform. This carbonate is interbedded with shale in some places, indicating transgressive and regressive sedimentary cycles (Fig. 3). However, the Palaeocene carbonate facies are confined to the platform, while the deep open marine facies are restricted to the structural low areas. The most important structural features in the area were extensional normal faults, which occurred at the basin margin. Most faults are truncated by the end of the Middle Eocene time (Fig. 2).

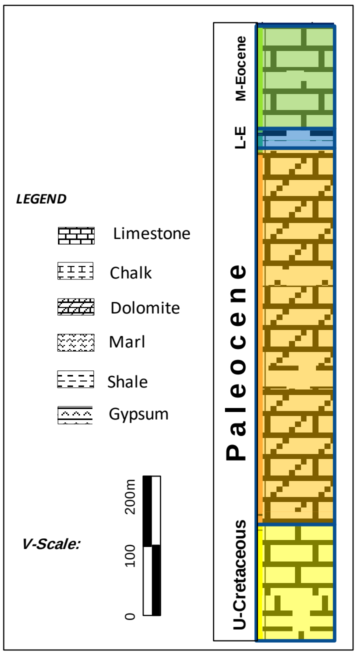

Fig. 3. Part of lithological log in well I1-41 summarised the lithology of the Palaeocene Sequence in the study area.

4. Rimmed Shelves vs Carbonate Ramps

Generally, the rimmed shelves are characterised by the development of reefs and carbonate bodies along the shelf margin, and the depths are shallow adjacent to the shelf-break, even subaerial if islands have formed (Fontaine *et al*., 1987). The shelf margin is characterised by a near-continuous rim of barrier reefs and/or skeletal-oolitic sand shoals. Increases in the basinward slope may occur tectonically, due to differential subsidence or extensional faulting, or it may occur as a result of differential sedimentation between the basin margin and the basin centre (El-Shari, 2008). However, a ramp may develop into a rimmed shelf through differential subsidence along a hinge-line. The carbonate ramp may evolve into rimmed shelves as a result of high carbonate production on the forming shelf edge or, through reef growth (Fig. 4).

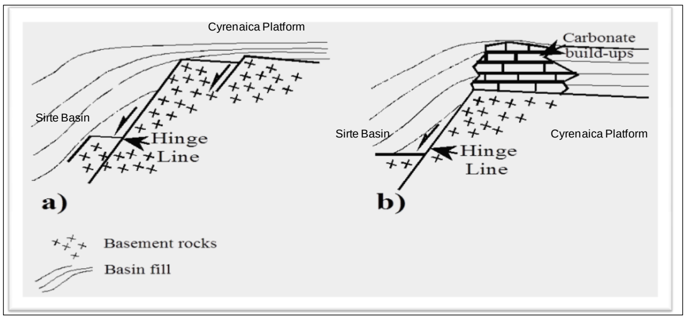

Fig. 4. Possible structures at carbonate margins across a hinge-line, a) open shelves, and b) rimmed shelves.

During highstand systems tract deposition, shallow-marine sedimentation rates are commonly greater than subsidence and the eustatic rise, thus leading to deposition of aggradational or progradational parasequence sets (Sarg, 1988; Tucker, 1991). These sediments include muddy and sandy shoreface deposits, platform-interior patch reefs and grainy shoals, shelf-edge reefs and shoals, and basin-margin and slope facies.

However, the shape of the northeastern margin of Ajdabia Trough, extending NW-SE, suggests a structural influence. The structures have played a very essential role in terms of controlling where deposition takes place (El-Shari, 2008). The earlier platform is faulted to form a series of horsts and grabens and has undergone rapid submergence, with carbonate upbuilding being localised on the highs, while the grabens become sites of deep-water sedimentation. Thus, this may give the possibility of development of carbonate bank or reef complexes above the hinge-line (Fig. 4).

5. Seismic Faceis Analysis

Many seismic sections, representing dip and strike profiles, are fully interpreted in this research. Two-way time structure map of the sequence shows a continuing dip of the horizon towards the southwest (Fig. 5). Major normal faults of the NW-SE trend and downthrown southwest have been interpreted on the top of the sequence.

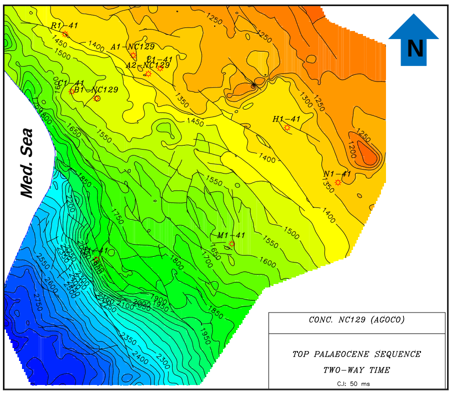

Fig. 5. Time structure contour maps of top Palaeocene sequence in the Northeastern part of Ajdabia Trough.

Based on the internal seismic reflection parameters such as the configuration, continuity, amplitude, interval velocity and external form of each seismic facies, the Palaeocene seismic sequences were interpreted. Seismic facies analysis were used to determine lithological and stratigraphic variations within the sequence, based on their position and lateral relationships to other seismic facies. The main significant features recognized in this seismic facies analysis are isolated mound features within the Palaeocene sequence in the north-eastern shelf area. The reefal construction is characterised seismically by a mound shape and onlap of surrounding reflections. Bubb and Hatlelid (1977) proposed definite criteria for recognising the buildups: the boundary outline, which includes the reflection configuration and onlap of overlying reflections, as well as seismic facies changes defining the buildup.

Generally, on the seismic section; the reefs topography can be identified by; mounded shapes; internally chaotic seismic facies; weak internal amplitude; draping of overlying sediments; onlapping of flanking reflection cycles; and pull-down phenomenon. However, complex sedimentary bodies such as carbonate mounds are characterized by a combination of geometric shapes from seismic reflections. It is generally an association of chaotic, subparallel and concave up features. According to these criteria and others, a number of mounds observed in the Palaeocene sequence are interpreted. Generally, the internal configuration within Palaeocene sequence is characterised by variable-amplitude and variable-continuity. On the platform, the Palaeocene seismic reflections are generally parallel or sub-parallel with variable amplitude and discontinuous reflection configuration (Fig. 6).

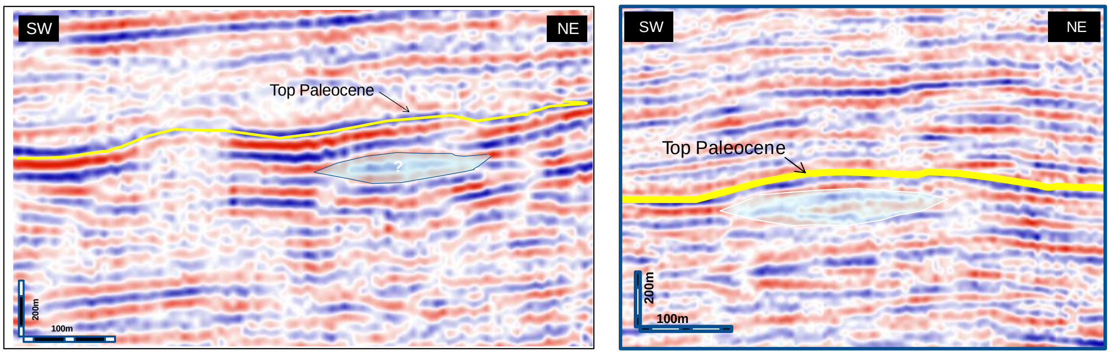

Fig. 6. Part of two seismic section, dip lines, clearly shows lateral seismic facies in the northern part of the area.

Furthermore, occasional discrete mounds of more diffuse seismic character have been identified in the extreme northeastern part of the area, in an SW-NE trending feature. Online NC129-89-56, a large mounded structure of about 600 m width is seen (Fig. 7). It is more than 200 ms thick and is composed of discontinuous, chaotic reflectors. Evidence for similar mound characters exists at the northeastern part of the study area. The isolated mounds are draped and onlapped by later Palaeocene sediments.

The observed mounds in the Palaeocene sequence are interpreted as carbonate buildups, which are usually mound-shaped biogenic deposits that display marginal onlapping reflections, whereas the overlying reflections drape the reefs, and the underlying reflections exhibit pull-down effect (Fig. 8). This pattern may indicate growth of carbonate buildup during the early Palaeocene time. Further evidence for such features already exists on the Amal Platform (the south-eastern margin of the Sirte Basin), where similar buildups have been interpreted within the Palaeocene section (Sola & Ozcicek, 1990).

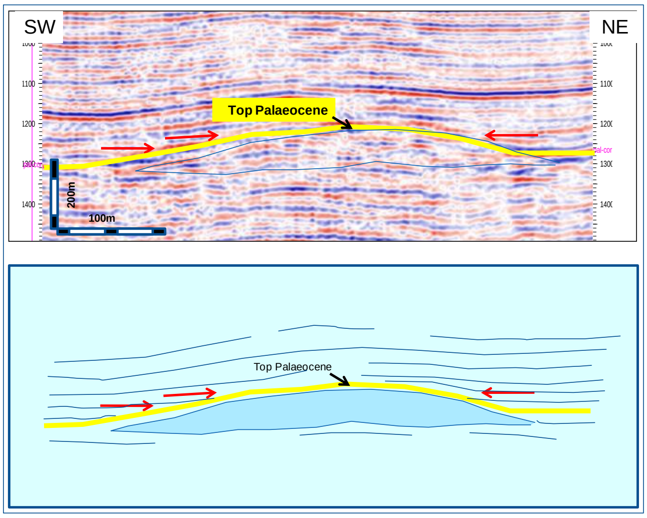

Fig. 7. Part of seismic line NC129-89 shows relatively large mound shape and onlap of surrounding reflections interpreted as reefal build-ups forming on a carbonate ramp during the early Palaeocene time.

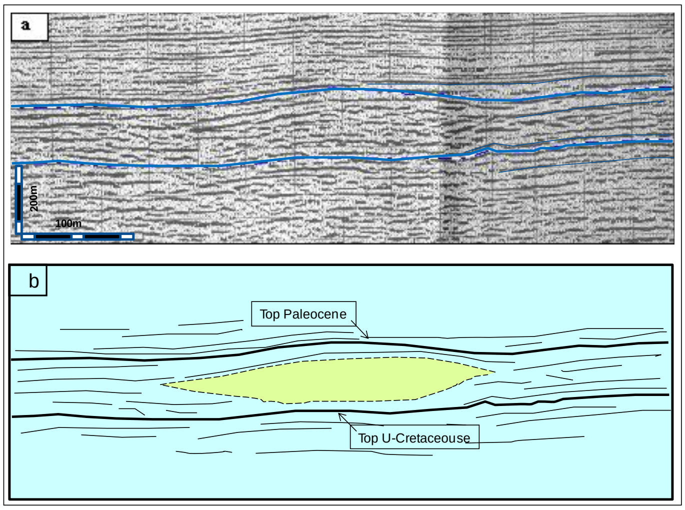

Fig. 8. Part of the seismic section in the study area shows a mound feature with clear internally chaotic seismic facies and pull-down effect.

6. Palaeocene Build-ups as Hydrocarbons Reservoir

In general, carbonate ramps form major reservoir zones with wide opportunities for stratigraphic and structural trapping and lateral variations in reservoir quality (Burchette & Wright, 1992). Organic build-ups in mid or outer-ramp locations commonly form ideal stratigraphic traps sealed by onlapping basinal facies or by down lapping mud-textured distal high stand sediments. In the Sirte Basin, the Palaeocene reservoirs have large amounts of hydrocarbon. In the eastern basin, the bioclastic coral-rich boundstones and grainstones of the Upper Sabil Formation form the main reservoir (Spring & Hansen, 1998). In addition, the Palaeocene rocks are composed of shoals and pinnacle reefs facies, and these are one of the major hydrocarbon reservoirs of the area (Brady *et al.,* 1980; Bezan, 1996).

However, in the last thirty years attempts to develop the hydrocarbon resources have been increased in this area. The existence of many sedimentary cycles with a corresponding source, reservoir, and seal rocks ranging in age from Upper Cretaceous to Miocene, suggest that exploration for hydrocarbons in this region could be potentially very successful. A better understanding of the stratigraphy in the north-eastern margin of Ajdabia Trouhg, may help to find out the prospective lithostratigraphic unit for hydrocarbon potential by identifying potential structural-stratigraphic traps (Fig. 9).

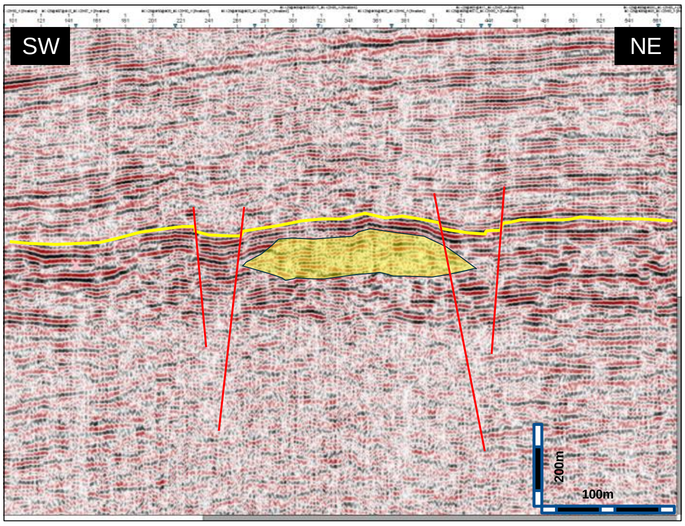

Fig. 9. Part of the the seismic section in the study areas shows possible combined hydrocarbon traps developed within the Palaeocene Sequence.

The main hydrocarbon reservoir in the northeastern Ajdabia Trough is the porous and permeable dolomitic rock unit of the Paleocene sequence. The reservoir properties are related to dolomitization processes. The cap rock for this reservoir in the area is the shales of the lower Shale sequence (Early Eocene). Furthermore, in the area, organic build-ups may form ideal stratigraphic traps sealed by onlapping basinal facies or by down lapping mud-textured distal highstand sediments. The overlying argillaceous Lower Eocene carbonate may provide a good seal facies.

7. Conclusions

In the north-eastern shelf margin of Ajdabia Trough, mound shape features have been identified within carbonate rocks within the Palaeocene sequence. These features interpreted as carbonate build-ups forming towards the basin margins on a carbonate ramp during the early Palaeocene time. They range in diameter between about 200 to 600 m and of more than 200 ms thick. However, these features had not been previously detected in the study area.

The common criteria observed on seismic sections on the development of carbonate build-ups in the Palaeocene Sequence are; marginal onlapping reflections, the overlying reflections drape the reefs, and the underlying reflections show a pull-down effect.

From an exploration point of view, hydrocarbon reserves may be stored in this carbonate build-ups. Potential seals over the drowned Palaeocene platform would be expected to be relatively good and really extensive because the section mainly consists of lime mudstone and shale.

8. Recommendations for Further Work

The main risk from this investigation; is the reservoir present or not? It means, is it reefal build-up? Or it is just a pop-up structure containing deep water non-reservoir facies. Furthermore, there are some uncertainties due to the lack of a consistent seismic response, as some of the mound features shows sub-parallel internal facies, which suggest off-reef facies. Therefore, ddetailed sedimentological work on the Palaeocene sequence sediments from existing core material, particularly in the north-eastern part of the area, would help to determine whether carbonate build-ups are present. In addition, a 3D-seismic survey in the area would lead to an increased understanding of the complex trap architectures and possibly result in new discoveries.

References:

Berggren, W. A. (1974) 'Palaeocene benthonic foraminiferal biostratigraphy, biogeography and palaeoecology of Libya and Mali', Micropalaeontology, 20, p. 449-465.

Bezan, A. M. (1996) The Palaeocene Sequence in the Sirte Basin; *In*: M. J. Salem, A. J. Mouzughi and O. S. Hammuda (*eds*.), Geology of the Sirte Basin, 1, pp.97-119.

Brady, T. J., Campbell, N. D. J and Maher, C. E. (1980) Intisar "D" oil field, Libya. *In*: M. Halbouty (*ed*.), Giant oil and gas fields of the decade, 1968-1978, *AAPG Memoir* 30, pp. 543-564.

Bubb, J. N. and Hatlelid W. G. (1977) Seismic stratigraphy and global changes of sea level, part 10: Seismic recognition of carbonate buildups, *In:* C. E. Payton (*ed*.), Seismic stratigraphy-Application to hydrocarbon exploration, *AAPG Memoir* 26, pp. 185-204.

Burchette, T. P. and Wrigh, V. P. (1992) 'Carbonate ramp depositional systems', *Sedimentary Geology*, 79, pp. 3-57.

Buxton, M. W. N. and Pedley, H. M. (1989) 'A standardised model for Tethyan Tertiary carbonate ramps', *Journal of the Geological Society, London*, 146, pp. 746-748.

Conley, L. D. (1971) Stratigraphy and lithofacies of the Lower Palaeocene rocks, Sirte Basin. *In*: M. J. Salem and M. T. Busrewil, (*eds*.) The Geology of Libya, Academic Press, 1, pp.127-140.

Del Ben, A. and Finetti, I. (1991) Geophysical study of the Sirte Rise, *In*: M. J. Salem, A. M. Sbeta and M. R. Bakbak (*eds*.), The Geology of Libya, Elsevier, Amsterdam, 6, pp. 2417-2432.

El-Shari, S. (2005) Subsidence Analysis at the Western Margin of Cyrenaica Platform, NE-Libya; 2nd North African/Mediterranean Petroleum and Geosciences Conference & Exhibition, Algeria.

El-Shari, S. (2008) 'Stratigraphic effects and tectonic implications at hinge-zone area between Sirte Basin and Cyrenaica Platform, NE Libya'; *Third Symposium on Sedimentary Basins of Libya- Geology of East Libya*, IV, pp. 269-281.

El-Shari, S. (2017) Seismic and Sequence Stratigraphy of the Palaeocene Carbonates at the Western Margin of Cyrenaica Platform, NE-Libya" Libyan Journal of Science & Technology 6:1, pp. 25-29.

Elwerfalli, H. O. and Stow, D. A. V. (1998). Early Tertiary carbonates in NE Libya; surface and subsurface facies analysis. (Abstracts), The First Earth Science Conference

Finetti, I. (1985) Structure and evolution of the central Mediterranean (Pelagian and Ionian Seas), *In:* D. J. Stanley and Forese-Carlo Wezel., (*eds.*), Geological evolution of the Mediterranean basins, Springer-Verlag, p.215-230.

Fontaine, J. M., Cussey, R., Lacaze, J., Lanaud, R. and Yapaudjian, L. (1987) 'Seismic interpretation of carbonate depositional environments', *AAPG. Bull*., 71, pp. 281-297.

Gumati, Y. D. and Kanes, W. H. (1985) Early Tertiary subsidence and sedimentary facies-northern Sirte Basin, Libya. *AAPG. Bull*, 69, pp. 39-52.

Gumati, Y. D. and Nairn, A. E. M. (1991) 'Tectonic subsidence of the Sirte basin, Libya', *Journ. petrol. Geol.*, 14, pp.93-102.

Pitman, W. C. (1978) 'Relationship between eustasy and sequence stratigraphy of passive margins', *GSA Bull*., 89, pp. 1389-1403.

Sarg, J. F. (1988) Carbonate sequence stratigraphy, *In:* C. K. Wilgus, B. C. Hastings, Kendall C. G. St. C., H. W. Posamentier, C. Ross and J. C. Van Wagoner (*eds.*), Sea-level changes: An integrated approach, SEPM. Special Publ., 42, pp. 156-181.

Spring, D. and Hansen, O. P. (1998) The influence of platform morphology and sea level on the development of a carbonate sequence: *In*: D. S. Maggrgor, R. T. J. Moody and D. D. Clark-Lowes (*eds.*), Petroleum Geology of North Africa, Geological Society, London, Special Publ. No. 132, pp. 317-334.

Sola, M. and Ozcick, B. (1990) 'On the hydrocarbon prospectivity of the north Cyrenaica region, Libya', *PRJ*, 2, pp. 25-41.

Tucker, M. E. (1991) Sedimentary Petrography: an Introduction to the Origin of Sedimentary Rocks, Blackwell Scientific Publ., Oxford, 260p.

Libyan Journal of Science & Technology 9:1 (2019) 31–37
The 2nd International Conference on Geosciences of Libya-GeoLibya 2 (2017), 14-16 October 2017, Benghazi-Libya

Faculty of Science - University of Benghazi
Libyan Journal of Science & Technology
journal home page: www.sc.uob.edu.ly/pages/page/77

Classification of hydrocarbons trapping systems of the Ghadames and Murzuq Basins in relation to Gargaf high, West Libya.

Al Fasatwi Yahya Ahmed.

Libyan Academy, Tripoli, Libya,

E-mail address: Alfasatwi@yahoo.com

Highlights

- **This paper provides comprehensive synthesis of the hydrocarbon trapping systems of the Ghadames and Murzuq Basins, Western Libya.**
- **The influence of the intervening Gargaf Arch on the trapping systems of the Ghadames and Murzuq basins has also been investigated in this paper.**
- **The paper provide an idea on the influence of the combination of tectonic, sedimentation, oil migration on forming trends of hydrocarbon accumulations in the Ghadames and Murzuq Basins. The resulted maps can be used for hydrocarbon exploration in the two basins.**

ARTICLE INFO

Article history:
Received 01 February 2018
Revised 22 March 2018
Accepted 29 March 2018
Available online 31 March 2019

Keywords:
Gargaf high, Ghadames, Murzuq, hydrocarbons, trapping systems, basin

ABSTRACT

The Ghadames and Murzuq Basins, West Libya, are major producers of hydrocarbons in Libya. The producing-bearing horizons of the two basins range in age from Cambro-Ordovician to Triassic. Reservoirs of Devonian and Silurian age are major producing horizons in the Ghadames Basin. In the Murzuq Basin, the main reservoirs are Cambro-Ordovician in age. The Silurian Tanezzuft shales are the main source rock of the hydrocarbons in the Ghadames and Murzuq Basins. The reservoir characteristics indicate that the hydrocarbons of the Ghadames basin have mainly accumulated mainly in combination and stratigraphic traps in areas close to Gargaf high, and in structural anticline traps in areas close to the centre of the basin. In the Murzuq Basin, hydrocarbons are trapped mainly in structural faulted traps.

The distribution of oil fields in the Ghadames and Murzuq Basins appears to be confined to a regional trend, which reflects the close relationship between tectonics, sedimentation, oil migration and accumulation.

1. Introduction

Recent oil discoveries within the Ghadames and Murzuq Basins indicate the necessity for a renewed examination of the tectonic and stratigraphical framework of both basins. This study provides an analysis of the hydrocarbon systems of the Ghadames and Murzuq Basins (Fig. 1). More than 150 exploratory wells have been drilled in these basins, resulting in the discovery of some 50 oil pools in the Ghadames Basin and some 20 in the Murzuq Basin. Fig. 1 illustrates the distribution of major known hydrocarbon resources across the region. Most of the hydrocarbon exploration carried out in the Ghadames and Murzuq Basins have been within their major depocentres. The primary objectives of this study are to compile a reliable data set of oil and gas fields in the Ghadames and Murzuq Basins and to develop criteria for subdividing these areas into zones or trends. It is believed that recognition of such processes is essential for a better understanding of the tectonic and stratigraphical framework of the region, and it is hoped that this regional approach will help to gain an insight in:

1. *Facies development (source rocks, reservoir rocks, cap rocks, etc.),*
2. *Structural development (migration, traps, etc.),*
3. *Establishing a tentative correlation between regional structural patterns and hydrocarbon accumulations.*
4. *Predicting possible hydrocarbon trends.*
5. *Comparing the Murzuq and Ghadames Basins.*

This understanding will be transferred to less explored and currently unproductive areas within the region, in an attempt to highlight areas and fairways of remaining exploration potential.

Hydrocarbons in the Ghadames and Murzuq Basin have been produced from several Paleozoic sandstone pay-zones (Fig. 2). The source rock is mainly Silurian shales of the Tanezzuft Formation, supplemented by Devonian and Cambro-Ordovician shales. The main producing horizons in the Ghadames Basin are the Silurian Acacus Formation in the northern and central parts of the basin and the Devonian Tadrart Formation in the southern and central parts of the basin. Other intervals with minor production are found in several parts of the basin. In the Murzuq Basin, the Ordovician Memouniat Formation is the main producing horizon; other Devonian formations are also producing. Structural traps are the most common types of trap in the Murzuq Basin; traps in the Ghadames Basin range from combination traps in the southern and northern parts of the basin (close to the rims of the basin) to structural traps in the central part of the basin. Minor discoveries are found in stratigraphical traps in the western part of the basin. All discovered oils are naphthenic crude.

2. Comparison of the hydrocarbon systems in the Ghadames and Murzuq Basins

2. 1 Introduction

Stratigraphy and hydrocarbon occurrence relationships within the Ghadames and Murzuq Basins are summarized in Fig. 2. Comparison of the hydrocarbon systems in the two basins indicates that there are some points of similarity and also some differences.

 ISSN 2663-1407; National Library of Libya, Legal number: 390/2018

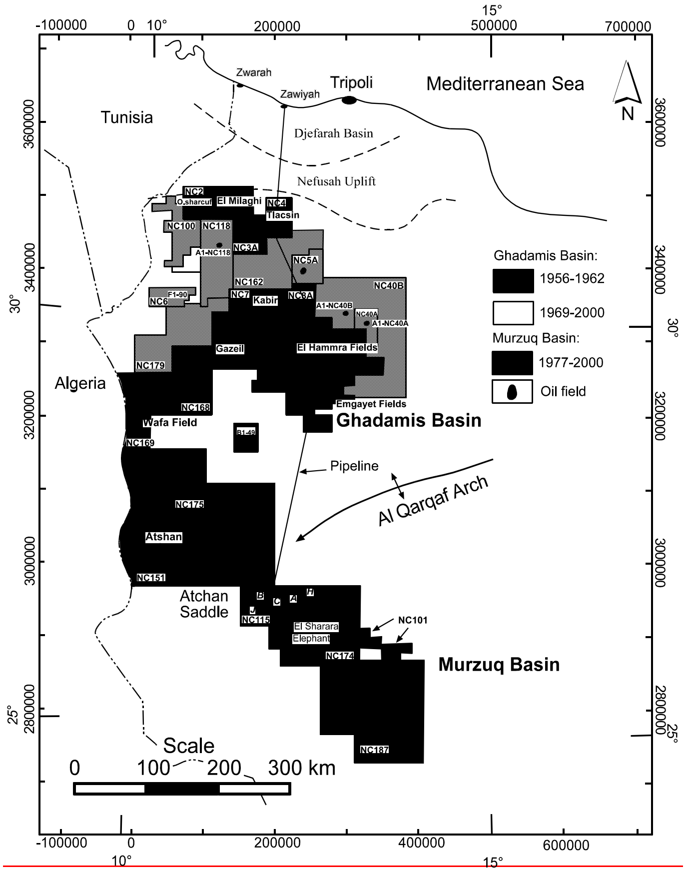

Fig. 1. Index map of the study area showing concessions, names and locations of main hydrocarbon-producing fields in the Ghadames and Murzuq Basins.

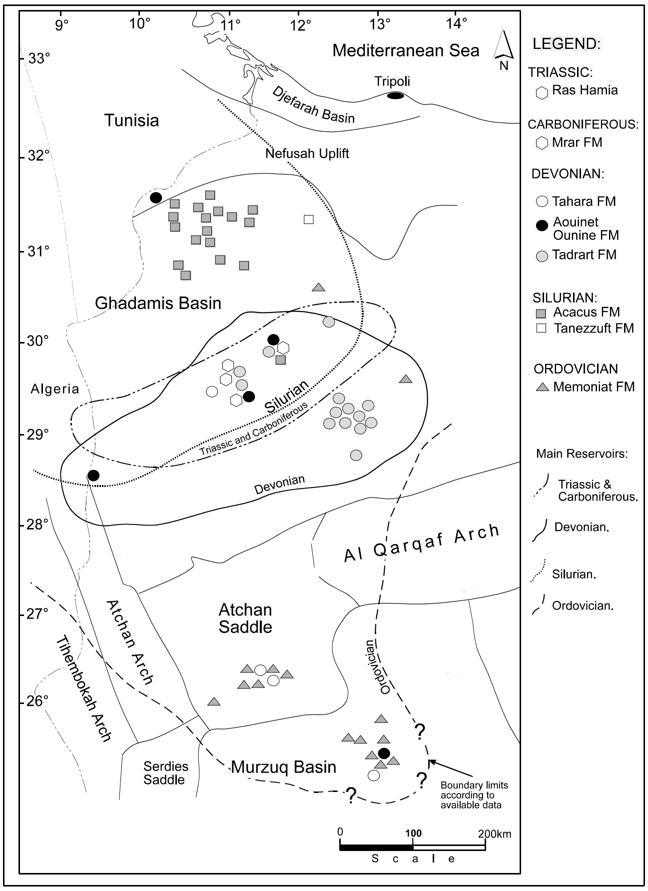

Fig. 2. Map showing regional distribution of reservoirs in the Ghadames and Murzuq Basins.

2. 2. Distributions of reservoirs in the Ghadames and Murzuq Basins

2.2.1 Spatial and stratigraphical distribution:

Fig. 2 presents the regional distribution of the reservoirs in the Ghadames and Murzuq Basins. In the north part of the Libyan part of the Ghadames Basin, the Upper Silurian Acacus Formation is the most productive horizon, and in the southeast of the basin the Lower Devonian Tadrart Formation. In the central part of the basin, there is a combination of different reservoirs, ranging from the Acacus Formation to the Lower Carboniferous Mrar Formation. The reason for this, according to Alvares (1956), is apparently to be sought in the source-cap relationship. The middle Acacus shale units have apparently acted as a cap, confining oil generated in the Tanezzuft shale to Lower Acacus sands, and preventing it from reaching the reservoirs of the Upper Acacus/Tadrart. As the Middle Acacus shale dies out to the southeast, the lack of barriers permits Tanezzuft oil to reach the Tadrart reservoirs.In the Murzuq Basin, the Cambro-Ordovician Memouniat Formation is the most important producing horizon. Two clusters of reservoirs are producing in the basin, the first one located in the central part of the basin, and the other one located in the area of the Atchan Saddle.

2.2.2 Depth distribution

Fig. 3 shows N-S cross sections with the reservoirs in the area. Most of the discovered hydrocarbon fields in the Ghadames and Murzuq Basins are almost similar in depth, ranging from 600 to 2200 m in both basins. The correlation with the depth to the top of basement map indicates that the discovered hydrocarbon fields are located in areas where the depth of the basement ranges from 1220 to 2740 m subsea in the Ghadames Basin and from 610 to 2440 m subsea in the Murzuq Basin.

2.2.3 Field size distribution

Fig. 4 represents the distribution of trap types and the initial recoverable reserves. The fields of the two basins have been subdivided into four groups, with less than 50, 50 to 100, 100 to 150, and more than 150×10^{6} barrels of initial recoverable reserves. In the north and central Ghadames Basin, the discovered hydrocarbon fields range in size between 50 and 100 MMBO. In the northern part of the Ghadames Basin, the traps are mainly a combination of structural and stratigraphical traps. The size of the fields increases to the south, where fields reach more than 150 MMBO close to Al Qarqaf Arch. Most of the traps in the south are combination traps. Mixed types of traps also characterize the central part of the Ghadames Basin. All the traps of the Murzuq Basin are structural, with two groups of reservoirs. The first is located in the area of the Atchan Saddle and is characterized by fields that have recoverable reserves of between 50 and more than 150 MMBO. The other group is located in the northeastern part of the Murzuq Basin and is characterized by fields of smaller size, generally less than 100 MMBO.

2.2.4 Play type distribution (classification of traps)

Analysis of well and seismic data over the Ghadames and Murzuq Basins indicates the existence of a wide variety of structural and stratigraphical trap types of different age. Three main classes of traps have been identified in the area (Figs. 4 and 5). In the Ghadames Basin, we indeed find structural traps in the centre of the basin and combination to stratigraphical traps towards the flanks. Most of the productive structures in the Ghadames Basin have an SW-NE orientation, especially in the southern parts of the basin where the influence of Al Qarqaf Arch is strong. In the Ghadames Basin, all Acacus Formation oil has been found in structural traps. Trap development in the Ghadames Basin has been assumed to be related to tectonism in the latter part of the Silurian (Caledonian) and in the Carboniferous and Permian (Hercynian). In the case of the Murzuq Basin, the story is different because all of the traps identified are structural and most of the faults trend NW-SE (almost perpendicular to the direction of Al Qarqaf Arch).

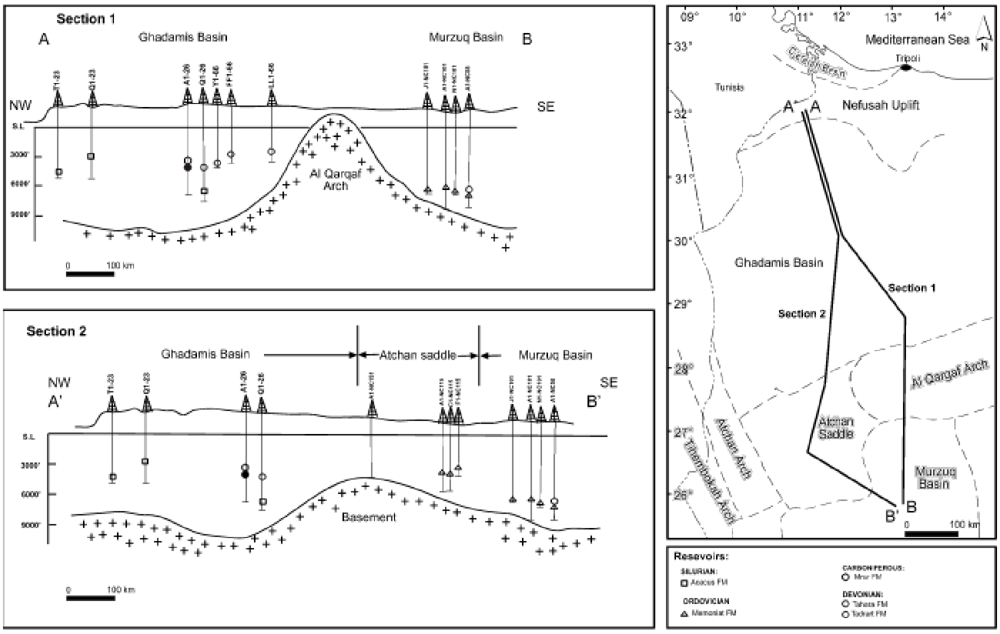

Fig. 3. Cross sections showing the depths of reservoirs in the Ghadames and Murzuq Basins.

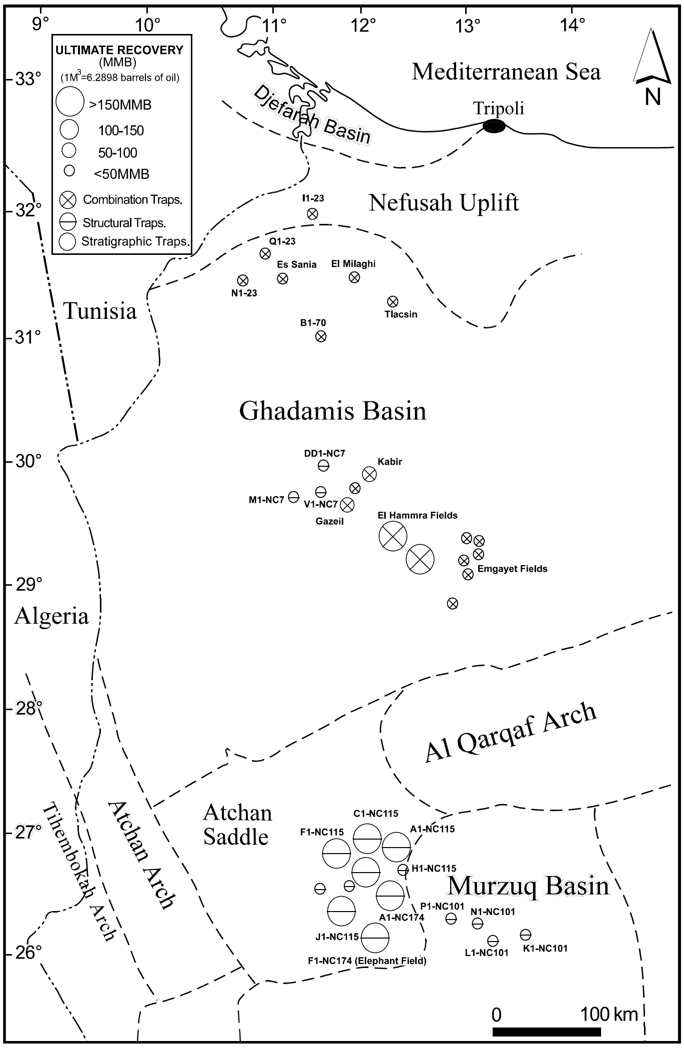

Fig. 4. Trap styles and ultimate oil recovery of hydrocarbon occurrences in the Ghadames and Murzuq Basins.

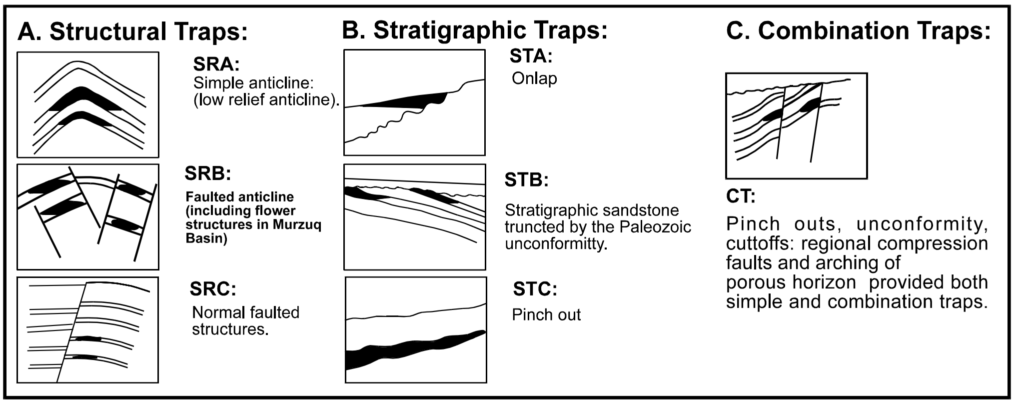

Fig. 5. Types of traps in the Ghadames and Murzuq Basins.

A. Structural traps

Most of the large hydrocarbon accumulations discovered in the Ghadames and Murzuq Basins occur in structural traps. In the Murzuq Basin, most structural traps of the Murzuq Basin were probably formed before or coincident with the first phase of oil generation in the Late Paleozoic. Fig. 7 shows a TWT structural map (Middle Devonian Unconformity) showing N-S en-échelon fault blocks. The fault system is part of the 10° wrench fault. The seismic windows A and B of Fig. 7 show flower structures associated with the wrench fault. The figure shows that the oil in the area of the Elephant oil field is trapped in a reverse faulted anticline over basement uplift. The structural history of the area of both basins has produced a wide variety of structural traps of different ages.

A.1 Simple low relief anticline (SRA)

This trap type is present mainly in central and northern parts of the Ghadames Basin (Figs. 6 and 7). These anticlines are generally broad low-relief structures and were formed during the Silurian and Devonian (Echikh, 1998).

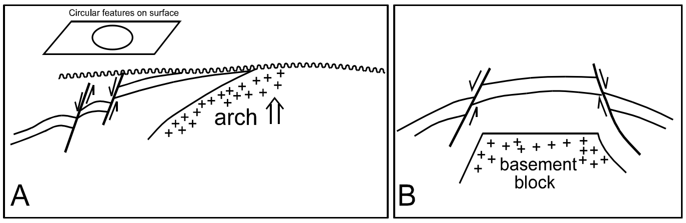

Fig. 6. Schematic sections illustrating the mechanism of faulted anticlines and normal faulted structures associated with arch structures and basement blocks.

A.2 Faulted anticline (SRB)

This type of faulting corresponds to the model of traps associated with the near surface arch. In this form of trap, entrapment was achieved by the faulting of anticlines (Fig. 5). This type of structure is found in the southern part of the Ghadames Basin, close to Al Qarqaf Arch. In this area, the beds have a regional NNW dip and are arranged in large tilted fault blocks, bounded to the south by major ENE trending faults, which are downthrown to the south. Oil and gas have accumulated in anticlines on the footwall side of the faults, the accumulations being locally sealed by these faults.

These fields are made up of several pools, some of which are divided into "sub-pools" separated by saddles or faults. In many cases. The faulted anticlines appear on the surface as circular and semi-circular features, which are interpreted from remote sensing images and are located in the southern part of the Ghadames Basin. It is likely that these semi-circular features are a result of the subsurface tectonics and are thus of practical interest in hydrocarbon prospecting. Two types of circular features appear from the interpretation of remote sensing images. They are located in the southern part of the basin and range from 5 to 35 km in diameter. These features coincide with the location of El Hammra and Emgayet oil fields and are located on the aeromagnetic map in an area of high magnetic anomalies.

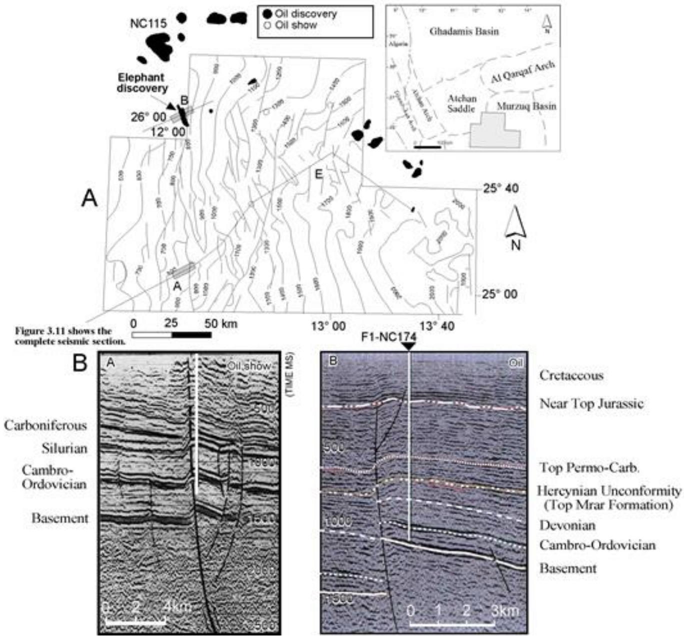

Fig. 7. A) TWT structural map (Middle Devonian unconformity), C.I.20 msec, showing N-S en-échelon fault blocks. The fault system is part of the 10° wrench zone. B) Seismic windows, the seismic sections showing flower structure in concession NC58 (window A) and reverse faulted anticline formed over a basement uplift (window B). Well F1-NC174 is a well in the giant Elephant field, while the other well is a dry hole in a smaller but well-defined closure to the south.

A.3 Normal faulted structures (SRC)

This type of trap is mainly related to the faulting of layers due to basement uplifting. In the Ghadames Basin, this type was formed during the Hercynian events. To date, available data indicate the presence of this type in the central and northern parts of the Ghadames Basin (Fig. 6). This type is mostly expected in flanks of Al Qarqaf Arch.

B. Stratigraphical traps

The traps formed by a lateral change in the reservoir. Two types of stratigraphical traps have been observed, namely:

B.1 Stratigraphical truncation on unconformity (STB)

This type consists of sandstone reservoirs that are truncated by the Paleozoic unconformity. It is present in the central and northwestern parts of the Ghadames Basin. According to Echikh (1998), in this type, hydrocarbons are trapped against the subcrop of the Silurian Acacus reservoirs against Triassic shales.

B.2 Permeability pinchout traps (STC)

In the Ghadames Basin, this type of trap is present in the western part of the basin, close to the Tihembokah Arch (Fig. 5). The sandstone bodies of the Aouinet Ouenine Formation are considered as the main target in this area, where they pinch out into shale. The extensive shale layers within the formation provide the seals. No information has been released on the reservoir characteristics.

C. Combination traps (structural-stratigraphical traps)(CT)

This is a combination of any two or more of the above. This type of trapping includes pinchouts, unconformity, fault-bounded closures, regional compressional faults and arching.

2.2.5 Seals:

In the Ghadames and Murzuq Basins, stratigraphical units possessing seal rock properties are like the reservoir rock and source rocks to be found at various levels within the Paleozoic succession. The Early to Late Silurian (Ludlovian) Tanezzuft shales are the regional seal deposited across the Murzuq Basin. Fig. 8 shows the model of the relationship between source rock, reservoir rock and sealing in the central and southern parts of the Ghadames Basin. Some layers of the Acacus Formation serve as a good seal for the hydrocarbons of the formation in the central and northern parts of the Ghadames Basin. The Tadrart reservoirs in the Ghadames Basin have as their top seal the shales that occur at the base of the overlying Early Devonian Ouan Kasa Formation. The extensive shales of the Early Carboniferous Mrar Formation provide seals for the Tahara reservoir.

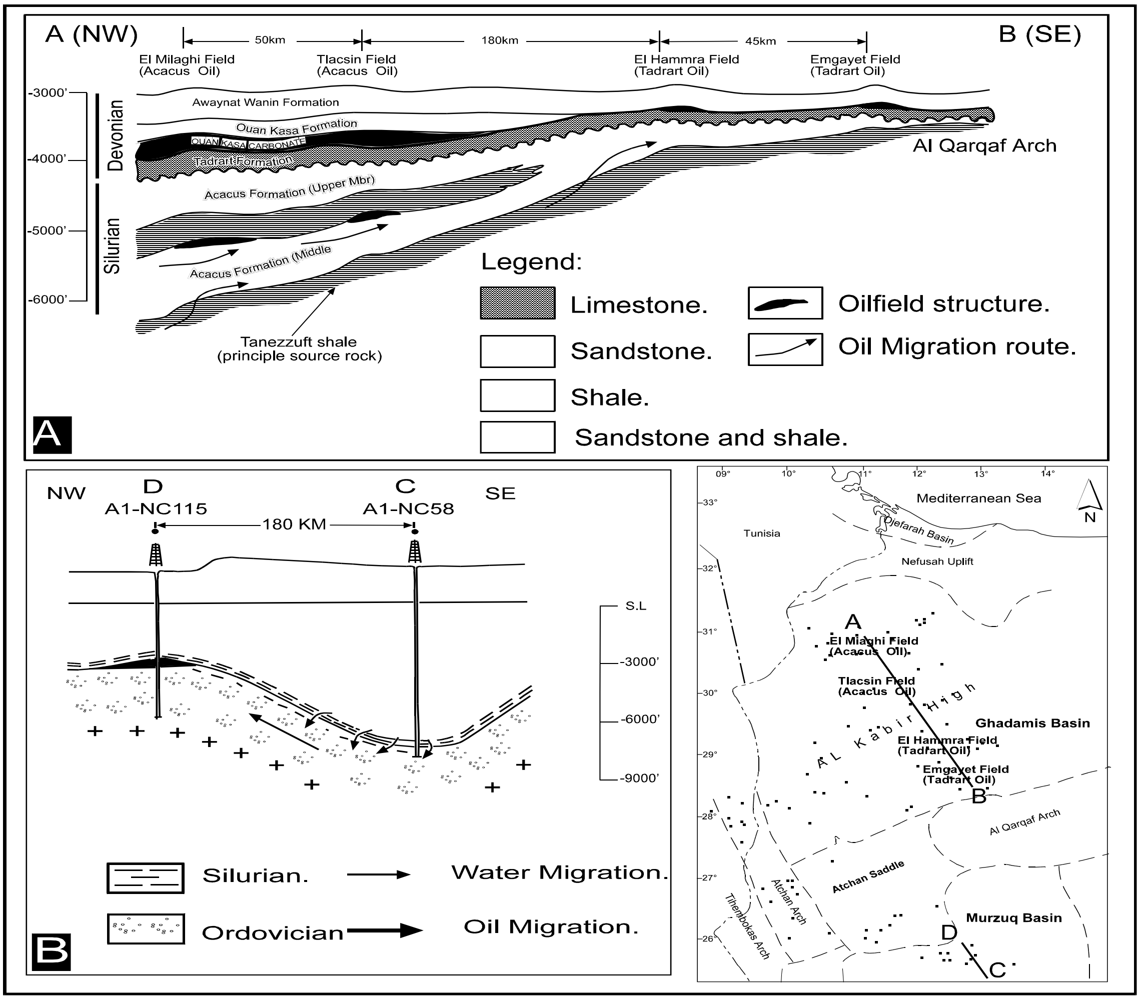

Fig. 8. Schematic cross sections showing hydrocarbon migration routes and trapping in (A) the Ghadames Basin (after Alvares, 1956) and (B) the Murzuq Basin (after Meister *et al.*, 1991).

2.2.6 Hydrocarbon generation, migration and trapping

The generation and expulsion of hydrocarbons of varying thermal maturation can be explained with reference to a source rock's thermal history (Fig. 8). Burial history curves of three wells in the Murzuq Basin show important geological horizons and key Time-Temperature Index (TTI) lines. These curves were used to estimate theoretical maturity and to determine the likely time of hydrocarbon generation. The Time-Temperature Index has been computed using Lopatin's method (Waples, 1980). This method is applied to three wells in the Murzuq Basin. The calculations and graphics indicate that the base of the Silurian sediments reached a Time Temperature Index of 15 at respectively 50, 107 and 112 million years before present for wells A, B and C. This means that Silurian rocks would have attained sufficient thermal maturity to start generating oil only since Cretaceous to Early Tertiary times. Peak generation was probably in Late Mesozoic (Early Cretaceous) time. Generation in source rock units younger than the Silurian was somewhat later. The Devonian may not have produced hydrocarbon until Cretaceous time. In general, traps older than Jurassic would be expected to be most favourable for oil accumulation (Massa *et al.*, 1994). Migration distance for the discovered fields in the Murzuq Basin, according to Meister *et al.* (1981), must have been in the order of 150 to 200 km. It is generally assumed that lateral migration played an important role since much of the shale underneath the producing areas is insufficiently mature to have provided hydrocarbon to the overlying reservoir zones.

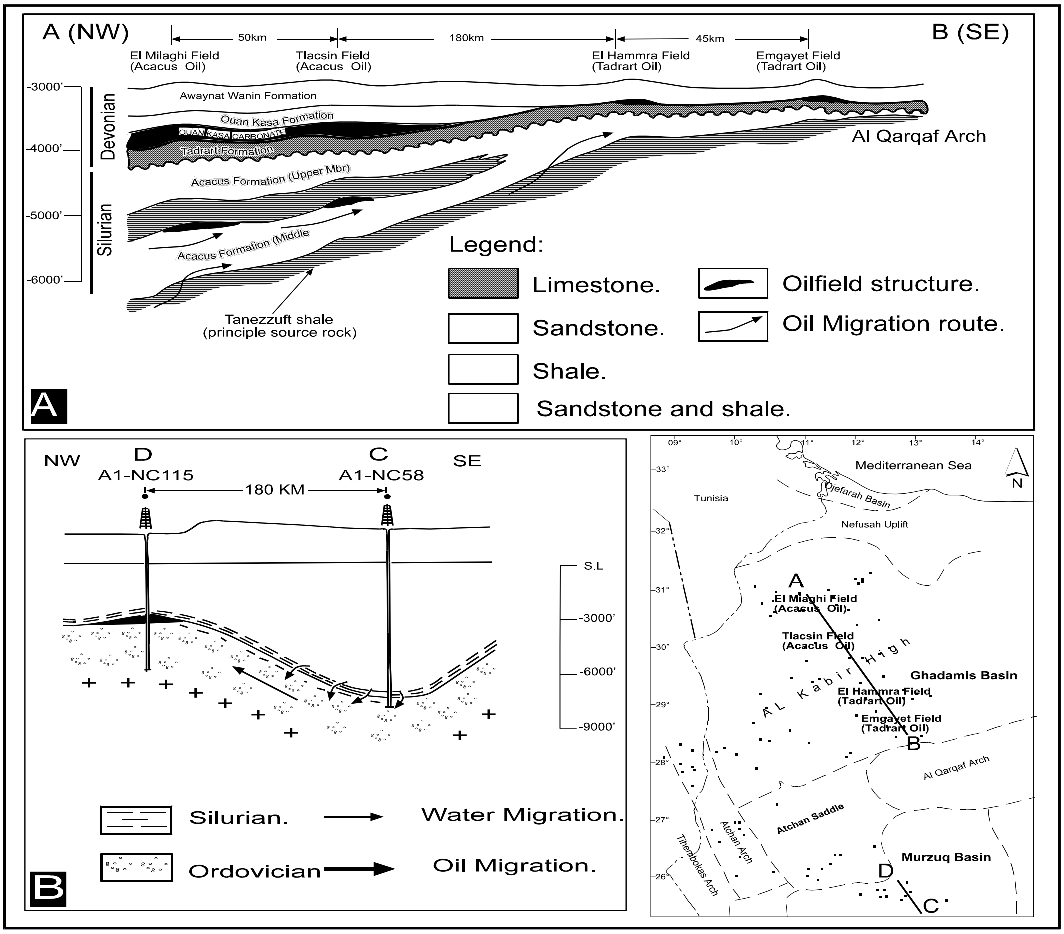

Fig. 8. Schematic cross sections showing hydrocarbon migration routes and trapping in (A) the Ghadames Basin (after Alvares, 1956) and (B) the Murzuq Basin (after Meister *et al.*, 1991).

3. Future trends:

Hydrocarbon prospectivity increases towards the basin margins, where traps tend to be structural and structural/stratigraphical. The structures tend to be low-amplitude anticlinal closures, and hydrocarbon columns are small. Most stratigraphical traps found so far are associated with the regional Hercynian Unconformity, which facilitates the overstep of dipping Paleozoic reservoirs by basal Mesozoic seals.

In the Murzuq Basin, the Late Ordovician Memouniat Formation is the primary prospective horizon. The Murzuq Basin is bounded by two major wrench zones. This type of faulting will produce flower structures, which are potential traps.

The hydrocarbons of the recently discovered giant Elephant oil field are trapped in a reverse faulted anticline formed over a basement uplift of compressional origin, with dip closure to the north, east and south. The structure resulted from several pulses of uplifts (Compton *et al.*, 1999). It can be concluded that the western and northern parts of the Murzuq Basin are highly prospective for hydrocarbon exploration. The eastern parts of the basin are less prospective due to the lack of source rock. As we have seen before, the structural and the hydrocarbon systems of the Ghadames and Murzuq Basins are quite different with respect to the influence of Al Qarqaf Arch. The influence of Al Qarqaf Arch on the structural and trapping systems in the Ghadames Basin is stronger than that in the Murzuq Basin.

Therefore, potential oil and gas plays are expected to be present in both basins include the following:

1. Pinchout of the reservoir units of the Late Silurian Acacus Formation could occur as the section thins against the Al Qarqaf Arch axis at the southern edge of the Ghadames Basin. The same could occur in the northern parts of the Murzuq Basin with the Cambro-Ordovician Memouniat Formation.
2. Structural doming of porous horizons along wrench faults on the western and central parts of the Murzuq Basin.

A sketch summary of the play concepts of the two basins is shown in Fig. 9, in which one can see the distribution of the major resources and source rocks and the principle migration routes.

4. Recommendations

1. A study of the distribution and maturity of all possible source rocks, and source rock-cap rock relationships, in particular around Gargaf high.
2. Investigation of the formation water salinities in the two basins, which may give clues to the nature and age relationships between oil emplacement, erosional stripping and fresh-water flushing. In some areas, oil may be emplaced after the erosional stripping and fresh-water flushing of the reservoir rocks. In such cases, anomalous salinity values are expected.
3. There are not enough data available to establish the pattern of diagenesis for the reservoir rocks occurring in the area, so further analysis is recommended.
4. Detailed work on the role of faults in migration in both basins is highly recommended.
5. The role of wrench faults in the trapping of oil in the Murzuq Basin should be investigated in more detail by integrated interpretation of seismic data over a large area.

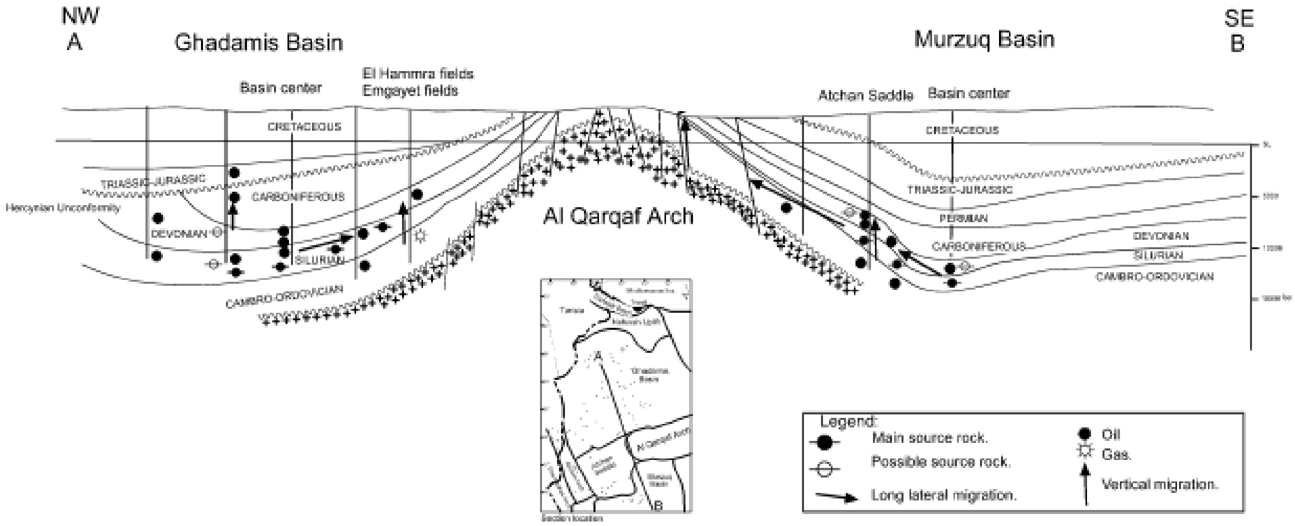

Fig. 9. Sketch summary of play concepts of the Ghadames and Murzuq Basins.

References

Alvares, W. (1956) The Upper Silurian-Lower Devonian (Sinawan Group) in Northwestern Libya. National Oil Corporation, Open File Report, 21p.

Compton, P., Hammali., A. and Walker, R. (1999) AAPG International Conference, Birmingham, England, Sept. 12-15, 132p.

Echikh, K. (1998) Geology and Hydrocarbon Occurrences in the Ghadames Basin, Algeria, Tunisia, Libya. In: (eds Macgregor, D. S., Moody, R.T.J. and Clark-Lowes, D.D.) Petroleum Geology of North Africa. Geological-Society Special Publication, pp. 109-129.

Massa, D., Oesterle, H. and Kirmanik, K. (1994) African Exploration Opportunities: Ghadames, Murzuq-Djado and Kufra-Edri Basins. Petroconsultant, 372p.

Meister, E. M., Ortiz E.F., Pierobon, E. S. T., Arruda, A.A. and Oliveira, A.M. (1991) The Origin and Migration Fairways of Petroleum in the Murzuq Basin, Libya: An Alternative Exploration Model. In: (eds Salem, M.J. and Busrewil, M.T.) The Geology of Libya. Academic Press, London, 2725-2741.

Waples, D.W. (1980) 'Time and Temperature in Petroleum Formation: Application of Lopatin's Method to Petroleum Exploration', *AAPG Bulletin*, 64(4), pp. 91

Libyan Journal of Science & Technology 9:1 (2019) 38–45
The 2nd International Conference on Geosciences of Libya-GeoLibya 2 (2017), 14-16 October 2017, Benghazi-Libya

Faculty of Science - University of Benghazi
Libyan Journal of Science & Technology
journal home page: www.sc.uob.edu.ly/pages/page/77

Taxonomical and biostratigraphical notes on *Nummulites* of Darnah Formation at Daryanah-Al Abyar area, Cyrenaica, NE Libya.

Mohamed S. Al Faitouri[a], Ahmed M. Muftah[a], Farag A. Al Tarhouni[a] and Rajab B. El Zaroug[b]

[a]*Department of Earth Sciences, Faculty of Science, University of Benghazi. Benghazi-Libya.*
[b]*Department of Engineering Geology, Faculty of Engineering, University of Tripoli. Tripoli-Libya.*

Highlights

- **The paper deals with taxonomy investigations of the genus Nummulites in Middle Eocene Darnah exposed rocks from Al Jabal al Akhdar based on biometric measurements and/or morphological features from which five species are identified and illustrated.**
- **The studied species assigned to the N. gizehensis biozone.**

ARTICLE INFO

Article history:
Received 01 February 2018
Revised 22 March 2018
Accepted 29 March 2018
Available online 31 March 2019

Keywords:
Taxonomical measurements, Biostratigraphical analysis, *Nummulites gizehensis,* Darnah Formation, Wadi Ekhil, Daryanah-Al Abyar Area, Cyrenaica

*Corresponding Author:
E-mail address: mohamed.alfaitouri@uob.edu.ly
M. S. Alfaitouri

ABSTRACT

Darnah Formation at Wadi Ekhil in Daryanah- Al Abyar area, Al Jabal al Akhdar, Northeast Libya has been subjected to micropaleontological and biostratigraphical analyses based on larger foraminifera "*Nummulites*" which has largely used as a time marker in the Tethyan region (Circum-Mediterranean). Taxonomical measurements were performed during this study from which the following five species were identified, *Nummulites gizehensis, N. lyelli, N. beaumonti, N. striatus* and *N.* sp.

The studied sections assigned to the i) *N. gizehensis* biozone Late Eocene "Late Lutetian" age due to the acme occurrence of the zonal marker species *N. gizehensis*; and ii) *N. lyelli* biozone Late Eocene "Biarritzian" due to the total range of the zonal marker species *N. lyelli*. The concerned nummulites-bearing sections of Darnah Formation indicate an inner neritic environment of bank settings as indicated by A/B ratio.

1. Introduction

Nummulites is a genus belonging to the order foraminiferida, with a shell made of a perforated low Mg-calcite hyaline wall. They are commonly extracted from limestones and dolomites but rarely with clastic sediments. The dimorphism phenomenon (alternation of generation between the asexually produced A-Form and the sexually produced B-Form) is well known in *Nummulites*. The speciation of *Nummulites* depends largely on morphological and structural features which depend largely on measurements done by using calibrated eyepiece micrometer, among these are 1) The relationship between diameter and thickness of the test; 2) Juvenile apparatus (protoconch); 3) Shape of both chamber and septa; 4) Septal filaments which are the only external morphological features besides granulations and nodes. 5) The spiral diagram which shows the relation between the number of whorls and the corresponding radii of both A- and B-forms as compared to Schaub (1981) and/or Racey (1995) spiral diagrams were also used in identifications of some species in the current study, depends on number of retrieved specimens.

Nummulites is the most useful diagnostic larger benthic foraminifera throughout the Paleogene of the Mediterranean region. The collected *Nummulites* tests used herein are retrieved from the Middle Eocene Darnah Formation in Al Jabal al Akhdar, NE Libya. The most valuable work using *Nummulites* in Al Jabal al Akhdar has been published by Abdulsamad (2000) who studied the larger foraminifera with detailed biometric descriptions of *Nummulites* from selected exposures in Al Jabal al Akhdar, NE Libya, where, *Nummulites gizehensis, N. lyelli, N. beaumonti, N. striatus, N. cyrenaicus*, and *N. discorbinus* are documented. Abdulsamad and Barbieri (1999), however, reported *N. gizehensis, N.* cf. *cuvillieri* and *N. subdiscorbinus* from Darnah Formation in the Well A1-36 drilled in Al Jabal al Akhdar southeast of Darnah city. Muftah and Boukhary (2013) reported the *N. fabianii* and *N. ruetimeyeri* as well as *Gaziryina pulchellus* from the Late Eocene Shahhat Marl Member of Al Bayda Formation. The main aim of this paper is to: 1) Produce a comprehensive systematic study of the retrieved *Nummulites* species from Darnah Formation in the area of study. 2) Establish the possible foraminiferal biozones with its regional extent. 3) Determine the depositional environment. The studied section of Wadi Ekhil is located in the lower escarpment of Al Jabal al Akhdar in the northeast of Libya (Fig. 1).

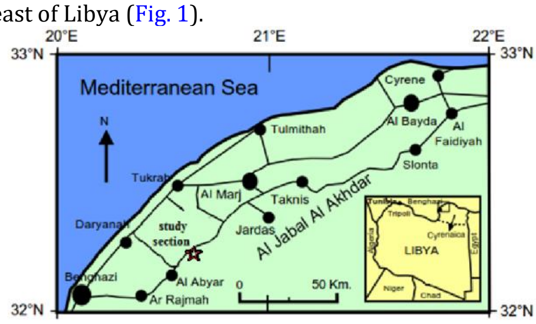

Fig. 1. Location map of the study area shows the location of Wadi Ekhil (Modified after Abdulsamad *et al.*, 2009).

2. Materials and methods of study:

The Fourteen rock samples have been collected from the measured section at Wadi Ekhil (Fig. 2). After the separation of the *Nummulites* tests from the contained sediments by the Standard Micropaleontological Techniques for the separation of *Nummulites* (see Schaub, 1981; Racey, 1995; Abdulsamad, 1999). The small-sized *Nummulites* were picked using the binocular microscope, whereas the large-sized ones were picked by the naked eye. Most picked nummulites-tests were heated in a Bunsen flame until it is glowed red hot, then quickly dropped into a glass beaker of cooled water. The *Nummulites* consequently became equatorially split apart into two identical halves and the internal morphological features were examined and biometrically measured under the binocular microscope. Measurements of protoconch size, chamber geometry, septa shape and radii of successive whorls were essential to build up the spiral diagrams. Spiral diagrams were drawn for the available *Nummulites* as a technique to identify the *Nummulites* species using Schaub's (1981) monumental monograph. The *Nummulites* were biometrically analyzed, photographed and thin-sectioned axially, equatorially and externally. To calculate the A/B ratio, Kondo (1995a) method on a quadrat of 15×15 cm is performed in the outcrops.

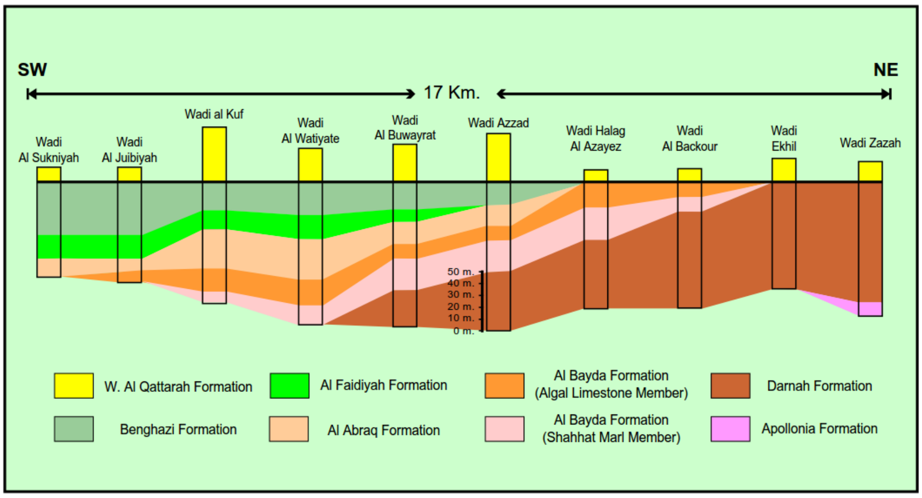

Fig. 2. Stratigraphic correlation of the study area including Wadi Ekhil (present study) (Abdulsamad *et al*., 2009).

3. Background and stratigraphy

The stratigraphy of the study area consists of five formations ranging in age from Middle Eocene to Late Miocene, which are Apollonia, Darnah, Al Bayda, Al Abraq and Wadi al Qattarah formations (see Abdulsamad *et al*., 2009). The best example to understand the stratigraphy of the study area and its environs are that conducted by Abdulsamad (2009), who included Wadi Ekhil in his stratigraphic logs correlation (Fig. 2). Only one outcrop has been sampled at Wadi Ekhil, from which only Darnah Formation are described herein and subdivided into two units (Figs. 3 and 4), the lower one is made of Foraminiferal wackestone-packstone, whitish yellow, very hard, massive bedded, rich in *Nummulites* spp. and some *Sphaerogypsina globula* with some echinoderm remains (Fig. 4a).

However, the upper one is nummulithoclastic packstone, white to creamy colored, moderately soft- medium hard, massive, and rich in *Nummulites* spp., nummulitic debris and some Gastropoda (Fig. 4b).

Darnah Formation at the study area yields a thickness of about 90m and consists of two nummulitic limestone units varying in texture between wackestone to packstone particularly in the lowermost two units (Fig. 3). The bioclastic grains are mainly *Nummulites* of small-sized *"N. striatus* and *N. beaumonti*" and large-sized "*N. gizehensis*, *N. lyelli* and *N.* sp.". Rare specimens of *Sphaerogypsina globula* are also occurred in the lowermost unit. Nummulithoclasts, with *N. beaumonti* and *N. lyelli*, *N. striatus* and *N.* sp. however, dominate the middle and upper part of the studied section (Fig. 3).

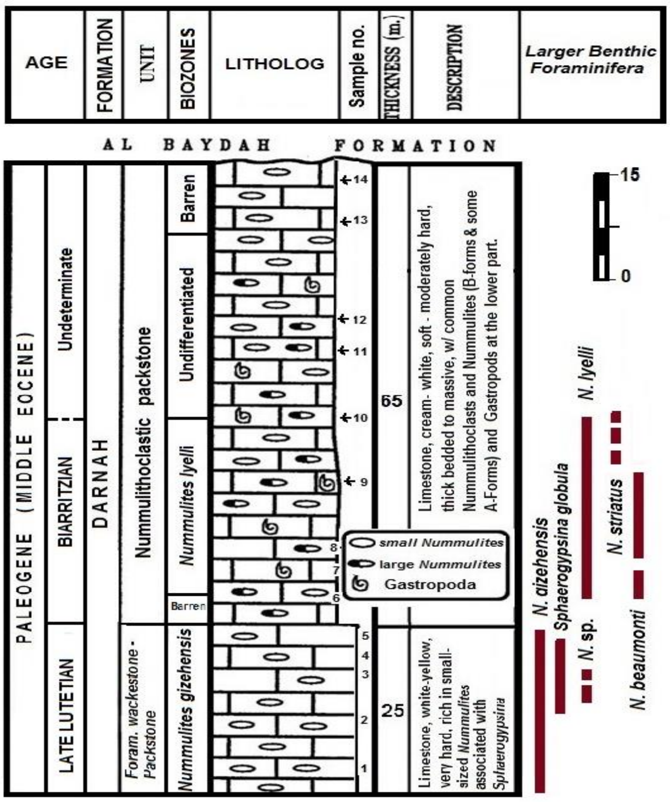

Fig. 3. Columnar section of Darnah Formation at Wadi Ekhil, with larger Foraminifera distribution chart.

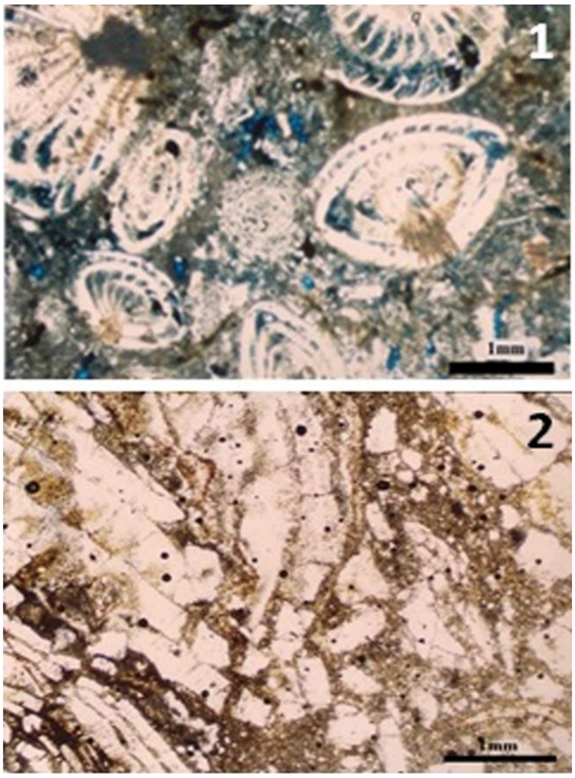

Fig. 4. a) Foraminiferal packstone of Darnah Formation, shows the *Nummulites* sp. (A- Form). and *Sphaeogypsina globula*; and b) Nummulithoclast wackestone-packstone dominated by nummulithoclasts and *Nummulites* sp. at Wadi EKhil.

4. Systematic paleontology

The classification of Loeblich and Tappan (1988) are followed herein for the suprageneric ranks. The studied material will have a final repository in the Geological Museum of the University of Benghazi (Benghazi, Libya).

Order: Foraminiferida Eichwald, 1830
Suborder: Rotaliina Delage and Herouard 1896
Superfamily: Nummulitacea de Blainville1827
Family: Nummulitidae de Blainville 1827
Genus: *Nummulites* Lamarck (1801)
Type species: *Camerina laevigata* (Bruguiere), 1792
Nummulites gizehensis (Forskål, 1775)

(Pl. I, Figs. 1-6)

1775 *Nautilus gizensis* (Forskål), p.140.

1965 *Nummulites gizehensis* (Forskål), Bozorgnia and Kalantari, pl. 6

1982 *Nummulites gizehensis* (Forskål), Boukhary, Blondeau and Ambroise, p. 72, pl. 1, Figs. 13, 14

Materials: 129 (B-Form) specimens and 402 (A-Form) specimens

Description:

*B-Form***:** Test lenticular, surface undulated, septal filaments flexuous to meandering, granulated in the juveniles while none granulated in the adults. Diameter ranges from 33-43.6 mm and thickness ranges from 7.8-9.8 mm.

Equatorial section: The spiral diagram (Fig. 5) the relation between the number of whorls and the corresponding radius in the median section. The spire is regular, the steps of coiling are lax and the number of whorls is as follows: 43 whorls in a radius of 23.1 mm, 41 whorls in a radius of 22.4 mm, 33 whorls in a radius of 18.3 mm 20 whorls in a radius of 9.4 mm and 10 whorls in a radius of 3.7 mm, septa are thin, regular, vertical at the base and then slightly arched near the end. The marginal cord is thick; chambers are mostly higher than long and longer than height in last whorls.

*A-Form***:** Test lenticular and truncated, septal filaments flexuous to sigmoidal, granulation present on and between filaments. Diameter ranges from 6-7.5 mm and thickness ranges from 3.3-4.3 mm.

Equatorial section: The spire is regular; all whorls are lax and regular. The numbers of whorls per radius are shown on the spiral diagram (Fig. 5) and as follows: 5 whorls in a radius of 3.6 mm, 4 whorls in a radius of 3.5 mm, and 4 whorls in a radius of 2.4-3.1 mm. The septa are arched at first whorls then straight at the base and inclined at the top. The marginal cord is thick; chambers are more or less isometric. The size of protoconch ranges from 1.15-1.8 mm. A characteristic taphonomical feature in form of boring tests is commonly observed in the B-Form tests (Fig. 6).

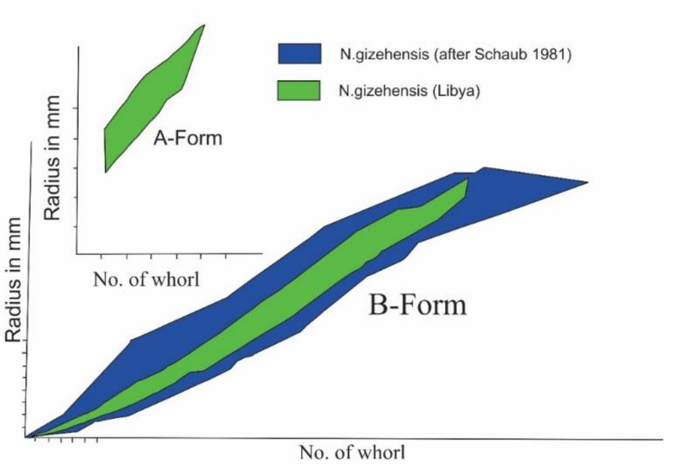

Fig. 5. Spiral diagram showing the relation between the number of whorls and the corresponding radius in equatorial section of *N. gizehensis*

Fig. 6. *Nummulites gizehensis* (A- and B-forms) shows the bored B-Form, Darnah Formation at Wadi Ekhil section.

Occurrence: *Nummulites gizehensis* are found in Darnah Formation at Wadi Ekhil at 185-190 meters above sea level. It also reported by Abdulsamad and Barbieri (1999) in the Darnah Formation from the surface exposure at Cyrene-Apollonia roadcut section as well as in subsurface A1-36 Well.

Age: Middle-Late Lutetian (Racey, 1995 and Hottinger *et al*., 1964).

Nummulites lyelli d'Archiac & Haime, 1853

(Pl. II, Figs. 1, 2, 4, 5)

1853 *Nummulites lyelli* d'Archiac and Haime, p.95, pl. 3, Figs.1a, 1b, 2

1981 *Nummulites lyelli* d'Archiac and Haime, Schaub, p. 116, table. 6, fig. e; pl. 38, figs. 18-20.

1995 *Nummulites lyelli* d'Archiac and Haime, Racey, p. 52, pl. 5, Figs. 7, 10-11

Materials: 65 (B-Form) specimens and 206 (A-Form) specimens

Description:

B-Form: Test flat with slight thickening at center, septal filaments flexuous to meandering, granulation appear in the juvenile test, while disappear on the adult's surfaces. Diameter ranges from 33.5–64.2 mm and thickness ranges from 6.2–11.6 mm.

Equatorial section: As shown on the spiral diagram "Winding diagram" (Fig. 7) the relation between the number of whorls and the corresponding radii in the median section, the spire is rather regular, the steps of coiling and number of whorls are as follows: 30 whorls in a radius of 12-18.95 mm, 40 whorls in a radius of 22.3 mm and 57 whorls in a radius of 26.8 mm. Septa are thin, regular, vertical straight in the first part and then slightly arched near the end. The marginal cord is thick; chambers are higher than length in the majority of the whorls and slightly longer than height in the peripheral whorls in some individuals.

*A-Form***:** Test lenticular with a sharp edge, septal filaments are flexuous to undulated, granulation is visible, with more concentration toward the periphery. Diameter ranges from 5 to 8 mm and thickness ranges from 2.1 to 3.69 mm.

Equatorial section: The spire is regular, lax in the early two whorls to tight in most part of the whorls. The number of whorls per radius is shown on the spiral diagram (Fig. 7) and as follows: 5 whorls in a radius of 2.6–3.5 mm, and 6 whorls in a radius of 2.9–4.1 mm. The septa in the internal whorls are inclined and somewhat irregular, while in the external part, they are regular or isometric and mostly straight to relatively inclined. Chambers are higher than length with some exceptions in the last two whorls. The size of protoconch ranges between 1.07–1.61 mm. The measurement of the present study of the *N. lyelli* in comparison with that of Schaub (1981) is listed in Table 1.

Remarks: Pillars in *Nummulites lyelli* de La Harpe are radiates from the pole, while in *Nummulites gizehensis* are zoned in the middle.

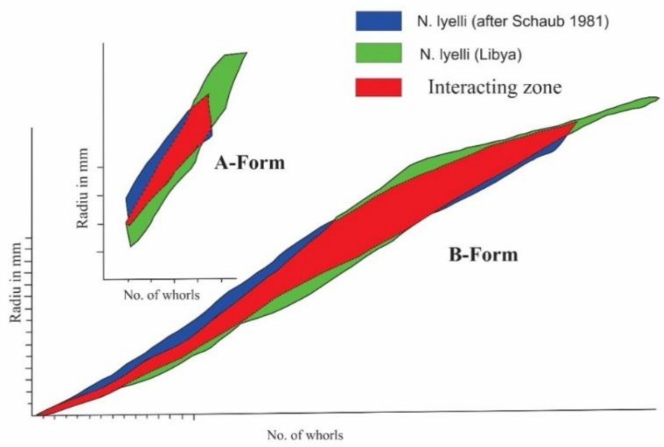

Fig. 7. Spiral diagram showing the relation between the number of whorls and the corresponding radius in an equatorial section of *N. lyelli*

Occurrence: Darnah Formation, at Wadi Ekhail 200 meters above sea level.

Age: Late Lutetian (Biarritzien) Racey, (1995); Hottinger *et al.*, (1964); and Boukhary and Kamal (2003).

Table 1

Dimensions of *Nummulites lyelli* (present study) compared with Schaub, (1964).

Measurements	*N. lyelli* Schaub, 1981	*N. lyelli* **(present study)**
Diameter & Thickness	B-form D/20-25 nan T/3-6.5 mm	B-form D/33.5-64.2 mm T/6.2-11.6 mm
	A-form D/5-7 mm T/2-3 mm	A-form D/6-8 mm T/2.1-3.6 mm
Granulation	Present	Present
No. of Whorls	B-form 50 whorls in a radius of 25 mm 44 whorls in a radius of 23-25.7 mm 41 whorls in a radius of 18.5 mm	B-form 57 whorls in a radius of 26.8 mm 41 whorls in a radius of 18 -22.3 mm 30 whorls in a radius of 12 – 18.95 mm
	A-form 5 whorls in radius of of3 4-3,7 mm 6 whorls in radius of 3.l-3.S mm 7 whorls in a radius of 4 mm	A-form 5 whorls in a radius of 2.6 -3.5 mm 6 whorls in a radius of 2.9-4. 1 mm
Protoconch size	B-form	A-form
	1-1.5mm	1.07-1.61 mm

Nummulites sp.

(Pl. II, Figs. 3, 6)

Materials: 2 (B-Form) specimens and 2 (A-Form) specimens

Description:

*B-Form***:** Test lenticular, surface undulated, with a thin margin. Diameter ranges from 33.5-38.5 mm and thickness ranges from 6.7-9.2 mm.

Equatorial section: The spire is irregular; the steps of coiling are more or less tight to lax. Septa are thin, vertical at the base then slightly arched near the end. The marginal cord is thick; chambers are isometric at first half of the whorls then subrectangular.

*A-Form***:** Test lenticular, granulation present all over particularly around the poles of the test. Diameter ranges from 6.1-6.6 mm and thickness ranges from 3.0-3.3 mm.

Equatorial section: The spires tend to be lax but start to be tight after the first two whorls. The septa are arched at first whorls then straight to inclined in the successive whorls. Chambers are higher than long. The size of protoconch ranges from 1.46-1.54 mm.

Occurrence: Darnah Formation, at Wadi Ekhail 185-190 meters above sea level.

Age: Middle Eocene (Lutetian)

Nummulites beaumonti d'Archiac and Haime, 1853

(Pl. III, Figs. 1-2)

1853 *Nummulites beaumonti* d'Archiac & Haime, p. 133, pl. 8, figs.1 a-e, 2, 3.

1981 *Nummulites beaumonti* d'Archiac & Haime; Schaub, p. 135, table 14, fig. p, pl. 53, figs. 17-19, 22-25.

Materials: 2 (B-Form) specimens and 2 (A-Form) specimens

Description:

*B-Form***:** Test lenticular with rounded margin, septal filaments flexuous from the center, granulation absent. Diameter ranges from 7.1-12.2 mm and thickness ranges from 3.1-5.6 mm.

Equatorial section: The spire is regular, septa start straight then inclined, and the marginal cord is thick and chambers sub rectangular.

*A-Form***:** Test lenticular and globular, septal filaments are flexuous, granulation absent. Diameter ranges from 3.2-3.5 mm. and thickness ranges from 1.6- 1.9 mm.

Equatorial section: The spire is regular and lax, the marginal cord is thick, and the chambers are sub rectangular. The size of the protoconch is very small and ranges from 0.1- 0.13 mm.

Occurrence: Found in Darnah Formation, in the Wadi Ekhail section at an elevation of 200 meters above sea level. It also reported by Abdulsamad (1999) from the Darnah Formation at Cyrene-Apollonia roadcut section.

Age: Middle Eocene (latest Lutetian –earliest Biarritzian) Racey, 1995; Blondeau, (1972).

Nummulites striatus (Bruguiere, 1792)

(Pl. III, Figs. 3-5)

1853 *Nummulites striata* d'Orbigny; Archiac & Haime, p. 135, pl. 8, Figs.9-12.

1972 *Nummulites striatus* (Bruguiere); Blondeau, p. 148, pl. 24, Figs. 1-10.

Materials: 2 (B-Form) specimens and 2 (A-Form) specimens

Description:

*B-Form***:** Test lenticular with a thin margin, septal filaments radiating from the center, granulation absent. Diameter ranges from 6.4-10.08 mm and thickness ranges from 3.08-4.9 mm.

Equatorial section: The spire is more or less tight to lax; septa are arched, vertical to inclined. The marginal cord is thick; chambers are higher than length

*A-Form***:** Test lenticular with a thin margin, septal filaments are radiating, granulation absent. Diameter ranges from 3.08-3.23 mm and thickness ranges from 1.54-1.8 mm.

Equatorial section: The spire is regular and lax, the marginal cord is thick, chambers are higher than length except in the earlier whorls chambers are isometric, and the size of protoconch is small and ranging from 0.12- 0.15 mm (two specimens are measured only).

Occurrence: Found at Darnah Formation, in Wadi Ekhail section at 200 meters above sea level.

Age: Middle Eocene (latest Lutetian –earliest Biarritzian), Racey (1995); Blondeau (1972).

5. Results and discussions

The collected ten samples from the Darnah Formation at Wadi Ekhil yield larger benthic foraminifers (i.e. *Nummulites*) *Nummulites gizehensis* and *N. lyelli* of both forms with minor elements of *N. striatus*, *N. beaumonti*, and *N.* sp. and *Sphaerogypsina globula*. The only established local biozones in Wadi Ekhil area are the *Nummulites gizehensis* Biozone and the overlying *Nummulites lyelli* biozone.

***Nummulites gizehensis* Biozone (Middle-Late Lutetian):**

The zonal marker *N. gizehensis* is widely distributed in the Eocene sediments of Mediterranean belt and is documented by Abdulsamad (2000); Abdulsamad *et al.*, (2009); Abdulsamad and Barbieri (1999) in Al Jabal al Akhdar region. *Nummulites gizehensis* bed are documented by Aigner (1982) in the Lutetian Mokattam Formation in Giza Pyramid Plateau West of Cairo and Mokattam Hill East of Cairo. It is recognized herein due to the common occurrence of the zonal marker *Nummulites gizehensis* to the occurrences (FO) of *N.* sp.. In association with *Sphaerogypsina globula.* It was described from Sirt Basin by Arni (1965). This biozone is established by Kenawy *et al.*, (1993) within Samalut Formation in the Nile Valley, who defined it as the interval from the first appearance of *N. gizehensis* to the first appearance of *N. beaumonti*. Bristot and Duronio (1985) covering the interval range of Early-Middle Lutetian also document it in Bouri Oil field as Nummulites gizehensis (Reineche horizon) Loculicytheretta semirugosa Biozone. However, the species is reported in Oman within Middle Lutetian *N. beucharnensis* biozone to Late Lutetian of *N. aturicus* by Schaub (1981) and Racey (1995).

***Nummulites lyelli* Biozone (Biarritzian)**

It is recognized herein due to the total range of the zonal marker *Nummulites lyelli.* In association with *Nummulites beaumonti, Nummulites striatus* with the absence of *Nummulites gizehensis*. It is widely distributed in the Eocene sediments of the Mediterranean belt. Abdulsamad (2000) documents the zonal marker from surface and subsurface successions, Abdulsamad *et al.*, (2009); Abdulsamad and Barbieri (1999) in Al Jabal al Akhdar region.

Depositional process:

The ratio between asexual form (Form-B) to sexual form (Form-A) in most recent works of normal ratio of A /B is 10/1 Moody (1998). Louks *et al.*, (1998) considered the A/B ratio due to the biological reproductive strategy and linked to changing environmental conditions and not by hydraulic sorting. The in-situ accumulation of *Nummulites* is expressed by A/B ratio of (10/1) as suggested by Blondeau (1972); Kondo (1995b) and Aigner (1982, 1983, 1985). In Middle Eocene of Pederiva di Grancona and Mossano sections in Veneto of northern Italy, the bank sediments with A/B ratio being low in comparison with the "normal" nummulitic limestone (Seddighi and Papazzoni, 2011). The A/B ratio in the present study has been calculated for *N. gizehensis* specimens and found to be of larger proportions 167/24 (≈7/1). This higher A/B ratio revealed that the original *Nummulites* assemblages were winnowed in situ with the extensive boring particularly within B-Form tests (Fig. 6), although good preservation noted in A-forms suggesting a bank depositional setting. In addition to that and due to the absence of the outer ramp indicators "discocyclinids and globigeriniids" as well as the inner ramp indicators "miliolids and textulariids" Cotton and Pearson, (2011), therefore, a shallow neritic bank environment is highly suggested to the lower part of the studied Darnah Formation at Wadi Ekhil section. A comparison of the A/B ratio with other studies is listed in Table 2, which shows close similarities except that of Braiser and Green (1993) from Barton Clay in the Isle of Wight.

Table 2

A/B ratio from present studies and others.

Author	A/B ratio	Formation	Age	Country
Aigner (1983)	7/1	Mokhattam	Eocene	Egypt
Abdulsamad and Barbieri, 1999	15/1	Darnah	Middle Eocene	Libya (Al Jabal al Akhdar) CA section.
Brasier and Green, 1993	59/1	Barton Clay	Late Eocene	Isle of Wight
Blondeau (1972)	10/1	Al Garia	Early Eocene	Tunisia
Present study	7/1	Darnah	Middle Eocene	Libya (Al Jabal al Akhdar) Wadi Ekhil

6. Conclusions

1- Darnah Formation at this section subdivided into two litho-units (foraminiferal wackestone-packstone and the overlying nummulithoclastic packstone).

2- Five *Nummulites* taxa "*N. gizehensis, N. lyelli, N. beaumonti, N. striatus* and *N.* sp. are identified, described and illustrated from Wadi Ekhil, at Daryana-Abyar area, NE Libya.

3- The *Nummulites gizehensis* and *N. lyelli* are recognized within the section.

4- The studied Darnah Formation at Wadi Ekhil section is deposited under a shallow neritic bank environment as suggested from the A/B ratio.

References:

Abdulsamad, E. O. (2000) 'Contribution to the Nummulites taxonomy from the Paleogene sequences of Al Jabal al Akhdar (Cyrenaica, NE Libya)', *Review de Paleontologie,* 19 (1), pp. 19-45.

Abdulsamad, E. O. (1999) Foraminiferal micropaleontology of the Tertiary deposits of Al Jabal al Akhdar (Cyrenaica, NE Libya). *PhD thesis*, Bologna University, Bologna, Italy, 140p.

Abdulsamad, E. O. (2000) 'Contribution to the *Nummulites* taxonomy from the Palaeogene sequences of Al Jabal al Akhdar (Cyrenaica, NE Libya)', *Review Paleobiol.,* Geneve, 19 (1), pp. 19-45.

Abdulsamad, E. O. and Barbieri, R. (1999) 'Foraminiferal distribution and paleoecological interpretation of the Eocene-Miocene carbonate at Al- Jabal al Akhdar (northeast Libya)', *Journal of Micropaleontology*, 18, pp. 45-65. England.

Abdulsamad, E. O., Bu-Argoub, F. M. and Tmalla, A. F. A. (2009) 'A stratigraphic review of the Eocene to Miocene rock units in the al Jabal al Akhdar, NE, Libya', *Marine and Petroleum Geology,* 26, pp. 1228-1239.

Aigner, T. (1982) Event-stratification in nummulite accumulations and in shell beds from the Eocene of Egypt. *In*: Einsele G. & Seilacher A. (Eds.), Cyclic and Event Stratification. Springer, Berlin, pp. 248-262.

Aigner, T., (1983) Facies and origin of nummulitic buildups: an example from the Giza Pyramids Plateau (Middle Eocene, Egypt)', *Neues Jahrbuch fur Geologie und Palaontologie,* Abhandlungen, 166, pp. 347-368.

Aigner, T., (1985) 'Biofabrics as dynamic indicator in Nummulite accumulations', *Journal of Sedimentary Petrology*, 55, pp. 0131-0134.

Arni, P. (1965) L'évolution des Nummulitinae en tant que facteur de modification des depots littoraux', *Mém. Bur. Rech. Géol. Min.*, 32, pp. 7-20.

Blondeau, A. (1972) Les Nummulites: Vuibert Vuibert, Paris, 254p.

Bozorgina, F and Kalantari, A. (1965) *Nummulites* of parts of Central and East Iran. Nation Iranian Oil Co., Téhéran, 28 p., 3 text. Fig., 24 pl.

Brasier, M. D., and Green, O. R. (1993) 'Winners and losers: stable isotopes and microhabitats of living Archaiadae and Eocene *Nummulites* (larger foraminifera)', *Marine Micropaleontology* 20, pp. 267-276.

Bristot, B. and Duronio, P. (1985) Bouri Oil Field Handbook for Wellsite Geologist. Agip Name, Libya Branch- Exploration Division. Tripoli.

Boukhary, M. and Kamal, D. (2003) 'What is *Nummulites lyelli*? Evolution in Larger Foraminifera during the Middle Eocene, Egypt', *Microplaeontoloie*, 49 (2), pp. 171- 187.

Boukhary, M., Blondeau, A. and Ambroise, D. (1982) 'Etude sur les nummulites de la region de Minia-Samalut, Vallee du Nil, Egypte: biometric et biostratigraphie', *Cahiers de Microplaeontoloie*, 1, pp. 65- 78.

Cotton, L. J. and Pearson, P. N. (2011) 'Extinction of larger benthic foraminifera at the Eocene/Oligocene boundary', *Palaeogeography, Palaeoclimatology, Palaeoecology*, 311, pp. 281-296.

D'Archiac, A. and Haime, J. (1853) Description des animaux fossils du groupenummulitiquede'l'Inde. *Précédé d'un résumegéologique et d'unemonographie des nummulitites*. Paris

Forskal, P. (1775) Descriptionesanimalium. Copenhagen: Hauniae, Carsten Niebuhr.

Hottinger, L, Lehmann, R. and Schaub, H. (1964) Données actuellessur la biostratigraphie du Nummulitique méditerranéen. L. Hottinger et H. Schaub: I. Les series paléogènes de quelques bassines méditerranéen. *Colloquesur le paleogene*. Bordeaux, 1962= Mém. Bur. Rech. Géol. Min. Nº 28.

Kinawy, A. I., Mohamed, H. K. and Mansour, H. H. (1993) Biostratigraphic zonation of the Middle Eocene in the Nile Valley, based on larger Foraminifera. Zitteliana, 20, Hagn/Herm-Festschrift: 301-309. Munchen.

Kondo, V. (1995a) 'Paleocurrent reconstruction, using imbricated tests of Nummulites in the Eocene of Hahajima, Ogasawara Islands', *Journal of the Geological Society of Japan*, 101, pp. 228-234.

Kondo, V. (1995b) 'Density and relative abundance of microspheric and megalospheric forms of Nummulites as sedimentologic and taphonomic indicators', *Trans. Proc. Palaeont. Soc. Japan*, N.S., No. 177, pp. 59-64, 4 Figs., April 30.

Loeblich, A., R. and Tappan, H. (1987) Foraminiferal genera and their classification. New York: *Van Nostrand Reinhold Co. Inc.*, 970 p.

Louks, R. G., Moody, R. T. J., Brown, A. A. and Bellis, J. K. (1998) Regional depositional model for larger foraminiferal Nummulite deposits in the Lower Eocene Metlaoui Group, Tunisia. Tertiary to Recent Larger Foraminifera their depositional environments and importance as Petroleum Reservoirs. *Conference – Workshop – field trip*. Kingston University, United Kingdom. (Abstract vol.).

Muftah, A. M. and Boukhary, M. (2013) 'New Late Eocene genus *Gaziryina* (Foraminifera) from the Al Bayda Formation (Shahhat Marl Member), Al Jabal al Akhdar; Northen Cyrenaica, Libya', *Micropaleontology*, 59 (2-3), pp. 103-109.

Moody, R. (1998) *Tertiary to recent Larger Foraminifera, Their depositional environment and importance as petroleum reservoirs* (field trip guide. Part 3, Background information on Metlaoui Carbonates). ARCO-BG plc – Carthage Oil- Vheveron. Northern and Central Tunisia. 1-84.

Schaub, H. (1981) 'Nummulites et Asssilines de la Téthys Paléogene. Taxinomie, Phylogenèse et biostratigraphie', *Schweizerische Paläontologische Abhandlungen*, 104, pp. 1-236.

Seddighi, M. and Pappazoni, C. A. (2011) Comparative quantitative analysis of a nummulite bank and a "normal" nummulitic limestone, Middle Eocene of Pederiva di Grancona and Mossano sections (Veneto northern Italy). *Berichete Geol*. B.-A., 85 (ISSN 1017-8880) – CBEP, Salzburg.

Racey, A. (1995) 'Lithostratigraphy and larger foraminiferal (nummulitid) biostratigraphy of the Tertiary of northern Oman', *Micropaleontology*, Supplement 41, pp. 1-123.

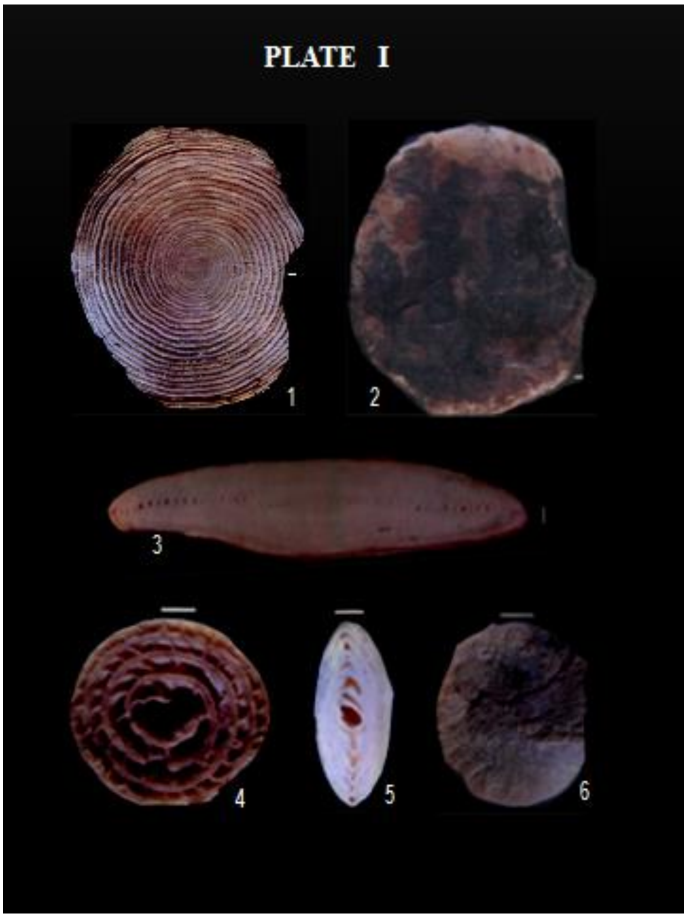

Explanation of Plate 1 (All scale bar = 1 mm)

1, 2, 3: *Nummulites gizehensis* (B-Forms) equatorial section, an external view and axial section respectively (each photograph represents a different specimen).

4, 5, 6: *Nummulites gizehensis* (A-Form) equatorial sections, axial section and external view respectively (each photograph represents a different specimen).

Explanation of Plate II (All scale bar = 1 mm)

1, 2: *Nummulites lyelli* (B-Form) axial section and equatorial section respectively (each photograph represents a different specimen).

4, 5: *Nummulites lyelli* (A-Form) equatorial and axial sections respectively (each photograph represents a different specimen).

3, 6: *Nummulites* sp. equatorial sections of B- and A-forms respectively.

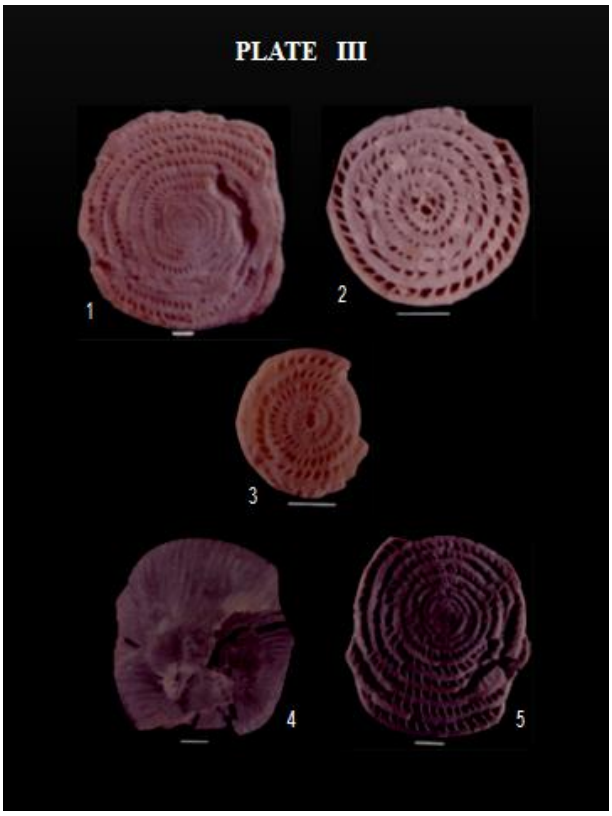

Explanation of Plate III (All scale bar = 1 mm)

1, 2: *Nummulites beaumonti* equatorial sections of B & A forms respectively

3, 5: *Nummulites striatus* equatorial section of A& B forms respectively.

4: *Nummulites striatus* external view.

Libyan Journal of Science & Technology 9:1 (2019) 46–52
The 2nd International Conference on Geosciences of Libya-GeoLibya 2 (2017), 14-16 October 2017, Benghazi-Libya

Faculty of Science - University of Benghazi
Libyan Journal of Science & Technology
journal home page: www.sc.uob.edu.ly/pages/page/77

Biostratigraphy of Palaeocene to Miocene Foraminifera in Concession 65, SE Sirt Basin, Libya

Esam O. Abdulsamad[a,*], Ahmed F. A. Tmalla[b], Fawzi M. Bu-Argoub[c]

[a] *Department of Earth Sciences, University of Benghazi, P. O. Box: 9480, Benghazi, Libya.*
[b] *Marine Biodiversity Group, Naturalis Biodiversity Center, Postbus 9517, 2300 RA Leiden, the Netherlands.*
[c] *Exploration Division, Arabian Gulf Oil Company, P. O. Box: 263, Benghazi, Libya.*

Highlights

- **Five wells were biostratigraphically examined from the Palaeocene to Miocene sequence in Concession 65, SE Sirt Basin, Libya.**
- **Study of the different foraminiferal faunae allowed the subdivision of the Palaeocene to Miocene sequence in Concession 65 into different foraminiferal zones.**
- **The recovered planktic foraminifera were used to subdivide the Palaeocene into the planktic foraminiferal zones of Berggren *et al.* (1995).**
- **The retrieved larger benthic foraminifera from the Late Palaeocene to Miocene, however, were examined biostratigraphically following the shallow benthic zones (SBZ) of Cahuzac and Poignant (1997) and Serra-Kiel, *et al.* (1998).**

A R T I C L E I N F O

Article history:
Received 01 February 2018
Revised 22 March 2018
Accepted 30 March 2018
Available online 31 March 2019

Keywords:
Libya, Sirt Basin, Concession 65, Biostratigraphy, Palaeocene-Miocene, Foraminifera.

*Corresponding Author:
E-mail address: esam000@yahoo.com
E. O. Abdulsamad

A B S T R A C T

Palaeocene to Miocene planktic and larger benthic foraminifera retrieved from ditch cuttings samples taken from 5 wells drilled in Concession 65, SE of Sirt Basin, Libya, have been studied biostratigraphically.
This study indicates that the Palaeocene sequence is composed of a shale unit overlain by a carbonate unit. The shale unit contains a rich assemblage of planktic foraminifera indicating Early Palaeocene age (Danian Stage), which is equivalent to the planktic foraminiferal zones P1 and P2.
The overlying carbonate unit is Late Palaeocene in age (Selandian-Thanetian) based on the occurrence of several planktic foraminiferal species of the planktic foraminiferal zones P3-P5. The recovery of few species of larger benthic foraminifers from this carbonate unit provides an additional evidence that it was deposited during the Late Palaeocene, corresponding to the shallow benthic foraminiferal biozones SBZ3-SBZ6, which correspond to the (Selandian-Thanetian) stages.
The Early Eocene sequence is mainly barren anhydrites and dolomites with rare badly preserved nummulitids in the Ypresian. The Middle Eocene (Lutetian-Bartonian) limestones contain a nummulitic assemblage with variable species, including *Nummulites gizehensis*/*Nummulites lyelli* group, which represent the SBZ14-SBZ16 in the Lutetian and the SBZ17-SBZ18 in the Bartonian.
The Late Eocene interval is dated on the presence of few reticulate medium-sized nummulitic species, including *Nummulites fabianii*, and assigned to the SBZ19.
The lowermost part of the Oligocene sequence is attributed to the SBZ21 (Rupelian) based on the occurrence of *Nummulites vascus* and *Operculina complanata* in the limestones. This is overlain by the SBZ22 (Chattian), as indicated by the last occurrence of *Nummulites vascus* and the first appearance of *Borelis melo melo* and *Amphistegina* sp. The uppermost deposits of the studied successions, which are mainly sandstones with hardly any fossils, belong to the Miocene.

1. Introduction

Most of the oil production in Libya comes currently from the Sirt Basin, which has received, since the 1950's, a lot of attention in terms of geological and geophysical studies, but micropalaeontological data are relatively few. In this study, the Palaeocene to Miocene intervals of five exploration wells (A1, A2, C13, C14 and C19), drilled by different oil companies in Concession 65, of SE Sirt Basin during the 60's and 90's of last century, have been investigated for their foraminiferal contents. Concession 65 covers a huge area (about 8000 km^2) and broadly located between 27° to 28° N latitudes and 21° to 23° E longitudes (Fig. 1). The Sarir oil field represents the major oil field in Concession 65 where around 100 wells were drilled.

The field went on production in December 1966 at 100.000 bbl/day. Production was gradually increased up to about 330.000 bbl/day in 2010. Almost everywhere, in the Sirt Basin, the late Mesozoic and Tertiary structures developed on a Precambrian and Paleozoic eroded surfaces (Conant and Goudarzi, 1967). According to Sanford (1970), the majority of oil fields are on the horst ridges or high fault edges of the regional tectonic features of the Sirt Basin. Local oil accumulation generally is associated with sedimentary cover and cross-faulting of these main trends. The stratigraphic setting of the study area (Fig. 2) represents the succession throughout the Sirt Basin, although there are some important local variations. The stratigraphic successions penetrated by the studied wells are generally similar, the difference being only the relatively slight thickness variations of individual rock units.

 ISSN 2663-1407; National Library of Libya, Legal number: 390/2018

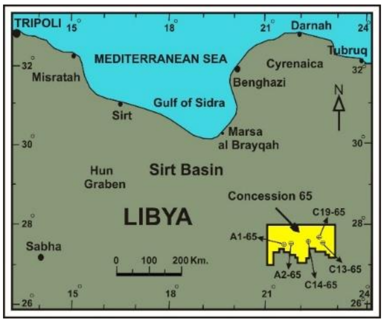

Fig. 1. Location map of Concession 65, SE Sirt Basin, and the studied wells

Previous studies by Sanford (1970), Gillespie and Sanford (1970), Lewis (1990), Ambrose (2000), Ahlbrandt (2001) and Hallett (2002) did help in explaining the geological, structural and development of the petroleum system in the region, but many stratigraphic aspects of the Cenozoic deposits remain poorly understood. Therefore, the objective of this paper is to refine the biochronostratigraphy of the Palaeocene-Miocene deposits in the region, based on planktic and larger benthic foraminiferal assemblages. A brief palaeoenvironmental assessment of the studied sequence was, however, presented by Abdulsamad *et al.*, (2008) and the main results are adopted here. They are summarized in Fig. 2:

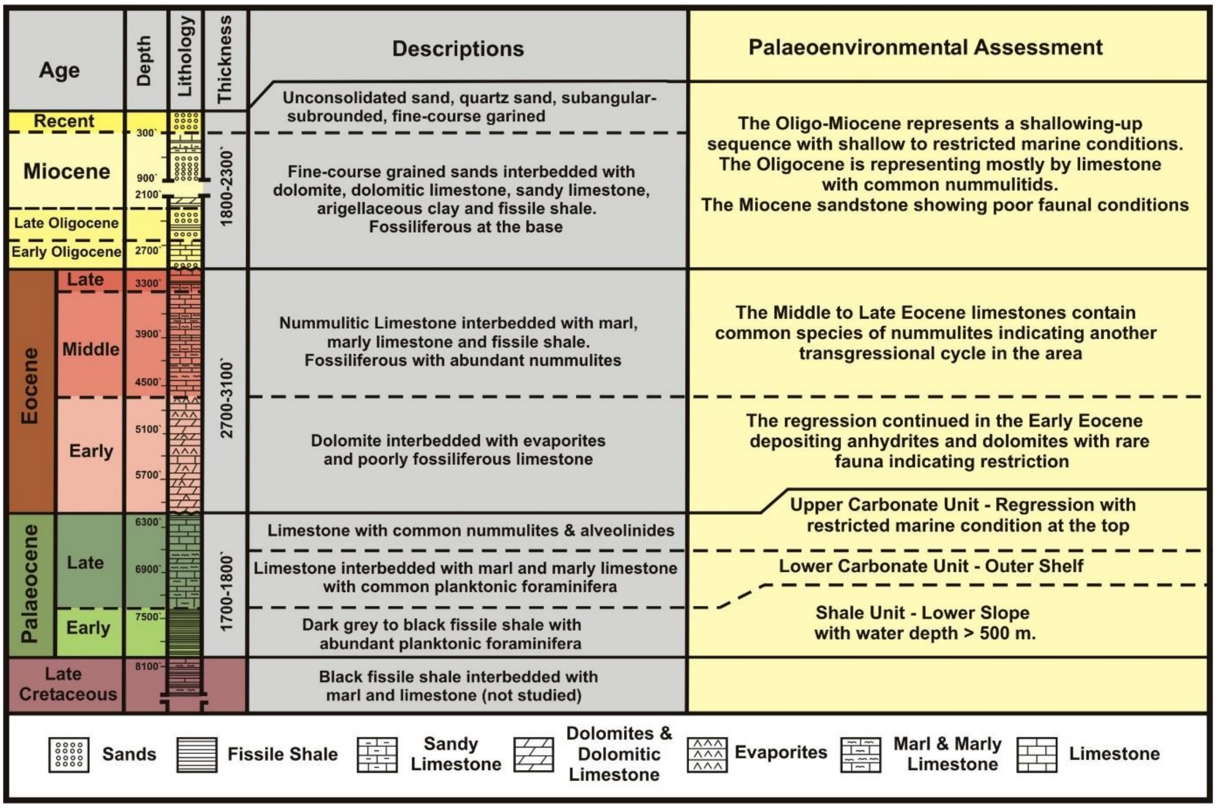

Fig. 2. General stratigraphy of Concession 65.

The Palaeocene sequence consists of a lower shale unit and an upper carbonate unit. The Lower Paleocene shale unit, overlying the Upper Cretaceous shales, contains very abundant deep marine planktic foraminifera indicating water depths in excess of 500 m. lower slope or deeper (Grimsdale and Van Morkhoven, 1955; Tipsword *et al.*, 1966). The carbonates of the lower part of the Upper Palaeocene unit contain rare planktic foraminiferal species with frequent to abundant nummulitic fauna, alveolinids and miliolids in the uppermost part of the Upper Palaeocene carbonates. This is an evidence of marine gradual regression introducing shallow to a restricted marine environment of deposition to the area during the Late Palaeocene time.

The regression continued throughout the Lower Eocene depositing anhydrites and dolomites with few badly preserved benthic microfauna, indicating restriction. The Middle to Upper Eocene limestone contains diverse and common species of nummulites, indicating another transgressional cycle in the area.

The Oligo-Miocene time interval represents a shallowing-up sequence with shallow to restricted marine conditions. Generally, the Oligocene sediments are represented, mostly, by limestone with common nummulitids, particularly at lower levels, whereas the uppermost sediments of the studied successions are mainly Miocene sandstones showing poor faunal habitat conditions. This is suggested by the occurrence of a few badly preserved specimens of alveolinids and miliolids.

2. Materials and Methods

About 350 ditch cuttings samples from five boreholes, provided by the Arabian Gulf Oil Company, were processed for micropalaeontological analysis. All samples were washed through a set of sieves (65-100 µm in diameter). Specimens were identified based on the overall morphology under a stereoscopic microscope and stored in reference slides. Isolated specimens of nummulites, however, were identified based on external and internal morphology. All laboratory analyses were undertaken at the Micropalaeontology Laboratory of the Earth Sciences Department of the Benghazi University, Benghazi, Libya. Scanning Electron Microscope (SEM) Photomicrographs, however, were taken at the Naturalis Biodiversity Center, Leiden, Netherlands.

3. Results and Discussion

To demonstrate the lateral variation of the studied deposits, a correlation of the investigated subsurface sections, based on stratigraphic criteria, is outlined in Fig. 3. Here, the stratigraphic successions penetrated by the wells are generally similar, the difference being only the relatively slight thickness variations of individual rock units. Fig. 4 represents a composite range chart for the studied wells and provides the stratigraphic distribution of most recovered foraminiferal species (Plates 1-6). The results were analyzed to have a biostratigraphic control based on the planktic foraminiferal zones of Berggren *et al.*, (1995) for the Palaeocene sequence. The recovered larger benthic foraminifera from the Late Palaeocene to Miocene were examined biostratigraphically according and assigned to the shallow benthic zones (SBZ) of Cahuzac and Poignant, (1997) and Serra-Kiel, *et al.*, (1998). Despite problems arising from using ditch-cuttings samples, facies changes, stratigraphic gaps, and barren intervals, analyses of the recovered foraminifera indicate that the studied sedimentary rocks show distinctive age-related foraminiferal content that can be described in the following order:

3.1 Palaeocene sequence

The Palaeocene sequence is about 550 m thick in the eastern part of the studied area. It is composed of a shale unit in the lower part overlain by a carbonate unit. The shale is dark grey to black with abundant planktic foraminifera. The recovered fauna from this unit (Fig. 4) includes *Eoglobigerina edita* (Subbotina), *Globoconusa daubjergensis* (Brönnimann), *Subbotina trivialis* (Subbotina), and *Praemurica inconstans* (Subbotina). This assemblage indicates an Early Palaeocene age (Danian Stage). Most of the Danian Stage, however, corresponds to the P1: *Parvularugoglobigerina eugubina-Praemurica uncinata* Interval Zone of Berggren *et al.* (1995). This zone has been subdivided into three subzones (P1a-P1c) based on the chronological appearances of *Subbotina triloculinoides* and *Globanomalina compressa/Praemurica inconstans* (Berggren and Miller, 1988). *Parvularugoglobigerina eugubina* has not been recovered from our samples and consequently the base of P1a zone can not be established. Although, the top of P1a and the base of P1b subzones can be established by the first occurrence datum (FAD) of *Subbotina triloculinoides* and the last occurrences (LAD) of *Praemurica inconstans*, we could not establish the boundary on the distribution chart (Fig. 4) due to caving problems, which make it very difficult to determine first occurrences. A similar conclusion has been reached for the overlying P1c subzone. The remaining time-interval of the Danian Stage is considered belonging to the P2: *Praemurica uncinata-Morozovella angulate* Interval Zone of Berggren *et al.* (1995). The biostratigraphic interval between the FAD of *Praemurica uncinata* and the FAD of *Morozovella angulate* can be recognized in Fig. 4.

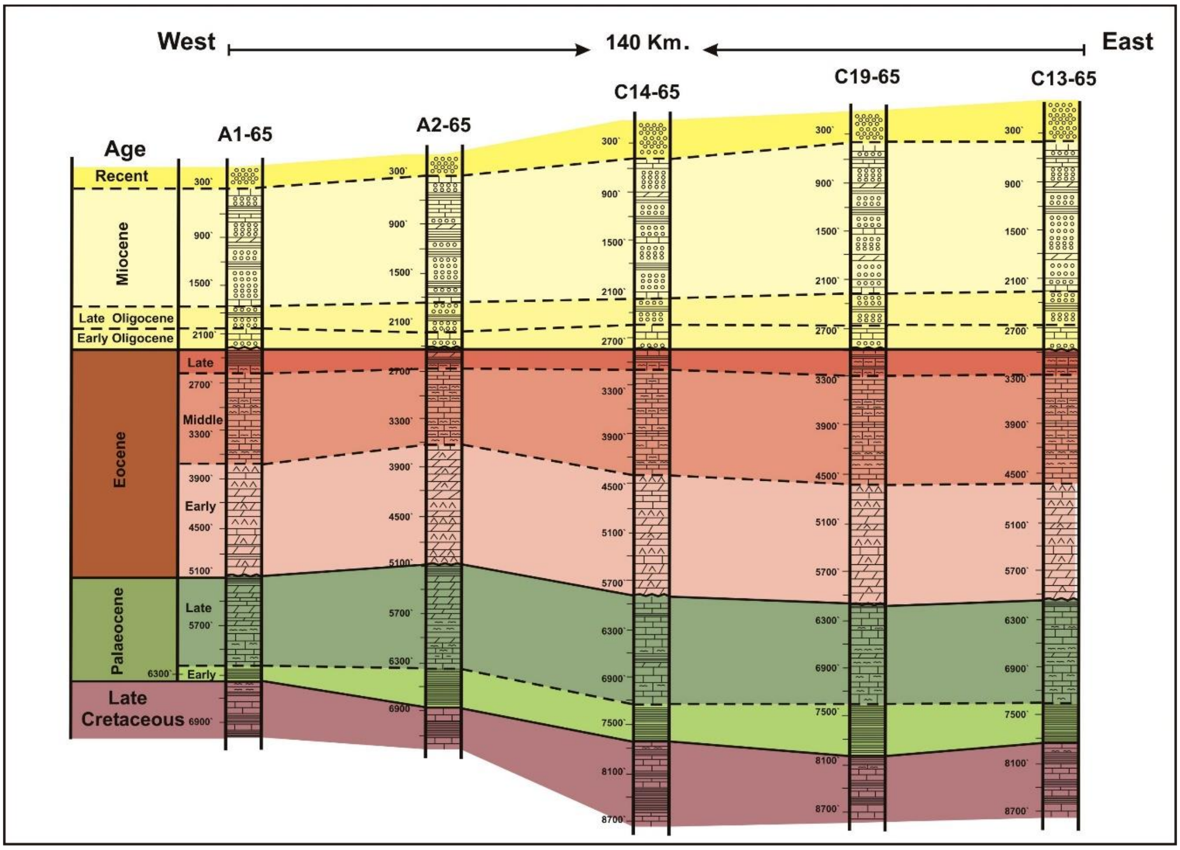

Fig. 3: Correlation chart of the studied w

The upper carbonate unit is mostly limestone interbedded with dolomite, dolomitic limestone and marl. This carbonate unit is considered here as Late Palaeocene based on the recovery of several planktic foraminiferal species including *Morozovella angulata* (White), *Igorina pusilla* (Bolli), *Globanomalina ehrenbergi* (Bolli), *Morozovella apanthesma* (Loeblich & Tappan), *Globanomalina chapmani* (Parr), *Morozovella parva* (Ray), *Morozovella aequa* (Cushman & Renz), *Acarinina soldadoensis* (Brönnimann), *Subbotina triangularis* (White), *Morozovella velascoensis* (Cushman) and *Morozovella subbotinae* (Morozova). This assemblage indicates broad Late Palaeocene age (Selandian-Thanetian). The Selandian Stage is equivalent to P3: *Morozovella angulata-Globanomalina pseudomenardii* Interval Zone of Berggren *et al.* (1995). The zone has been subdivided traditionally into a lower (a) subzone and an upper (b) subzone based on the (presumed) FAD of *Igorina pusilla* in the lower third of the biostratigraphic interval by Berggren and Miller (1988). Currently, the subdivision of zone P3 is based on FAD of *Igorina pusilla* descendant form *Igorina albeari* (= *Igorina pusilla laevigata*), which occurs about midway within Zone P3. This occurrence has been used to define the existing subdivision of Zone P3 (Berggren and Norris, 1993). Since we did not recover the latter species from our samples, we are not able to subdivide zone P3.

The Thanetian Stage corresponds to the P4: *Globanomalina pseudomenardii* Total Range Zone and P5: *Morozovella velascoensis* Interval Zone of Berggren *et al.* (1995). *Globanomalina pseudomenardii* has not been recovered and consequently no criteria can be used to recognize zone P4. The last occurrence of *Morozovella velascoensis* and associated planktic taxa has been used to establish the upper limit of the Late Palaeocene (see Fig. 4). The Early/Late Palaeocene boundary, however, has been established based on the last occurrence of *Praemurica inconstans* and the first appearance of *Morozovella angulata*.

The recovery of few species of larger benthic foraminifera, such as *Ovalveolina primaeva* (Reichel), *Chordoperculinoides* cf. *georgianus* Cole & Herrick, and *Nummulites deserti* de la Harpe from the upper carbonate unit are quite significant and provide additional evidence that the deposition was during the Late Palaeocene. This assemblage of larger foraminifera belongs to the Selandian-Thanetian stages and corresponds to the shallow benthic foraminiferal biozones SBZ3 to SBZ6 of Serra-Kiel *et al.* (1998). The total range of *Ovalveolina primaeva* (see Fig. 4) which corresponds approximately to the upper part of the Selandian and the lower part of the Thanetian stages defines the biozone SBZ3. According to Serra-Kiel *et al.*, (1998) the stratigraphic range of *Nummulites deserti* in the Tethyan realm is confined to biozones SBZ5 and SBZ6 which correspond to the uppermost Thanetian and lowermost Ypresian (Early Eocene). The presence of this species below this stratigraphical interval reflects the problem of ditch cuttings samples and the consequent contamination by caving. A similar conclusion has been noted for *Chordoperculinoides* cf. *georgianus*. According to Haynes *et al.* (2010), the latter species indicates an age close to the Palaeocene/Eocene boundary.

3.2 Eocene sequence

The Eocene sequence is 820-945 m thick. The Early Eocene interval consists of evaporates interbedded with some dark grey shale, off-white limestone and dolomites. The biotic components of this interval have low diversity and contain several fragments of small inflated, lenticular to biconical nummulites. This stratigraphic level has been dated broadly, as Early Eocene (Ypresian Stage) based on its stratigraphic position, since no taxa can be identified at species level. The boundary between the Early and Middle Eocene has been established based on the first occurrence of *Nummulites gizehensis* group (Fig. 4). The Middle Eocene interval, however, is represented by nummulitic and argillaceous limestone and marl. It carries numerous species of nummulites, including *Nummulites gizehensis* (Forskål), *Nummulites lyelli* d'Archiac & Haime, *Nummulites cyrenaicus* Schaub, *Nummulites beaumonti* d'Archiac & Haime, *Nummulites discorbinus* (Schlotheim) and *Nummulites bullatus* Azzaroli. This assemblage indicates Lutetian-Bartonian stages, which correspond to SBZ14-SBZ18 of Serra-Kiel *et al.* (1998). In general, the occurrences of *Nummulites gizehensis* and *Nummulites bullatus* in the lower and middle parts of the studied sections are indicative of the SBZ14-SBZ16 of Serra-Kiel *et al.* (1998). *Nummulites discorbinus* and *Nummulites beaumonti* have been also recovered from the same stratigraphic interval. The last occurrence of *Nummulites gizehensis* and first occurrences of *Nummulites lyelli* mark the contact between the Lutetian Stage (SBZ16) and Bartonian Stage (SBZ17). The boundary between Middle and Late Eocene (Bartonian/Priabonian), however, is defined by the last occurrences of *Nummulites lyelli* and *Nummulites cyrenaicus* and the first appearance of *Nummulites fabianii* (Fig. 4).

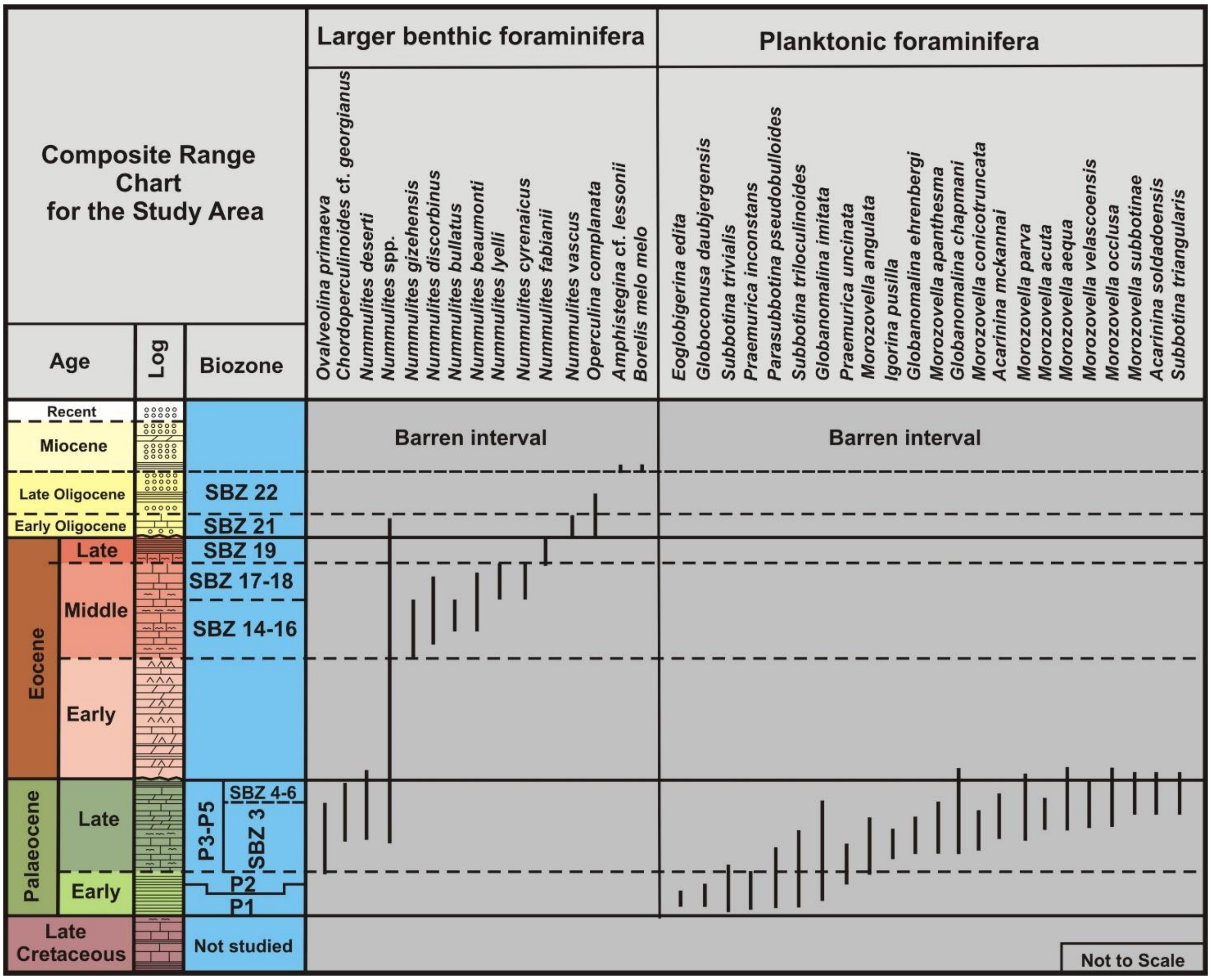

Fig. 4. Composite foraminiferal range chart for the studied area.

The Late Eocene is reduced (<90 m thick) throughout the studied subsurface sections and consists of interbedded limestone, dolomite, marl and shale. The sequence has been dated on the presence of a few medium sized and reticulate nummulites. The Eocene/Oligocene boundary is defined by the last stratigraphic occurrence of *Nummulites fabianii* and the first stratigraphic appearance of *Nummulites vascus* Joly & Leymerie (Fig. 4). This boundary (see Fig. 3) has been selected as a datum for correlation in Concession 65 since it coincides with high levels of gamma radiation on the studied logs.

3.3 Oligocene-Miocene sequence

The Oligo-Miocene sequence is up to 800 m thick in the eastern part of the studied area, and consists of sands interbedded with some limestones, dolomites, shales, and clays. The Early Oligocene interval, however, is condensed (<90 m thick) and defined based on the total range of *Nummulites vascus*. *Operculina complanata* (Defrance) is also present, but has no stratigraphic value in this time-interval. According to Cahuzac and Poignant (1997), SBZ21 can be determined based on the occurrence of *Nummulites vascus* and *Nummulites fichteli*. Although, the latter taxon has not been recovered in the current research, the studied deposits have been tentatively assigned to SBZ21. This biozone corresponds to the Rupelian Stage and can be correlated with Berggren's *et al.* (1995) P18-P21a zones. The overlying deposits have been assigned tentatively to SBZ22 (Chattian). The Lower boundary of this zone is defined based on the last occurrence of *Nummulites vascus*, while the upper boundary (Oligo-Miocene boundary) is based on the first appearance of *Borelis* sp, (Fig. 4). The washed samples from the Oligocene period yield also several small benthic foraminifera of Oligocene to Miocene age, such as *Gyroidina soldanii* (d'Orbigny), *Textularia schencki* Cushman & Valentine and *Cancris oblongus* (Williamson).

The uppermost studied deposits belong to the Miocene period due to the occurrence of few badly preserved specimens of *Borelis melo melo*, *Amphistegina* sp and *Eliphidium* cf. *crispum* (Linnaeus) (Fig. 4). The stratigraphical distribution of the genus *Borelis* ranges from Eocene to Holocene (Jones *et al.*, 2006). In the Miocene, however, the genus is largely distributed in the Mediterranean province and essentially represented by *Borelis melo melo* (Fichtel & Moll). Based on the stratigraphic data provided by Jones *et al.*, (2006), one can conclude that *Borelis melo melo* (Fichtel & Moll) is abundant from the Middle Miocene deposits of the Mediterranean region, whereas this subspecies is infrequent from the Upper Miocene in the same region (see Betzler and Schmitz, 1997). *Borelis melo melo* (Fichtel & Moll) has been observed in Libya by Berggren (1967) and Sherif (1991) from the Middle Miocene Al Khums Formation (northwest Libya), by Abdulsamad and Bu-Argoub (2006) from Ar Rajmah Group (northeast Libya) and more recently by Abdulsamad and El Zanati (2013) from the same rock units in the southeast of Benghazi City.

4. Conclusions

About 350 ditch cuttings samples from five wells were biostratigraphically examined from the Palaeocene to Miocene sequence in Concession 65, SE Sirt Basin, Libya. Study of the different foraminiferal faunae retrieved from these ditch cuttings allowed the subdivision of the Palaeocene to Miocene sequence in these five wells into different foraminiferal zones. The planktic foraminifers allowed subdividing the Palaeocene into the planktic foraminiferal zones of Berggren *et al.* (1995). The recovered larger benthic foraminifera from the Late Palaeocene to Miocene, however, were examined biostratigraphically following the shallow benthic zones (SBZ) of Cahuzac and Poignant (1997) and Serra-Kiel, *et al.* (1998).

The planktic foraminiferal taxa recovered from the Early Palaeocene interval (Danian) represent the planktic foraminiferal zones P1 and P2, whereas the Late Palaeocene (Selandian-Thanetian) foraminiferal taxa represent the planktic foraminiferal zones P3-P5 and the shallow benthic foraminiferal biozones SBZ3-SBZ6.

The Eocene sequence is represented mainly by *Nummulites gizehensis-Nummulites lyelli* group and has been ascribed to the SBZ14-SBZ16 in the Lutetian and the SBZ17-SBZ18 in the Bartonian.

The Late Eocene interval, however, has been dated based on the presence of *Nummulites fabianii* and ascribed to the SBZ 19.

The Oligocene sequence has been attributed to the SBZ 21 (Rupelian) and to the SBZ 22 (Chattian) based on *Nummulites vascus* and associated taxa. The uppermost deposits of the studied successions belong mostly to the Miocene with hardly any fossils.

Acknowledgments

We would like to express our gratitude to the management of the Exploration Division, Arabian Gulf Oil Company for providing the samples and the necessary log data as well as granting permission for publication. We are extremely grateful to the personnel of the Geology Laboratory and the postgraduate unit of the Earth Sciences Department, the University of Benghazi, especially Mr. N. Al-Selini, for processing part of the samples and for his assistance during the lab-work. Our thanks are also due to the Management of Naturalis Biodiversity Center, Leiden, The Netherlands, for the use of their facilities, including the Scanning Electron Microscope (SEM), with which all the photomicrographs in this article were taken. Last and not least, we also thank the laboratory Staff of Naturalis, especially Mr. D. van der Marel for his assistance with the SEM technical work.

References

Abdulsamad, E.O., and Bu-Argoub, F.M., (2006) 'Sedimentary Facies and Foraminifera of the Miocene Carbonates of the Ar Rajmah Group in Cyrenaica, NE- Libya', *Petroleum Research Journal*, 19, pp. 49-60. Tripoli, Libya.

Abdulsamad, E.O., Bu-Argoub, F.M., and Tmalla, A.F. (2008) 'Stratigraphic Distribution of Paleocene to Miocene Foraminifera in Concession 65, SE Sirt Basin, Libya', *Abstract (poster) to the Symposium of Geology of southern Libya, Tripoli*.

Abdulsamad, E.O., and El Zanati, S.M. (2013) 'Miocene benthic foraminifera from the Soluq area, NE Libya: biostratigraphy and environmental significance', *Journal of Mediterranean Earth Sciences*, 5, pp. 245-256. (University of Roma "La Sapienza") doi: 10.3304/JMES.2013.002.

Ahlbrandt, T. S. (2001) 'The Sirte Basin Province of Libya -Sirte-Zelten: Total Petroleum System', *U. S. Geological Survey Bulletin*, 2202-F, pp. 1-29.

Ambrose, Greg, (2000) 'The geology and hydrocarbon habitat of the Sarir Sandstone, SE Sirt Basin, Libya', *Journal of Petroleum Geology*, 23, pp. 165-192.

Berggren, W. A., (1967) Biostratigraphy and planktic foraminiferal zonation of the Tertiary System of the Sirte basin of Libya, North Africa. *In:* Brönnimann, P. & Renz, H.H. (Eds), *Proceedings of the First International Conference on Planktic Microfossils,* I: 104-120, E.J. Brill, Leiden.

Berggren, W.A., and Miller, K.G., (1988) 'Paleogene tropical planktic foraminiferal biostratigraphy and magnetobiochronology', *Micropaleontology*, 34, pp. 362-380.

Berggren, W. A., and Norris, R. D., (1993) Origin of the genus *Acarinina* and revision to Paleocene biostratigraphy: *Geological Society of America, Annual Meeting,* Abstract with Programs, Vol. 25, p. 359.

Berggren, W. A., Kent, D., Swisher, C. C., and Aubry, M. P., (1995) A revised Cenozoic geochronology and chronostratigraphy. *In:* Berggren, W.A., Kent, D. (Eds.), *Geochronology Time Scales and Global Stratigraphic Correlation*. SEPM, Special Publication, *No*. 54, pp. 134–175.

Betzler C., and Schmitz S., (1997) 'First record of *Borelis melo* and *Dendritina* sp. in the Messinian of SE Spain (Cabo de Gata, Province Almeria)', *Paläontologische Zeitschrift*, 71, pp. 211-216.

Cahuzac, B., and Poignant, A., (1997) 'Essai de biozonation de l'Oligo-Miocène dans les bassins Européens à l'aide des grands foraminifères néritiques', *Bulletin de la Société Géoleologique de France*, 168 (2), pp. 155–169.

Conant, L. C., and Goudarzi, G. H., (1967) 'Stratigraphic and tectonic framework of Libya, *American Association of Petroleum Geologists Bulletin*, 51, pp. 719-730.

Gillespie J., and Sanford, R.M. (1970) The geology of the Sarir Oilfield, Site Basin, Libya. *Proc. 7th World Petrol. Congress* 2: pp. 181-193.

Grimsdale, T. F., and Van Morkhoven, F.P.C.M. (1955) The ratio between pelagics and benthonic foraminifera as a means of estimating depth of deposition of sedimentary rocks. Proc. Fourth World Petrol. Congr., Sect. 1/D, Paper 4: pp. 473- 491.

Hallett, D. (2002) Petroleum Geology of Libya. Amsterdam; New York: Elsevier, 503 pp.

Haynes, J. R., Racey, A., Whittaker, J. E., (2010) A revision of the Early Palaeogene nummulitids (Foraminifera) from northern Oman, with implications of their classification. *In:* Whittaker, J.E., & Hart M.B., (Eds.), Micropalaeontology, Sedimentary Environments and Stratigraphy: A Tribute to Dennis Curry (1912-2001). *Geological Society of London*, pp. 2010 - 286.

Jones, R. W., Simmons, M. D., and Whittaker, J. E. (2006) 'On the stratigraphic and palaeobiogeographical significance of *Borelis melo melo* (Fichtel & Moll, 1798) and *B. melo curdica* (Reichel, 1937) (Foraminifera, Miliolida, Alveolinidae)', *Journal of Micropalaeontology,* 25, pp. 175-185.

Lewis, C.J., (1990) Sarir field. In: *American Association of Petroleum Geologists* Treatise of Petroleum Geology, Structural Traps II: pp. 253-263.

Sanford, R. M. (1970) Sarir oil field, Libya–desert Surprise, *In*: Halbouty, M.T., (Ed.). Geology of Giant Petroleum Fields: *American Association of Petroleum Geologists Memoir* 14, pp. 449-476.

Serra-Kiel, J., Hottinger, L., Caus, E., Drobne, K., Ferrandez, C.,; Jauhri, A. K., Less, G., Pavlovic, R., Pignatti, J., Samso, J. M., Schaub, H., Sirel, E., Strougo, A., Tambaru, Y., Tosquella, J. and Zakrevskaya, E. (1998) 'Larger foraminiferal biostratigraphy of the Tethyan Paleocene and Eocene', *Bulletin de la Société Géologique de France*, 169 (2), pp. 281–299.

Sherif, K. A. T. (1991) Biostratigraphy of the Miocene in Al Khums area, northwestern Libya . *In:* Salem M.J., Hammuda O.S., Eliagoubi B.A. (Eds.) *The Geology of Libya*, Elsevier, Amsterdam, pp. 1421-1455.

Tipsword, H. L., Setzer, F. M., and Smith, F.L.Jr. (1966) Interpretations of depositional environment in Gulf Coast Petroleum exploration from paleoecology and related stratigraphy. Tran. Gulf Coast Assoc. Geol. Soc., 16, pp. 119-130.

Explanation of plates 1-6

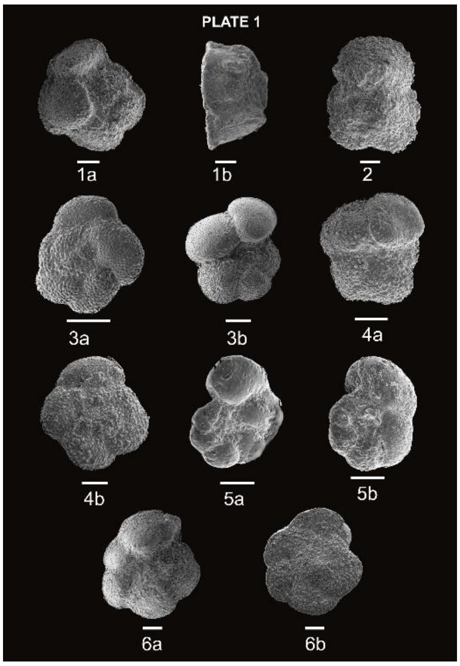

Plate 1 (Scale bars for all figures represent 100 µm; depths are in feet):
1a-1b: *Morozovella acuta* (Toulmin), 1a-umbilical view, 1b-side view - sample C13-65: 6650′
2: *Morozovella aequa* (Cushman & Renz), umbilical view - sample C19-65: 7450′
3a-3b: *Morozovella angulata* (White), 3a-Spiral view, 3b-umbilical view - sample C19-65: 7700′
4a-4b: *Morozovella apanthesma* (Loeblich & Tappan), 4a-umbilical view, 4b-spiral view - sample C19-65: 7450', 4b- sample C13-65: 6560′
5a-5b: *Globanomalina chapmani* (Parr), 5a-5b oblique Spiral views - sample C19-65: 7900′
6a-6b: *Morozovella conicotruncata* (Subbotina), 6a-umbilical view, 6b-spiral view - sample C19-65: 7450′

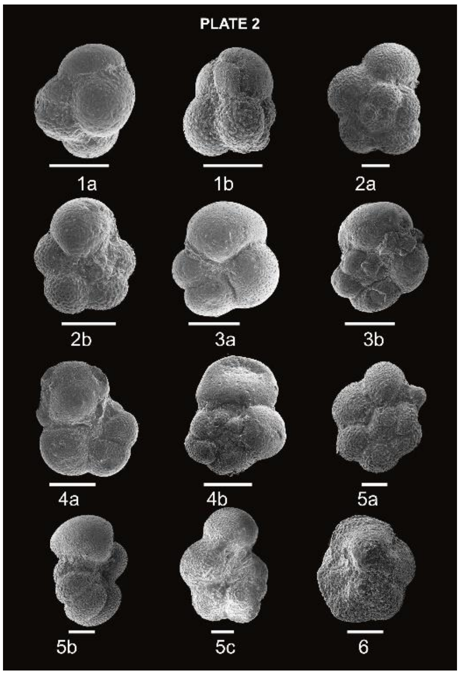

Plate 2 (Scale bars for all figures represent 100 µm; depths are in feet):
1a-1b: *Globoconusa daubjergensis* (Brönnimann), 1a-tilted umbilical view and 1b-side view of the same specimen - sample C19-65: 8010-70′
2a-2b: *Eoglobigerina edita* (Subbotina), 2a-spiral view, 2b-umbilical view - sample C19-65: 8010-70′
3a-3b: *Globanomalina imitata* (Subbotina), 3a-umbilical view - sample C19-65: 8010-70′; 3b-spiral view, sample A1-65: 6134′
4a-4b: *Globanomalina ehrenbergi* (Bolli), 4a-umbilical view - sample C19-65: 8000', 4b-spiral view, sample C19-65: 8010-70′
5a-5c: *Praemurica inconstans* (Subbotina), 5a-spiral view, 5b-side view, 5c-umbilical view - sample C19-65: 8000′
6: *Igorina pusilla* (Bolli), umbilical view, sample C19-65: 7700′

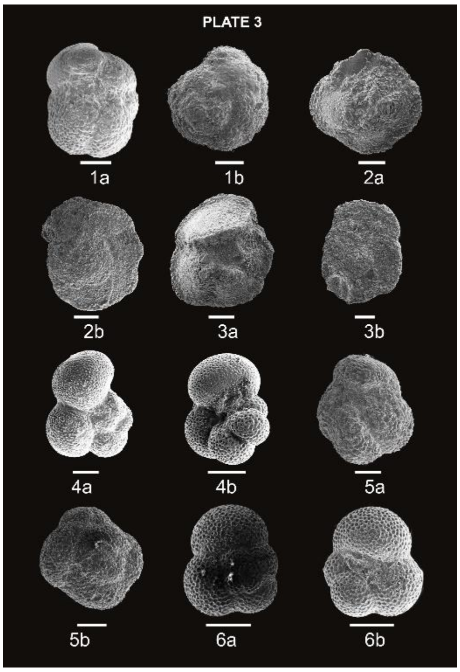

Plate 3 (Scale bars for all figures represent 100 µm; depths are in feet):
1a-1b: *Acarinina mckannai* (White), 1a-umbilical view, 1b-spiral view - sample C13-65: 7190′
2a-2b: *Morozovella occlusa* (Loeblich & Tappan), 2a-umbilical view, 2b-spiral view - sample C19-65: 7450′
3a-3b: *Morozovella parva* (Ray), 3a-umbilical view - sample C19-65: 7200', 3b-spiral view, sample C13-65: 6650′
4a-4b: *Parasubbotina pseudobulloides* (Plummer), 4a-spiral view - sample C19-65: 8000', 4b-tilted umbilical view, sample C19-65: 7550′
5a-5b: *Acarinina soldadoensis* (Brönnimann), 5a-umbilical view - sample C19-65: 7350', 5b-spiral view, sample C19- 65: 7450′
6a-6b: *Subbotina trivialis* (Subbotina), 6a-spiral view, 6b-umbilical view, sample -C19-65: 7700′

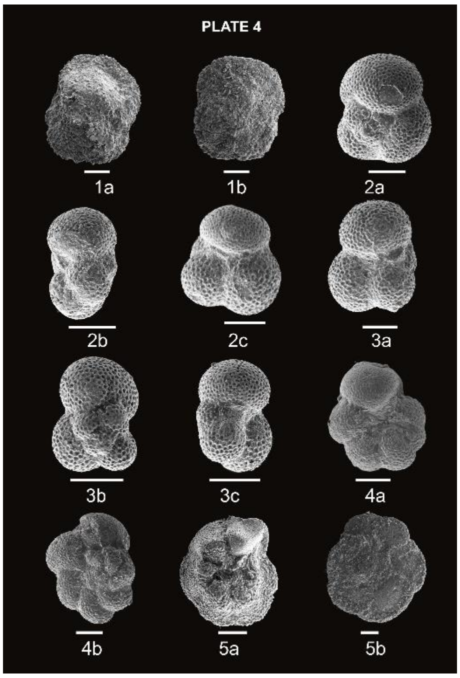

Plate 4 (Scale bars for all figures represent 100 µm; depths are in feet):
1a-1b: *Morozovella subbotinae* (Morozova), 1a-umbilical view - sample C19-65: 7350′ 1b-spiral view, sample C13-65: 6650′.
2a-2c: *Subbotina triangularis* (White), 2a- spiral view, 2b-side view, 2c-umbilical view - sample C19-65: 8010-70′.
3a-3c: *Subbotina triloculinoides* (Plummer), 3a-umbilical view, 3b-spiral view - sample C19-65: 8010-70′, 3c-side view - sample C19-65: 7300′.
4a-4b: *Praemurica uncinata* (Bolli), 4a- umbilical view, 4b-spiral view - sample C19-65: 8000′.
5a-5b: *Morozovella velascoensis* (Cushman), 5a-umbilical view, 5b-spiral view - sample C19-65: 7550′.

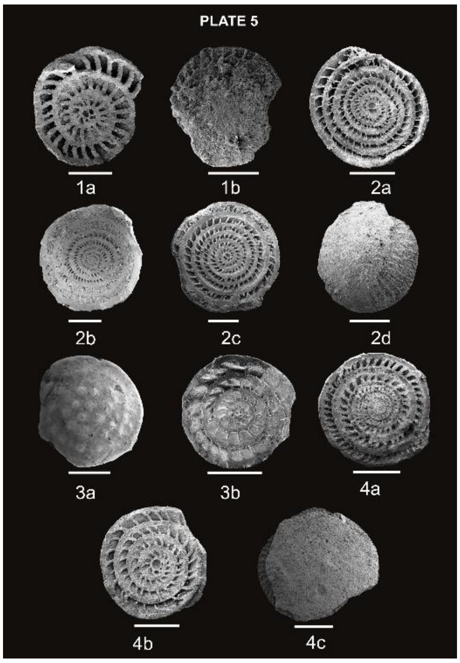

Plate 5 (Scale bars for all figures represent 1mm; depths are in feet; all sections are natural):
1a-1b: *Chordoperculinoides* cf. *georgianus* Cole & Herrick, equatorial section and surface of A-forms - sample C13-65: 6900′.
2a-2d: *Nummulites beaumonti* d' Archiac & Haime, 2a, 2c-equatorial sections of A- forms, 2b-equatorial section of B-form, 2d-surface of A-form, all from core sample A2-65: 2791-2806′
3a-3b: *Nummulites bullatus* Azzaroli, 3a- surface of A-form - sample C19-65: 3900′, 3b-equatorial section of A-form sample C19-65: 3650′.
4a-4c: *Nummulites cyrenaicus* Schaub, 4a, 4b- equatorial sections of B- and A-forms, 4c-surface of B-form, all from sample A1-65: 3527′ (core sample).

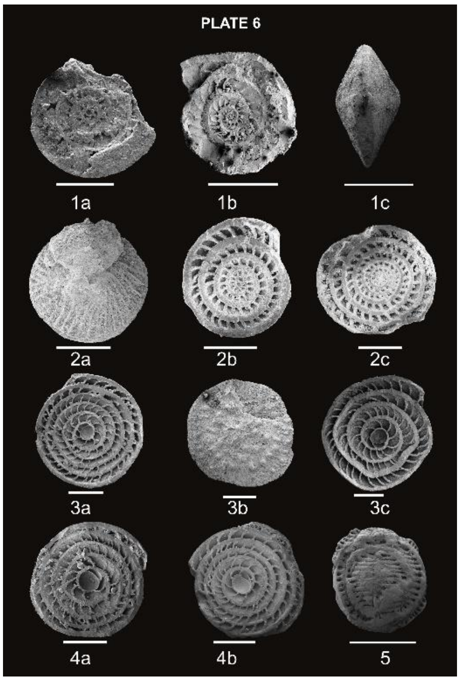

Plate 6 (Scale bars for all figures represent 1mm; depths are in feet; all sections are natural):
1a-1c: *Nummulites deserti* de la Harpe, 1a- equatorial section of A-form - sample A1-65: 6300′, 1b-equatorial section of B-form, 1c-axial view of A-form, both from sample C13-65: 6560′.
2a-2c: *Nummulites discorbinus* (Schlotheim), 2a, 2b-surface, and equatorial section of A-forms, 2c-equatorial section of B-form, all from core sample A1-65: 3593′.
3a-3c: *Nummulites gizehensis* (Forskål), 3a, 3c-equatorial sections of A-forms - sample A2-65: 3690′, 3b-surface of A-form, sample C13-65: 4400′.
4a-4b: *Nummulites lyelli* d 'Archiac & Haime, equatorial sections of A-forms - sample A2-65: 3490′.
5: *Ovalveolina primaeva* (Reichel), partly broken specimen - sample C13-65: 6700′.

Libyan Journal of Science & Technology 9:1 (2019) 53–56
The 2nd International Conference on Geosciences of Libya-GeoLibya 2 (2017), 14-16 October 2017, Benghazi-Libya

Faculty of Science - University of Benghazi
Libyan Journal of Science & Technology
journal home page: www.sc.uob.edu.ly/pages/page/77

3D Seismic to absolute acoustic impedance inversion of the Lower Devonian Tadrart Sandstone in Ghadames Basin, NW Libya

Ahmed Ali M Zeglam, Belgasem M. El-Saiti*

Department of Earth Sciences, Faculty of Science, University of Benghazi, Benghazi, Libya

Highlights
- **Improving the seismic interpretation by converting 3D post-stacked seismic data into 3D absolute acoustic impedance.**
- **Hydrocarbon detection by predicting 3D porosity from the 3D absolute acoustic impedance.**

ARTICLE INFO

Article history:
Received 01 February 2018
Revised 01 March 2018
Accepted 01 April 2018
Available online 31 March 2019

Keywords:
Seismic Inversion, Acoustic Impedance Inversion, Seismic Interpretation, Reservoir Seismic Properties, Reservoir Characterization, Rock Physics.

*Corresponding Author:
E-mail address: elsaitti@yahoo.com
B. M. El-Saiti

ABSTRACT

The aim of this study is to map 3D acoustic impedance from 3D post-stacked seismic data, and then predict 3D porosity values from the acoustic impedance results for the Lower Devonian Tadrart reservoir sandstone using seismic inversion. Theoretically, seismic inversion is the process of transforming seismic reflection data into qualitative rock properties such as acoustic impedance and porosity, which is also very important for reservoir evaluation. Seismic inversion can be performed on pre or post stacked seismic data, it can be applied when the conventional seismic interpretation may become misleading under certain conditions. Most of oil and gas companies use the seismic inversion to improve the seismic interpretation by removing the side lobes and tuning effects from seismic data, to improve the estimation of rock properties, and to increase resolution and reliability. Inversion of seismic reflection data for various lithological and petro physical attributes is broadly used for reservoir characterization and hydrocarbons detection. Rock property related attributes are easier to interpret than the seismic reflectivity, which is related to boundaries between zones of contrasting acoustic impedance properties. Broadly, the commonalities between all impedance type properties are in their relations to the values measured from the seismic traces. The fundamental problem is the lack of low-frequency information in the seismic data leading to many uncertainties in the solution. The absolute acoustic impedance inversion is the method that has been applied in this study, and it is applied in Hamra field, northwest Ghadames basin, the approach of this work by extrapolating the well logs information into the seismic properties, this is, in turn, better estimations of reservoir properties such as porosity and an additional benefit that the interpretation efficiency is greatly improved.

1. Introduction

The Lower Devonian Tadrart sandstone is the proven productive and prospective reservoir target in the study area. The application of absolute acoustic impedance inversion technique, using 3D post-stacked seismic data integrated with the borehole data. Acoustic impedance model, in turn, used to evaluate important reservoir characterizations and their implication on the petroleum entrapment.

2. Seismic Inversion Theory

Seismic inversion aims to put a spiked (earth's reflectivity) response at the geological boundaries (lithology changes) and the main reservoir characteristic interfaces. This is done by the inversion of the 3D seismic cube into 3D acoustic (or elastic) impedance cube. The link between the seismic cube and the acoustic impedance cube is the "seismic wavelet". In seismic acoustic impedance inversion, we assume that the seismic amplitudes represent a band-limited expression of the earth's reflectivity (at normal incidence), this is can be expressed by the convolution equation:

$$S(t) = r(t) * w(t)$$

For making more complicated equation by adding the noise function:

$$S(t) = r(t) * e(t) + n(t)$$

Where S(t) is the seismic trace, r(t) is the earth's reflectivity series, w(t) is the seismic wavelet, and n(t) is the noise. If we can determine the seismic wavelet then we can deconvolve it from the seismic trace to recover the earth's reflectivity series. For normal incidence, the reflectivity r(t) at a given layer boundary is determined by the contrast in acoustic impedance Z(t) between the layers and is given by:

$$r(t) = \frac{\rho_2 v_2 - \rho_1 v_1}{\rho_2 v_2 + \rho_1 v_1} = \frac{z_2 - z_1}{z_2 + z_1}$$

The Zoeppritz equations define the reflection coefficient for non-normal angles of incidence of a seismic pulse at Z(t) boundary, these equations are applied in a simplified form (e.g., Shuey,1985). By integrating r(t) we can obtain a band-limited measurement of acoustic and impedance, combining with additional information such as "low-frequency trend from well logs or seismic velocities" to obtain the absolute acoustic impedance. After getting the extracted wavelet from the 3D seismic data at all well locations, the

 ISSN 2663-1407; National Library of Libya, Legal number: 390/2018

next step is to run the low-frequency background model as part of the inversion process. Low-frequency model is also called "prior model" due to the low-pass filtering that in most cases is applied, such a prior model can be constructed by extrapolating laterally the calibrated impedance logs from well sites, then using a number of interpreted horizons as a model guide. The background geologic model provides the initial estimate of impedance values and provides constraints for subsequent updates in the internally iterative inversion procedure; one of these critical constraints includes the incorporation of these low-frequency components that are actually missing from the surface seismic data during the acquisition and/or the processing. Consequently, the background geologic model is used to control both inversion non-uniqueness and accuracy. The background model is often created from sparse well log data and seismic interpretation data using geostatistical procedures. Through geostatistics, well log information (e.g., P-wave impedance logs) is interpolated following the structure style within the project area to create the impedance volumes (Wang *et al.*, 2009).

Unfortunately, seismic acoustic impedance inversion has several limitations, the seismic frequency band is limited to about ~ 20Hz to 120Hz and the low- and high-frequency input data for inversion are missing, therefore using well log data will provide the information at these missing frequencies. Non-uniqueness of the solution is another problem, and seismic data can lead to multiple possible geologic models, which are consistent with the observations. In addition, in the inversion method itself, multiple reflections, transmission loss, geometric spreading and frequency-dependent absorption are ignored. The common way to reducing these uncertainties is to use additional information (mostly coming from well logs) which contains low and high frequencies and constrains the deviations of the solution from the initial-guess model. Therefore, the results rely on the seismic data as well as on this additional information, and on the details of the inversion methods themselves.

3. Rock Physical Properties

Rock physics is the science, which defines the relationship between measured elastic properties of rocks and reservoir properties. Accordingly, rock physics is the crucial link between geophysics, reservoir engineering and reservoir geo-mechanics. The ultimate goal of rock physics analysis is to gain insights into the physical properties of a reservoir. These can be bulk properties, or dynamic properties. A geophysical rock physic analysis uses the measured elastic properties from seismic data to generate attributes that yield information about the reservoir rocks.

Seismic reservoir properties are affected in complex ways by many factors, such as pressure, temperature, saturation, fluid type, porosity, pore type, etc. These factors are often interrelated or coupled in a way that may also change when one-factor changes. The effect of these changes on seismic data can be either additive or subtractive. As a result, investigation of the effect of varying a single parameter while fixing others becomes imperative in understanding rock physics applications to seismic interpretations. Several other sources of rock physics information that can be used to assist the analysts in understanding the study area, these other sources can be petrophysical, geophysical, and/or geological in nature. Ultimately, the more tools we use to assist in our understanding of the reservoir, the more we reduce the risk associated with an exploration/exploitation undertaking (Pelletier and Gunderson, 2005).

Rock physics modeling can help us understand the behavior of the reservoir and non-reservoir zones and correct for some of the problems encountered in well log data (Avseth *et al.*, 2001). It is the process of finding a rock physics model that is consistent with the available well data. One purpose of rock physics modelling is to allow reliable prediction and perturbation of seismic response with changes in reservoir conditions. The rock physics is part of the study area included the following steps:

1- Logs from all the wells were loaded and quality checked.

2- If there are missing sections in density log and/or sonic log, this issue can be solved using Gardner substitution based on the velocity information from the log data for all wells.

3- Geophysical acoustic impedance logs were generated from sonic and density relationship for each wells.

4- Porosity logs quality check and making sure that the porosity goes through the target of interest for all wells.

In general, when creating empirical models to describe the relationship between elastic properties and petrophysical properties using the regression function method, there are different ways of using simple regression functions. This approach can give good results within the data interval or the reservoir interval, which are used as input for the modeling, and sometimes-poor extrapolation from another data interval. The best extrapolation can be found by using an appropriate regression function. If the regression function is chosen fluid or lithology independent, then it can be proven that rock physics is consistent through the formation. This method can only work in case the relationship between elastic properties and petrophysical properties linear relationship. Figs. 1, 2 and 3 show cross plots between porosity and acoustic impedance logs using well 1, well 2, and well 3 for the Tadrart reservoir sandstone.

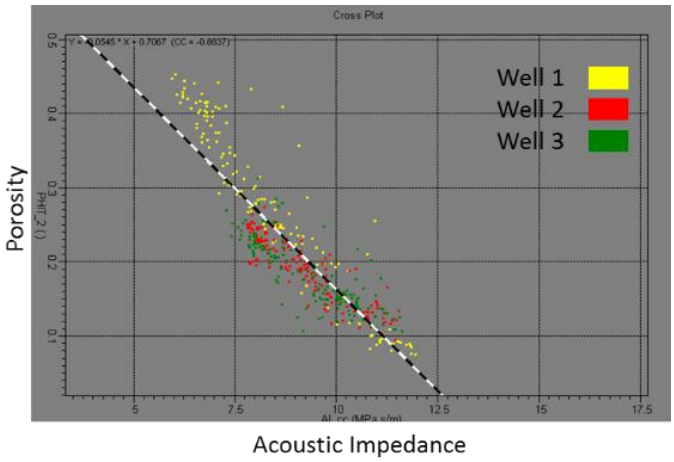

Fig. 1. Cross plot between porosity and acoustic impedance logs using the wells; well 1, well 2, and well 3, within Tadrart D1 formation, indicated a good linear relationship.

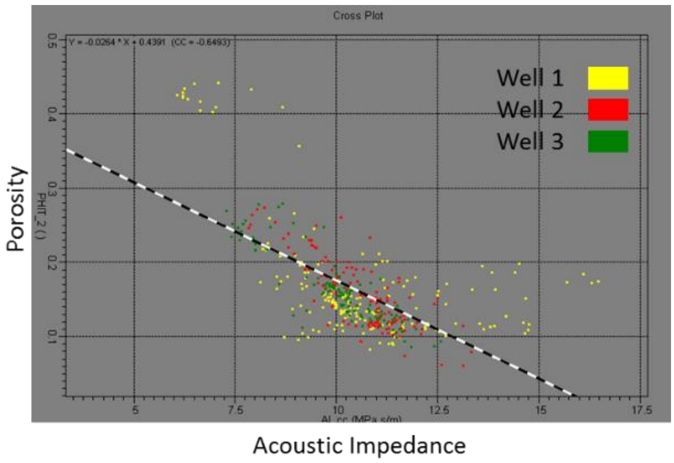

Fig. 2. Cross plot between porosity and acoustic impedance logs using the wells; well 1, well 2, and well 3, within Tadrart D2 formation, indicated a poor to good linear relationship.

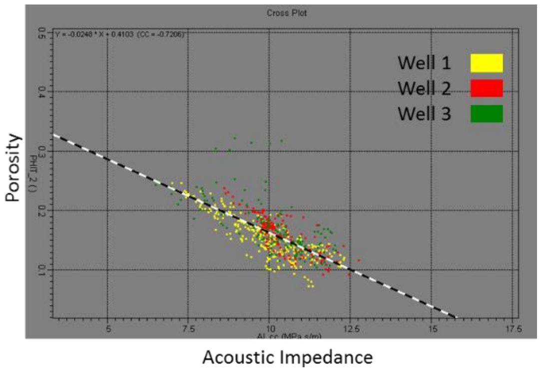

Fig. 3. Cross plot between porosity and acoustic impedance logs using the wells; well 1, well 2, and well 3, within Tadrart D3 formation, indicated a good linear relationship.

4. Inversion and Porosity Results.

High resolution of the absolute acoustic impedance inversion will reduce the uncertainty about reservoir by increasing well information and greater confidence and accuracy in modeling the reservoir. The result of acoustic impedance model achieved with high resolution when comparing it with seismic data, the inversion resolution is increased and the interpretation of data are improved. The acoustic impedance model is related to the important physical properties of the reservoir target. Figs 4, 5, and 6 showing modeling of the porosity distribution from seismic data is achieved through a strong correlation between the acoustic impedance model and the porosity model of the Tadrart reservoir sandstone, this can be used as a guide in reducing drilling risk in some interesting drilling locations.

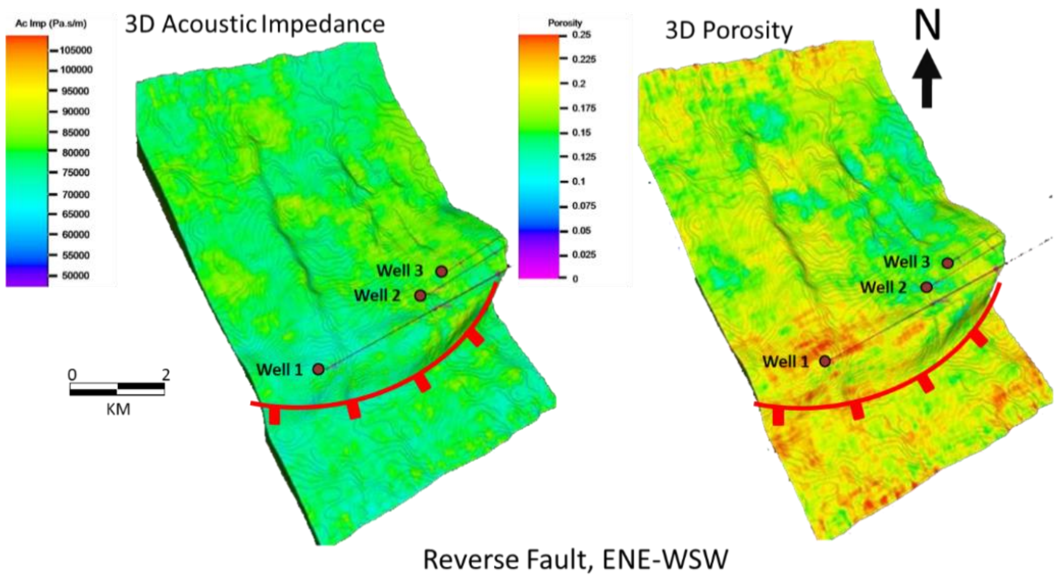

Fig. 4. Comparisons between 3D acoustic impedance model (left) and 3D porosity model (right), for Tadrart D1 formation.

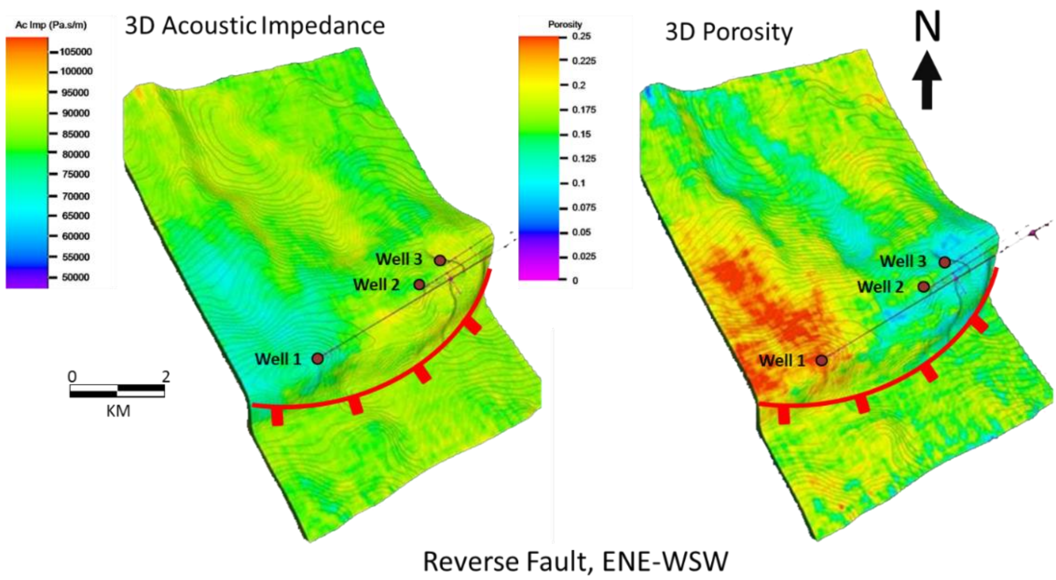

Fig. 5. Comparisons between 3D acoustic impedance model (left) and 3D porosity model (right), for Tadrart D2 formation.

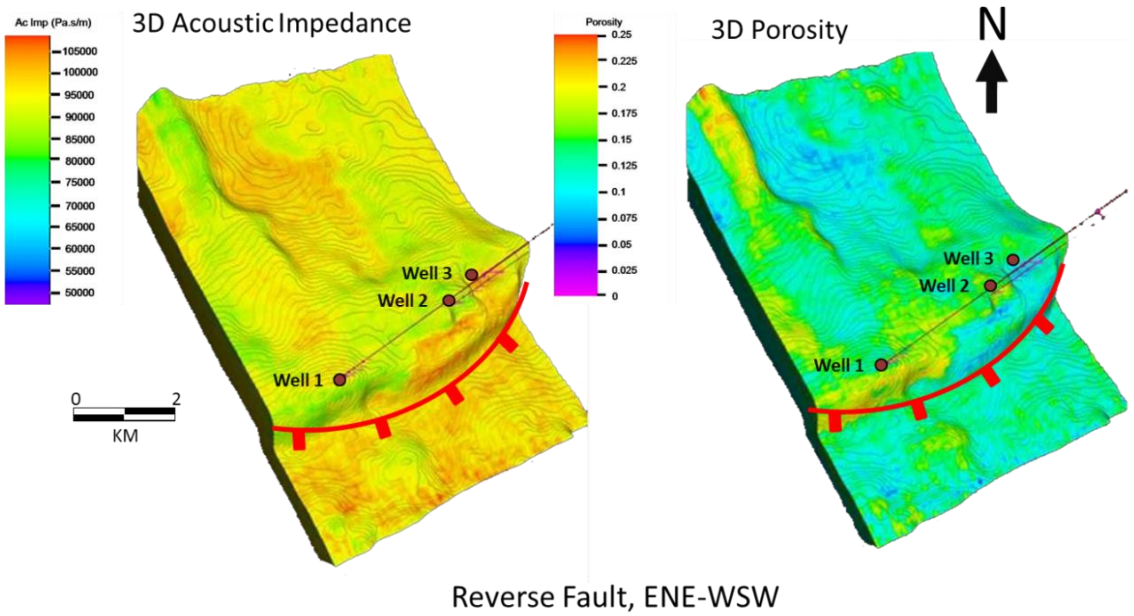

Fig. 6. Comparisons between 3D acoustic impedance model (left) and 3D porosity model (right), for Tadrart D3 formation.

5. Discussion

The ultimate goals of absolute acoustic seismic inversion are to identify reservoirs, delineate them, and determine the distribution of their relevant physical properties, which will provide an early determination of the reservoir economic potential.

The resulted acoustic impedance model captures the main characteristics of all well acoustic impedance logs, and comparing it with the acoustic impedance log at the well 1 is highly correlated with small quantitative deviations. The model was used to predict the acoustic impedance results in the two other wells; well 2, and well 3, the prediction deviation for them are also similar to well 1. The acoustic impedance models for the reservoir target of Tadrart formation tops at all well location generally show a good match with the acoustic impedance log, except in some intervals of Tadrart formation, where the match somehow was not clear enough. This could be related to the seismic resolution in these intervals or the complexity of the physical properties that could not be modeled.

The resulted porosity model captures the main characteristics at well 1, although not with the same precision at the other two wells. The variation in the porosity and acoustic impedance well logs are much larger and less smooth in the transitions. The porosity model shows difficulty in the continuity in some locations is mainly because the model is based on the seismic data, which have lower resolution than the well logs. Actually, the porosity values are smoothed and averaged out in the model compared to the porosity at the well.

The relationship between acoustic impedance and porosity is lithology dependent and can be approximated as a linear relationship for each lithological unit, this means that to apply a non-varying linear function to the acoustic impedance results, derived from seismic data, to estimate porosity, is only valid for a uniform geology. Porosity – acoustic impedance equations were derived for: Tadrart D1, Tadrart D2, and Tadrart D3 formations separately, which showed a strong empirical relationship existed between acoustic impedance and porosity distribution.

The porosity maps had a significant impact on defining prospective drilling locations, increased priority was given in some locations corresponding to the higher porosity zones (~15% to 25%) and in some locations the porosity was decreased (bellow to 10%), with these results, well placement can be designed to maximize contact with high porosity zones in these formations. Finding these high porosity zones within the Tadrart reservoir sandstone is very important for oil entrapment taking in account the major fault structure trend ENE-WSW that is associated with good trapping mechanism.

Regarding all the acoustic impedance and the porosity results, it is highly recommended to drill a well within these high porosity anomalies especially around the well 1, however, the Tadrart-D2, and Tadrart-D3 are the most interested zones to be drilled in order to increase the oil production of the Tadrart sandstone.

Acknowledgments

I would like to thank Dr. Belgasem El-Saiti for his scientific guidance and moral support. I really appreciate his constructive critical comments and the brainstorming discussions, which eventually led to my progress. My special thanks extend to the exploration management of the Arabian Gulf Oil Company (AGOCO) for the release of data and information needed for this research, and I would like to thank Schlumberger for providing me the tools and the experience using one of the finest software in oil markets.

References

Avseth, P., Mukerji, T., Jorstad, A., Mavko, G., and Veggeland, T., (2001) 'Seismic reservoir mapping from 3-D AVO in a North Sea turbidite system', *Geophysics, Soc. of Expl. Geophys.*, 66, pp. 1157-1176.

Pelletier, H., and Gunderson, J. (2005) 'Application of rock physics to an exploration play: A carbonate case study from the Brazeau River 3D', *TLE 24*, 5, pp. 516-519.

Shuey, R. T. (1985) 'A simplification of the Zoeppritz equations', *Geophysics*, 50, pp. 609-614.

Wang, J., Jayr, S., and Dopkin, D. (2009) 'Geologic modeling for seismic inversion', *Hart's E & P*, 82(2), pp. 33-34.

Libyan Journal of Science & Technology 9:1 (2019) 57–65
The 2nd International Conference on Geosciences of Libya-GeoLibya 2 (2017), 14-16 October 2017, Benghazi-Libya

Faculty of Science - University of Benghazi
Libyan Journal of Science & Technology
journal home page: www.sc.uob.edu.ly/pages/page/77

Utilization of seismic attributes for structural pattern detection In Bualawn, Dor Mansour fields, Western Sirt Basin, Libya.

Mohammed N. El-farsi[a,*], Saad M. El-Shari[b]

[a]*Department of Exploration, AGOCO, Benghazi, Libya*
[b]*Department of Earth Science, Benghazi University, Libya*

Highlights

- **Conjugate growth faults in NW-SE and NE-SW direction, dipping toward SW with antithetic faults dipping in opposite direction to the growth faults and other minor faults were identified manually and then tested by discontinuity attributes.**
- **Fault system is represented by a fracture system comprising long en echelon seismic faults and several discontinuities. This system of en echelon faults was initiated by left-lateral wrenching movements. This wrenching system has been identified by negative and positive flower structure along the releasing and restraining bends.**
- **A periodic strike-slip movement along deep seated basement faults has developed many structural features, such as horst-graben styles, which is the orientation of the transtensional movements linked to the Upper Cretaceous Succession.**

ARTICLE INFO

Article history:
Received 01 February 2018
Revised 22 April 2018
Accepted 29 April 2018
Available online 31 March 2019

Keywords:
Seismic cube; Tectonic evolution; Conjugate faults; Bualawn, Dor Mansour fields; Seismic attribute analysis.

*Corresponding Author:
E-mail address: m.alfarsi@yahoo.com
M. N. El-farsi

ABSTRACT

An integrated approach to the study of fault patterns carried out in the complex geological structures of Bualawn, Dor Mansour fields by using multiple seismic attributes of 3-D seismic data. Each type of geological structure event usually generates a unique seismic signature that can be recognized and identified. This paper highlights the practical importance of analyze integrated attributes and interpret them within the context of an appropriate structural deformation. Many of discontinuity attributes such as variance, 3DEE (3D edge enhancement), ant tracking, chaos and structure smoothing have been selected to delineate fault styles and their displacement effectively, which cannot be fully delineated using seismic amplitude data. Conjugate growth faults in NW-SE and NE-SW direction, dipping toward SW with antithetic faults dipping in opposite direction to the growth faults and other minor faults. The faults were identified manually and then tested by discontinuity attributes. Fault system is represented by a fracture system comprising long en echelon seismic faults and several discontinuities. This system of en echelon faults was initiated by left-lateral wrenching movements. This wrenching system has been identified by negative and positive flower structure along the releasing and restraining bends. The current understanding that these faults are strike-slip faults despite the absence of extensive horizontal displacements along them as shown on different time slices. A periodic strike-slip movement along deep-seated basement faults have developed many structural features, such as horst-graben styles, which is the orientation of the transtensional movements linked to the Upper Cretaceous Succession.

1. Introduction

The interpretation of faults in any seismic interpretation process has significant importance during the exploration. Faults are important in trapping hydrocarbon into accumulation for drilling. The identifying and mapping of fault structures often help in the determination of the size, geometry and the level of compartmentalization of hydrocarbon reservoirs (Jibrin, 2009). Fault interpretation is an important component in determining the structural information in the Bualwan, Dor Mansour fields to understand the impact of regional stress during its evolutionary history. The conventional way of interpreting fault is achieved by manual picking of fault on a 3D seismic volume. It is most times not suitable for using these approaches to interpret fault since sometimes these faults are not seen clearly, due to the presence of noise.

Seismic attributes provide a quick way to visualize the trends of faults, which are hard to see or most times not visible on a different conventional seismic sections. Seismic attributes defined as all the information obtained from seismic data, either by direct measurements or by logical or experience based reasoning (Liner *et al.*, 2004). In this paper, we discuss the use of volumetric attributes such as structural smoothing, chaos, variance attributes, and 3D edge enhancement (3DEE) on 3D seismic data. The information from different seismic attributes is used to form fault geometry to interpret the structural pattern to examine the relationship between observed fault kinematics (fault polygon) and tectonic evolution, to try understanding important role of strike-slip fault system in the structural configuration and can generally be used to optimize well locations as prospect identification.

1.1 Location of Study Area

The area under investigation is the Bualawn Dor Mansour Fields located in the central part of west of Sirt Basin, Its cover an area about 450 Km^2, which is located between (latitude; 28° 30' and 28° 35' north, and longitude; 18° 35' and 18° 45' east) (Fig. 1A).

 ISSN 2663-1407; National Library of Libya, Legal number: 390/2018

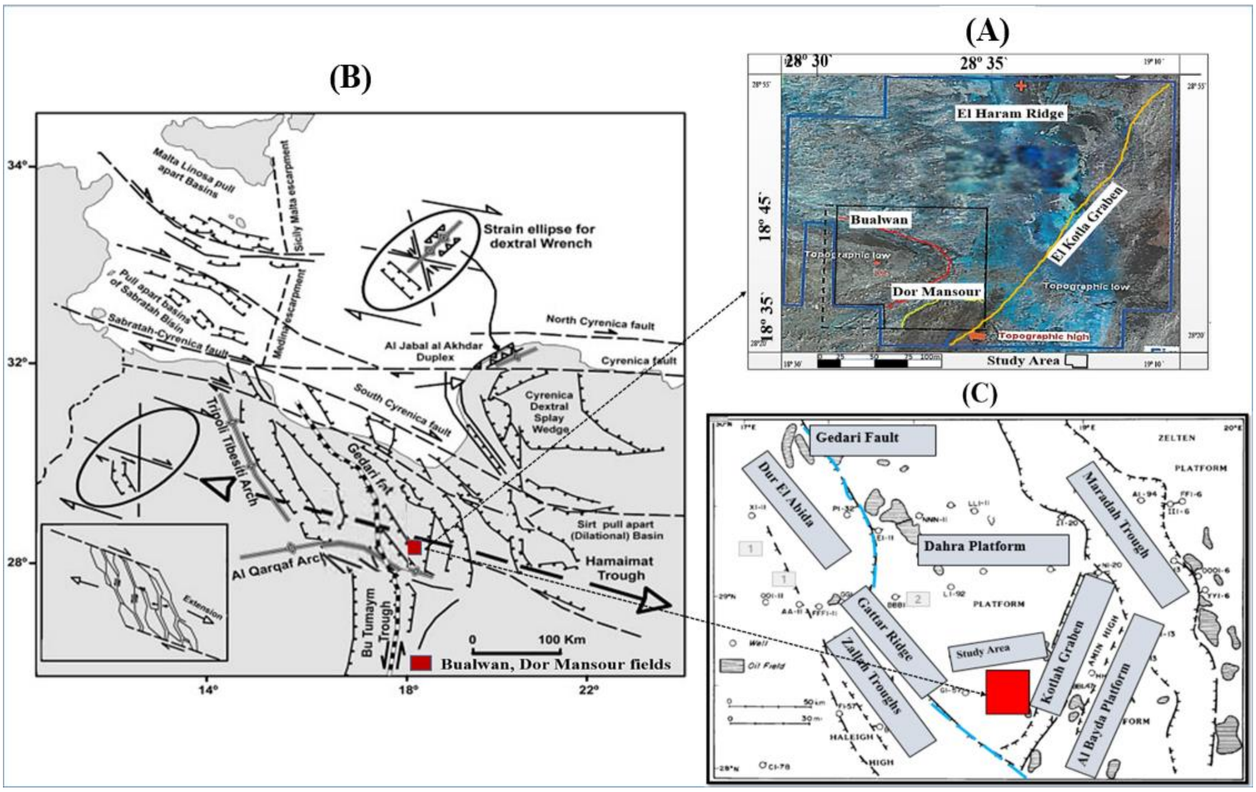

Fig. 1. (A) Tectonic interpretation of Sirt rift complex (Anketell, 1996), (B) Satellite image shows boundary and topography of the study area Bualwan, Dor Mansour Fields and (C) structural elements within study area (Gumati and Kanes 1985).

2. Geologic and tectonic setting

The structural pattern of the Sirt Basin being a rift type has evolved by strike-slip tectonics, which is originates from the major regional right lateral movement along the Sahara Cyrenaica Fault Zone (SCF) related to the opening of the Atlantic Ocean (Anketell, 1996), which is divided the basin into Horsts and Grabens during the Early Cretaceous period (Fig. 1). Consequently, this has in turn to varying degrees impacted on the attitude of the overlying formations (Abadi, 2002).

This rift basin of the Early Cretaceous has evolved Pre-rift sediments (Paleozoic-Triassic) NNE-SSW trend, followed by Upper Cretaceous Syn-rift basin, subdivided into three stages which are; began with continental-marine siliclastic rocks, to marine siliclastics and carbonate rocks and finally continental siliclastic strata NW-SE trend. The third cycle is Post-rift basin fill, deposition characterized by Carbonate and evaporate strata NNW-SSE (Roohi, 1996). In the Bualwan, Dor Mansour fields syn-depositional structures are prevalent and characterize the nature of rift subsidence.

2.1 Major impact of structural elements in the study area

The study area is located in the southwestern part of Dahra Platform, where it occupies a 40,000-km^2 area. Bounded by Dur El Abida and Zallah Troughsto the west, which is separated by Gedari Fault Zone (GFZ). Gedari Fault is trending NNE-SSW, which provide a sense of relative down throw across the fault zone (Jerzykiewicz, *et al*., 2002). On the southwest margin, the Gattar Ridge is formed by down faulting to the WSW, and by the Maradah Trough to the east, and is bounded on the south by the NNE-SSW trending Kotlath Graben, which separates it from Al Bayda Platform (Fig. 1C).

2.2 Evolution of regional stress regime

A multi-phase subsidence from the Cretaceous to recent periods in respect to the changes of regional stress, a combined strike-slip movement along SCFZ and normal extension mechanism along has been occurred. The initiation of rift oblique basement lineaments during extension can yield geometries similar to those formed during strike-slip (transtensional) movement. Understanding the variation between the two structural styles and their stress regime is important (Morley *et al*., 2004).

3. 3 D Seismic Data and Attributes conditions

The 3D seismic data volume imported to Petrel Software 2015, contains 500 inline and 600 crosslines, where inputted seismic was zero-phased. Seismic attributes are often sensitive to noise present in seismic data. It is advisable to run a spatial filtering filter to remove the noise while retaining the geometrical details. This can be achieved by applying structural smoothing to reduce background noise and to improve the spatial continuity of the seismic signal. Fig. 2 shows the raw data before and after the application of structural smoothing, it can be seen that the data quality has been enhanced, a better result since the faults are more pronounced in the data.

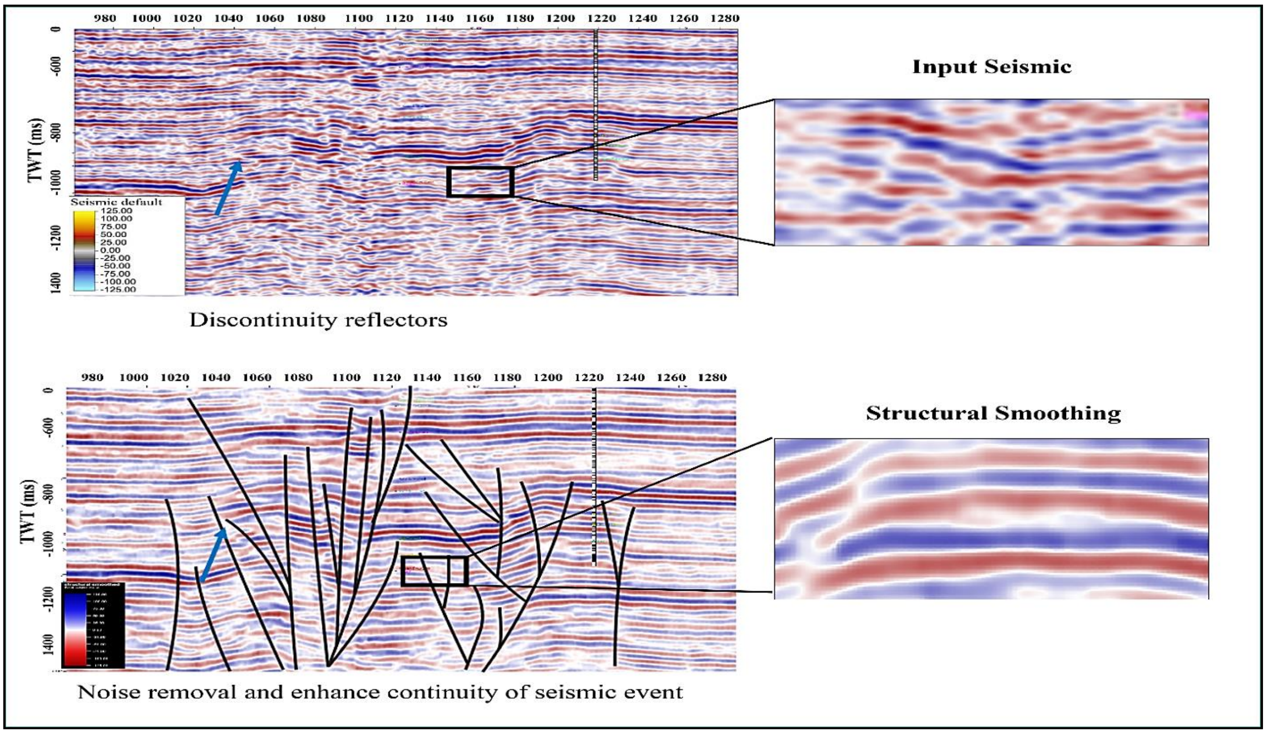

Fig. 2. Structural smoothing attribute reduce noise effects and enhance the quality.

3.1 Complex seismic trace

The Hilbert transform is used to calculate attributes in seismic interpretation includes amplitude, phase and frequency instantaneously (Hardage, 2010). The recognition of the recorded signal representing as the kinetic portion of the energy flux. Hilbert transform programs used to compute the potential component from its kinetic part, then realizing the potential component for extracting useful instantaneous information, which made possible practical and economical computation of all of the complex trace attributes.

The complex trace z (t) is comprised of the real seismic trace x (t) and an imaginary seismic trace y (t). The imaginary trace y (t) is calculated using the Hilbert Transform to apply a 90 degrees phase shift to every sinusoidal component of a signal (Fig. 3). At any time on this trace, a vector a (t) can be calculated that extends perpendicularly away from the time axis to intercept z(t) from this point, instantaneous amplitude, instantaneous phase, and instantaneous frequency can be calculated.

4. Automatic fault extraction technique/ant tracking

In this study, ant tracking used as seeds to interpret areas with discontinuity, to deliver automatic fault extraction process for the models. Generating ant track volume starts by preconditioning the seismic volume, as following steps:

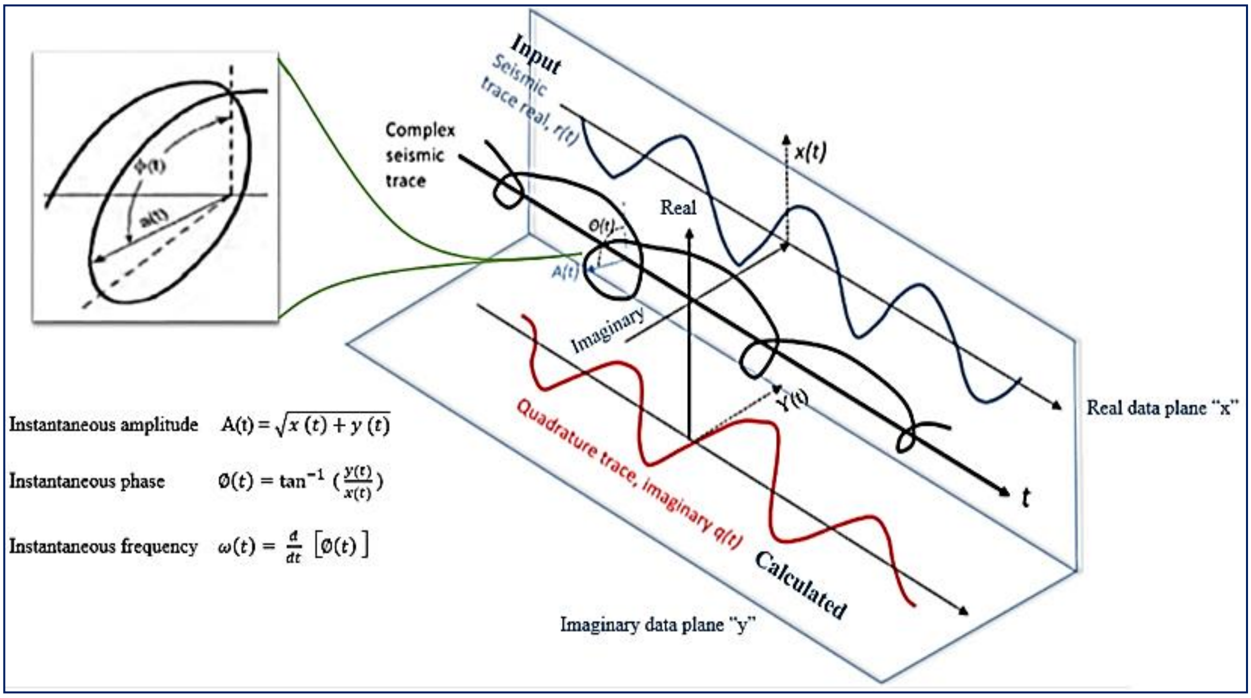

Fig. 3. Calculate instantaneous seismic attributes from the complex seismic trace (modify after Hardage, 2010).

4.1 Attribute Segmentation

Segmentation techniques are used to isolate or decompose seismic sections into meaningful of the desired object or region. The process subdivided an image into its constituent parts. Quantitative measurement of object features allows classification and display of the attribute image.

Cropped used to isolate specific depths interval include Upper Cretaceous succession ranging from 600 ms to 1200 ms entire seismic volumes (Fig. 4). To all extra advantage of speed in carrying out interpretation by minimizing the size of the store to be much easier and quicker, and to validate properties of the sub volume before making general applications. Attribute analysis such as ant track process of fault extraction cropped at specific target zones to pre-test before final parameter application to the whole seismic volume. The time taken for this attribute to run completely depends on the number of faults in the data, and the parameters used.

4.2 Attribute collection

The effective implementation of the attributes can be achieved by collecting two or more kind of attribute with each other. In such a faulted area, we used, structural smoothening and Chaos attribute, because these attributes are sensitive to faults, so these attributes were used as input data to run the ant attribute separately to see faults clearly that where difficult to display on the dataset.

4.2.1 Structural Smoothing

Smoothing attribute played an important role to understand structure revolution and their effects in the sediment deposits by delineating features in terms of horizons and faults, extending of faults in the deeper depth with different intensities and styles, reflect activity tectonic deformation.

4.2.2 Chaos Attribute

The study used chaos attribute to distinguish lithology variation based on different sediment facies, Upper Cretaceous marine deposits includes dolomite, limestone and shale, can be either in continuity or discontinuity bed. As shown in Fig. 5 uncolored values indicate minimum chaoticness correspond to continuity, and zones of maximum chaoticness indicate discontinuity of reflector character, which forms a basis to detect faults for automatic extraction.

4.3 Filters and Fault patches

Stereo net used to provide orientation filters for the ant agents, which places restriction to the azimuths and dips (Fig. 6) that the agents would allow for searching the seismic in lines and crosslines. Select aggressive mode, which is applied to detect discontinuities. Create fault patches, which gives information to the fault details as to their trends/nature and provides a much faster structural overview for interpretation (Fig. 7).

5. Manual fault interpretation

The fault picked manually starts by assigned fault segments picking on inline sections of seismic with the trace appearing on the corresponding cross lines, within the Upper Cretaceous succession into a basement from 600 ms to 1400 ms. Many of the faults were identified and interpreted as fault sticks then converted to fault polygon. These represent line data of the interpreted faults and their geometry, some extending through the extent of the field known as major regional growth faults; few flank faults appearing on few of the lines (Fig. 8).

5.1 3D Edge Enhancement (3DEE)

Applied 3DEE attribute helped to increase the number of faults and fractures have been identified and further enhance their resolution. This makes the workload easier to get effective fault interpretation. 3DEE in In line 1040 (Fig. 9) detected the tilted fault blocks related to extension normal fault with strike-slip, produce negative flower structure below TWT 600 ms because of the Cretaceous rift, which ends in Paleocene.

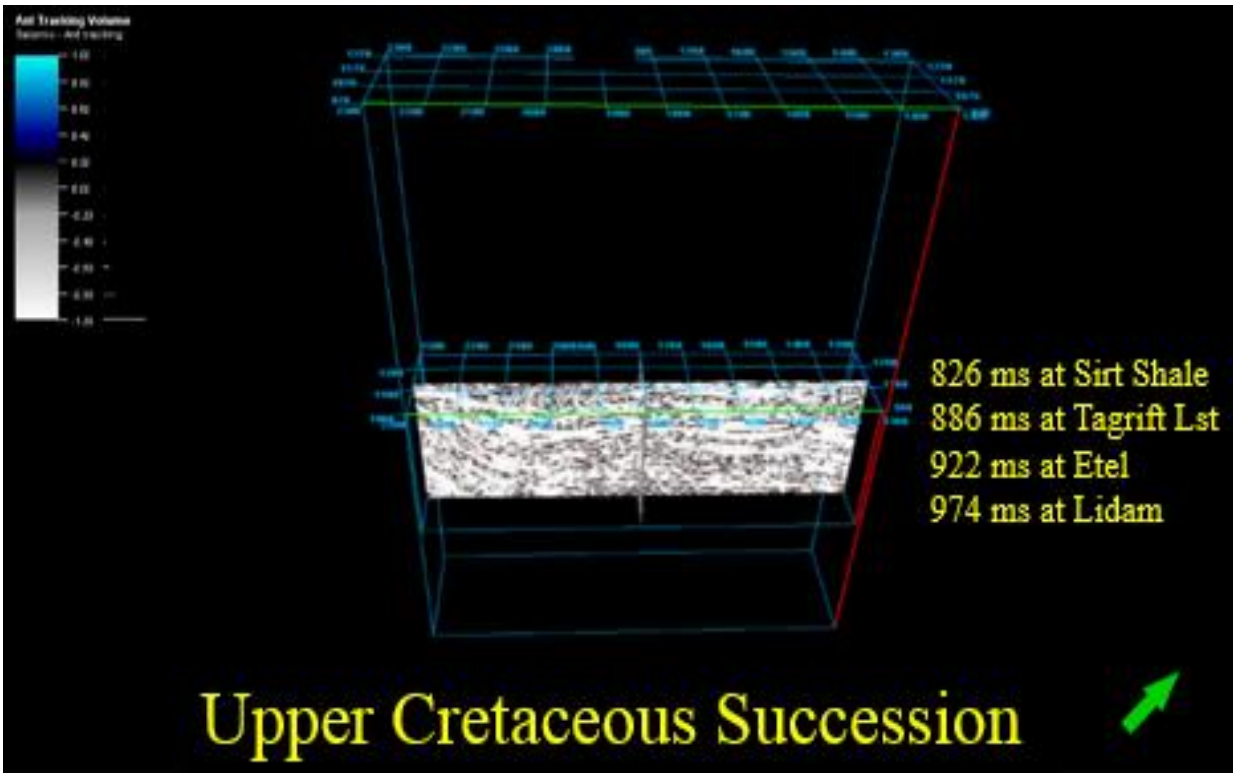

Fig. 4. Creation of a cropped volume of the active seismic cube and interactively use handles to manipulate size and shape zone of interest for ant track process and visualization.

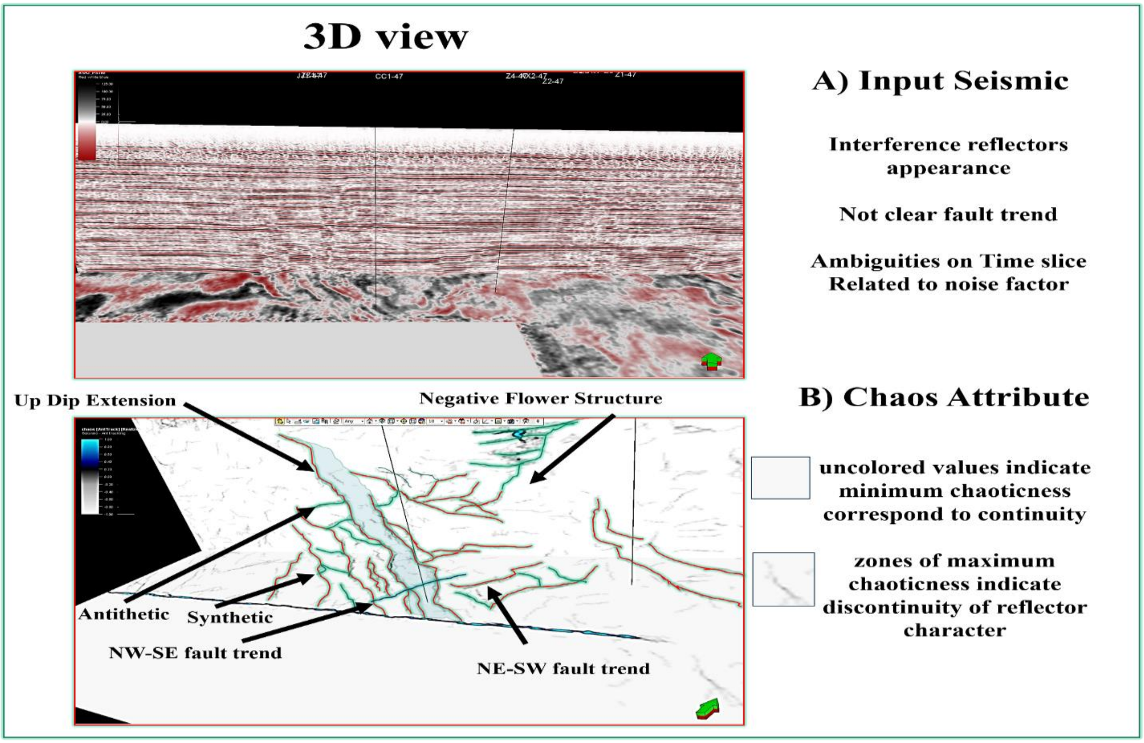

Fig. 5. 3D view display inline crossed by time slice, (A) original seismic (B) chaos attribute.

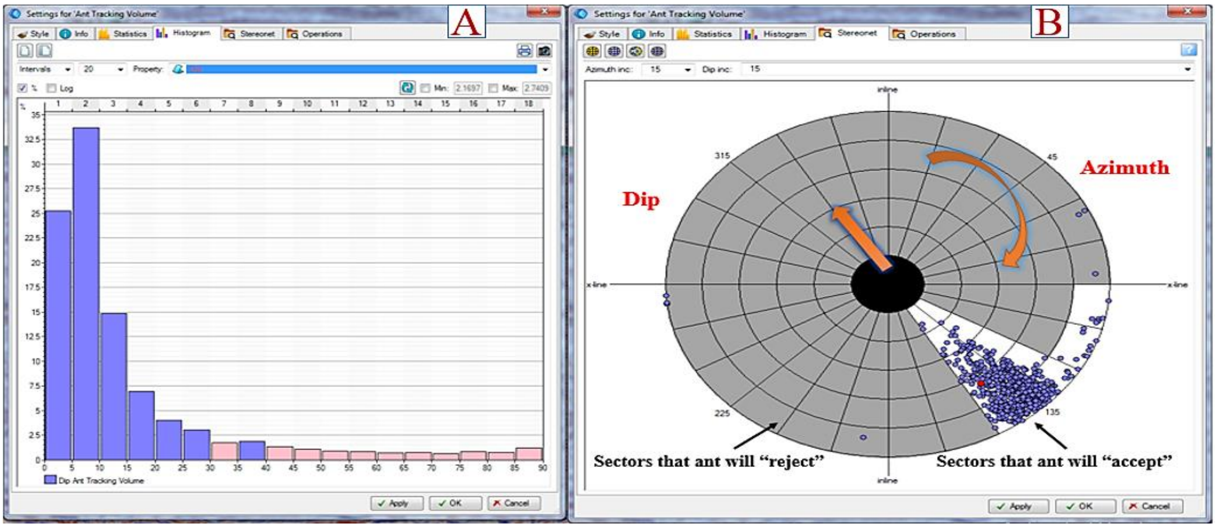

Fig. 6. Frame (a) shows the ant parameter with ant mode, ant track deviation, ant step size. Frame (b) shows the stereo net sectors of the dip and azimuth with the seismic inline/cross lines.

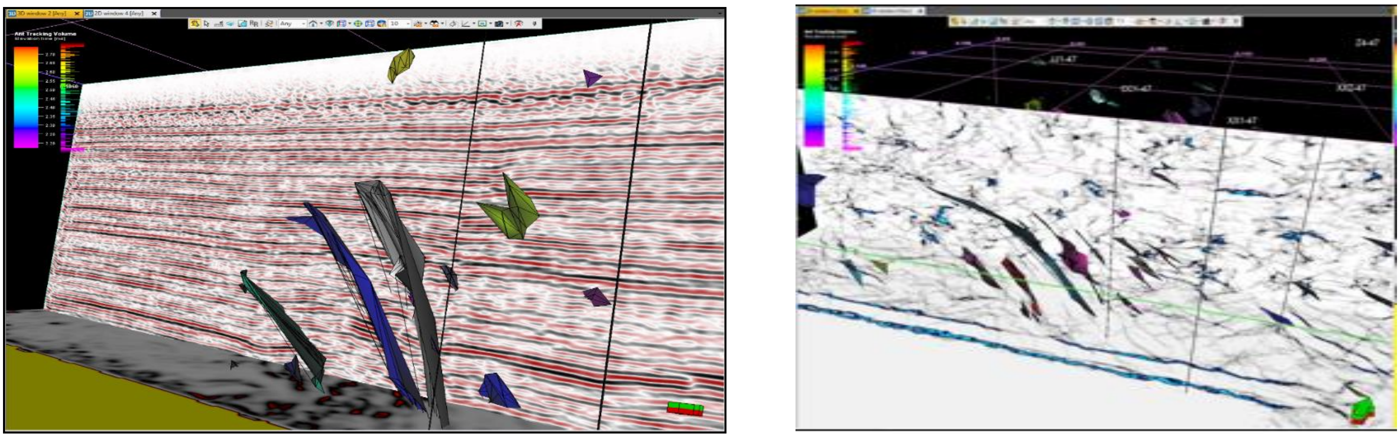

Fig. 7. (A) Fault patches generated with a cropped seismic section of the whole seismic volume. (B) Extracted fault patches with the chaos attribute within the cropped seismic section.

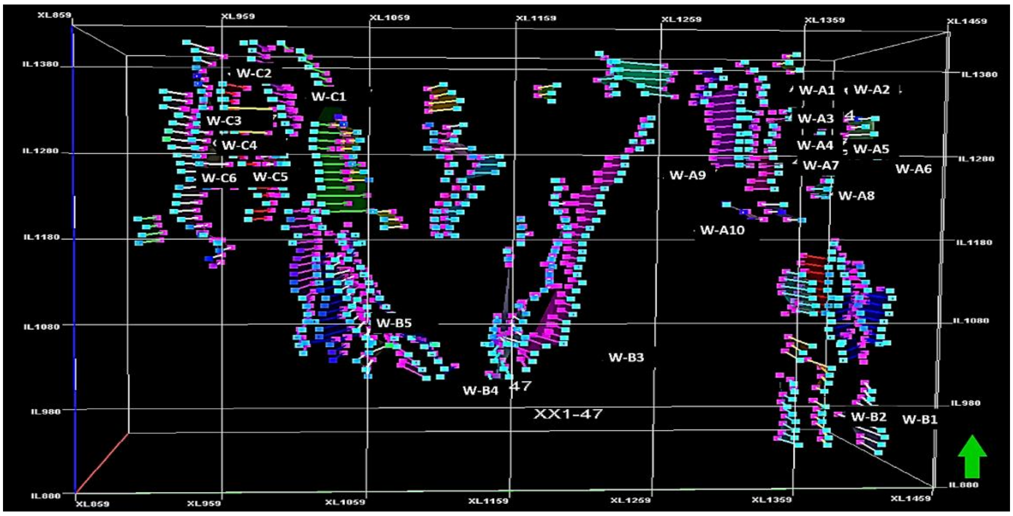

Fig. 8. Fault sticks show main fault segments.

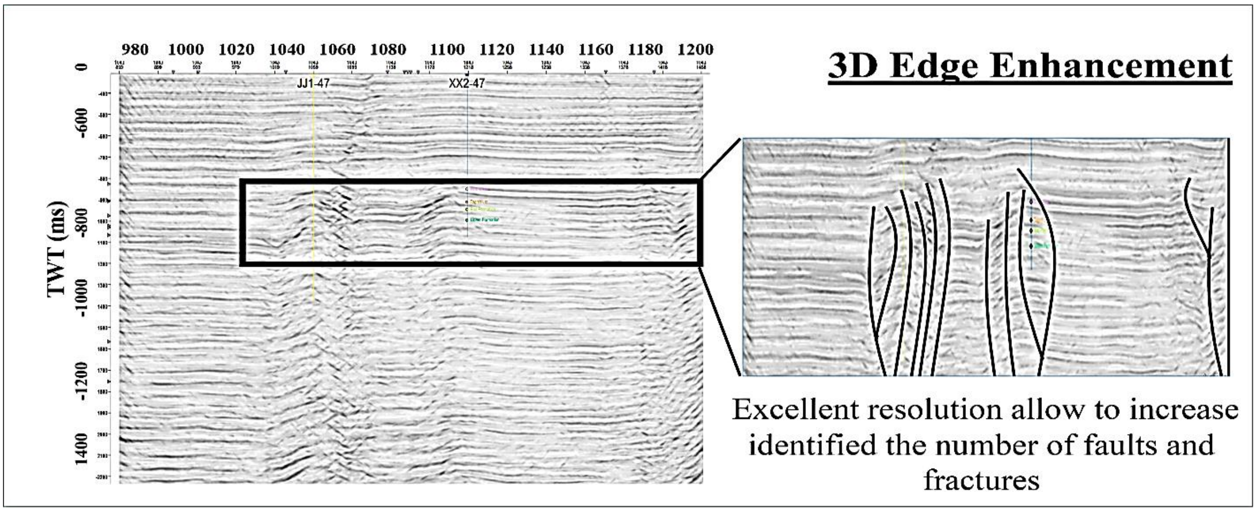

Fig. 9. Shows 3D Edge Enhancement attribute.

5.2 Structural architecture

The internal structure of the investigation area have been studied along two seismic profiles AA' and BB" as shown in the Lidam Time structure map (Fig. 10A). The study delineates the along-dip and across-strike variations in the distributions and thicknesses of the stratigraphic units, using the well-recognized seismic interfaces, and map the fault geometries and patterns affecting the stratigraphy at depth.

5.2.1 Profile A-A'

Inline1040 seismic profile in the southern part of the study area (Fig. 10) represents major faults have divergent style showing a negative flower structure of strike-slip fault. However, produce a pull apart opening in E-W blocks with opposite up thrown horst structure trending to NW-SE, steeply dipping in southwestern part as distinctive depression, and to NE-SW dipping in the northwest as a subsidence in the north-central part between to master fault, which was related to the extension, accumulate sediment load, and reactivation in Paleocene period. These two faults intersect in the basement at nearly 1200 ms, with high angle faults that bound horsts and grabens, which is represent extension related fragmentation. The second is low-angle detachments faults with associated basement (Fig. 10B). Both types of faults are related to the development of two superimposed stress fields, one related to tectonic and the other to gravitational collapse. The NW-SE faults that are parallel to the major structural trend of the basin controlled the rate of rifting and subsidence. Whereas the NE-SW structure modifies the pattern formed by the previous system to form the block structures.

Geoseismic model speculative possible propagation of secondary faults above major faulting resulting in horst and grabens and half-grabens, these secondary faults have parallel and sub vertical geometry influenced on sedimentary arrangement. Changes of stress on both side of fault gravitational sliding in transtesional stress to the SW, and contracted vertical and lateral duplexing in the transpressional stress to the NW and NE as triangle uplifted shape, this reflects changing in the tectonic event, because of strike-slip fault system corresponds to ancient deep fault related to basement.

5.2.2 Profile B-B'

Inline 1260 seismic profile goes through several structural domains. In the west of the profile, a mild structural high in the pre-Cambrian basement has been observed, above which the seismic reflectors are displaced by positive flower structure. In the mid-section of the profile, all formation and member boundaries display downward sagging, and the formation thicknesses increase, particularly that of Upper Cretaceous Formations. These observations occurred in this part of the basin during the Upper Cretaceous. In the western end of the profile, it is suggested that a major episode of subsidence might be basement beneath the sedimentary strata (Fig. 10C). A series of high angle, west reverse faults and fault-propagation folds, interpret these reverse faults and the associated asymmetrical folds as transpressional structures, which helped create the Uplift within the field. Diminishing effects of reverse faulting and folding stratigraphically upwards in the Upper Cretaceous (the Sirt Shale Formation) sedimentary units indicate that the main episode of transpressional deformation was completed by the Santonian age.

5.3 Variance Attribute

In order to test the accuracy of manually interpreted faults represented by fault sticks. Variance has the advantage to reveal the discontinuities, so in this study variance used as a structural guide by make the comparison. An overlay of variance detection with the manual seismic interpretation sticks and polygon showed excellent agreement between variance attribute showing fault highlighted by the darkest regions and manual fault interpretation displayed by fault polygon. Using variance seismic attribute maps on 3D seismic data at different time depths in order to delineate the fault and fold patterns of specific time frames in plan views.

The interpreted map (right) and its trace (left)(Fig. 11) of the Sirt Shale Formation at a time depth of 826 millisecond show the linear geometry of the NW-NE master fault with a left bend (releasing bend) along its strike and the distribution of en echelon normal faults in its hanging wall. The orientation of these en echelon faults (closely-spaced, parallel or subparallel, overlapping or step-like minor faults) is compatible with the main strike of extensional normal faults. Tagrift, Etel and Lidam formations at a time depth of 886, 922, 974 millisecond respectively, at this higher structural level in the study area show geometry of the NW Fault, which subdivided into two uplifted closure separated by constraining trough in the NW, having a left-bend along its strike. The occurrence of the en echelon normal faults associated with both the NW Fault systems indicates that transtensional deformation continued to affect the Cretaceous deposits in the North Sag (Fig. 10A). The NE-SW fault system has a major left-bend (restraining bend), where transpressional deformation produced en echelon fold trains oblique to the general orientation of the shear couple. The orientation of these en echelon faults with the main strike of extensional normal faults are consistent with the transpressional deformation patterns on seismic profiles B-B' (Fig. 10C). Strike-slip activity indicates that locally developed transpressional and transtensional deformation domains continued all the way through the Cretaceous times.

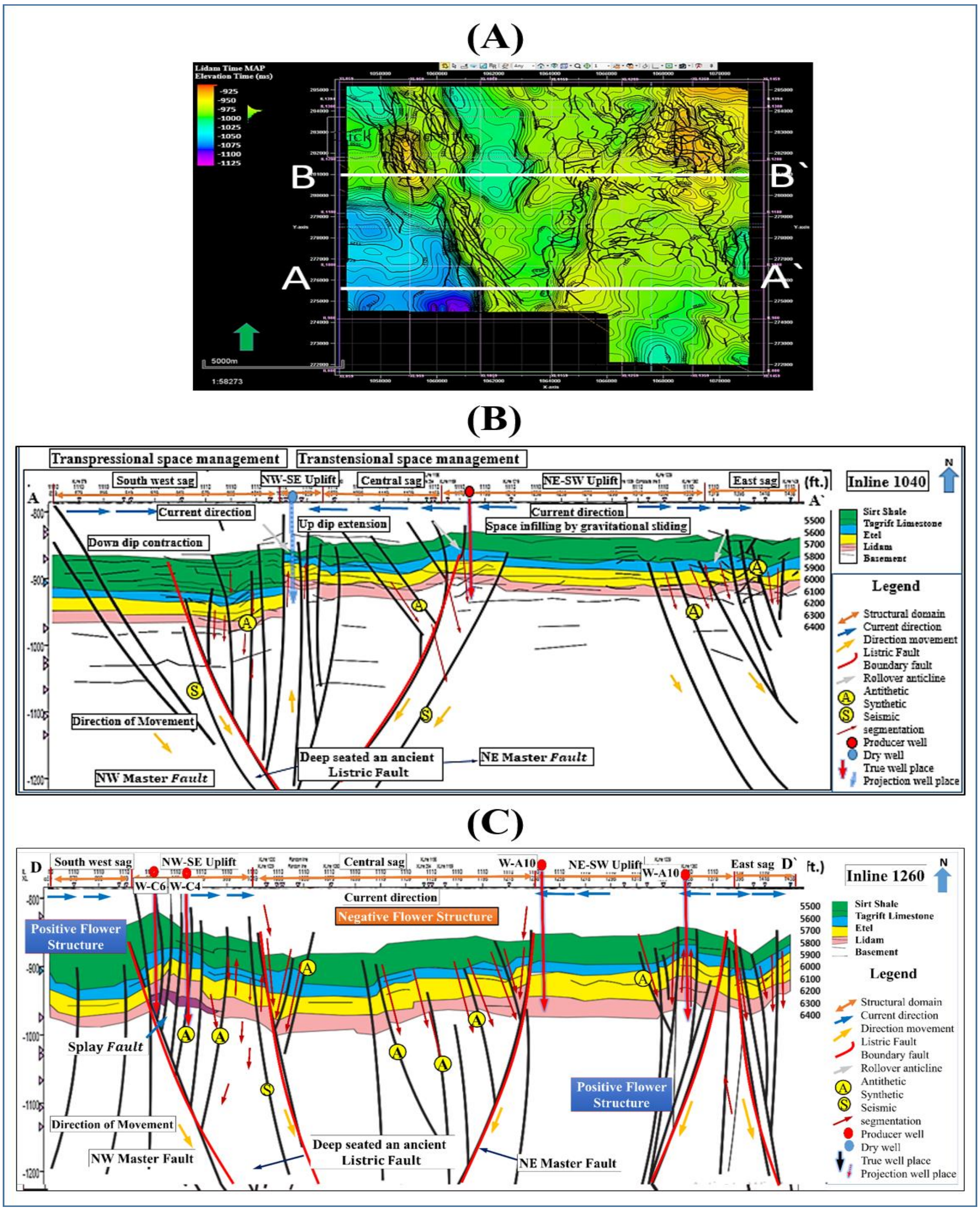

Fig. 10. (A) Lidam Time Structure Map with Cross Section Index AA` and BB`, (B) and (C) Typical Geological Profiles of Inline 1040 and 1260 respectively.

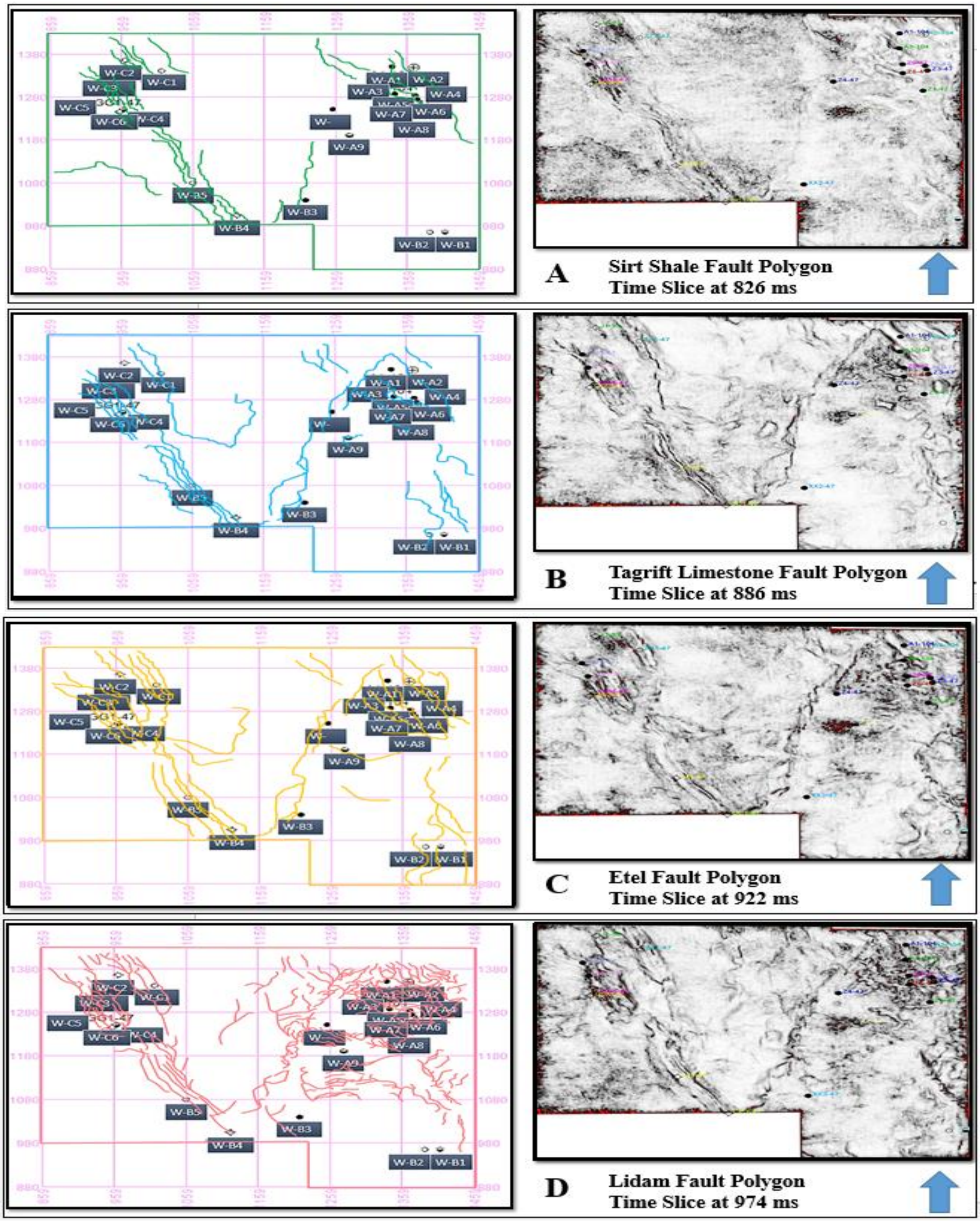

Fig. 11. Plan view of fault polygons, interpreted from the 3D seismic data for each formation showing the spatial and temporal changes in Upper Cretaceous geometry of faults that initiated and was re-activated during the Syn-rift phase (A) Sirt Shale, (B) Tagrift Limestone, (C) Etel and (D) Lidam Faults.

6. Interpretation of structure pattern

Prevailing fault orientation is NE-SW, dipping northwesterly and trending NW-SE direction, dipping southwesterly (Fig. 8). This is in response to the alternating compressional and extensional forces from the underlying strike-slip fault in the basement rock (Fig. 10C).

The marked similarities between the fault pattern in Bualwan, Dor Mansour fields and the Riedel shear pattern, suggests that their origin should be considered in terms of Riedel shear mechanisms. The major characteristic of Riedel shear is their en echelon pattern, it is obvious that minor faults are arranged like ridge ranges seem to consist of a linear group of minor individual ridges in en echelon pattern. The dominated NW-SE fault trend is, more or less, parallel to the fault zone trend. These faults are accompanied by NNW-SE trending fault related to the GFZ (Fig. 1).

Based on Naylor (1986), the orientation of the early Riedels are determined by initial stress state and that for maximum principle stress parallel and perpendicular to basement fault, the shear respectively low and high strike. This clearly suggests that the initial stress in Bulawan, Dor Mansour fields was oriented at a high angle to the trend of the fault zones, probably in an NE-SW alignment. Speculate en echelon pattern is developed in the NE-SW trend.

The formation of fault zone being with small overlapping fractures with tensional opening or shearing (Fig. 10B), the existence of R and P in place of tension gashes allows determining the sense of movement along the fault zone. The anticlockwise orientation (relative to the controlling slip vector) of the Riedel with respect to the trend of the major fault zones further indicates that the sense of displacement on the basement shear was sinistral, the research shows R-shear movement are antithetic with respect to the main fault. On the other hand, the maximum principal stress represented by vertical principal stress in the oblique extension.

7. Implication on hydrocarbon exploration

Bualwan, Dor Mansour fields have the appearance of a symmetric graben or half-graben structure, with similarities to an oblique extensional structure in rift basin. Hydrocarbon structural trap is complex and small size, which controlled the petroleum migration, accumulation and preservation. The main oil supply was from Sirt Shale Formation source rock, from Kotal-Graben by vertical migration along the fault (Hallet, 2002). Faulting was fairly active for a long time and occurrence of more new small faults, since the Early Cretaceous period caused oil escaping.

The transtensional movement of the NW-SE trend developed rollover anticline (Fig. 10B & C). The lateral movement of the master fault NE-SW trend (Figure 10B & C) released the compressional stress. The highly prospective area identified in the areas of flower structures but there are relatively small prospects.

8- Conclusion

Seismic attributes are very useful for the characterization of faults and fractures in 3D seismic data volumes. For example, Ant Tracker attribute is an effective tool suitable to enhanced fault interpretation in 3D seismic data set. As well as, Volumetric attribute such as chaos and structural smoothing attributes are very sensitive for fault detection.

Variance attributes are more suitable to show major faults that are not seen in the amplitude data. Especially after applied signal enhancing filters to remove residual noise to have an optimal result.

The structural patterns are complex and the major fractures are comprised of zones of minor faults arrange as en echelon. Riedel shear formed due to pure strike-slip are concave upwards "tulip shaped shear wedge", and Plam tree structure Riedel convex upward; there has a component of a dip-slip, particularly where dip-slip displays reverse displacement.

In case of palm tree fault wedge, the study suggests in such a structural framework. The basement fault related to the strike-slip movement. The sinistral strike fault or oblique-dip slip is the manner of the deep-seated reactivation not simple dip-slip.

Two major fault zones would represent Riedel connected by P-shear and have developed in response to sinistral slip on major basement fault. Overall NW-SE trend consistent with the regional pattern NNW-SSE. Whereas the NE-SW structure modifies the pattern formed by the previous system to form the block structures. The highly prospective areas identified based on this study are the areas of positive flower structure but they are relatively small prospects.

Acknowledgments

We are grateful to the Arabian Gulf Oil Company (AGOCO) for their generous help for providing the Petrel software workstation and for the permission to publish. We express our sincere thanks and appreciation to all who helped us in whatever capacity in preparing this work.

References

Abadi, A. M. (2002) Tectonics of the Sirt Basin".PhD Dissertation. Vrije Universiteit (Amsterdam), ITc (Enschede), pp.187.

Anketell, J. M. (1996) Structural history of the Sirt Basin and its relationship to the Sabratah Basin and Cyrenaican Platform, northern Libya. First Symposium on the Sedimentary Basins of Libya, Geology of the Sirt Basin, vol. 3. (eds. M.J. Salem, M.T. Busrewil, A. A. Misallati, and M. A. Sola), Elsevier, Amsterdam, pp. 57-89.

Gumati, Y. D. and Kanes, W. H. (1985) 'Early Tertiary subsidence and sedimentary facies, northern Sirte Basin, Libya', *Bull. Amer. Assoc. Pet. Geol*., 69, pp. 39-52.

Hallett, D. (2002) Petroleum Geology of Libya". Elsevier, Amsterdam. 503 p.

Hardge, B. (2010) Instantaneous seismic attributes calculated by the Hilbert transform. Search and discovery article #40563 (2010), adapted from the geophysical corner column, prepared by the author, in AAPG Explorer, posted July 17, 2010, 7p., http://www.searchanddiscovery.com/documents/2010/40563hardage/

Jerzykiewicz T., Czarnecki M., Elazezi M., HickeyP.and Edwards K. (2002). Geological History of the Ghedari Fault Zone in Western Sirt Basin, Libya". Abstract.

Jibrin. B. W., Turner, J. P., Westbrook, G., Huck, A. (2009) Application of volumetric seismic attributes to delineate fault geometry: Examples from the outer fold and thrust belt, deep water Niger Delta (Joint Development Zone). https://dgbes.com/index.php/software/attributes-references

Liner, Christopher, L. (2004) "Elements of 3D Seismology", Second Edition. Copyright PennWell Corporation 2004 under license agreement with Books24x7, Tulsa, Oklahoma.

Morley, C. K. Haranga, C., Phosongsee, W. Pongwappe, S., Kornsawan, A., Wonganan, N., (2004) 'Activation of rift oblique and rift parallel preexisting fabric during extension and their effect on deformation style: example from the rifts of Thailand', *J. Struct. Geol*., 26, pp. 1803-1829.

Naylor, M.A., Mandl, G. and supersteijn, C.H.K. (1986) 'Fault geometries in basement-induced wrench faulting under different initial stress state', *J. Struct. Geol*., 8, pp. 737-752.

Roohi, M. A. (1996) A geological view ofsource-reservoir relationship in the western Sirt Basin". In: Salem, M. J., El-Hawat, A, S. and Sbeta, A.M (Eds). The geology of Sirt Basin, p 323-336.

Libyan Journal of Science & Technology 9:1 (2019) 66–71
The 2nd International Conference on Geosciences of Libya-GeoLibya 2 (2017), 14-16 October 2017, Benghazi-Libya

Faculty of Science - University of Benghazi
Libyan Journal of Science & Technology
journal home page: www.sc.uob.edu.ly/pages/page/77

Geological, geomorphological and structural characterization features of Al Bordi area, Libya

Mahmoud Ali Al Mabrouk[a,*], Ibrahim M. Abou El Leil[b]

[a]*Faculty of Natural Resources and Environmental Sciences, Tobruk*
[b]*Petroleum Engineering Department, Faculty of Engineering, Tobruk*

Highlights

- **The exposed rocks of Al Bordy area are characterized by carbonate sequences of Late Eocence to Middle Miocence age.**
- **Various geological factors have affected the area structurally and geomorphologically.**

ARTICLE INFO

Article history:
Received 01 February 2018
Revised 28 April 2018
Accepted 05 May 2018
Available online 31 March 2019

Keywords:
Geological features, Stratigraphy, Lithology, Software, Geographic Information System (GIS), Geomorphology.

**Corresponding Author*:
E-mail address: mohmodali1979@gmail.com
M. A. Al Mabrouk

ABSTRACT

This study has been conducted on Al Bordy area, which lies between latitudes N31°48'16.51 N31°43'14.91and E25°00'18.09 E25°06'55.07 on the sea coast of eastern Libya, The area has specified geological features, where the different rock formation exhibit good exposures that give a clear view about the stratigraphic column. The exposed formations are Al Gaghbub, Al Faidiyah and Al Khowaymat.

The target of study is to evaluate some characterization features e.g. lithology, stratigraphic analysis, fossil distribution, structural and tectonic setting.

The technical simulation models and geographic information system (GIS) software have been applied to interpret some geologic structures such as faulting, fractures, cracks and folding as well as the effect of stresses on formation strata.

The field observations and the obtained data revealed that the area has affected by variable geological factors and changes in depositional environments, in addition to tectonic movements that led to the formation of various structures such as anticline and syncline folds, normal faults and unconformities.

1. Introduction

Al Bordy area received many geological attention since the last century. Being located on the northeast part of Libya between Egypt in the east, the Mediterranean coast in the north and traversed by the crossroads leading to the spiritual Al Jaghbub Oasis in the south is a unique position for the present area. The earliest geological work in the area was made by Schweinfurth (1883a) who visited Tobruk and Al Bordy. He described a Miocene fauna identified by Beyrich from the limestone beds in the area. Much work on the nearby Egyptian outcrops has also led to a better understanding of the geology of Al Bordy area. of importance is Said's work (Schweinfurth, 1883b) who classified the Miocene rocks in the western desert of Egypt. Gindy (1970), Gindy and El Askary (1970), Gindy *et al.* (1972) discussed the stratigraphy, structure, microfacies, petrography and heavy mineral detritals of the Miocene section north Salum.

Al Bordy area is divided into two main geomorphic units; a southern flat surface and a northern-scarped physiographic terrain. This study is concerned with the second unit. The northern part of the area is marked by the rise of several prominent scarps running in an east southeast–west northwest direction. It comprises several scarps one of them overlooks the Mediterranean Sea, is the lowest of averages 90 m above sea level and extends for 85 km in Al Bordy area (Anthony and Athol, 1994).

2. Study Objectives

This study has been carried out on this area aiming to evaluate some characterization parameters e.g. lithology, stratigraphic analysis, fossil distribution, structural patterns.

3. Materials and Methods

The methodology of the study has been carried out through the repeated field trips, a collection of different rock samples that represent the different formations beds, as well as paleontological study throughout tracing the distribution of various fossil types in the different formation beds. In addition to determining the various structural types using measuring tools and determination their main directions and identifying their magnitudes as well as the main forces that lead to form these structural patterns.

4. Location of the Area

The studied area lies at the eastern of Libya on the coast Mediterranean Sea, between N31°48'16.51 N31°43'14.91 and E25°00'18.09 E25°06'55.07 .The area characterized by its elevation location, where the elevation above sea level is ranging from 80-120 m. The area comprises three main wadis namely, Wadi Al Rahib, Wadi Al Rezg and WadiBordi (Fig. 1). The study was concentrated on these wadis due to their location importance and their good exposures of rock formations (Industrial Research Centre Tarabulus, 1984).

 ISSN 2663-1407; National Library of Libya, Legal number: 390/2018

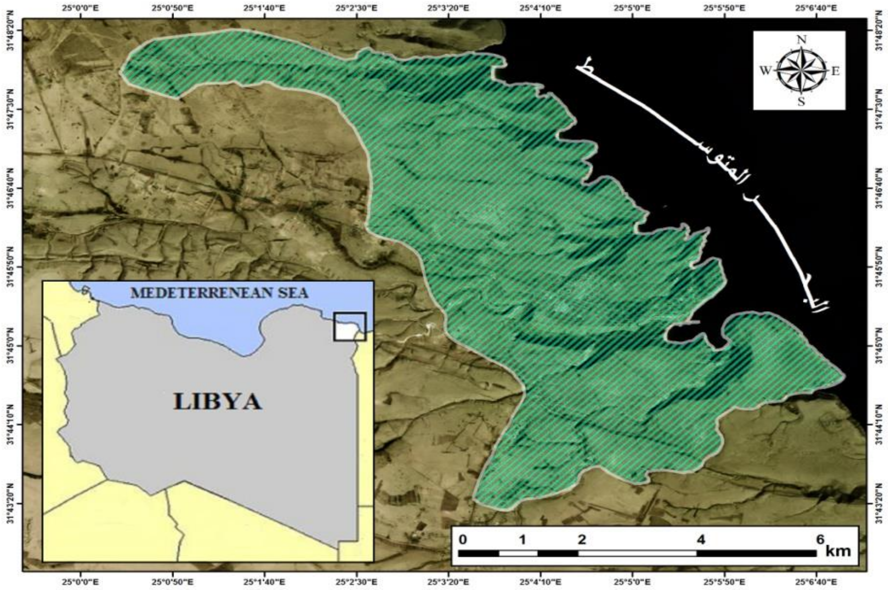

Fig. 1. Satellite map depicts Al Bordi area and the investigated locations

5. Results and Discussion

5.1. Lithology and Stratigraphy

In general, the characterization lithology of the studied area is encountered in a few rock types that represented by calcareous fossiliferous rocks, shale, sandy shale and conglomerate (Syamadas Banerjee, 1980; Megerisi and Mamgainn, 1980). The stratigraphic succession shows some variation from wadi to another in thickness and extent due to the variation of depositional factors and the tectonic movements. The thick sedimentary section exposed in Al Bordy area, especially noticed along the cliffs overlooking the Mediterranean Sea (Fig. 2) are classified into three main stratigraphic formations belonging to Early Tertiary. Besides, several, four in number, quaternary deposits were recognized near the foot slopes of the cliffs and inward covering older units. The following units were recognized in the field as given below:

Fig. 2. Anticline fold and rock avalanches at the coastal area

Quaternary:

Alluvium deposits.
Beach and coastal sand dune.
Sabkha sediments.
Eolian deposits.

Tertiary:

Lower-Middle Miocene: Al Jaghbub Formation
Upper Oligocene-Lower Miocene: Al Faidiyah Formation
Upper Eocene-Lower Oligocene: Al Khowaymat Formation
The section exposed at Wadi al Rahib; latitude 31˚ 48' 15" N and longitude 25˚ 03' 15" E described as following:

Al Khowaymat Formation: dolomitic limestone, yellowish white, hard compact, fossiliferous including; Globgerina spp., Globorotalia spp. and Nummulites.

Al Faidiyah Formation: limestone, faint brown to dark yellow, sandy and marly.

Lithologically the formation is made of alternating limestone, marly limestone and clay beds. The beds are nearly horizontal, thin to thin-bedded and highly fossiliferous (Fig. 3). It is including the following assemblage of macrofauna: Cardiumgallicum, Strombus sp. Worm tubes, Brissoposisfrassiand Tllina lacunose.

Al Jaghbub Formation: marly limestone, dark yellow and moderately hard. It is including the following assemblage of macrofauna: Ostreaverleti, Ostreadigitalina, Cardiumerinaceum and Pectencristato.

Fig. 3. Fossiliferous limestone

5.2. Geological Structures and Simulation Model analysis

The structural patterns of Al Bordy area are mainly determined by tensional faults. Faults planes are steep 75˚ to 80˚ and their extension are widely varied from one to another. It is seamed from the investigated area that it has been exposed to high tectonic movement and suffering from high stresses. The tectonic movement leads to the formation of different structural patterns represented by faulting, folding, fractures and cracks. On the other hand, another geologic structure formed later through depositional younger strata to yield disconformity and angular unconformity structures. However, the software technical simulation models have been applied to interpret some geologic structures e.g. faulting and folding to give us clear pictures of the tectonic movements and the effect of stresses on formation strata. Figs. from 4 to 7 show the mechanisms of faulting formation with time.

5.3. Geomorphological Features of Sea Coast

The coast of the studied area varies in its morphological aspects; this is due to different factors involved variation in lithology and the weathering due to wave's action. The rock type mainly formed of calcareous and soft rocks that highly affected by chemical and physical weathering owing to the formation of different types of Geomorphological features.

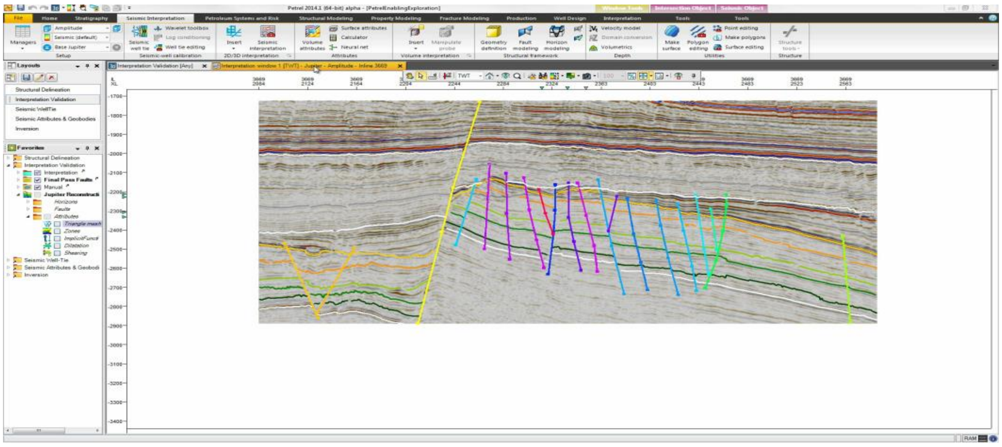

Fig. 4. Geological Rules (sequences) applied: Conformable, Erosional, Discontinuity

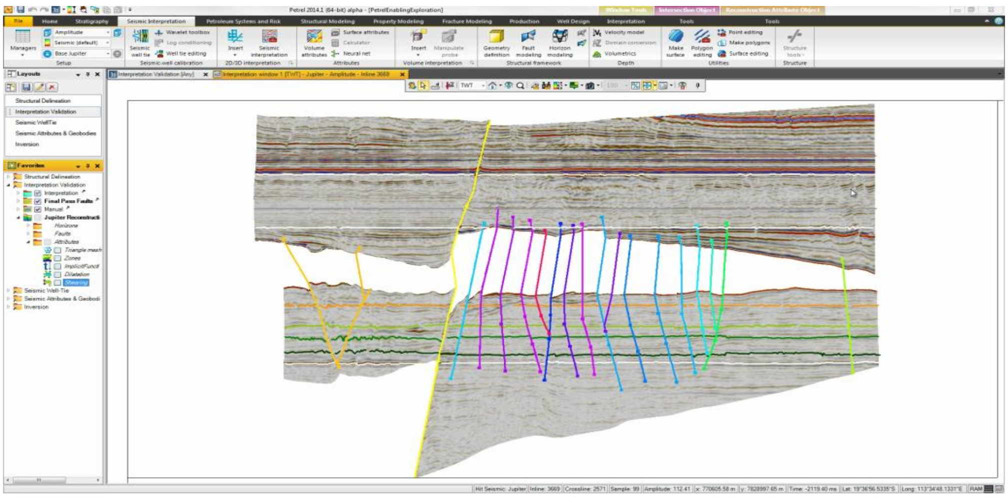

Fig. 5. Interpretation of geological structures

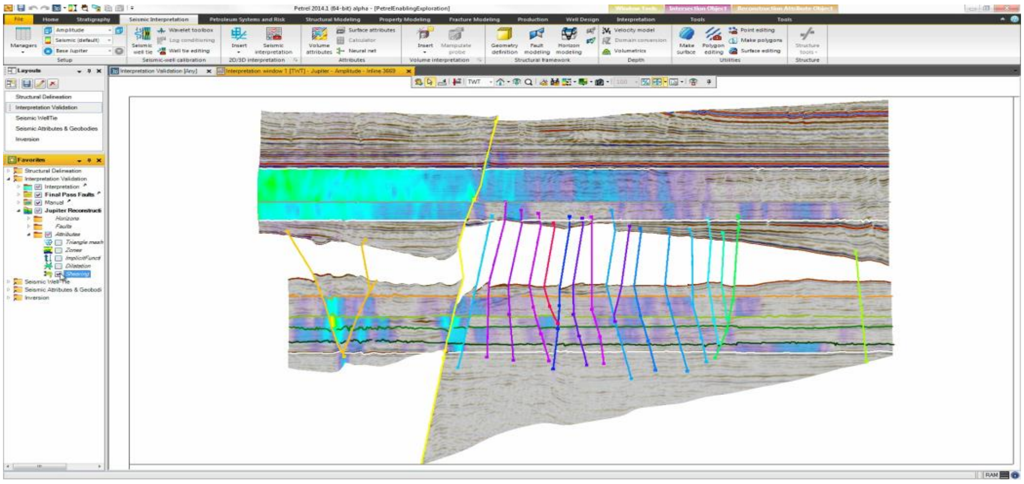

Fig. 6. Understand structure through time (Look for areas of high stress)

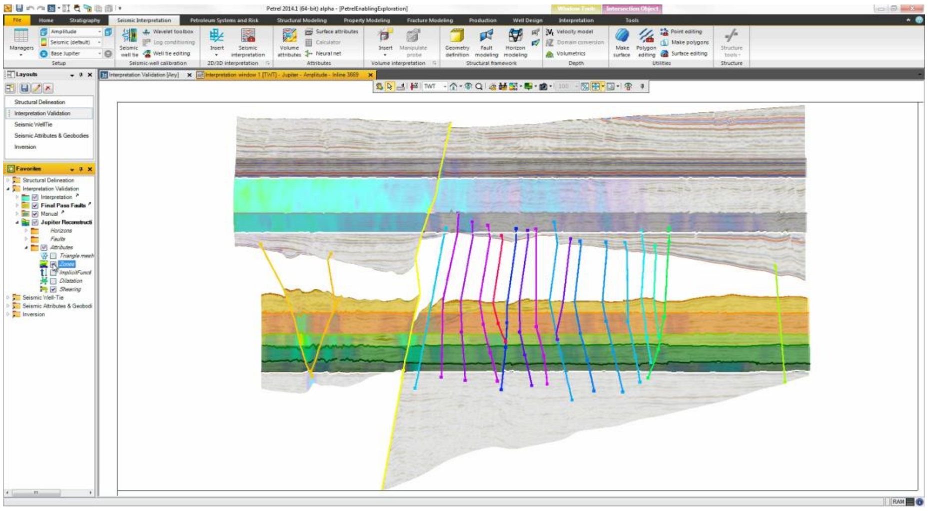

Fig. 7. Understand structure through time

5.3.1. Weathering Pits

These pits outcrops at rocks exposures on the slopes formed by calcareous rocks all over the area and usually associated joints and cracks, and also what is called taffonis pits that arises due to the solution solubility (Fig. 8)

Fig. 8. Weathering pits at the eastern ends of Wadi Al Jarfan

5.3.2. Honey Comb

These are holes and small pits are adjacent together, and characterized those small sizes compared with taffonis pits and formed due to chemical processes (Fig. 9)

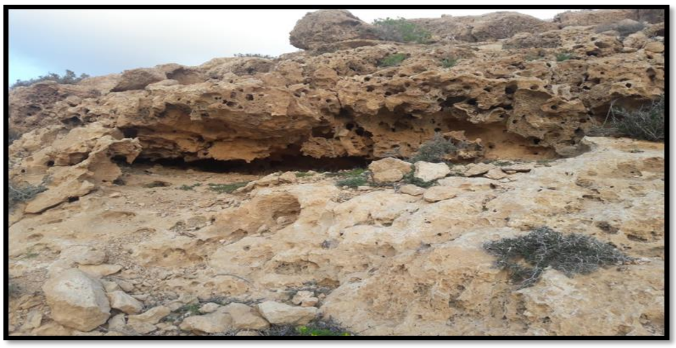

Fig. 9. Honeycomb due to weathering

These features include sea bay, sea caves, cliffs, sea plateaus and steep slopes as illustrated in Figs. from 8 to 10.

5.3.3. Coastal Cliffs

The edges that overlooking to the sea called coastal cliffs with slope ranging from 45-90˚ and affected by waves motions. These geomorphological aspects show a widespread on the coastal of study are with an elevation ranging from 50 to more than 100 m (Fig. 10).

Fig. 10. Coastal cliffs

The coastal cliffs include different geomorphological e.g. rock sliding and sea platforms, which appear at the foot of cliffs due to wave, cut platforms (Fig. 10).

5.3.4. Coastal Caves

The coastal caves and voids show a wide spread in the area, that indicate the active erosion process at cliffs feet due to wave actions. These caves ranging from 1.5 to 5.0 m with an average of 2 m, while its elevations ranging from 0.75 to 4.0 with an average of 0.50 to 4.0 m (Fig. 11).

Fig. 11. Coastal caves

5.3.5. Sedimentary Platforms

They are regarded as the most predominant Geomorphological features in the different valleys that indicate the variation in climatic conditions and amount of rainfall. Their elevations ranging from 0.20 m to 1.50 m above valleys drainage (Fig. 12).

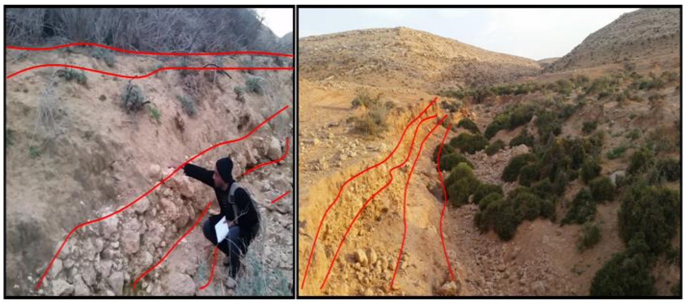

Fig. 12. Sedimentary platforms at Wadi Al Jarfan

5.3.6. Coastal area and coastal sand dunes

The downstream of wadis covered by coastal sand dunes with very fine-grained (Fig. 13), where they are formed of fine sands and calcareous deposits in addition of medium to coarse-grained of sands and remains of detrital shells. The mechanical analysis of hand specimens revealed that the dominant sand deposits have an average value 25.8% very fine sand, 35.7% medium sand, 7.6% coarse sand and 4.6% very coarse sand.

Fig. 13. Coastal sand at Wadi El Rahib

5.3.7. Coastal Lagoons and Swamps

Swamps and Sabhka are subjected to all changes affecting on the coastal area. They are represented by clay, sand and silt deposits. Sabhka includes evaporite deposits that made up of gypsum and halite minerals (Fig. 14).

6. Conclusion

The geology of the exposed rocks in Al Bordy area dated back to the Late Eocen-Middle Miocene times. The deposits of the area were correlated with Al Khowaymat Formation, Al Faidiyah Formation and Al Jaghbub Formation. They exhibit similarity between lithology, stratigraphy, structures and fauna distribution. Earth movements that forming normal faults, anticline folds and joints that show variable trends have affected the area. AlFaidiyah Formation shows a major anticline trend north south. The unconformable relationship between Al Khowaymat and the overlying Al Faidiyah is also revealed by different joints sets observed in both units. Al Jaghbub Formation covers most of the area studied and thick sections were measured from the scarps overlooking the coast. The fauna of Al Jaghbub Formation belongs Lower Miocene to Middle

Miocene. The area deposits show more or less a variation in lithological distribution that reflects the variety of marine environment under the oscillation of sea level. Software programs were used to the simulation of some geological structures such as faulting to interpret the mechanism of movements affected on the area.

Fig. 14. Swamps and sabhka along the coastal area

References

Anthony, J., Parsons, Athol, D., Abrahams, (1994) Geomorphology of Desert Environments, Library of Congress 2008939014_c Springer Science + Business Media B.V. Second Edition.

Egypt. Procc. Egypt. Acad. Sci. v. XXIII, p. 9-30.

Gindy, A. R., (1970) The stratigraphic succession of the exposed coastal Miocene sediments north of Salum town, its diagenesis and correlation with that of the Siwa Depression, Western Desert of Egypt. Procc. Egypt. Acad. Sci. v. XXIII, p. 9-30.

Gindy, A. R. and El Askary, M. A., (1970) Heavy mineral detritals of the exposed Miocene of Siwa Depression, Western Desert of Egypt and their stratigraphic and paleoecologic significance. Bull. Faculty Sci., Alexandria, v. IX., p 227-249.

Gindy, A. R., Abdu H. F., and El Askary, M. A. (1972) Litho and biostratigraphy of the exposed Middle Miocene succession of Siwa Depression, Western Desert of Egypt. Part I. Procc. Sixth Arab Sci. congress, Damascus, p. 905-921.

Industria Research Centre Tarabulus (1974) Geological map of Libya, Explanatory Booklet (Al Bordiya sheet , 1:250.000.

Megerisi, M. F. and Mamgainn, V. D. (1980) The upper cretaceous-Teriaryformatios of northern Libya asynthesis, department of geological researches and mining bulletin Industrial Reserch Centre, Tripoli no12.

Schweinfurth, G. (1883a) Unavisita a TobrukL'Esploratore, v.7, p. 207-222, Milano.

Schweinfurth, G., (1883b) EinBesuch in Tobruk an der Kuste von Marmarica. Beiheftezum Marineverordnugsblatt, no. 47, p. 14-27.

Syamadas Banerjee (1980) Stratigraphic Lexicon of Libya, Department of Geological Researches and Mining, Industrial, Research, Center, Tripoli.

Libyan Journal of Science & Technology 9:1 (2019) 72–92
The 2nd International Conference on Geosciences of Libya-GeoLibya 2 (2017), 14-16 October 2017, Benghazi-Libya

Faculty of Science - University of Benghazi
Libyan Journal of Science & Technology
journal home page: www.sc.uob.edu.ly/pages/page/77

Sedimentation, tectonic subsidence and hydrocarbon maturation history of the Gabes-Tripoli Basin, western offshore, Libya

Ibrahim Y. Mriheel

Exploration Department, National Oil Corporation, P. O. Box 2655, Tripoli, Libya
E-mail address: imriheel@noc.ly

Highlights

- **This paper provides comprehensive synthesis of the sedimentation and tectonic history of the Gabes-Tripoli Basin, Western offshore of Libya. HC maturation history has also been investigated and explained in the light of the tectonic setting and thermal regime of the basin.**
- **The paper provide new paleogeographic maps, new thermal regime maps, new HC maturation maps and tectonic model explaining Gabes-Tripoli Basin, Western Libyan Offshore formation and evolution history.**
- **New paleogeographic maps constructed based on chronostratigraphic well-well correlations can be used for petroleum paly fairway analysis.**
- **New corrected thermal regime maps can be used for HC maturation analysis of the Gabes-Tripoli Basin.**
- **The thermal regime of the Gabes-Tripoli Basin, Western Libyan offshore has been constructed considering spatial crustal thickness variation and corrected Bottom-Hole Temperatures.**
- **Tectonic model proposed explaining Gabes-Tripoli Basin formation and evolution.**

ARTICLE INFO

Article history:
Received 01 February 2018
Revised 30 May 2018
Accepted 06 June 2018
Available online 31 March 2019

Keywords:
Sedimentation, Tectonic subsidence, HC maturation history, Libyan offshore

ABSTRACT

The Gabes-Tripoli Basin (G-T Basin) is a Mesozoic-Cenozoic basin which was initiated as a result of widespread, middle Triassic, Jurassic and early Cretaceous extensional movements that developed over a broad zone of strain between the African and European plates.
The sedimentary succession in the G-T Basin ranges in age from Triassic-Recent. The tectonostratigraphic units comprise of 7 main second-order sequences reaching a 10 km-thick succession of Early-Middle Triassic, non-marine and marine clastics, late Triassic-Middle Jurassic, predominantly shallow marine carbonates and evaporites and Middle Jurassic-Recent marine carbonates and clastics.
The analysis of the basin-fill history of the G-T Basin from the Triassic until the Holocene reveals that the basin underwent development from a continental sedimentary basin located on Gondwana to an epicratonic rift basin. When main Mesozoic extensional movements ceased, the basin subsided thermally and developed as part of a passive continental margin on the North African plate margin. The basin has been subjected to compressional movements lead to inversion during late Cretaceous and Eocene time.
The dominant driving mechanism of subsidence seems clear to have been subsidence due to cooling following lithospheric thinning and the tectonic subsidence history shows that a simple stretching model successfully predicts the overall characteristics of the long-term patterns of the tectonic subsidence of the basin.
The central and northern regions of the basin have similar stretching values; however, the central area is characterized by older timing of HC generation and shallower depth of oil window. In other words, the crustal nature contributing to the heat flow spatial variation and depth of burial influence the changes in the level of HC window within the G-T Basin.
Geochemical analysis and basin modelling have confirmed the source potentiality of the early Eocene-late Cretaceous sequences to generate and expel hydrocarbon in the study area. Hydrocarbon has been generated in a wide span of time from several proven late Cretaceous-early Eocene organic-rich sources. However, none of the sequences younger than the early Eocene had the capability to expel out hydrocarbon in the basin.

1. Introduction

The G-T Basin, in northwestern Libya offshore (Fig. 1), is one of the Mesozoic-Cenozoic sedimentary basins on the North African continental margin. It was formed as a result of extensional tectonic movements that commenced during Triassic and continued during Jurassic and Early Cretaceous. These rifting phases are affecting other Mediterranean regions in the Pelagian and Ionian Seas (Finetti, 1982). Late Cretaceous – Eocene witnesses compressional tectonic phases lead to basin inversions. The ultimate Oligocene-Quaternary rifting phase has resumed its activity and was accompanied by strike-slip movements (Mriheel and Alhnaish, 1995). Fig. 2 shows the location of the study area and the drilled exploration wells used in correlations, facies analysis and paleogeographic reconstruction of depositional sequences. In this study, the subsurface analysis of the whole succession within the G-T Basin was carried out to unravel the subsurface aspects of the different depositional sequences and to interpret the overall basin evolution history. In this study, the tectonic subsidence history of the basin has been analysed and a tectonic model explaining the observed subsidence history and basin initiation mechanism has been proposed. The thermal maturation history will be analysed and the consequent hydrocarbon windows pattern will be discussed, providing insight into the hydrocarbon prospectively of the basin.

 ISSN 2663-1407; National Library of Libya, Legal number: 390/2018

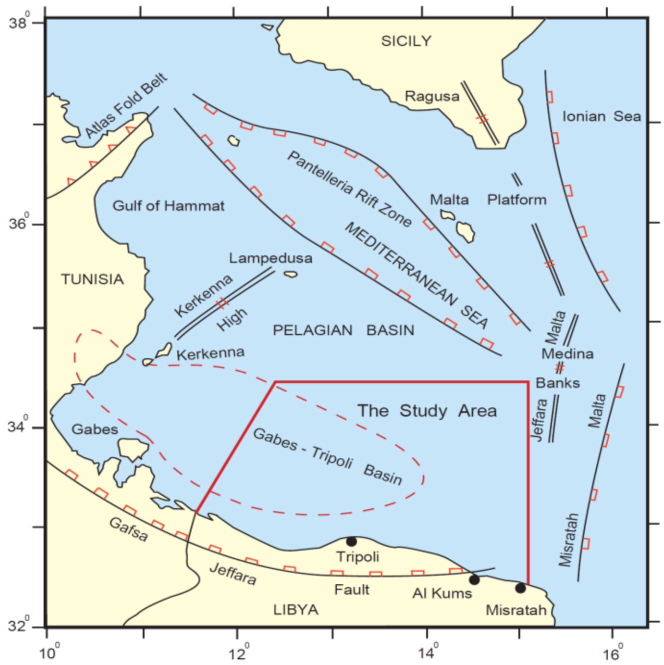

Fig. 1. Map showing the study area relative to the Pelagian Basin

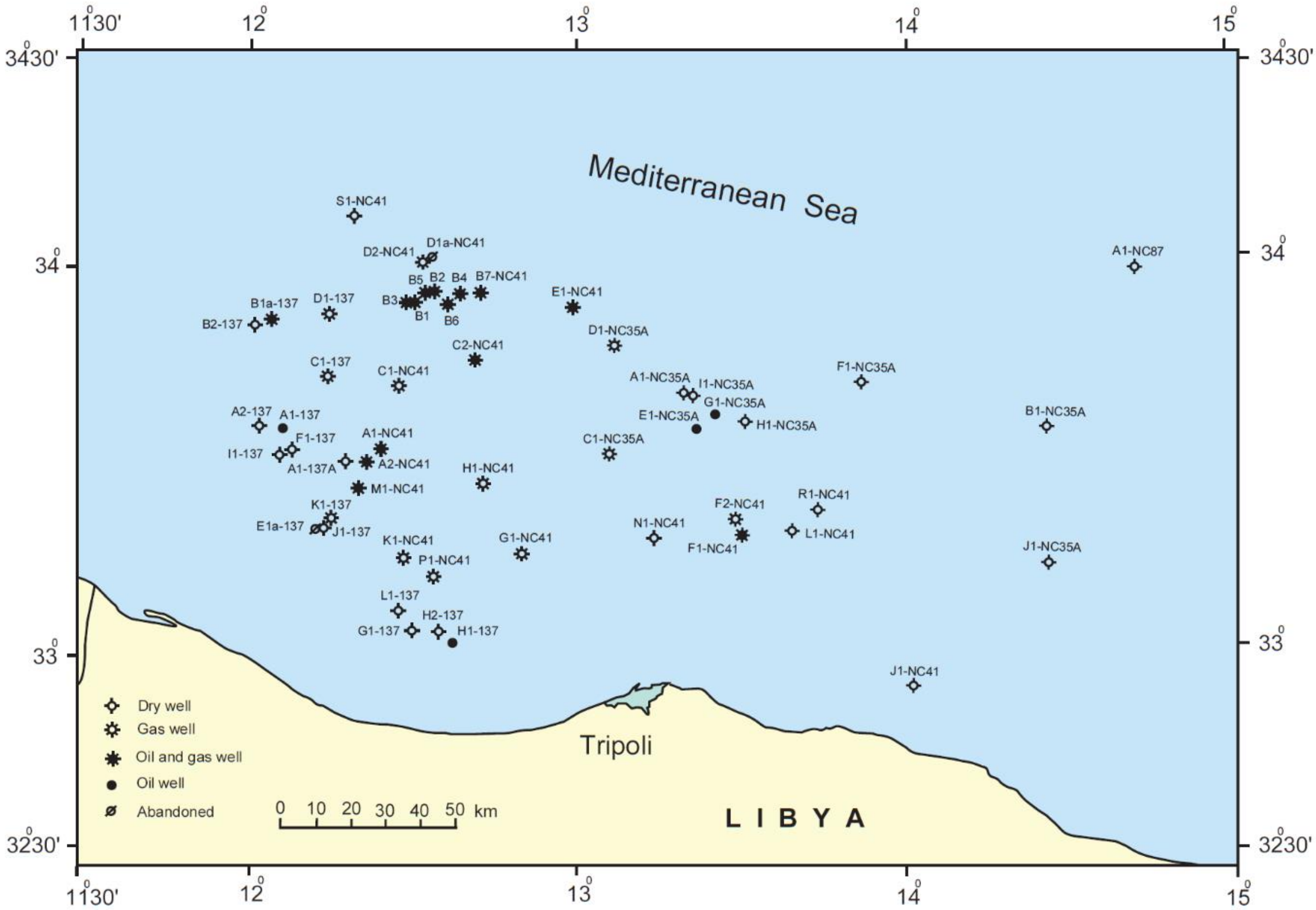

Fig. 2. Location map showing the distribution of the studied wells

1.1 Data and methods

This study presents an integrated basin analysis study involving subsurface geological and geophysical data, basin subsidence, thermal regime and maturation history analyses. The study utilises a multi-disciplinary approach to the problem of identifying and investigating the factors that control basin initiation, thermal regime, maturation history and hydrocarbon accumulations. Thus, the study uses a wide variety of techniques and draws on data obtained from geophysical well logs, seismic, and geological data.

1.1.1 Subsurface analysis

The subsurface study of the whole succession within the G-T Basin was carried out to unravel the subsurface aspects of the different depositional sequences and to interpret the overall basin evolution history. In order to investigate the G-T Basin evolution in the light of the global tectonic regime, a different approach from previous studies was followed to explain the stratigraphy, sedimentation history and mechanism of basin formation. The method simply involves the subdivision of the whole sedimentary succession into tectonostratigraphic mega sequences, all of which are linked in one way or another to regional tectonic episodes that can be correlated with the Mediterranean basin tectonic history. Thus, it was possible to interpret the development of the different depositional sequences and their bounding hiatuses in terms of relationships to eustatic sea level changes and regional tectonics. To fulfil the planned objectives, after well to well correlation had been achieved, and tops throughout the whole succession were calculated, a series of subsurface maps and diagrams were prepared. The constructed maps and diagrams include facies maps; palaeogeographic maps; isopach maps; structural maps and depositional models.

1.1.2 Basin subsidence history analysis

This part of the study involves numerical analysis of the basin subsidence history based on stratigraphic data obtained from drilled boreholes within the basin. The one-dimensional basin modelling software (Genex) of the French Institute of Petrol (IFP) was used to model subsidence in the G-T Basin. Subsidence analysis or backstripping was carried out at various localities within the region using lithologic and stratigraphic information from exploration wells. The tectonic subsidence can be estimated by quantitatively removing the effects of subsidence caused by sediment loading and basin water-depth changes.

Basins subsidence in the G-T Basin was reconstructed using a 'standard' method and the procedure used is similar to that of Steckler and Watts (1978). The 24 sites used for backstripping analysis were carefully selected from 50 available exploration wells. Using subsurface data and seismic lines as a guide, only those wells without significant faulting, or possible disruption by salt movement, were chosen. The location of the selected wells encompasses the overall tectonic evolution across the basin. Stratigraphic thicknesses and lithologic data were obtained from exploration geophysical well logs. Estimates of palaeobathymetery is based on palaeontological assemblages and sedimentary facies. Total subsidence of the stratigraphic column was corrected for sediment compaction. Tectonic subsidence was further corrected for the load effect of the sediments on total subsidence, using a one-dimensional Airy isostatic model, and is intended to reflect the tectonic forces driving basin subsidence. The amount of tectonic subsidence was computed and subsidence curves were automatically constructed.

1.1.3 Hydrocarbon maturation history

Burial history curves were constructed for 44 wells to evaluate the thermal and maturation history of the basin. The burial curves and thermal maturity calculations were made using Genex, developed by Institute Francais du Petrole (1995). This uses the kinetic maturity models developed by Tissot and Espitalie (1975) and Ungerer *et al*., (1988) and can account for any burial history, geothermal gradient and various types of organic matter represented by a range of activation energies. The burial history curves are representative of the different thermal scenarios across the G-T Basin. The results should be considered as reliable, given the fact that all exploration wells from this large basin were examined in detail.
Thermal histories of the drilled wells from the G-T Basin were first evaluated using the corrected measured temperatures to generate a range of thermal histories compatible with the observed TAI and Tmax data. Calibrating heat flow and thermal conductivity to match observed subsurface temperatures is frequently done in thermal modelling. When there are no other thermal indicator data (e.g. vitrinite reflectance, T_{max}, TAI) to calibrate the model, the fit to present-day temperatures is the only measure of the accuracy of the thermal model (McKenna and Sharp, 1998). Maturation reliability is confirmed by the predicted vitrinite values since these are in accord with the observed data. Finally, this work has seen a determination of all factors that controlled the petroleum generation and migration within the G-T Basin with mapping of the oil windows, and determination of the time of petroleum generation. The migration pathways have been constructed from palaeoheat flow anomalies, structural and seismic time maps on the top of the principal reservoir rocks.

2. Geological setting

The G-T Basin is located on the passive continental margin offshore the city of Gabes and Tripoli and oriented in an east-west direction, parallel to the NW Libyan coastal line (Fig. 1). The basin is about 400 km long and 170 km wide and covers an area of approximately 60 000 km^2. To the north, the basin is bounded by Malta – Medina Plateau and, to the south; it is bounded by the Jefarah Plain.

The tectonic evolution of the G-T Basin is dominated by Mesozoic rifting of the northern African margin, resulting in the break-up of Pangaea and resulting in the development of several Mediterranean basins (Finetti, 1982). Deposition of the Mesozoic mega-sequences took place during several rifting phases affecting the Mediterranean basins along the North African plate, starting from Triassic and passing through the Jurassic and terminated during early Cretaceous. The basin witnessed compressional phases during late Cretaceous and Eocene followed by Oligocene-Quaternary rifting (Fig. 3). The tectonostratigraphic evolution of G-T Basin can be subdivided into three cycles (Fig. 3).

- *The pre-rift megasequence*:

  The first stage of basin evolution involved uplifting and faulting during the Palaeozoic, which caused erosion of the pre-Triassic sediments and development of a broad arch during the Hercynian orogeny. This phase preceded the break-up of Gondwana, which began in the early Jurassic. During the early Triassic, the pre-rift phase sequence was formed in initially faulted basement blocks and contains continental siliciclastics (Figs. 3 and 4).
- *The rifting megasequences: can be subdivided into three supersequences.*

  The first one is made up of middle-upper Triassic shallow marine sediments, representing the first seawater inflows from the north. This section developed during sea level rise, combined with mild tectonism during Middle Triassic, led to widespread deposition of shallow shelf siliciclastics and carbonates of Kurush and Al Aziziyah Fms respectively (Fig. 3).

The overlying Upper Triassic-Middle Jurassic sequence consists of continental siliciclastics, shallow restricted shelf carbonates to hypersaline lagoonal evaporites and mixed siliciclastics and shallow marine carbonates. This section corresponds to a period of a relatively active tectonics and continuing subsidence indicated by the deposition of a thick admixture of lithologies and development of major erosional boundary during the whole Upper Jurassic (Fig. 3).

The remaining Lower Cretaceous section is characterized by deposition of marginal marine siliciclastic and carbonate, shallow carbonate shelf and deep shelf to basinal settings. On the neighboring onshore vicinity, fluvial sediments are ubiquitous. The start of Lower Cretaceous time witnessed uplifting of the Jifarah Plain which acted as a source of the clastic influx toward the G-T Basin (Figs. 3 and 4).

- *The post-rifting megasequences: is comprised of four main second-order sequences.*

The advent of Late Cretaceous marks initially the start of a long period of sea level rise in the basin resulting in the development of abroad Cenomanian carbonate ramp overlained by deep shelf to basinal facies corresponding to the Makbaz, Jamil, Bu Isa and Lower Aljurf Fms. A combination of sea-level rise during the late Cretaceous, corresponding to Haq *et al.* (1987) eustatic sea-level curve, and tectonism lead to deposition of pelagic shale, marl and carbonates in the deep shelf-basinal environmental setting. This section was locally affected by the Santonian inversion phase, which marks the start of the Mediterranean compressional tectonic event (Fig. 3).

The second one is made up of Paleocene-Lower Eocene shallow shelf carbonates developed over the southern and central parts of the basin and passed northward into its equivalent pelagic facies. During the Palaeocene, the offshore area was subjected to severe regressive episodes concomitant with tectonic uplifting induced by volcanism along the southern margin of the G-T basin. The latest Palaeocene-early Eocene time witnessed a relatively quiescent tectonic phase, during which the carbonates of the Farwah Group were developed. To the north of the offshore region, the Farwah Group passes into pelagic facies of the Hallab Formation (Fig. 3). The overlying Middle-late Eocene section consists of shallow shelf carbonates and shales of the Tellil Group and its deeper water equivalent Ghalil Formation. The Cenozoic closure of the Neotethys has contributed to the Eocene inversion of the basin (Fig. 3).

The remaining Neogene section represents a shallowing upward sequence that commenced with rapid sea level rise and flooding during Oligocene-early Miocene. This leads to deposition of the pelagic facies and development of Dirbal reefal carbonates over local highs. The subsequent increase in clastic influx augmented by subsidence leads to deposition of a muddy shallow shelf with sandy beach sediments of the Al Mayah Formation (Fig. 3). The Tortonian time witnessed quiescent tectonics that encouraged the resumption of carbonate deposition. The end of the sequence is marked by a lowering of the sea level concomitant with the Messinian crises that lead to the deposition of the sabkha-restricted shallow shelf evaporites and carbonates. The sedimentary sequence of the G-T Basin ends with shallow siliciclastic shelf of Pliocene-Recent age (Fig. 3).

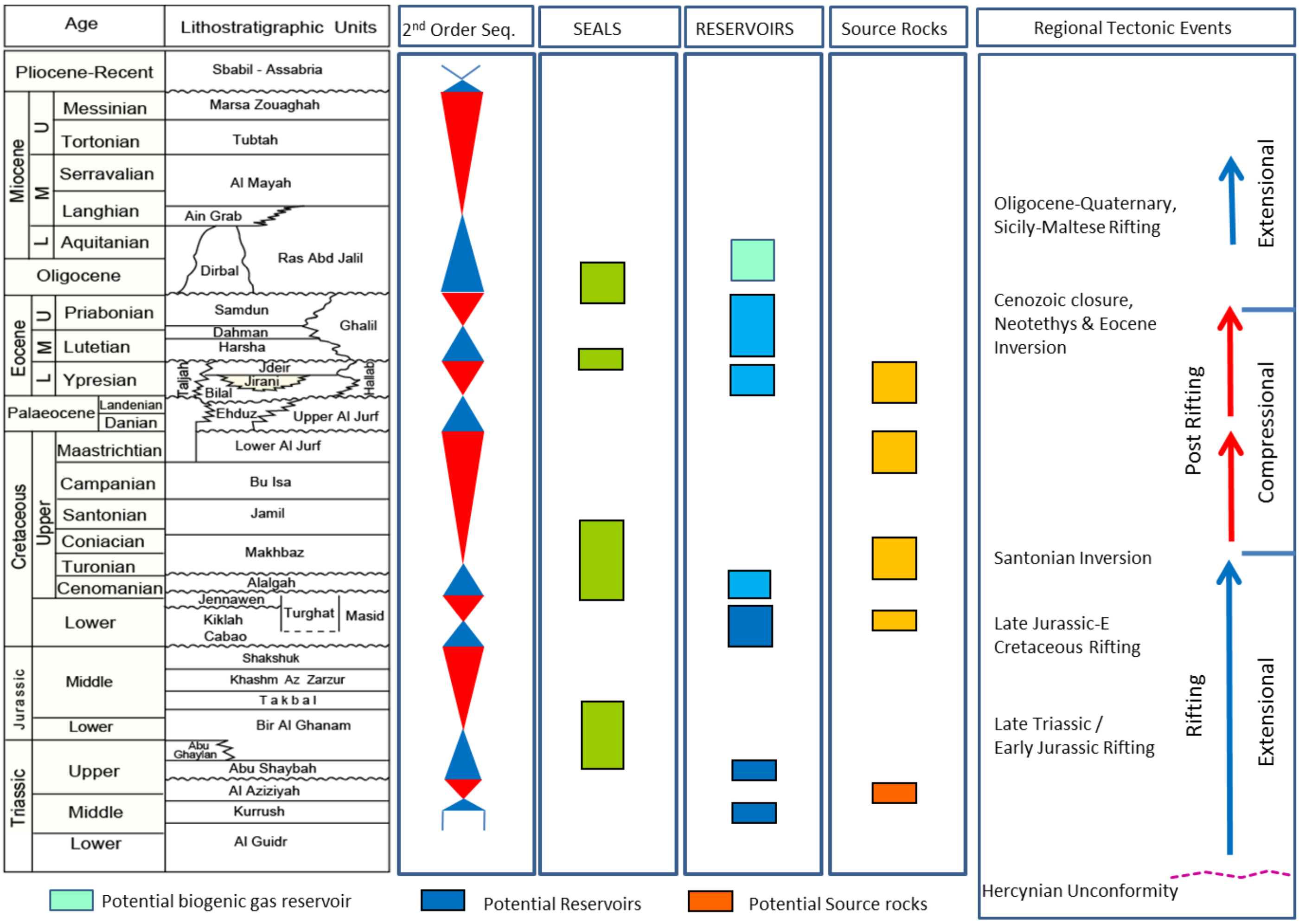

Fig. 3. Showing the G-T Basin Stratigraphy, regional tectonic events and petroleum plays, after Mriheel, 2014 and 2017.

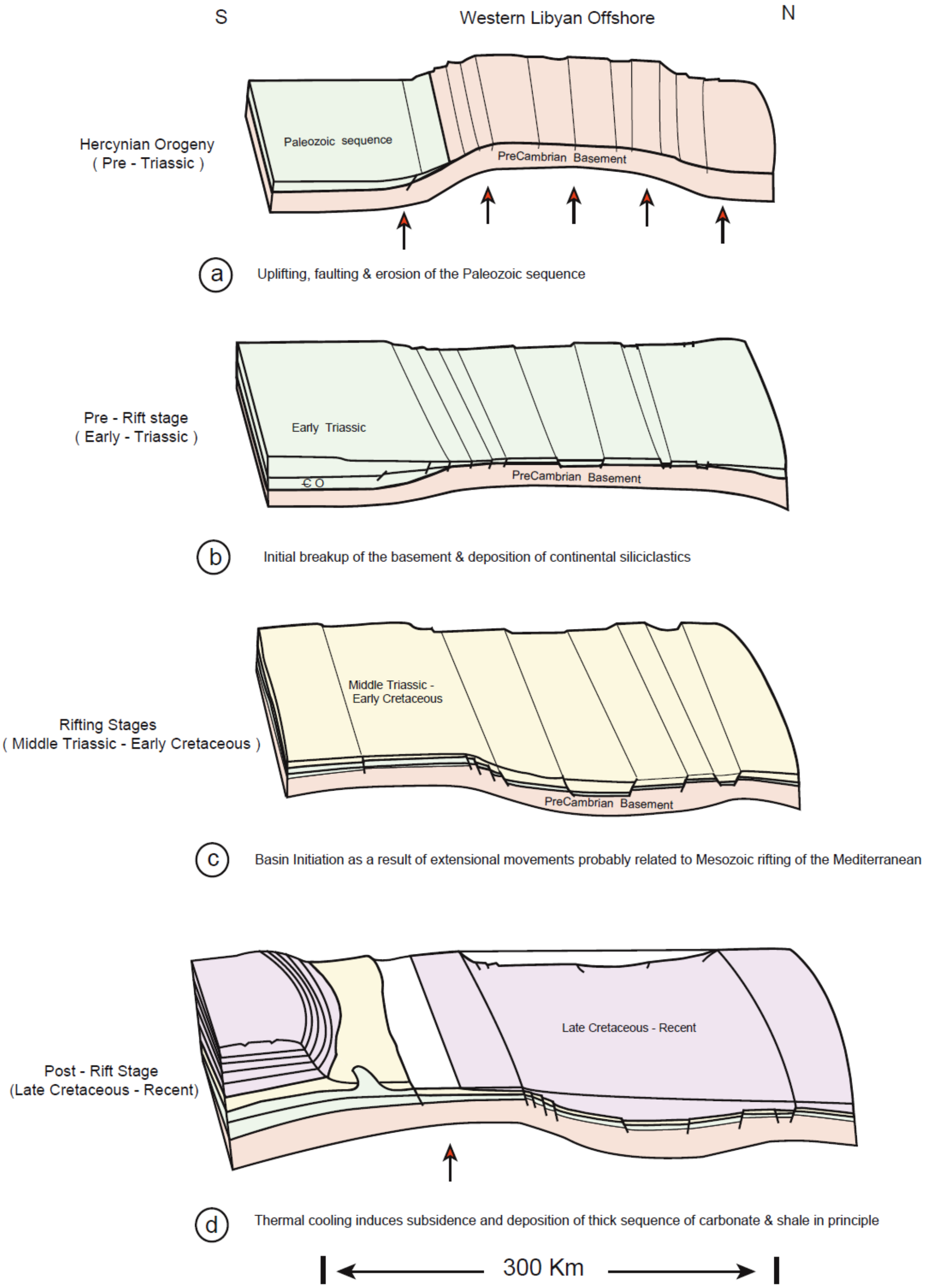

Fig. 4. Summary of the Evolution of the Gabes-Tripoli Basin

3. Stratigraphy and sedimentation history

The sedimentary succession in the G-T Basin ranges in age from Triassic- Recent. In this study, the basin stratigraphy and evolution have been discussed based on global tectonic events linked with the break-up of the Gondwana land, opening of the Atlantic Ocean, and motion of the African plate. The sedimentation history and basin evolution are explained in pre-rift, rifting, and post-rifting stages (Fig. 3).

The sedimentary sequences forming the bulk stratigraphy of the G-T Basin comprises a 10 km-thick succession of Early-Middle Triassic, nonmarine and marine clastics, Late Triassic-Middle Jurassic, predominantly shallow marine carbonates and evaporites and Middle Jurassic-Recent marine carbonates and clastics. The tectono-stratigraphic units comprise 7 main sequences on the time scale of second-order sequences (Fig. 3). For most sequences and sequence boundaries, either a eustatic or tectonically enhanced origin can be established.

3.1 The pre-rifting megasequence

The first stage of basin evolution involved uplifting and faulting during the Palaeozoic, which caused erosion of the pre-Triassic sediments and development of a broad arch during the Hercynian orogeny (Fig. 4). This phase preceded the break-up of Gondwana and the opening of the Neo-Tethys Ocean, which began in the Early Jurassic (Guiraud, 1998). Based on geophysical data, no sediments of Pre-Triassic age appear to be present in the G–T Basin. The oldest encountered sedimentary succession so far is of Late Triassic–Early Jurassic age (Mriheel, 2000). Therefore, the source of information about the Pre-rift megasequence comes largely from the adjacent outcrops in the Jefarah region to the south and from many boreholes drilled in proximity to the offshore region (Hammuda *et al.*, 1985). The pre-rift sediments in the basin consist of Early–Middle Triassic sandstones and shales of the Al Guidr Formation (Fig. 5). Deposition during this phase was predominantly continental siliciclastics (Hammuda *et al.*, 1985). The Al Guidr sediments overlie the basement and are probably witness to the first sedimentation period to take place in the initially faulted and fractured basin.

3.2 The rifting megasequences

- *Middle Triassic-Early Jurassic*

The subsequent rise in sea level followed Al Guidr deposition, combined with mild tectonism during Middle Triassic, led to widespread deposition of shallow shelf siliciclastics corresponding to the Kurrush Formation (Fig. 5). In the subsurface, the Kurrush Formation consists of shallow shelf sandstones, and shales, dolomite and limestone (Menning *et al.* 1963). The Kurrush Formation is conformably overlain by the Al Aziziyah Formation and overlies the Al Guidr sandstone with gradational contact (Fig. 3).

During the subsequent phases of Middle Triassic-Early Jurassic rifting, the major faults and structural elements of the G-T Basin were either initiated or rejuvenated and significant subsidence of the basin allowed major sedimentation of shallow shelf carbonates and fluvial-shallow marine siliciclastics and restricted shelf-hypersaline lagoon evaporites of the Al Aziziah, Abu Shybah and Bir Al Ganam formations respectively (Fig. 5).

This late Triassic-Middle Jurassic tectonic activity laid the foundation of the extensional G-T Basin on the northern margin of the African Craton. This phase was concomitant with the break-up of Gondwanaland and the opening of the Atlantic Ocean (Guiraud, 1998).

- *Middle Jurassic*

At the western Libyan offshore area, Middle Jurassic is represented by the upper Bir Al Ghanam, Takbal, Khashm Az Zarzur and Shakshuk formations (Fig. 3) and is comprised of shallow restricted shelf sandstone, siltstone and shale, evaporates, dolomites and limestones. The subdivision of these lithostratigraphic units is well established in the neighboring area of Jifarah Escarpment. However, due to scarce subsurface information about deeper sequences, hence their subdivision remained arbitrary.

- *Early Cretaceous*

The last event of Mesozoic rifting is corresponding to the Lower Cretaceous phase (Figs. 3 and 4). The advent of Early Cretaceous time witnessed uplifting of the Jifarah plain, which acted as a source of the clastic influx toward the G-T Basin (Mriheel, 2000). Early Cretaceous sedimentation continued over the Jifarah Plain with fluvial deposits of the Kiklah Formation (Fig. 5). On the offshore shallow shelf environments are ubiquitous. At the end of the Early Cretaceous (Aptian–Albian), Kiklah, Turghat and Masid formations were deposited (Figs 3 and 5) and are comprised of marginal marine siliciclastic and carbonate, shallow carbonate shelf and deep shelf to basinal settings respectively (Fig. 5). This stage was contemporaneously occurred with Sirt basin rifting. Differential block movements toward the offshore that followed the Kiklah deposition continued as the area was invaded by the Late Cretaceous sea. Initial transgression was first started during Late Albian-Early Cenomanian as the marginal marine sediments of the Jennawen Formation would suggest (Mriheel, 2013 and 2014).

3.3 The post-rifting megasequences

- *Late Cretaceous*

The advent of Late Cretaceous marks initially the start of a long period of sea level rise in the basin resulting in development of abroad Cenomanian carbonate ramp corresponding to the Alalghah formation (Fig. 5). Progressive transgression continued from Turonian to Maastrichtian and lead to the deposition of the deep shelf to basinal facies corresponding to the Makbaz, Jamil, Bu Isa and Lower Aljurf formations (Figs 3 and 5). A combination of sea level rise during the Late Cretaceous, corresponding to the Haq *et al* (1987) eustatic sea level curve, and tectonism lead to deposition of pelagic shale, marl and carbonates in deep shelf-basinal environmental setting. This section was locally affected by the Santonian inversion phase (Fig. 3) which mark the start of the Mediterranean compressional tectonic event.

During the Late Coniacian, the western Libyan Coastal Fault system and structural elements of the basin were rejuvenated. As a result, the Jifarah Plain emerged as a landmass, and significant sedimentation onshore is thought to have ceased since then. This continuous rise in sea level and rejuvenation of the western Libyan coastal fault system appears to have slightly exceeded the uplift of the peripheral palaeohigh around the G-T basin. Consequently, a long period of non-deposition and erosion persisted over the emergent area of the Jifarah Plain (Mriheel, 2000).

- *Tertiary*

Subsequent to the deposition of the Maastrichtian shales, the depositional style in the G-T Basin changed as a prism of shallow-marine sediments prograded seaward across the basin. This broad progradational wedge defines the shallowing Tertiary depositional sequences, which range in age from the Palaeocene to Recent (Fig. 3). The shallowing Tertiary deposits encompass three main second order depositional sequences: Late Palaeocene-Early Eocene, Middle-Late Eocene, and Oligocene-Late Miocene (Fig. 3). The later is capped by thin and incomplete sequence of Pliocene-Recent age (Fig. 3). These depositional sequences are characterised by several stacking patterns during their development and throughout the Tertiary period, shallow shelf carbonates and siliciclastics predominate the southern region. To the north, in deeper water, shales, marls and limestones were deposited in deep shelf–basinal setting (Figs. 6 and 7).

During the Palaeocene, the offshore area was subjected to severe regressive episodes concomitant with tectonic uplifting induced by volcanism along the southern margin of the G-T basin. This was accompanied by exposure of the Late Cretaceous sequence toward the southern margin of the basin and deposition of a narrow belt of Ehduz shallow shelf carbonates and its equivalent pelagic facies of Upper Al Jurf Formation (Fig. 6).

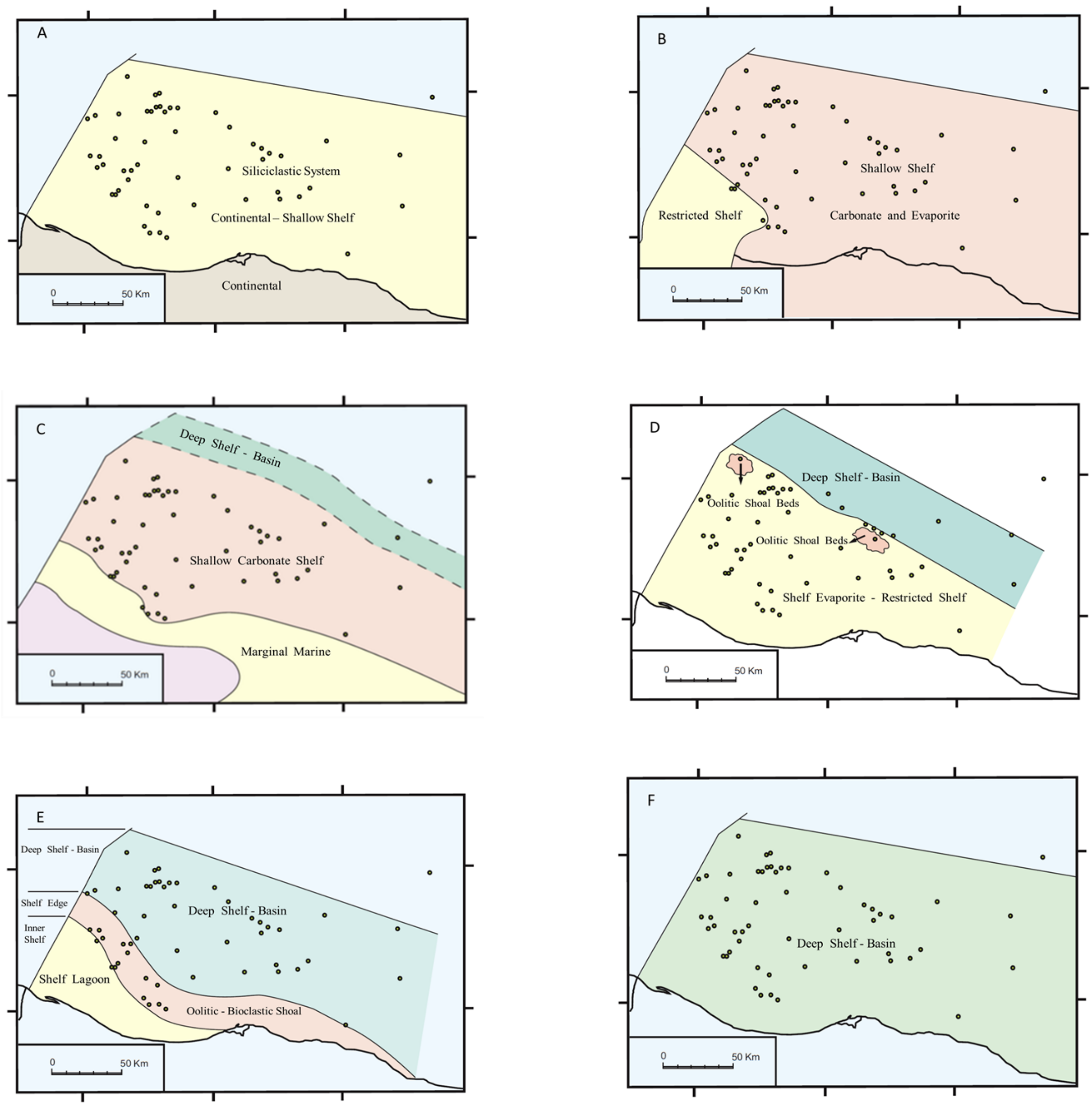

Fig. 5. Showing the paleogeography of the Mesozoic Megasequences. (A) Main facies and depositional environment of the early-middle Triassic AlGuidr-Kurrush Fms. (B) Depositional environment of the Al Aziziyah, Abu Shaybah and Bir Al Ghanam Fms during late Triassic-middle Jurassic. (C) Main depositional settings and facies belts of the early Cretaceous Kiklah, Turghat and Masid Fms. (D) Depositional facies and environment of the Cenomanian Alalghah Fm. (E) Main facies belts and environments of the Turonian- Coniacian Makbaz Fm. (F) Depositional environment of the Santonian-Maastrichtian Jamil, Bu Isa and Lower Al Jurf Fms.

The latest Paleocene-Early Eocene time witnessed a relatively quiescent tectonic phase, during which the carbonates of the Farwah Group were developed over the southern and central parts of the basin. To the north of the offshore region, the Farwah Group passes laterally into its equivalent pelagic facies of the Hallab Formation (Fig. 6). After a short period of erosion or non-deposition of the early Eocene sediments, sedimentation resumed with the rise of sea level in the Middle Eocene. The Middle-Late Eocene shallow shelf intercalations of carbonates and shales of the Tellil Group and its deeper water equivalent Ghalil Formation were developed (Fig. 6). Again, after uplifting and erosional event related to the closure of the Neotethys during Eocene inversion (see Fig. 3), a shallowing upward sequence that commenced with rapid sea level rise and flooding during Oligocene-Early Miocene was established. The Oligocene-Miocene sequence is bounded by obvious hiatuses and consists of the RasAbdJalil, Dirbal, Al Mayah, Tubtah, and Marsa Zouaghah formations (Fig. 7; Mriheel, 2000 and 2014).

The subsequent increase in clastic influx augmented by subsidence lead to deposition of a muddy shallow shelf with sandy beach sediments of the Al Mayah Formation (Fig. 7). The Tortonian time witnessed quiescent tectonics that encouraged the resumption of carbonate deposition of the Tubtah Formation (Fig. 7). The end of the Miocene section is marked by a lowering of the sea level concomitant with the Messinian crises that lead to the deposition of the sabkha-restricted shallow shelf evaporites and carbonates of the Marsa Zouaghah Formation (Fig. 7). The sedimentary sequence of the G-T Basin ends with siliciclastics of Pliocene-Recent age. The sequence is represented by the Sbabil and Assabria formations (Fig. 7).

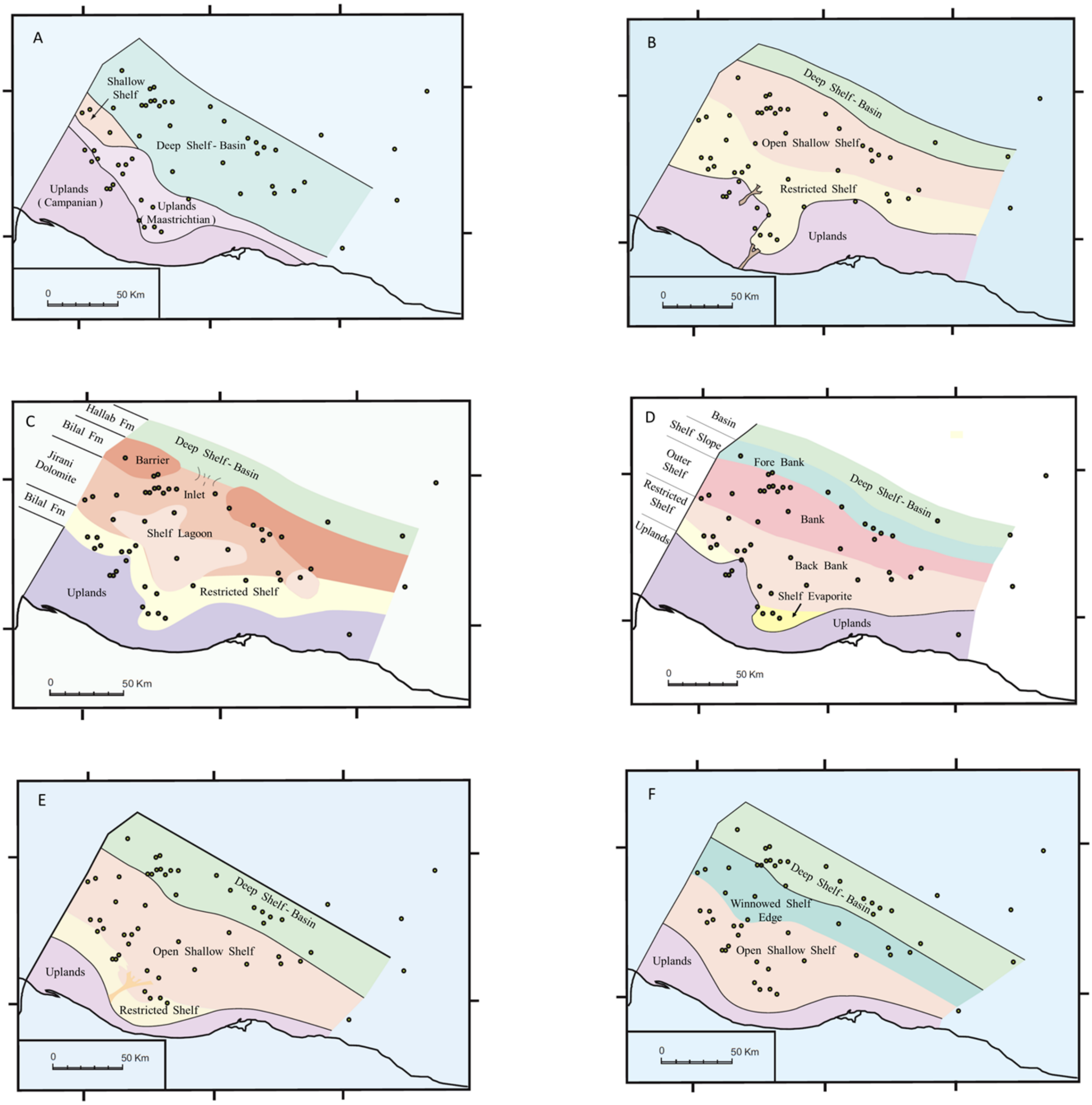

Fig. 6. Showing the paleogeography of the Early Tertiary Megasequences (Paleocene-Middle Eocene). (A) Main facies and depositional environment of the Paleocene Halab Fm. (B) Environmental settings and facies belts of the late Paleocene-early Eocene Bilal Fm. (C) Main depositional settings and facies belts of the Jirani Dolomite and its equivalent upper Bilal Fm. (D) Facies belts and depositional environment of the early Eocene Jdeir, Taljah and Hallab Fms. (E) Main facies belts and environments of the middle Eocene Harash Fm. (F) Main facies belts and depositional environment of the middle Eocene Dahman Fm.

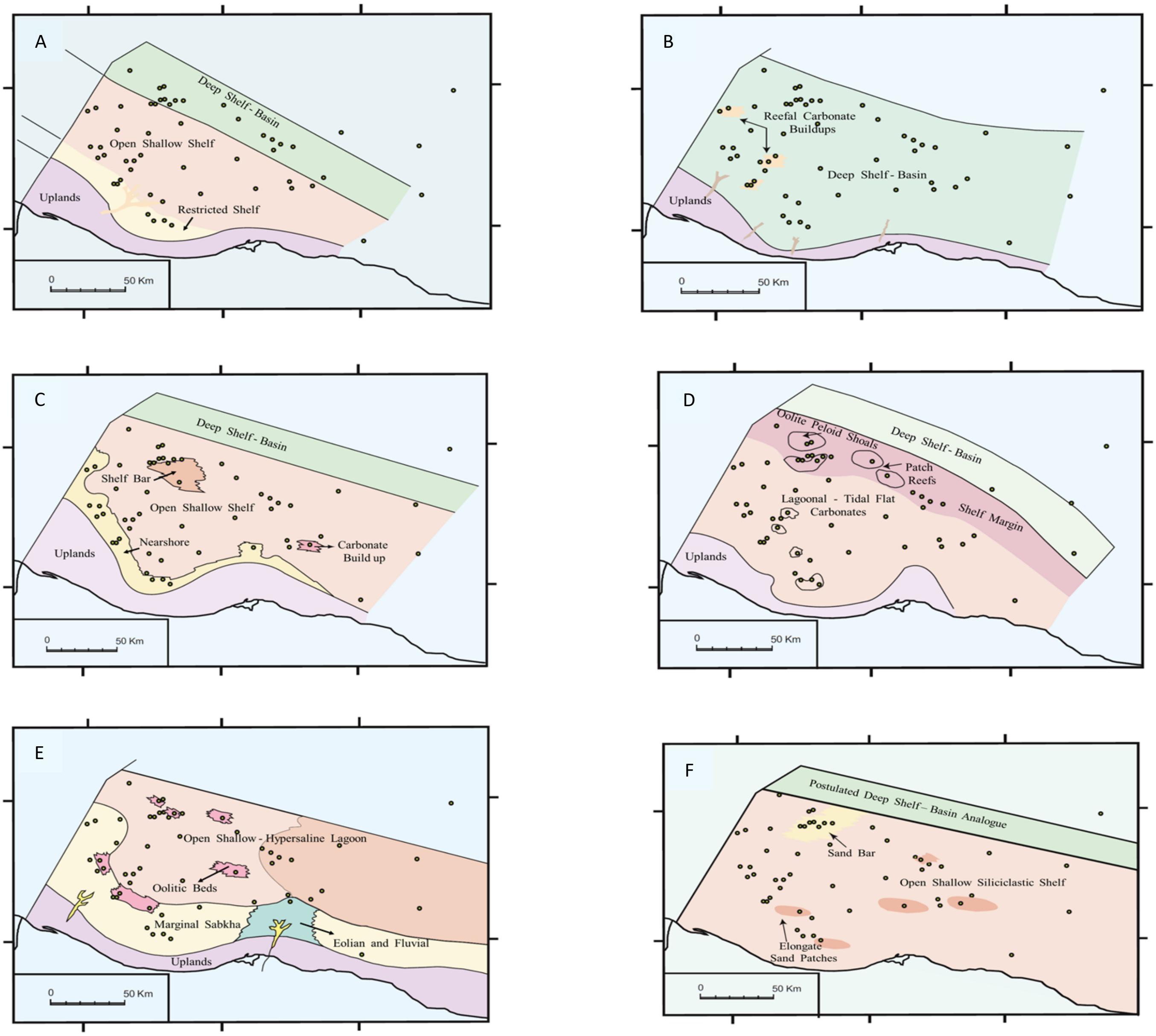

Fig. 7. Showing the paleogeography of the Late Tertiary Megasequences (late Eocene-Recent). (A) Main facies belts and depositional environment of the late Eocene Samdun Fm. (B) Depositional environment of the Oligocene-middle Miocene Ras Abd Jalil Fm and its equivalent Dirbal Fm (C) Main depositional settings and facies belts of the middle Miocene Al Mayah Fm. (D) Facies belts and depositional environment of the Tortonian Tubtah Fm. (E) Main facies and depositional environments of the Messenian Marsa Zouaghah Fm. (F) Depositional environment of the Pliocene-Recent Sbabil and Assabria Fms.

4. G-T Basin subsidence history

Tectonic subsidence analyses of selected sites were carried out to compare patterns of subsidence at different areas in the G-T Basin, using standard backstripping techniques similar to that of Steckler and Watts (1978) and was carried out at 24 localities within the G-T Basin using lithologic and stratigraphic information from exploration wells. The 24 sites used were carefully selected from 50 available exploration wells (Fig. 8). Stratigraphic thicknesses and lithologic data were obtained from exploration geophysical well logs. Estimates of palaeobathymetry are based on palaeontological assemblages and sedimentary facies. Total subsidence of the stratigraphic column was corrected for sediment compaction. Tectonic subsidence was further corrected for the load effect of the sediments on total subsidence, using a one-dimensional Airy isostatic model, and is intended to reflect the tectonic forces driving basin subsidence.

Up to the present time, the oldest penetrated succession in the G-T Basin is the Late Triassic-Early Jurassic sediments in well L1-137. Both stratigraphic and seismic data, as well as the constructed subsidence curves (Figs. 9-11), reveals that the subsidence of the G-T Basin was induced thermally. The thermal phase of subsidence began in the Late Cretaceous. Thus, the beginning of the thermal sag phase marked the end of the primary stretching phase. The post-Jurassic subsidence of the G-T Basin, after backstripping analysis, fits with the overall pattern of the theoretical subsidence curves predicted for a thermal sag phase that would follow whole lithosphere extension. The basement subsidence curves (Figs. 9-11) show that the tectonic subsidence in the G-T Basin behaves in accordance with the thermal cooling model of Mackenzie (1978). Thus, the basin subsidence of the G-T basin is attributed to lithospheric extension induced subsidence followed by a long period of exponentially decreasing thermal subsidence as the underlying thinned mantle cooled and thickened. Therefore, the Mckenzie (1978) lithospheric extension model can best explain the basin evolution. The amount of tectonic subsidence was computed and subsidence curves were automatically constructed using Genex software.

4.1 Subsidence curves

The stratigraphic accumulation and tectonic subsidence curves for wells in the G-T Basin are shown in Figures 9-11. These Figures (note scale change) show example curves from three locations, wells J1-NC41 and L1-137 in the south, coastal region, wells H1-NC41 and J1-NC35A from the basin centre and wells A1-NC35A and B1-NC35A from a platform in the northern margin of the G-T Basin. These locations are distant from the areas affected by salt domes and have been selected to represent examples of the tectonic evolution of the basin uninfluenced by halokiniesis. The main results are as follows: Magnitudes of total subsidence, tectonic subsidence and stratigraphic accumulation increase from margins to the basin centre (see also Figs. 12 and 13).Generally, the subsidence curves (Figs. 9-11) show that sediment loading accounts for over one-half of the total observed subsidence. The basement subsidence curves (Figs. 9-11) show that the tectonic subsidence in the G-T Basin behaves in accordance with the thermal cooling model of Mckenzie (1978). Hence, the overall pattern of these subsidence curves (Figs. 9-11) suggests that thermal cooling of the continental lithosphere induced considerable basement subsidence during the post-rift stage. The shape of the tectonic curves shows the thermal subsidence was a result of exponential cooling of the basement with time.

Figs. 9 through 11 show that the regional subsidence in the G-T Basin (during post-rift), which followed the extensional event, is broad and well recognized. As a result, the magnitude and the rate of the basement subsidence curves can be directly compared with the predictive model (Mckenzie, 1978) based on simple stretching. The consistent increase of both basement tectonic subsidence curves with the total subsidence curves supports the fact that basin subsidence during later stages of the post-rift phase is augmented by sediment loading.

The tectonic subsidence curves (basement subsidence) shows that low basement subsidence rates correspond to wells on the southern and northern shoulders of the basin (Figs. 9 and 11). This is also supported by stratigraphic accumulation. Hence, stratigraphic accumulation and total subsidence continued in the central main trough of the basin. Vertical motion continued along major faults bordering the G-T Basin in response to loading in the central rift basin. Examination of the constructed tectonic subsidence curves, which were corrected for compaction and sediment and water loads across the G-T Basin reveals the following results. The total basement subsidence curve at the southern margin, in well J1-NC41 (Fig. 9) shows the subsidence is low (does not exceed 1000 m). This subsidence figure represents the last 84 my. On the contrary, during the last 60 my only a high total basement subsidence of 1600m was observed at the basin depocentre in well H1-NC41 (Fig. 10). At the northern margin of the basin in well B1-NC35A (Fig. 11), 1600 m of total basement subsidence was accounted for by the last 98 my. By considering the time duration difference of the total tectonic basement subsidence across the basin a subsidence rate of 12 m/my, 26 m/my and 16 m/my were calculated for the southern, central and northern parts of the basin respectively. Thus, the rate of basement subsidence from the basin margin to the centre increases in magnitude and indicates differential tectonic subsidence across the basin. The variation of tectonic subsidence is best explained by the variation in the amount of crustal extension in the basin. It was found that the crust thinned by more than half of its original thickness at the basin centre (H1-NC41) and about a quarter of its original thickness in the south, at the coastal region. In summary, the total unloaded basement subsidence of the G-T Basin reveals that low basement subsidence rate corresponds to wells L1-137 and J1-NC41 (Fig. 9) on the southern margin of the basin and to B1 and A1-NC35A wells (Fig. 11) on the northern margin. However, the maximum total tectonic subsidence rate of the basement corresponds to well H1-NC41 (Fig. 10) on the basin center.

4.2 Estimates of crustal extension

Estimation of the amount of extension cross the G-T Basin in this study was achieved from deep seismic reflection (Allen and Allen, 1990, p. 90) and the results are summarized in Figure 13. The constructed subsidence curves (Figs. 9-11) represent the post-rift stage of the G-T Basin and their shape shows the thermal subsidence as a result of exponential cooling of the basement augmented by sediment loading with time. Using deep seismic reflection section (see Figs. 14a and 14b) the amount of crustal stretching across the basin has been calculated and the results achieved suggest an appropriate tectonic model for the basin subsidence mechanism. In order to show the variation in crustal thickness across the basin, both the constructed tectonic subsidence curves and cross section were used as a guide to select the best sites to measure the total sedimentary succession at each chosen location within the basin. Assuming that the pre-stretching original thickness of the crust is 35 km thick in the region and taking into consideration depth changes of Moho across the basin from 32 km below the southern coast and 26 km over other parts of the basin (see Fig. 13) the β factor and crustal thickness variation in the basin has been calculated (see Fig. 13). The following are three selected examples from different parts of the basin. At the southern margin in J1-NC41 location, the G-T Basin contains about 6 km of sediments and Moho is approximately 32 km from the surface. The amount of crustal attenuation, in this case, is estimated to be 1.38, which corresponds to 38% extension of the crust beneath the southern margin.

However, remarkably higher values of crustal extension are found in the central parts of the basin i.e. H1-NC41 location, the thickness of the sedimentary section is 11 km and the Moho rises to 26 km of the surface. The range of the extension factor over the basin depocentre is 2.33, which corresponds to 133% extension of the crust. Toward the northern margin at B1-NC35A location, the total sediment thickness is about 8.3 km and depth to the Moho is 26 km. The range of the extension factor is $\beta = 1.97$, which corresponds to 97% extension of the crust beneath the northern margin. Thus, the proof is established that a stretching-driving mechanism is a valid assumption for the basin formation and that the Mckenzie model accurately accounts for the basin evolution.

4.3 Mechanisms of G-T Basin subsidence

Passive continental margins evolve through the initiation of spreading and divergent plate motion within a pre-existing continent (Falvey and Mutter, 1981). Passive continental margins (Atlantic–type margins) are characterized by seaward thickening prisms of marine sediments overlying a faulted basement with syn-rift sedimentary sequences, often of continental origin. The post-rift seaward-thickening prisms of sediments consist predominantly of shallow water deposits (Allen and Allen, 1990). By comparing the compatibility of the Western Libyan offshore with the subsidence mechanisms and their characteristics, the stretching hypothesis was adopted and the Mckenzie model (1978) is believed to explain the subsidence mechanism of the G-T Basin. Moreover, this is considered as a reliable passive margin tectonic model, which is characteristic of subsidence history and maturation depth. Hence, it can be used as a useful exploration tool on the Western Libyan Continental margin. In the Mckenzie model, a rapid stretching of continental lithosphere produces a thinning and passive upwelling of the hot asthenosphere.

This stage is associated with block faulting and subsidence. The lithosphere then thickens by cooling, and slow subsidence occurs not associated with faulting. The slow subsidence and the heat flow depend only on the amount of stretching, which can be estimated from these quantities and from the change in thickness of the continental crust caused by the extension. The model is therefore easily tested using the subsidence results, the heat flow interpreted from temperature structure and thermal regime in this study and the form of basement topography as well as variations in Moho relief over the basin (Fig. 13). It is concluded that the Mckenzie (1978) lithospheric extension model is compatible with geological and geophysical data of the G-T Basin and explains its evolution. The following evidence supports the proposed model.

- The overall shape and pattern of the constructed tectonic subsidence curves reveal the exponential decline of subsidence and fit with those developed as a result of thermal cooling of the stretched lithosphere (see Fig. 12).
- The depth changes of Moho across the basin from 32 km below the southern margin of the basin to 26 km over other parts of the basin and thinning of the crust to more than half of its original thickness at the central parts of the basin (Fig. 13) suggests lithospheric stretching is appropriate deriving mechanism of the basin subsidence.

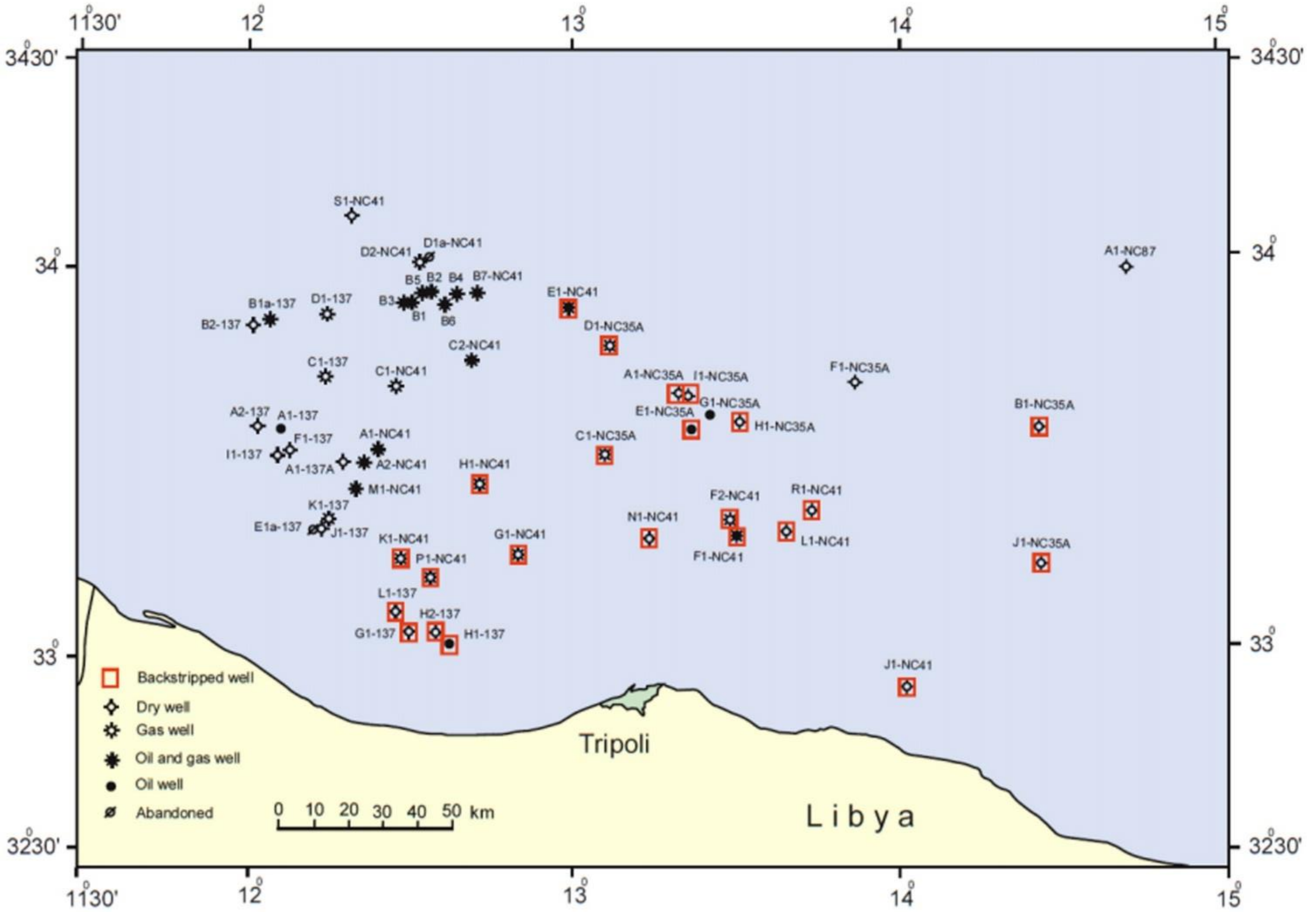

Fig. 8. The selected exploration Wells for backstripping

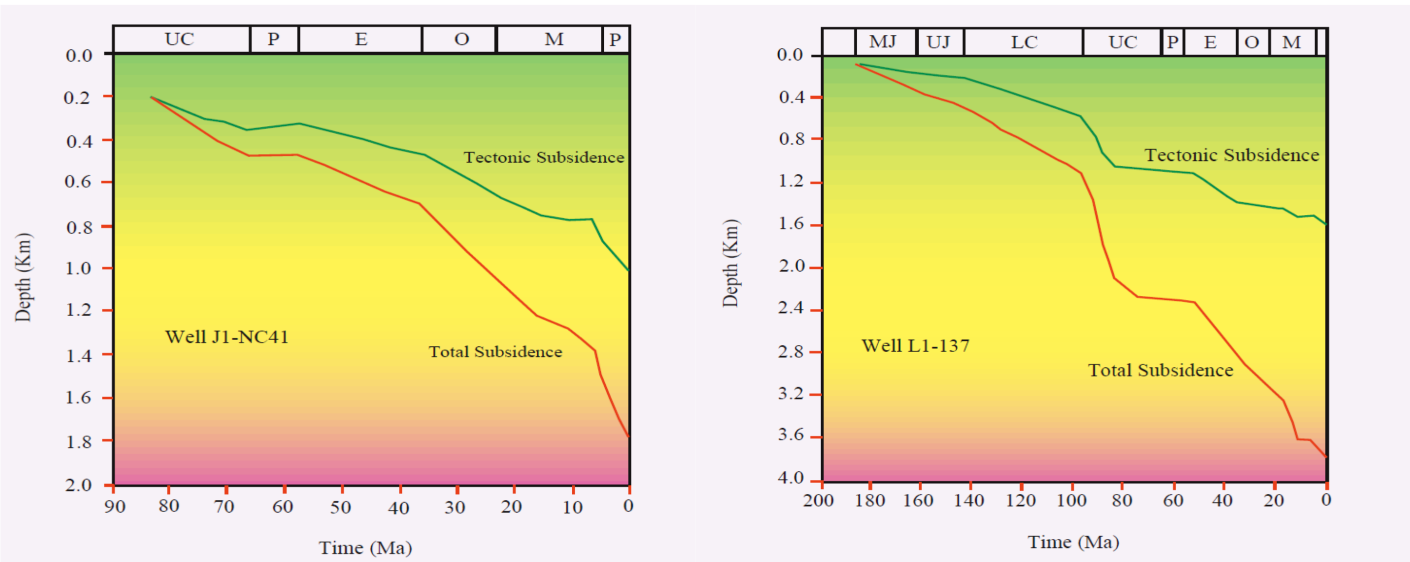

Fig.9. Total and tectonic subsidence curves at the southern margin of the G-T Basin. See Fig. 8 for well location.

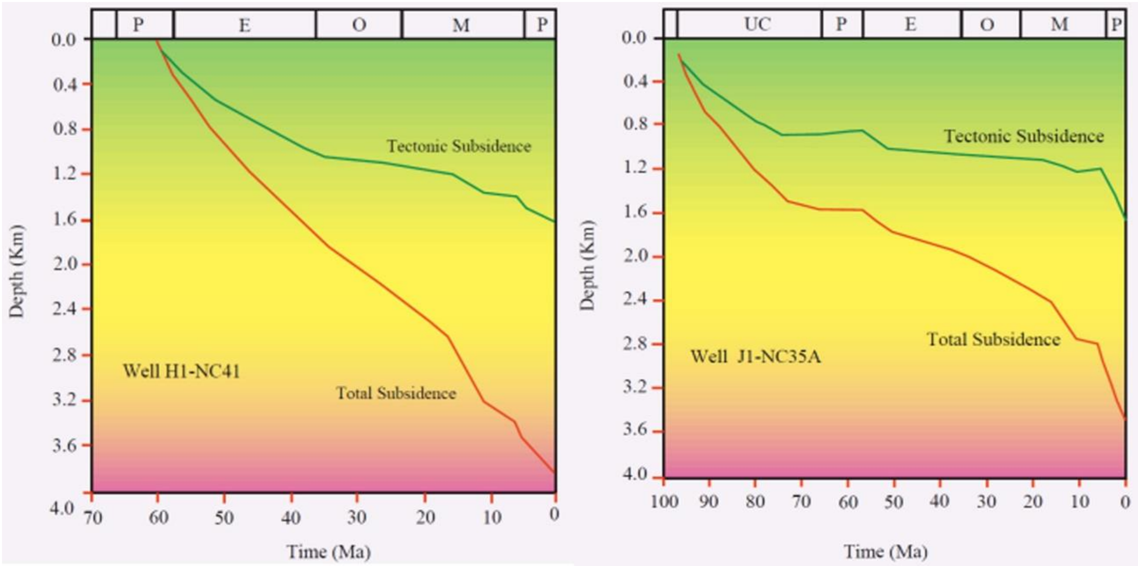

Fig.10. Total and tectonic subsidence curves at the central part of the G-T Basin. See Fig. 8 for well location.

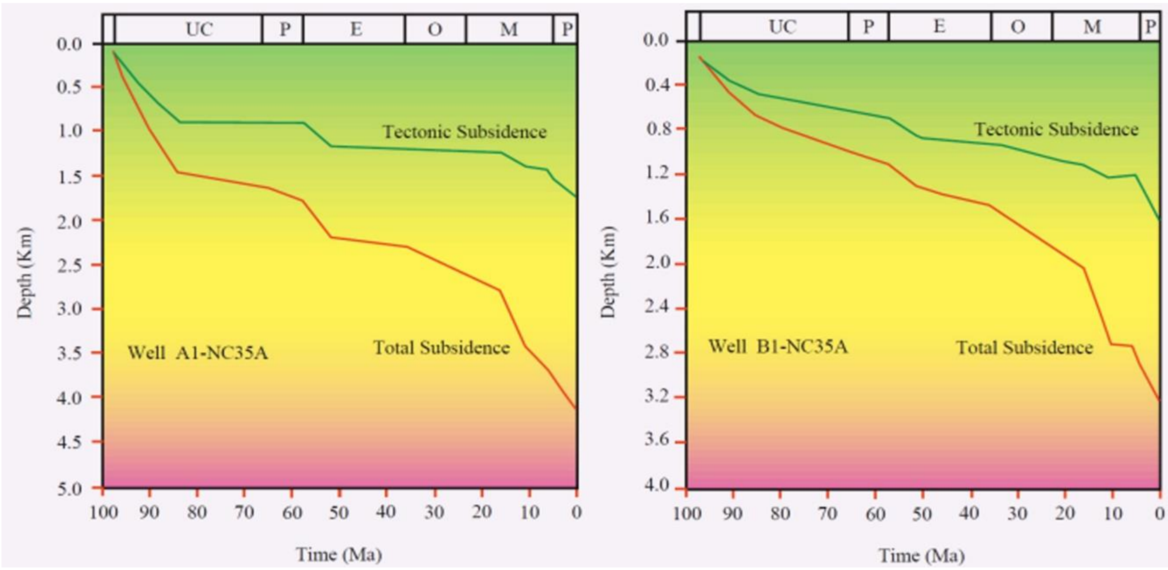

Fig.11. Total and tectonic subsidence curves at the northern margin of the G-T Basin. See Fig. 8 for well location.

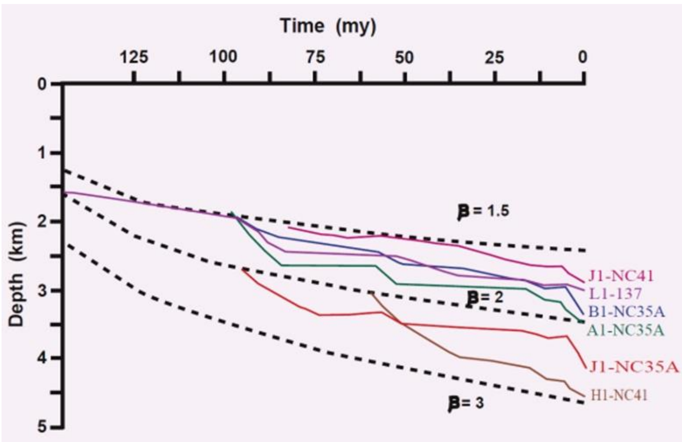

Fig. 12. Comparison between the predictive subsidence model (Beta) and the calculated tectonic subsidence curves at the G-T Basin. See Fig. 8 for well location.

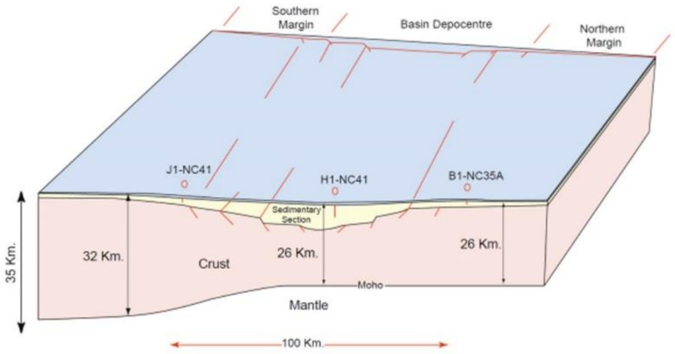

Well No.	Depth to the Moho (Km)	Thickness of Sedimentary Section (Km)	Extension Factor (β)	Extension of the Crust
J1-NC41	32	6	1.38	38%
H1-NC41	26	11	2.33	133%
B1-NC35A	26	8.3	1.97	97%

Fig. 13. The β factor of the crustal thickness variation in the basin has been calculated assuming pre-stretching original thickness of the crus is 35 km. thick in the region and considering the depth changes of the Moho across the basin.

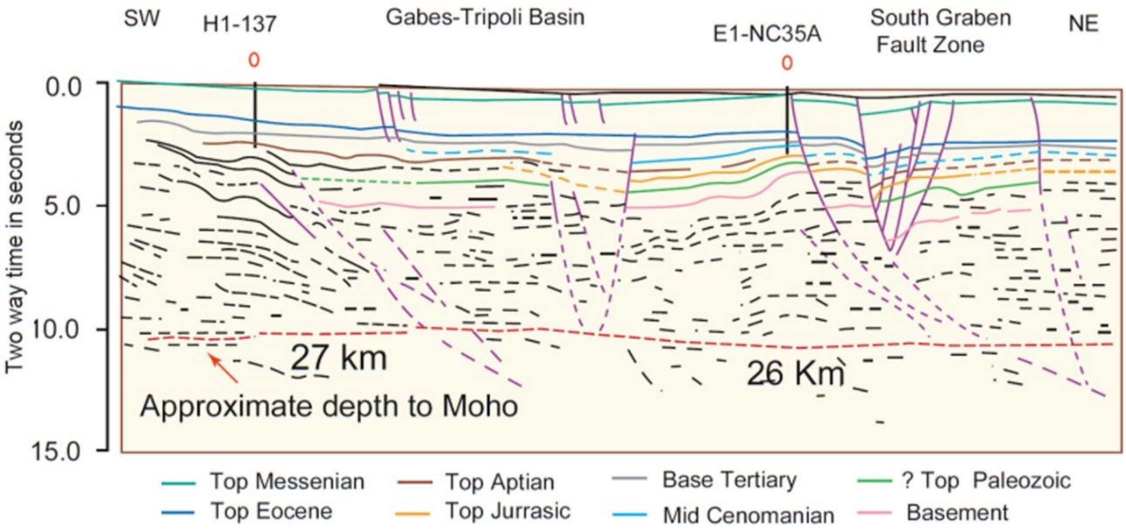

Fig. 14a. Interpreted deep seismic deep reflection section showing the crustal thickness changes across the Gebes-Tripoli basin after (Faux *et al.*, 1988)

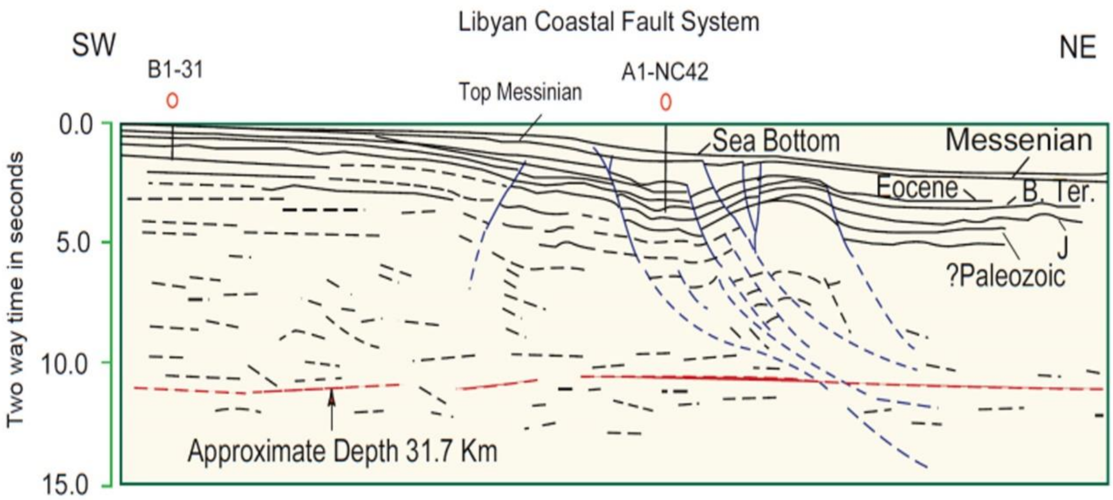

Fig. 14b. Interpreted deep seismic deep reflection section showing the crustal thickness changes across the faulty costal system after (Faux *et al.*, 1988)

5. Hydrocarbon maturation history

Thermal maturation history of the G-T Basin has been conducted in order to reduce exploration risk and enhance future exploration in the offshore area. To fulfill this objective the one-dimensional basin modeling software (Genex) of IFP has been used to model the oil window and time of oil generation in the region. Areas of potential petroleum source rocks were mapped after correction of the bottom hole temperature (BHT) and the thermal maturation history of the basin was assessed after preparation of new geothermal gradient and heat flow maps (Figs. 15 and 16). Burial history and oil window curves were constructed for all exploration wells and maturation maps of principal source rocks were prepared.

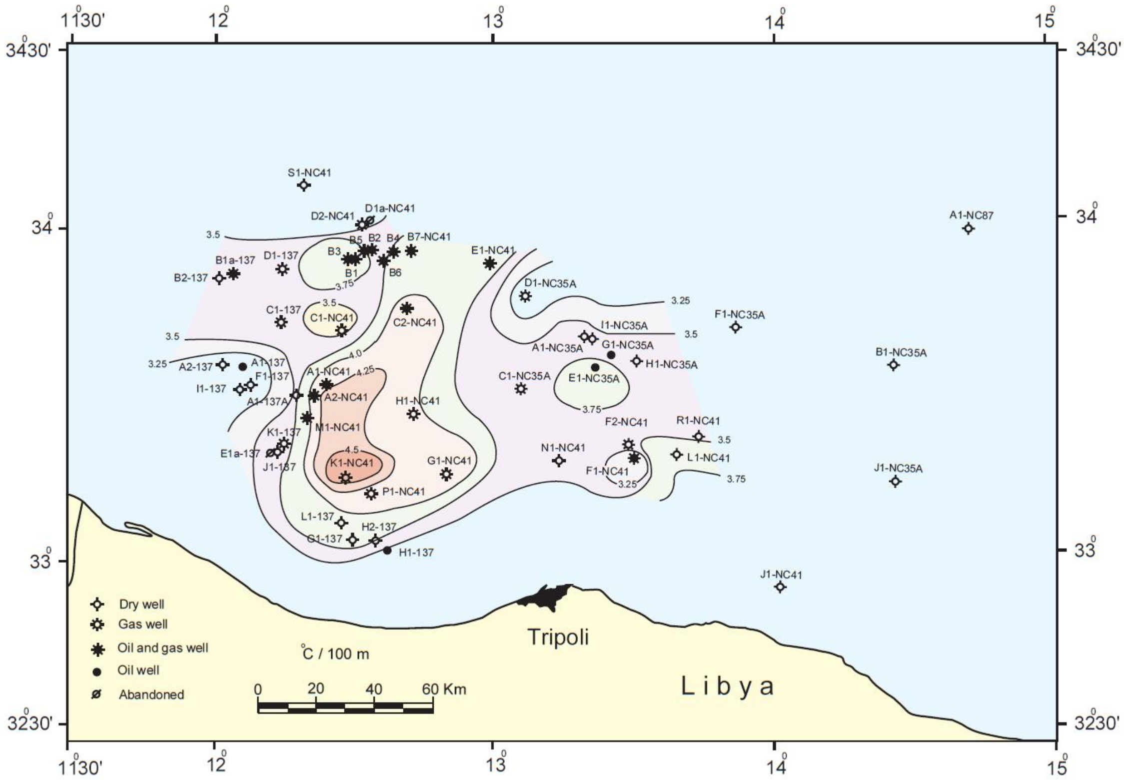

Fig. 15. Geothermal gradient map of the study area.

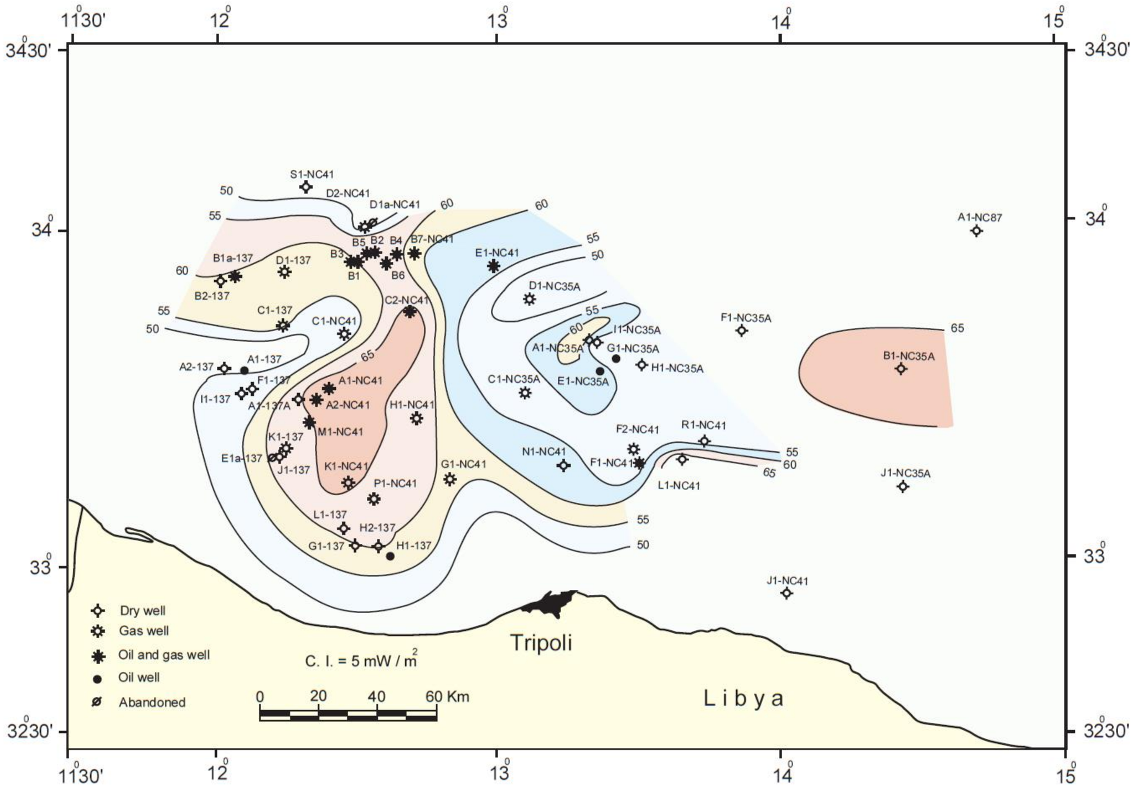

Fig. 16. Heat Flow map of the study area

5.1 Quantitative modelling of maturity data

Hydrocarbon maturation and diagenesis are functions of the thermal history of the host sediments and sedimentary rocks (McKenna and Sharp, 1998). Numerical modelling is one of the primary tools used to reconstruct this thermal history. Measured organic geochemical indices are routinely applied in the petroleum industry to determine the level of maturity of source rocks and hence to evaluate the petroleum potential of a basin. These indices reflect the cumulative effect of time and temperature on organic matter maturation and consequently can fix only the present position of the oil-generative window (OGW) (Ejedawe *et al.*, 1984). They are inadequate in interpreting the maturation history of a source rock or the basin (Ejedawe *et al.*, 1984). Knowledge of the latter is important to the accurate assessment of the timing of oil generation and expulsion, and in predicting variations in the type of hydrocarbons reaching the trap at various times. To evaluate the thermal and maturation history of the G-T basin, burial history curves were constructed for 44 wells. These, (Figs. 17-20) are representative of the different thermal scenarios across the basin. Given the fact that all exploration wells from this large basin were examined in detail, the results may be considered reliable.

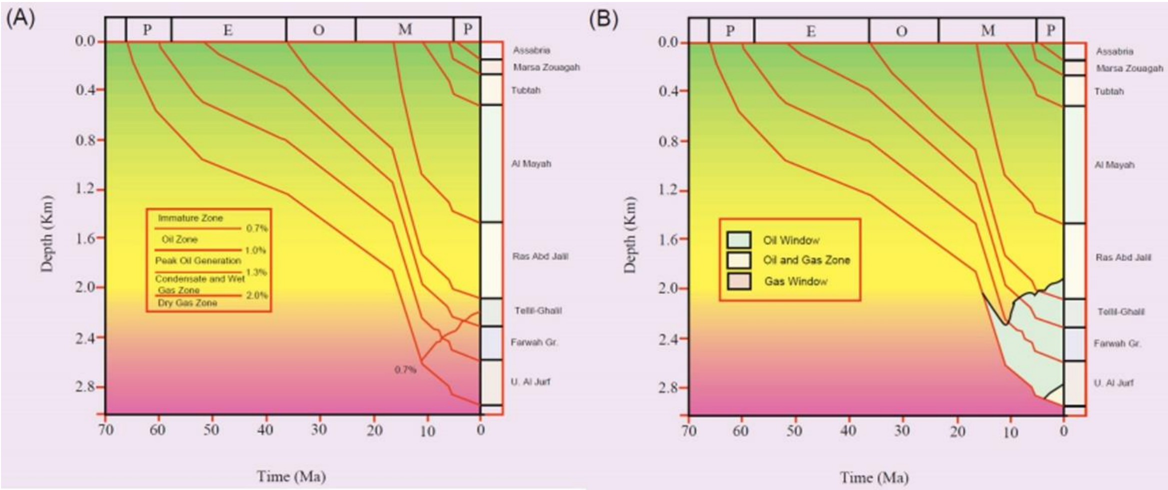

Fig. 17. Burial history curves for well B2-NC41 showing (A) Maturity windows and (B) Hydrocarbon windows

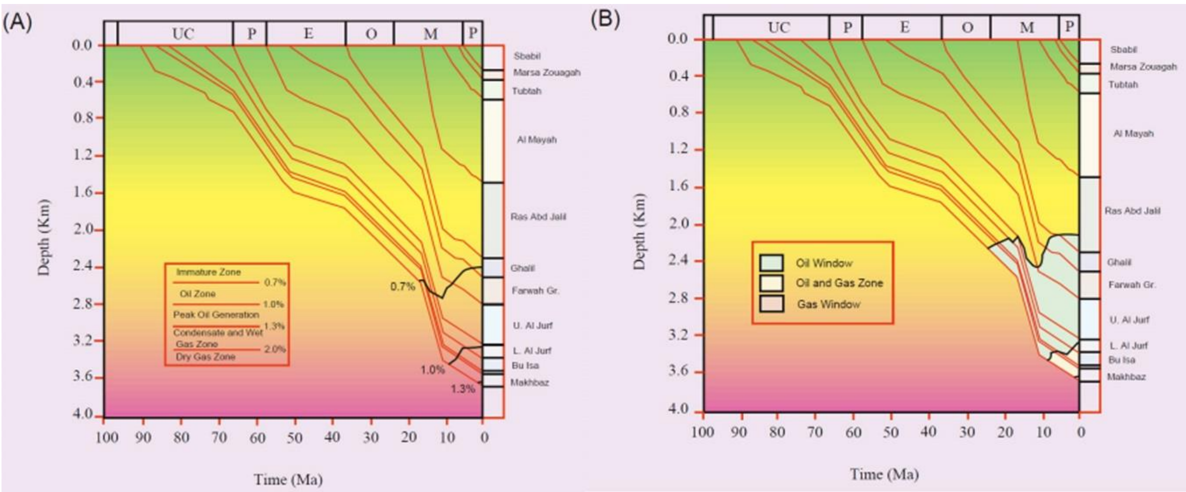

Fig. 18. Burial history curves for well D2-NC41 showing (A) Maturity windows and (B) Hydrocarbon windows

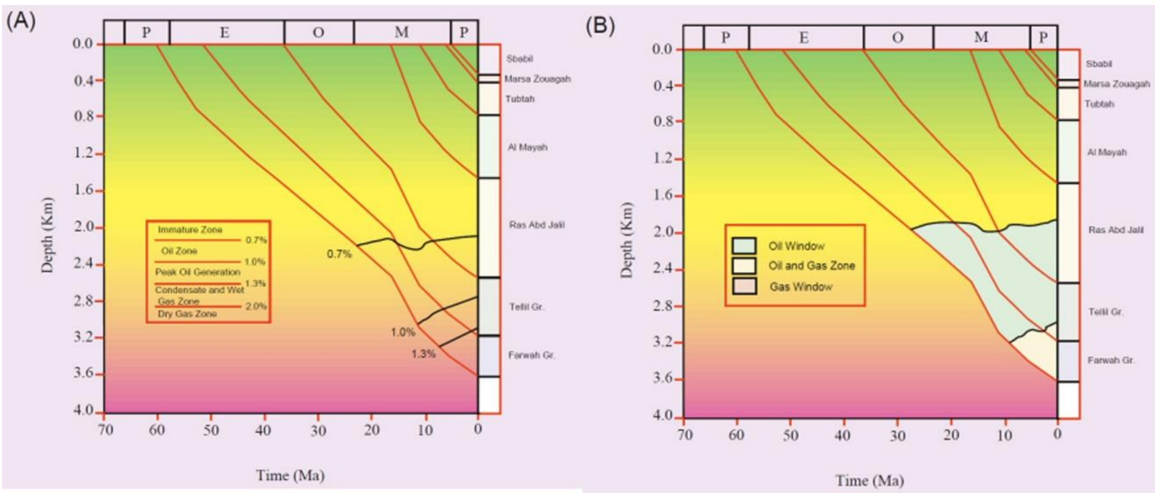

Fig. 19. Burial history curves for well H1-NC41 showing (A) Maturity windows and (B) Hydrocarbon windows

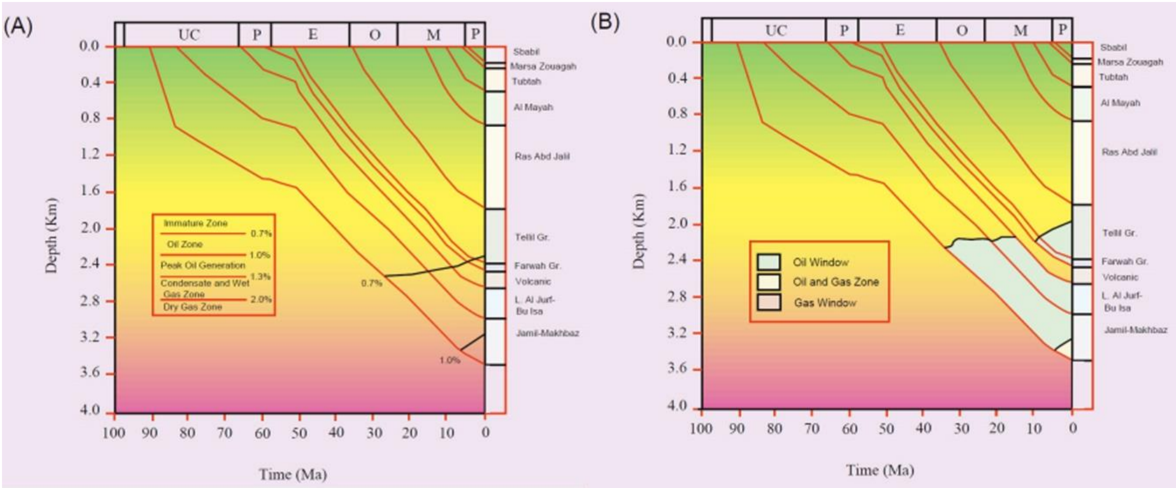

Fig. 20. Burial history curves for well H1-137 showing (A) Maturity windows and (B) Hydrocarbon windows

Thermal histories of the drilled wells were first evaluated using the corrected measured temperatures to generate a range of thermal histories compatible with the observed TAI data (Fig. 21). Calibrating heat flow and thermal conductivity to match observed subsurface temperatures is frequently done in thermal modelling. When there are no other thermal indicator data (e.g. vitrinite reflectance, T_{max}, TAI) to calibrate the thermal model, the fit to present-day temperatures is the only measure of the accuracy of the model (McKenna and Sharp, 1998). Maturation reliability is confirmed by the predicted vitrinite values, and are in accord with the observed data. The calculated Ro is in general agreement with observed thermal TAI, T_{max} and Ro. The decrease in depth to the oil window from the margin to the basin centre generally agrees with the measured geothermal gradient and heat flow.

Modelling of the B2-NC41 and D2-NC41 locations (Figs. 17-18) in the vicinity of the giant Bouri oil field and D structure respectively, indicates that the principal source rocks Farwah Group and Al Jurf formation, as well as the whole late Cretaceous sequence, are in the mature stage. The depth to the oil window at B2-NC41 and D2-NC41 wells is at 2200 and 2400 respectively. In fact, only the lower parts of the Middle-late Eocene Tellil Group has reached the Ro of 0.7% (the upper limit of the oil window). In contrast, in the central parts of the basin at H1-NC41 (Figs 19a and 19b), the model shows about 320m decrease to the top of the oil window compared with the northern margin at well D2-NC41 (Figs 18a and 18b). The depth to the main stage of oil maturity at this location is 2080 m (Fig. 19a). This depth corresponds to the middle section of the Oligocene-early Miocene Ras Abd Jalil Formation. Thus, as a result of increasing palaeoheat flow toward structurally low areas at the depocentre of the G-T Basin, sequences younger than the Eocene have entered the oil window since 8 Ma. The current depth to the top and base of the oil window ranges from 2080-3100 m giving a total thickness of 1020 m (Fig. 19a).

In contrast, at D2-NC41 location, the depth interval of the oil windows extends from 2400-3650 m giving a 1250 m thick oil zone (Fig. 18a). The model thus shows an increase of 230m in the oil window toward the northern margin from the depocentre of the basin at H1-NC41. This clearly demonstrates the impact of the thermal regime on the maturity level, thickness of oil windows, and timing of hydrocarbon generation. Modelling of the H1-NC41 well indicates that the Farwah Group was mature enough to begin generating oil in the early Miocene at 22.5 My (Fig. 19a). However, at the northern margin (B2 and D2-NC41 wells) oil was generated from the Farwah source much later at about 8 my (Figs. 17a and 18a). This is considered by this author as a crucially important result that could have a significant effect on exploration strategy in the basin.

Earlier oil generation and thinner oil zone toward the depocentre of the basin is simply explained by the constructed heat flow and geothermal pattern, which are both higher in the central parts than the basin margins (see Figs. 15 and 16). This hypothesis suggests that hydrocarbon generation at the central parts started 14 My earlier than at the basin margins. Hence, an enormous amount of this earlier-generated hydrocarbon has been subjected to secondary cracking into gas and condensate. This conclusion is supported by the explored gases and condensate fields at the central parts of the basin at H, F and C structures and liquid hydrocarbon discoveries at the Bouri structure toward the northern margin.

In the vicinity of the H1-137 location, the Farwah Group first entered the early oil maturation stage in the early Pliocene (at 5.0 Ma.), and has continued to the present (Fig. 20a). Today, the early Eocene-late Cretaceous section lies within the oil maturity window (Fig. 20b), and most of this section has been in a generative state since the end of the Oligocene (26 Ma.) (Fig. 20a). The depth interval of the zone of oil maturity (%Ro=0.7-1.0) is approximately 2300-3150 m and the base of the oil window of %Ro =1.3 could extend to more than 3500 m (Fig. 20a). The increased depth to the top of the oil maturity zone and greater range of the zone in the northern and southern margins compared to the central basin are due to the lower heat flow over the basin margins. The earlier maturation time in the central basin is primarily a function of the higher heat flow compared to the northern and southern parts of the basin.

Modelled thermal histories that satisfy the observed maturity data (Fig. 21) indicate a gradual increase of thermal maturity with depth and lack of significant cooling episodes. Analysis of TAI, T_{max} and thermal maturation data provides some constraint on the depositional and evolutionary history of the sedimentary succession within the G-T Basin. Both measured (TAI and Tmax) and predicted Ro maturation data for the basin indicate that palaeotemperatures were invariant and persisted without predictable changes since at least the post-rift stage. The maturity data indicate that cooling has not occurred since the deposition of the principal source rocks (late Cretaceous-early Eocene). Because significant regional uplifting and erosion during the post-rift stage is not evident, and water flow in the basin is limited, cooling has not occurred and probably the present thermal regime reflects the post-rift palaeoheat flow of the basin. However, exceptions locally exist toward the southern flanks of the basin where the stratigraphic record confirms the presence of a major gap in the sedimentary sequence from the Campanian to the Middle Eocene time during which cooling episodes possibly occurred.

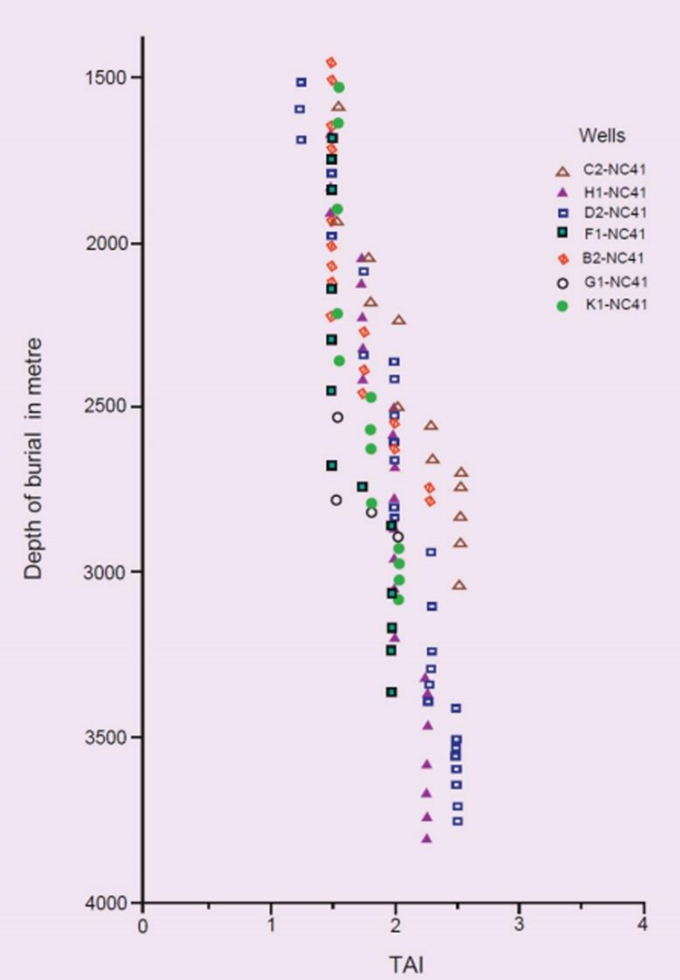

Fig. 21. Plots of the observed thermal maturity indictors (TAI) showing gradual increase of maturity with depth.

5.2 Timing of hydrocarbon generation

Geochemical analysis and basin modelling have confirmed the source rock potentiality of the early Eocene-late Cretaceous to generate hydrocarbon in the study area. They suggest that rich source intervals in both the Farwah Group and Al Jurf Formation would yield major oil and gas to associated reservoirs. Based on the interpreted thermal regime and thermal maturation levels the main Petroleum kitchen has been mapped within the G-T Basin. The area of major hydrocarbon generation occupies the central parts of the basin (Fig. 22 and 23). It has the capacity to generate major hydrocarbons, which have undergone a short-range migration to fill the Eocene Farwah and Tellil reservoirs. It is proposed here that hydrocarbon has been generated in a wide span of time and from several proven organic-rich sources, which have been encountered at various drilling depths. The impact of the thermal regime and temperature structure proposed in this study is conspicuously manifested in variation across the basin of the timing of hydrocarbon generation, of depth to the oil window and depth interval of the oil zones. The results match observed petroleum occurrences in the G-T Basin and can be used as a sensible approach to asses migration pattern and reduce exploration risk in the study area. Hydrocarbon has been generated from the Al Jurf and Farwah sources during Oligocene and early Miocene in the central G-T Basin. The model shows that hydrocarbon in the H1-NC41 location has been initiated at 22.5 my from Farwah source and probably at about 30 my from the Al Jurf source (Fig. 19a). Both of the principal source rocks are presently at the condensate and wet gas zone (Ro = 1.3-2.0%). However, at the northern margin of the basin, toward the vicinity of D2-NC41 location (Fig. 18a), the Al Jurf Formation has reached the peak of oil generation (Ro=1.0-1.3%) and the timing of oil generation from this source began 14 my ago (later than the central basin by 16 my). This scenario is repeated toward the southern margin at well H1-137 (Fig. 20a) where the Al Jurf Formation started to generate hydrocarbon since only 15 my ago, again much later (by 15 my) than generation time at the basin depocentre. The model also indicates that the late Cretaceous-Palaeocene Al Jurf Formation is in the early stage of thermal maturity in the oil zone i.e. Ro = 0.7-1.0%. This result matches with the observed oil shows that have been found at H1-137 well. Similar results, however, are obtained when the second important source, the Farwah Group, is examined. Hydrocarbon generation from the group source at the northern margin (D2-NC41) (Fig. 18a) and the southern margin (H1-137) (Fig. 20a) of the G-T Basin, commenced at 8 my and 5 my respectively and in both locations the group is in the early stage of thermal maturation (Ro=0.7-1.0%). Nevertheless, at the central parts of the basin (H1-NC41), hydrocarbon generation started at 22.5 my ago (Fig. 19a). A time difference ranging between 14.5-17.5 my occurs from the basin centre to the margins. Thus, basin modelling yields consistent results and clearly matches with the observed petroleum occurrence, which is, gas discoveries at the central parts and liquid hydrocarbon accumulations toward the north and minor, but also liquid, accumulations at the southern parts. These facts have crucially important strategic values in the near future petroleum exploration programs. Most known traps were formed post-Eocene, and the major generation-migration and accumulation of petroleum commenced during early Miocene and continues to the present; however, the timing of oil generation for each of the potential source rocks varies throughout the study area as a function of the heat flow and depth of burial. Because of the timing of peak oil generation varies spatially, overlaps in the timing of generation exist among the different source rocks. This relationship enhances the prospectivity of this area because it allows late migration in multiple source rocks, and early migration and accumulation into numerous porous Eocene reservoirs. The structural traps within or close to the interpreted petroleum kitchen are here rated as highly prospective. Exploration risks generally increase with the distance from the principal area of hydrocarbon generation and significant hydrocarbon accumulation are remained to be discovered in the basin.

In conclusion, basin modelling results and burial history analysis of the G-T Basin show that hydrocarbon generation took place during a wide time span. It has been found that oil started to generate in the basin depocentre from the principal Al Jurf and Farwah sources during 30 and 22.5 my respectively but at the northern and southern margins it started some 15 my later. Since then hydrocarbon has migrated out of the basin depocentre, where the main petroleum kitchen is located, toward the basin flanks in a radial pathway pattern. However, an enormous amount of oil has also been proven to be generated and expelled out of the Al Jurf and Farwah Groups within the northern flanks. Thus, most but not the entire liquid hydrocarbon in the vicinity of the giant Bouri oil field probably originated from these.

Variation of palaeoheat flow undoubtedly controlled the changes in the timing of hydrocarbon generation across the basin and depth to the top of the oil windows as well as the depth interval of the different hydrocarbon liquid and gas windows. The present-day heat-flow regime is a key factor to the understanding of the hydrocarbon habitat in the basin and offers a valid answer to the explorationist as to where, how and when hydrocarbon can be found in the basin. The difference between the timing of oil generation and the beginning of Farwah source rocks deposition is more than 40 my, which indicates that a normal rather than high palaeoheat flow regime prevailed since source rocks deposition. It is found that in basins of high heat flow i.e. Pattani Basin, Gulf of Thailand, hydrocarbon generation started since 5-7 m.y. after deposition (Bustin and Chonchawalit, 1997).

5.3 Source rock potential of the G-T Basin

Source rock maturity maps are presented for the Middle-Upper Eocene, late Palaeocene-early Eocene and Maastrichtian-Palaeocene sequences in terms of vitrinite values (Figs. 22-24). The maturity maps were constructed using all available geochemical data, the basis of which is derived from Agip oil company and Petroleum Research Centre labs (Rock-Eval pyrolysis data on well A1-NC35A). All types of maturity indicators were considered including thermal alteration index (TAI), actual vitrinite reflectance and Rock-Eval pyrolysis Tmax. Two principal rock intervals are recognized in the study area. They are the Al Jurf formation and the Bilal formation of the Farwah Group. Both intervals are classified as very good source rocks.

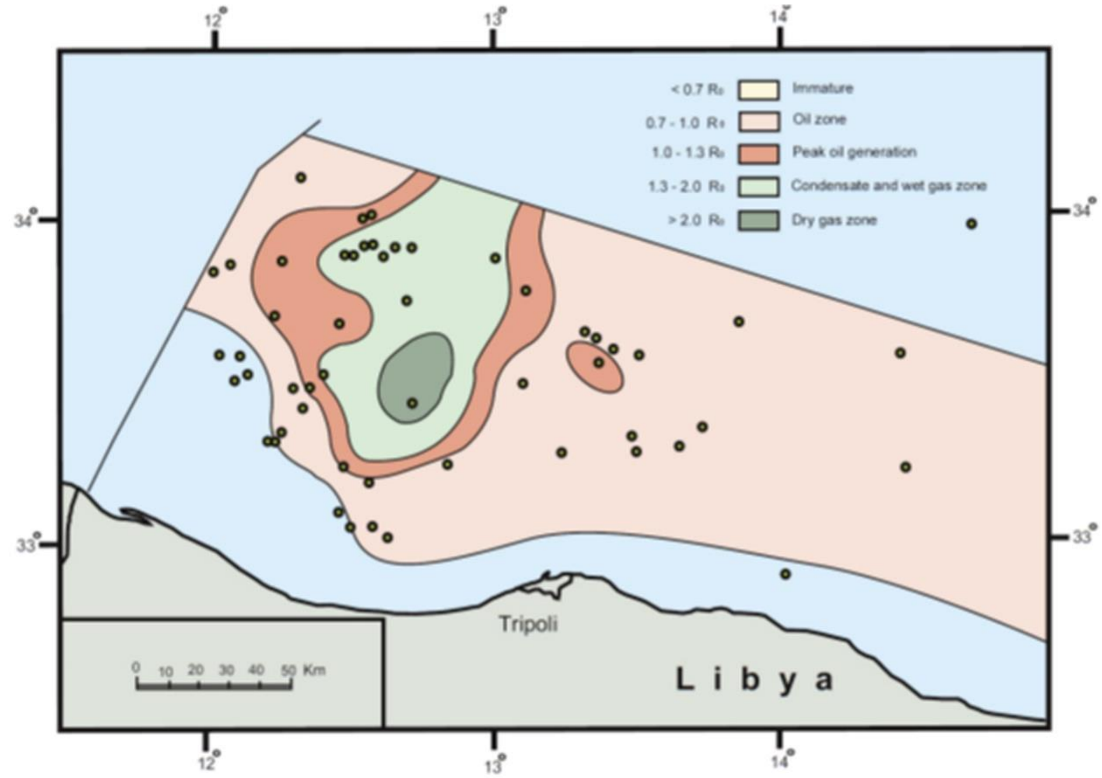

Fig. 22. Thermal maturity of the base of the lower Aljurf formation at 0.0 Ma

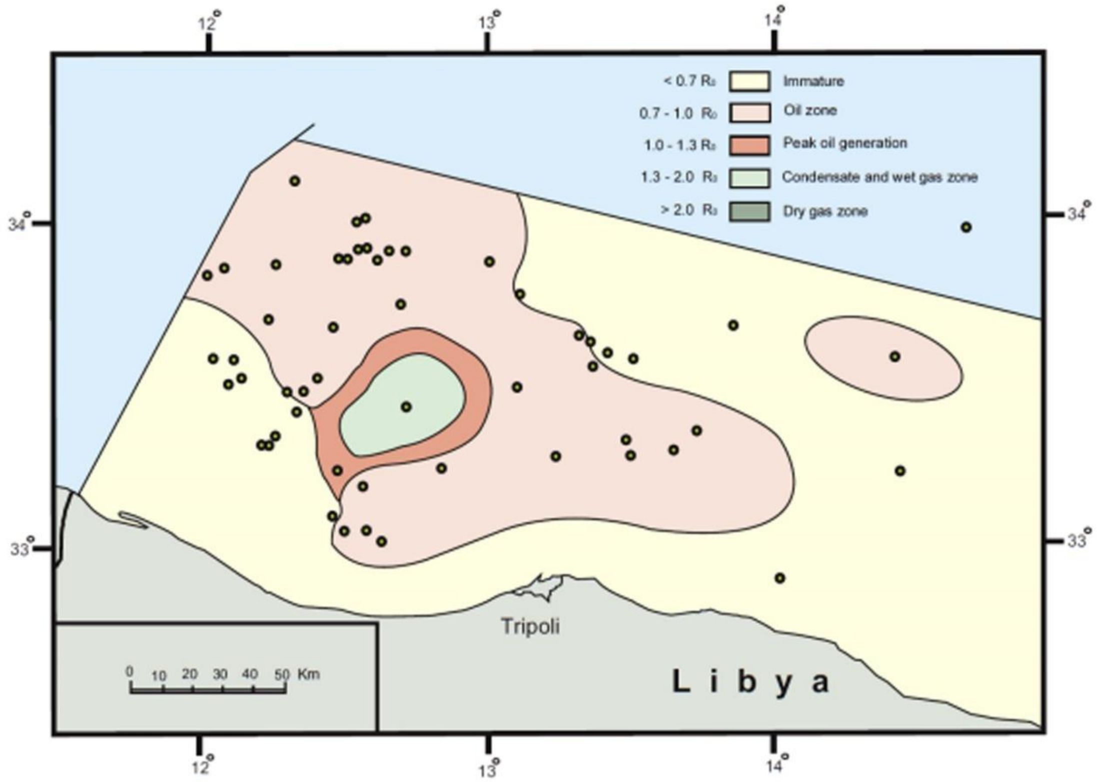

Fig. 23. Thermal maturity of the base of the Farwah group at 0.0 Ma

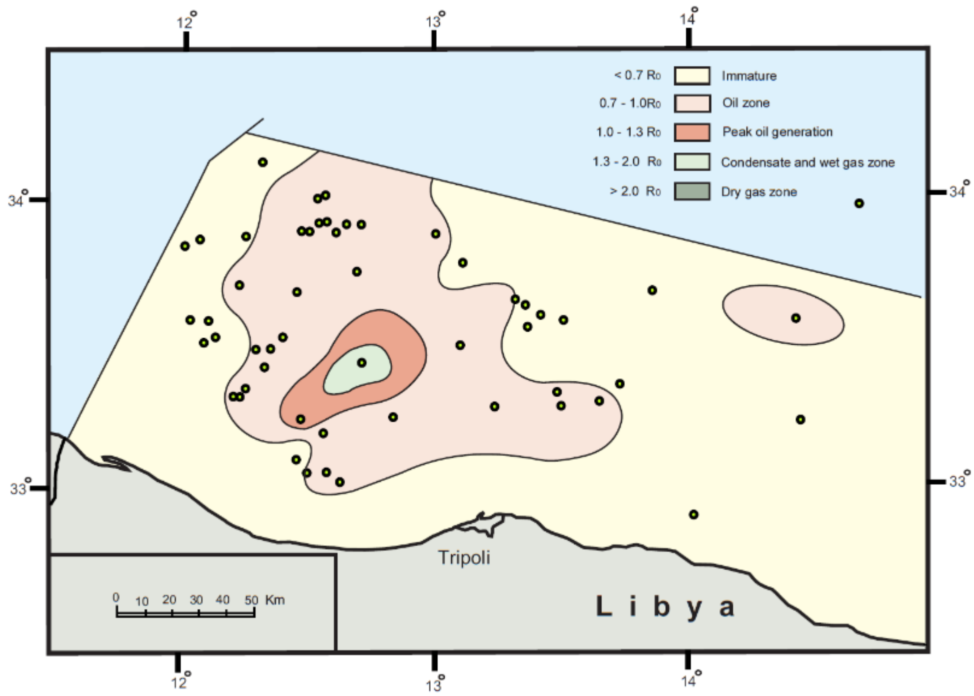

Fig. 24. Thermal maturity of the base of the Tellil group at 0.0 Ma

For mapping purposes, all maturity data are presented in vitrinite reflectance values. The constructed maturity maps of the late Cretaceous-Palaeogene sequences were prepared to show maturity levels referred to the present time. Data concerning the sequences were available from all exploration wells at 44 locations distributed over all the basin, therefore the maps constructed can be considered reliable. Maturity windows are almost similar to that of Tissot and Welte (1984) and were defined as follows:

< 0.7 Ro immature
0.7-1.0 Ro oil zone
1.0-1.3 Ro peak oil generation
1.3-2.0 Ro condensate and wet gas
> 2.0 Ro dry gas zone

5.3.1 Source potential of the Al Jurf Formation

The Maastrichtian lower Al Jurf formation is comprised of deep shales and limestones with planktonic foraminifera. The quality of the kerogen evaluated geochemically from 13 wells in the basin shows that the upper and lower Al Jurf formations are composed of fair to very good quality source rocks with levels of excellent potential to generate hydrocarbon i.e. at wells B1 and C1-NC41. The maturity maps related to the base of the Lower Al Jurf Formation show the complete maturation of the area (Fig. 22). The constructed maturity maps show a central over mature zone in the deep parts of the basin (Ro = 1.3-2.0 and > 2.0) surrounded by a narrow belt of mature facies in the peak of oil generation (Ro = 1.0-1.3). These zones then pass laterally into mature facies in the oil zone (Ro = 0.7-1.0) over all parts of the basin.

5.3.2 Source potential of the Farwah Group

The late Palaeocene-early Eocene Bilal Formation of the Farwah Group contains a good petroleum source potential. TOC contents from geochemical analysis of 13 wells reveal fair-very good organic richness in the range of 0.2-4.74%. This formation is mature-overmature in most parts of the basin and is actively generating oil at present. Kerogen content is highly oil and gas prone and basically comprises continental herbaceous phytoclasts, continental woody debris and amorphous organic matter. The maturity map for the late Palaeocene-early Eocene, of the Bilal Formation (Fig. 23) shows large portions of the G-T Basin are immature (Ro = < 0.7). The immature areas are well established toward the east, south and almost the northeastern parts of the basin. Nevertheless, mature zone (Ro = 0.7-1.0) extends over large areas of the central basin (Fig. 23) and coincides generally with areas of relatively higher heat flow. Locally, toward the centre at H1-NC41 location, the sequence attained over mature stage and is in the condensate and wet gas zone (Ro = 1.3-2.0). Lower maturity values in the southern, eastern and northern G-T Basin can be attributed to the higher structural position and lower heat flow through time relative to the deeper central G-T Basin.

5.3.3 Source potential of the Tellil Group

The Middle-Upper Eocene Tellil Group is generally of poor-fair quality source rock. In most parts of the study area, the TOC ranges from 0.2-0.8%. The sequence is either immature or mature locally in its lower part. Since it is lean in organic carbon, and in many parts of the basin, only partially mature, it is not considered as important as the earlier deposited sequences of Farwah and Al Jurf. The maturity map (Fig. 24) of the Tellil Group clearly mimics the same pattern of the Farwah Group (Fig. 23), and is again consistent with the modelled thermal regime and temperature structure of the basin. The maturity map (Fig. 24) shows a large mature area in the oil zone (Ro = 0.7-1.0) located in the basin depocentre and coincides with the interpreted principal petroleum kitchen of the basin which delineates the area of highest heat flow. A narrow belt exhibiting a bull's eye closure of mature and over mature zones is present at the basin centre (Fig. 24). Although, the group is in the mature stage over large areas in the central parts, its hydrocarbon potentiality is not considered here. This is because the shallow shelf carbonates and shales have poor source potential with an average of less than 0.5% and basin modelling yields strong evidence that the sequence is not capable of expelling hydrocarbon. The hydrogen index measured at well A1-NC35A is less than 100 and the type of organic matter in most parts of the basin comprises of rare algae and a mixture of continental herbaceous and woody debris with amorphous materials that indicate the environment of deposition was anoxic.

5.3.4 Hydrocarbon potential of other source rocks

In most parts of the study area, all the Eocene and late Cretaceous source rocks are mature or overmature but only the Farwah and Al Jurf formation are organically rich enough to generate and expel major quantities of hydrocarbon. However, the possibility of other older sources is not ruled out. This is supported by the fact that in many parts of the basin they have not been penetrated by drilling. Moreover, in a few cases, however, when they have been encountered and geochemically analyzed. Geochemical evidence from the Tunisian extension of the G-T Basin, have confirmed the source rock potentiality of Cenomanian-Turonian limestones of the Bahlol formation (Ben Ferjani *et al*., 1990). It is considered as the main source rock for the late Cretaceous reservoirs and for the early Eocene reservoir where tectonics allow the migration of the Bahloul oil into the Ypresian reservoir.

It is crucially important to mention that, the early Eocene Bou Dabbous Formation (equivalent to Hallab Formation in Libyan offshore) source for the offshore oils implies either the absence of Cretaceous-based petroleum system or the presence of an effective seal, which prevents Cretaceous-derived oils from reaching Tertiary reservoirs in the Gulf of Gabes. The occurrence of Cretaceous-derived oils immediately onshore suggests the latter possibility is the case and makes pre-Tertiary reservoirs attractive targets in the offshore (Hughes and Reed, 1995). If this hypothesis is true then the difference between the early Tertiary and late Cretaceous pressure systems in the Libyan offshore may simply be attributed to the presence of the same seal between the two systems. It is here proposed that the potentiality of the late Cretaceous reservoirs is similarly augmented in the Libyan offshore and that enormous amount of hydrocarbon yet remain to be discovered within the basin. For the first time, a new temperature structure and thermal regime have been constructed based on corrected BHT and are consistent with observed thermal maturity indicators. This new heat flow regime is remarkably lower than that of the AGIP oil company (Benelli, *et al*., 1985) as the long time lapse between source rock deposition and hydrocarbon generation would suggest. This fact enhances the chance of finding more liquid hydrocarbon within the basin.

6. Summary and conclusions

The G-TBasin is a Mesozoic-Cenozoic basin which was initiated as a result of widespread, late Triassic, Jurassic and early Cretaceous extensional movements that developed over a broad zone of strain between the African and European plates. A detailed facies and sequence analysis carried out in the G-T Basin has resulted in a stratigraphic correlation scheme and construction of depositional models for the entire Mesozoic-Cenozoic succession. The sedimentary sequences forming the bulk stratigraphy of the G-T Basin comprises a 10 km-thick succession of Early-Middle Triassic, nonmarine and marine clastics, late Triassic-Middle Jurassic, predominantly shallow marine carbonates and evaporites and Middle Jurassic-Recent marine carbonates and clastics. The tectono-stratigraphic units comprise 7 sequences on the time scale of second-order sequences. For most sequences and sequence boundaries, either a eustatic or tectonically enhanced origin can be established.

The analysis of the basin-fill history of the G-T Basin from the Triassic until the Holocene reveals that the basin underwent development from a continental sedimentary basin located on Gondwana to an epicratonic rift basin. When major extensional movements ceased (late Cretaceous), the basin subsided thermally and developed as part of a passive continental margin on the North African plate margin. The basin also has been subjected to strike slip movements and compressional events lead to inversion during the late Cretaceous and Eocene time. The dominant driving mechanism of subsidence clearly seems to have been subsidence due to cooling following lithospheric thinning and the tectonic subsidence history shows that a simple stretching model successfully predicts the overall characteristics of the long-term patterns of the tectonic subsidence of the basin. Regional deep seismic reflection profiles in the G-T Basin shows that the Moho shallows from 32 km beneath the unrifted coastal region to about 26 km below other parts of the basin. The observed stretching factor, in the range β=1.38-2.33, corresponds to a crustal extension of 38-133%. The highest values of the stretching factor are associated with the basin centre; values diminish outward toward the basin margins. The region of greatest thinning is directly below the region of greatest sedimentary thickness in the G-T Basin depocentre.

The crust has been thinned a half and less than a half of its original thickness at the central and northern parts respectively and only thinned to a quarter of its original thickness at the coastal region. The central and northern regions of the basin have similar stretching values; however, the central area is characterized by the older timing of HC generation and shallower depth of the oil window. In another words, similar stretching factor but different depth of maturity windows and different timing of HC generation characterize these areas. Therefore, crustal nature (age and composition) cause important HF variations and depth of burial is causing spatial variation in the depth of HC window within the G-T Basin. Hence, both the proposed stretching hypothesis as well as depth of burial are useful exploration tool in the basin and are considered as paramount to the understanding of basin evolution and hydrocarbon accumulation.

The observed organic thermal maturity measurements in the G-T Basin indicate that the pre-Middle Eocene sequences are at a mature to over mature stage. The Middle-Upper Eocene Tellil sequence attained an early mature stage while locally the Oligocene-Early Miocene is in a mature stage. The rest of the Tertiary sequence is immature. The depth variation to the modelled top of the oil maturity 0.7 Ro ranges from 2000-2400 m in the G-T Basin. The highest Ro maturity values in the principal source rocks (Farwah and Al Jurf) are in the basin centre, and that Ro values change gradually toward the basin margins. This anomaly is attributed to the spatial variation in depth of burial and crustal thinning toward the basin centre, as is witnessed by the deep seismic interpretation across the basin.

The calculated organic maturities indicate that the early Eocene-late Cretaceous sequences are either mature or over mature with respect to the oil window. The current depth to the top of the oil window ranges from 2000 to 2400m, and the base of the oil window ranges from 3000 to 3650 m. Combined geohistory and basin modelling indicates that the main phase of hydrocarbon generation from the Farwah source began 22.5 to 5.0 Ma, and continues until the present. A relatively late generation (approximately 30-50 my after deposition) is ascribed to the lack of high palaeoheat flow and moderate burial, which is consistent with a passive margin and post-rift thermally subsiding basin. Hydrocarbon has been generated from the Al Jurf and Farwah sources in the basin centre first and earlier than the basin margins by about 15 my. Hydrocarbon generation commenced about 30 my from the Al Jurf Formation and at 22.5 my from the Farwah source in the basin centre. It began, however, to generate 15 my later from both principal sources at the basin margins.

6. Acknowledgments

Editors of the 2nd International Conference on Geosciences of Libya reviewed the manuscript and made helpful suggestions and comments. The author wish to thank the management of the National Oil Corporation (NOC) for the sponsorship and permission to publish the data and interpretations in this paper. A major part of this work was carried out at the Earth Sciences department of the University of Manchester as part of the requirements for a PhD under the supervision of Dr. Mike Anketell. His support and encouragement are greatly appreciated. Further improvements of the results were added to the discussion based on the author working experience in the Mediterranean region.

References

Allen, P. A. and Allen, J. R. (1990) Basin analysis principles and applications. Blackwell Scientific Publications, London, 451p.

Benelli, F., Mcavaggion, M. and El Ashuri, O. (1985) Oil habitat in concession NC41, Agip N.A.M.E., Tripoli.

Bustin, R. M. and Chonchawalit, A. (1997) 'Petroleum source rock potential and evolution of Tertiary strata, Pattani Basin, Gulf of Thailand', *Am. Assoc. Petrol. Geologists*, 81, pp. 2000-2023.

Ejedawe, J. E., Coker, S. J. L., Lambert-Aikhionbare, D. O., Alofe, K. B. and Adoh, F. O. (1984) 'Evolution of oil-generative window and oil and gas occurrence in Tertiary Niger Delta basin', *Am. Assoc. Petrol. Geologists*, 68, pp. 1744-1751.

Falvey, D. A. and Mutter, J. C. (1981) 'Regional plate tectonics and the evolution of Australia's passive continental margins', *BMR Journal of Australian Geology and Geophysics*, **6**, pp. 1-29.

Faux, F. A., Johnson, W. R., Kienzle, J. K. and Mcdowell, E. H. (1988) Regional Geophysical studies. In: Mccrossan, R. G. and Booth, J. E. (eds.) *Geology of western offshore Libya and adjacent regions*. Sirt Oil Company, 1, pp. 37-79.

Hammuda, O. S., Sbeta, A. M., Mouzughi, A. J. and Eliagoubi, B. A. (1985) *Stratigraphic Nomenclature of the north-western offshore of Libya*. The Earth Sciences Society of Libya, Tarabulus, Libya, 166p.

Haq, B. U., Hardenbol, J. and Vail, P. R. (1987) 'Chronology of fluctuating sea levels since the Triassic', *Science*, 235, pp. 1156-1167.

Hughes, W. B. and Reed, J. D. (1995) Oil and source rock geochemistry and exploration implications in the northern Tunisia. In: *The proceedings of the seminar on source rocks and hydrocarbon habitat in Tunisia*, ETAP, Memoir No. 9, pp. 49-67.

Institute Francais Du Petrole. (1995) Genex user's guid. An IFP basin modelling software, marketed and maintained by Beicip-Franlab.

Lopitan, N. V. (1971) 'Temperature and geologic time as factors in coalification', *Akad. Nauk, SSSR, Izv. Ser. Geol*., 3, pp. 95-106.

Mckenna, T. E. and Sharp, J. M. (1998) 'Radiogenic heat production in sedimentary rocks of the Gulf of Mexico Basin, South Texas', *Am. Assoc. Petrol. Geologists*, **82**, pp. 484-496.

Mckenzie, D. (1978) 'Some remarks on the development of sedimentary basins', *Earth and Planetary Science Letters*, 40, pp. 25-32.

Mriheel, I.Y. and El Bakai, M. T. (1992) Petroleum geology of the Western Libyan offshore (Abstract). In: *the 29th International Geological Congress*, Kyoto, Japan.

Mriheel, I. Y. and Alhnaish, A. S. (1995) 'Study of the Messinian carbonate-evaporite lithofacies offshore Western Libya', *Terra Nova*, 7, pp. 213-220.

Mriheel, I. Y. (2000) 'Basin Modelling and Reservoir Geology of the Principal Reservoir, Farwah Group, Gabes-Tripoli Basin, Western Offshore, Libya', *PhD. thesis*, Manchester University, UK.

Mriheel, I. Y. (2013) Jennawen Formation, a new stratigraphic unit at Jifarah Escarpment, Western Libya. *Report*, 5 p.

Mriheel, I. Y. (2014) Paleogeography and Sedimentation History of the Western Libya Offshore, Central Mediterranean (Extended Abstract). In: *The International Conference and Exhibition, Am. Assoc. Petrol. Geologists,* Istanbul, Turkey

Steckler, M. S. and Watts, A. B. (1978) 'Subsidence of the Atlantic-type continental margin of New Yourk', *Earth and Planetary Science Letters*, 41, pp. 1-13.

Tissot, B. P. and Espitalie, J. (1975) L'evolution thermique de la matiere organique des sediments: applications d'une simulation mathematique: Revue de l' Institut Francais du Petrole, 30, pp. 743-777.

Tissot, B. P. and Welte, D.W. (1984) *Petroleum formation and occurrence*, 2nd edition. Springer-Verlag, Berlin-Heidelburg-New York, 699p.

Ungerer, P., Espitalie, J., Behar, F. and Eggen, S. (1988) Modelization mathematique des interactions entre craquage thermique et migration lors de la formation du petrole et du gaz: Compte Rendu a l'Academie des Sciences, serie II, p. p. 927-934.

Libyan Journal of Science & Technology 9:1 (2019) 93–97
The 2nd International Conference on Geosciences of Libya-GeoLibya 2 (2017), 14-16 October 2017, Benghazi-Libya

Faculty of Science - University of Benghazi
Libyan Journal of Science & Technology
journal home page: www.sc.uob.edu.ly/pages/page/77

Geology of Ayn Al Majdoub Karstic Lake, Benghazi, NE Libya

Mousa S. AlShible

National Oil Corporation N.O.C. Benghazi, Libya

E-mail address: mousaalsheble1993@gmail.com

Highlights

- **Ayn Al Majdoub Karstic Lake belongs to Ayn Zayanah Karstic system.**
- **This lake was formed by dissolution of the soft units in the bottom of Benghazi Formation (middle Miocene).**
- **Lithology, Structure and Hydrology are main agents contributed to the formation of this karstic feature.**

A R T I C L E I N F O

Article history:
Received 01 February 2018
Revised 04 July 2018
Accepted 11 July 2018
Available online 31 March 2019

Keywords:
Benghazi Formation, Karst, Doline, Ayn Zayanah, Ayn Majdoub and the Blue Lagoon.

A B S T R A C T

The major karstic area in Libya known as Ayn Zayanah system is a unique phenomenon of concentrated karstic surface and subsurface dolines and channels.

By focusing on Al Majdoub Lake, as a case study, we can better understand how lithology, structure and hydrology contribute to the regional formation of the Karstic system.

Geologically, the limestones of the middle Miocene, Benghazi Formation is forming the northern side of Benghazi region, which is characterized by well-developed surficial, interface, surface and subsurface karstic features that are open or filled with sediment. The formation of Ayn Majdoub doline is filled with saline water, which is attributed to the dissolution of a buried carbonate layer by fresh groundwater due to the drop of the Sea level and the associated groundwater levels. This is combined with epeirogenesis movements, which have caused the development of karstification to reach a depth of 130-150 m below present sea level in the Benghazi plain. Through this Karstic system, groundwater seeps from Benghazi Basin towards the Ayn Zayanah (The Spring) and then to the Blue Lagoon (The Lake) finally to the sea.

1. Introduction

Dolines are natural enclosed depressions found in karst landscapes (Ford and Williams, 2007). They are subcircular in plain view, tens to hundreds of meters in diameter, and can range from a few meters to about a kilometer in width. They are typically a few meters to tens of meters in depth, but some are hundreds of meters deep. Their sides range from gently sloping to vertical, and their overall form can vary from saucer-shaped to conical or even cylindrical.

Ayn Al Majdoub doline is located about ~5 km north East the center Benghazi city (Fig. 1), defined by the coordinates (32° 09' 18.1" N) and (20° 07' 44.1" E). The lake is oval shaped with a length of 250 m, width of 135 m and estimated depth of 40 m (Fig. 2). The Ayn Zayanah water system is one of several natural lakes (dolines) that has an electrical conductivity of 9,320 (μmhos/cm) recorded in 2016. This doline and the others represent the outlet of aquifer complex system flowing within the Neogene limestone. The lithology of study area represented by Middle Miocene algal limestone Benghazi Formation of Ar Rajmah Group. The aim of this study is to see how does the geological factors (lithology, structure and hydrology) are involved in forming the Ayn Majdoub lake.

Fig. 1. Satellite images show Al Majdoub Lake**.**

 ISSN 2663-1407; National Library of Libya, Legal number: 390/2018

Fig. 2. General view of Ayn Al Majdoub Lake.

2. Geology

2.1 Karstic System

The karst is formed by a solution of calcium carbonate in the rocks by water containing carbon dioxide (Bates and Jackson, 1987). The major karstic area in Libya is concentrated in AL Jabal Al Akhdar region, it is mostly composed of carbonate rocks, and it has moderate amounts of precipitation which is important for the generation of different features of karstification. These features are mostly found in the exposed rocks of the study area, and similar to those existing in other parts of the whole region. Karst landforms are characterized primarily by underground drainage in areas of massive limestone, and by the formation, at the ground surface, of hollows and pits where water enters the rock and enlarges joints and fissures by solution (Blair, 1986).

Karst development is most effective where a very thick, hard, and well-jointed limestone occurs in an area of high relief with a humid climate. Thin limestone do not permit the development of underground drainage; soft limestone such as chalk does not permit the survival of deep surface depression or the formation of caves and passages underground, and in arid regions; the water is insufficient water for such solution to occur.

2.2 Karst Development on Benghazi Plain

- **Spatial distribution**

Despite the fact that Benghazi Plain is mainly composed of Miocene limestone rocks the relatively low rainfalls have led to a very irregular development of the karstic patterns within the groundwater basin (Guerre, 1980). Although the sinkholes are numerous and generally have wide openings, especially on Miocene outcrops, horizontal karst patterns are well developed, except in the Benghazi plain where the groundwater flow from the whole basin has been concentrated. Elsewhere, karstic development below the water table remains locally related to peculiar structural conditions which are almost completely unconnected, as in the central part of Al Marj plain (Rohlich, 1974).

- **Depth of Karstification**

In the study area, due to their stratigraphic position, the Miocene limestones are more intensively karstified than the Eocene limestone's. However, the friability of the Miocene limestones and their important clay or sandy contents has led to rapid fossilization of part of the early karstic patterns by collapsing and filling up with residual materials.

2.3 Karst Controls

The control factors on karsts formation include seven main factors that contribute to the evolution of karsts terrain (lithology, structure, relief, hydrology, climate, vegetation and time) (Blair, 1986). The solution process begins with carbon dioxide combining with water to form carbonic acid, as shown in Eq. 1.

$$CO_2 + H_2O \leftrightarrow H_2CO_3 \quad (1)$$

Eq. 2. illustrates that the carbonic acid dissolves limestone, and it goes into solution,

$$C_aCO_3 + CO_2 + H_2O \leftrightarrow Ca^2 + 2HCO \quad (2)$$

2.3.1 Lithology

Although karst develops primarily on carbonate rocks (mostly limestone), not all carbonate rocks possess the proper combination of physical and chemical properties that are conductive to a generation of karst topography (Palmer, 1977). Most of the world's karst regions are developed on limestone, which by definition consists of at least 50 % calcite and/or aragonite (CaCO3). Isomorphism substitution of magnesium for calcium in the carbonate mineral structure forms the mineral dolomite, the rock is dolostone. In general, the purer the limestone (CaCO3), the greater its ability to form karst. Some evidence suggests that about 60 % CaCO3 is necessary to form karst, and about 90 % may be necessary to fully develop karst. However, even pure limestone may not produce karst because lacking the important factors. Some karst features may form on dolomite, but their permeability is typically lower than that in limestone (Herman and White, 1985). Therefore, the occurrence of karst in dolomites is usually relatively minor.

2.3.1.1 Lithostratigraphy of Ayn Majdoub

Benghazi Formation consists of bioclastic packstone grades to algal boundstone, the bioclasts are dominated by rich coralline red algae, echinoids and benthonic foraminifers with sparse bryozoan remain at some levels. This formation is partly dolomitized and shows vuggy porosity. It was deposited in a shallow neritic environment with affinity to reefal build up. This formation is well karstified, due to the low porosity and massive limestone, which is characterized by algal boundstone textures (Muftah *et al*., 2009). It is well jointed in the Kuwiffia -Ayn Zayanah region near Benghazi City and is providing weak zones for water percolation in order to develop karst (Abdulmalik *et al*., 2007). The beds of Benghazi Formation are thick and gradually become thinner upward. It is represented by five limestone units, they are from oldest to youngest as follows (Fig. 8 and Table 1):

Unit (1)

Oysterid-Algal Boundstone, white color, soft, massive with common algae (Rhodoliths) 3.5 cm in diameter, (Fig. 3. a&b) Echinoids, peleceypoda fragments also present. The thickness of this unit is about 1 meters.

Unit (2)

Pelecepoda-Echinoidal-Algal boundstone, white color, moderately hard, massive with common Rhodoliths algae ranging in size from 1.5 to 2.5 cm in diameter and echinoids (Clypeaster sp. and Scotela sp.), (Fig. 4). The thickness of this unit is about two meters.

Unit (3)

Calcarenitic grainstone, yellowish white color, moderately hard, massive with algaes, echinoid (*in situ* at the base) and commonly borrowed. The thickness of this unit is about (1.5) meters.

Unit (4)

Algal Bound stone, white color, moderately hard, massive with common Rhodoliths algae ranging in size from 3 to 5 cm diameters and corals, (Fig. 6). In addition, this unit is highly jointed with extended oblique and vertical joints with the sliding surface. The thickness of this unit is about 2.5 meters.

Unit (5)

Algal limestone Packstone texture, white color, hard, thinly bedded with algaes (Fig. 7). The thickness of this unit is about 1.33 meters.

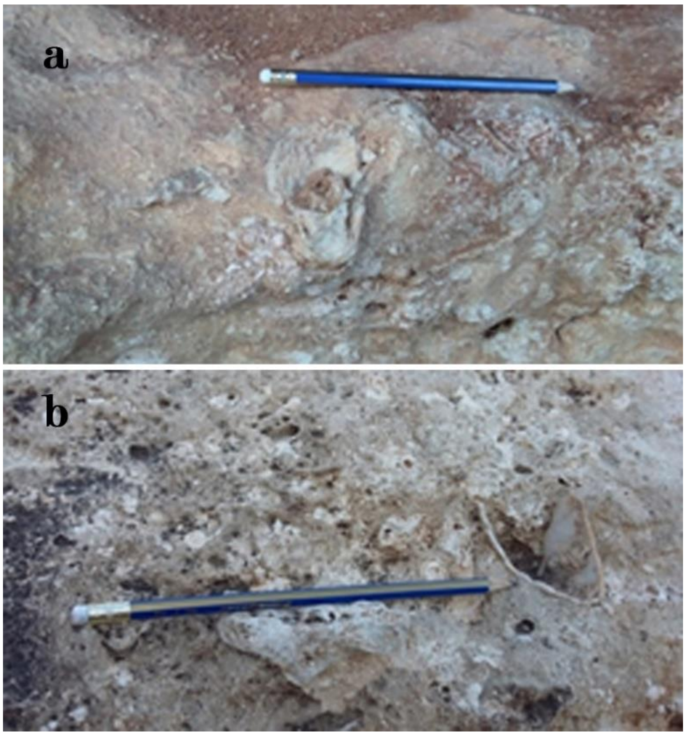

Fig. 3. Unit 1 in Benghazi Formation.

Fig. 4. Unit 2 in Benghazi Formation.

Fig. 5. Unit 3 in Benghazi Formation.

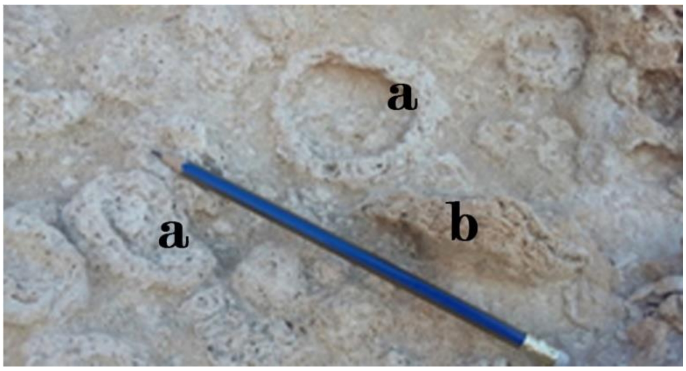

Fig. 6. Unit 4 in Benghazi Formation shows Formation (**a**) Rhodolith algaes and (**b**) corals.

Fig. 7. Hand specimen for unit 5 in Benghazi Formation.

Table 1

Description of Ayn Al Majdoub lake lithology.

	Name	Texture	Color	Hardness	General Notes
Unit 1	Oysteried-Algal Limestone	Boundstone	White	Soft	
Unit 2	Pelecepoda-Echinoidal-Algal Limestone	Boundstone	White	Moderately Hard	
Unit 3	Calcarenite	Grainstone	Yellowish White	Moderately Hard	* Because of the physical properties (such as: purity, low porosity and hardness); These units acts as a favorable rock type in forming karast. * Structurally, these rock units highly jointed.
Unit 4	Algal Limestone	Boundstone	White	Moderately Hard	
Unit 5	Algal Limestone	Packstone	White	Hard	

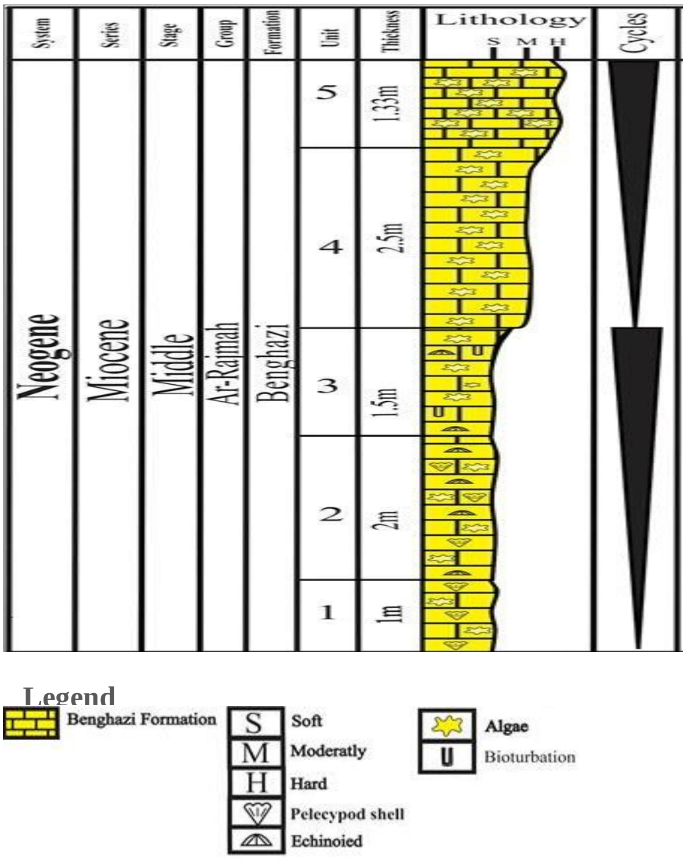

Fig. 8. Stratigraphic columnar section of Ayn Al Majdoub outcrop.

2.3.2 Structure

Geologic structure is an important factor in karst development. Palmer (1977) has stated that structure is the main factor in the development of karst features. In the study area, the carbonate rocks consist of the joints and when weathered they act as conduits for groundwater circulation. The spacing of joint sets is also important. Meaning, if intersecting joint planes are spaced at long intervals circulation is impeded; but if they are too closely spaced, the rock may be too structurally weak to support karst features, even though the rock may be highly permeable. Faults can also transmit water, but their spacing is usually much greater than that of joints, so they are not as effective in developing karst (Palmer, 1977).

Considering the above-mentioned factors, optimum lithology and structural conditions for full karst development include the following: Thick, pure calcite, crystalline limestone uninterrupted by insoluble beds. Intersecting joint sets that allow free circulation of ground water along discrete flow paths with enough discharge to create or enhance significant solution openings (Palmer, 1991).

Fig. 9. View of highly jointed sides of the lake.

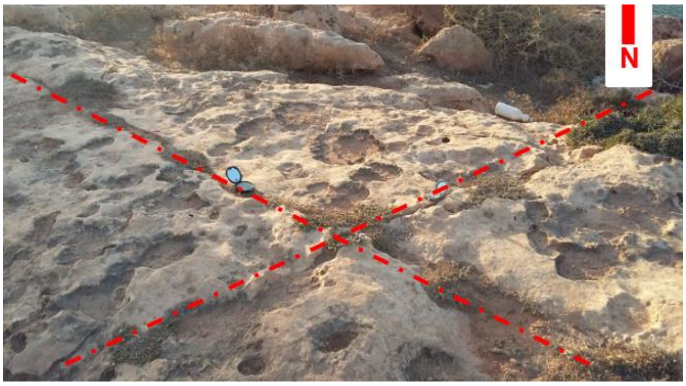

Fig. 10. The two major dip strikes.

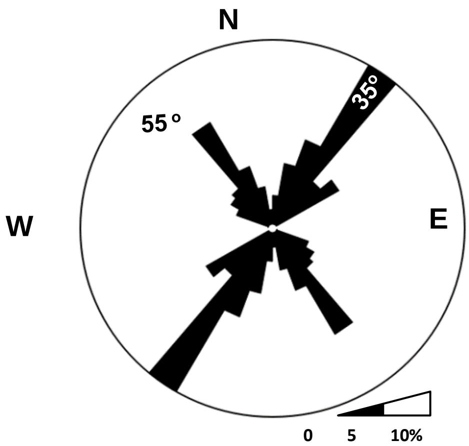

Fig. 11. Rose diagram represents the major joints.

3. Conclusions

Most of the karstologic literature explains formation of dolines through dissolution effects of rainwater discharge via fissures in the lowest (weakest) point of the doline. Herein, the development of the dolines in Benghazi Formation was originally undertaken by dissolution at the surface and infiltration by water and collapse in depth due to change (from wet to dry seasons) in the water level. Since the most dominant process on karst is dissolution. Ayn Al Majdoub doline was formed by dissolution of the soft units in the bottom of Benghazi Formation followed by the collapse of overlying strata. To sum up, the development of Ayn Al Majdoub karstic feature is mainly controlled by the followings:

a) Lithology, the rock formation in the study area possess horizontal, well bedded, well-jointed, hard limestone as the fundamental condition for karst. Elsewhere, this limestone is rich in fossils and coral reefs that give chance for a selective solution and, in turn, voids and more effective by percolating water.

b) Structure, this doline was formed along or at the intersection points of joints, which greatly enhanced the circulation of the solution by water at the surface, which aided the collapse in depth. Collapse or slumping noted on the doline sides is created from the free surface expansion of the walls inward the dolines due to stress relief and opening up of the surrounded structural lines.

c) Hydrology, the change of groundwater level depends on the amount of recharge and amount rain-water leaking vertically through faults and joints. Continuous seasonal variations in rainfall, from wet to dry, reflect in-depth fluctuation of groundwater levels on the lower part of Benghazi Formation, leading to discernible differences in hydraulic pressure and hence induce the collapse more likely within the zone of water-table change.

4. Recommendations

Karstic areas are always representing the major source of land instability; therefore, hazards resulted from this have to be taken into the government's consideration. However, the study is an only a small portion of the huge active karstic phenomena, in other words, karstic features are dangerous in NE Benghazi near Al Kuwafia and north Al Laithi areas. Serious studies and control should be considered in near future.

Acknowledgments

I thank my advisors Dr. Fathi Salloum, Dr. Ahmed Al Kuwafi, Dr. Saad El Shari, Dr. Muftah Al- Showaihdi and Msc Student Ahmed Al Amin for their help in the field.

References

Abdelmalik, M. B, El-Moursi, M. E. And Salloum, F. M. (2007) 'The Environmental impact of the karstic features of Ayn Zayanah–Kuwiffia sector, Near Benghazi, Libya', Speleologia Iblea, 12, pp. 147-152. Ragusa, Italy.

Bates, R.L. and Jackson, J.A. (1987) Glossary of Geology, 3rd Edition, American Geological Institute, Alexandria, p. 788.

Blair, R. W. Jr. (1986) Karst of landforms and Lakes, in short, N. M. Sr and Blair, R. W. Jr. (eds), Geomorphology from space. NASA Special Publication 486, pp, 402-446.

Ford, D., Williams, P. D. (2007) Karst hydrogeology and geomorphology. Chichester, Wiley, 576 pp.

Guerre, A. (1980) Hydrological Study of the Ayn Zayanah karstic Spring, J. Salem and M. Buscrewil, eds. Proc. Sypm, Geology of Libya volume II, pp. 685-710

Herman, J. S., and White, W. B., (1985) 'Dissolution kinetics of dolomite: Effects of lithology and fluid flow velocity', Geochimica and Cosmochimica Acta, 49, pp. 2017–2026.

Muftah A. M., Abdulsamad E. O., Ali R. A. & Alsonusi A. H. (2010) 'Stratigraphy-Karst Relationships In The Eocene - Miocene carbonates of Al Jabal Al Akhdar, (Cyrenaica, Ne Libya)', Speleologia Iblea, 14, pp. 53-60. Ragusa, Italy.

Palmer, A. N., (1977) Influence of geologic structure on ground water flow and cave development in Mammoth Cave National Park, USA. In Tolson, J. S., and Doyle. L., Karst hydrology: International Association of Hydrogeologists, 12th Memoir, pp. 405-414.

Palmer, A. N., (1991) 'Origin and morphology of limestone caves', *Geological Society of America Bulletin*, 49, pج. 50-66.

Rohlich, P. (1974) 'Geological map of Libya, 1:250,000, Al Bayda sheet NI34-15, explanatory booklet', *Indust. Resear. Cent., Tripoli, Libya*, 70 pp.

Williams, P. D. (2003) Doline. In A. Goudie (Ed.) Encyclopedia of Geomorphology. New York, Routledge, pp. 266–270.

Libyan Journal of Science & Technology 9:1 (2019) 98–101
The 2nd International Conference on Geosciences of Libya-GeoLibya 2 (2017), 14-16 October 2017, Benghazi-Libya

Faculty of Science - University of Benghazi
Libyan Journal of Science & Technology
journal home page: www.sc.uob.edu.ly/pages/page/77

Description and characteristics of chert nodules in Appollonia Formation, Al Hmmeda road-cut, Al Jabal Al Akhdar, NE Libya

Omar B. Elfigih[a,*], AL- Moatasem Bellah K. El Degheeli[b]

[a]*Department of Earth Sciences, Faculty of Science, University of Benghazi, Benghazi-Libya*
[b]*Department of Geology, Exploration Division, Arabian Gulf Oil Company, P. O. Box 263, Benghazi Libya.*

Highlights

- **The characteristics of physical, petrographic and bulk elements of the Appollonia chert nodules in Al Hmmeda area is documenting its origin by replacement.**
- **Low crystallized silica of possible organic origin composed mainly the Appollonia Formation chert nodules.**
- **Partial to total dissolution of low crystallized silica is under the influence of increasing temperature and pH.**
- **Local porosity and permeability variations in the examined Appollonia chert, mostly produced mixing of the diffused digenetic fluids resulted in the formation of nodular form of this chert.**

ARTICLE INFO

Article history:
Received 01 February 2018
Revised 19 February 2018
Accepted 22 September 2018
Available online 31 March 2019

Keywords:
Chert nodules, Appollonia Formation, Al Hmmeda road-cut, physical properties.

*Corresponding Author:
E-mail address: omar.elfigih@uob.edu.ly
O. B. Elfigih

ABSTRACT

Physical, petrographic and bulk elements analysis of Chert Nodules in Appollonia Formation, Al Hmmeda road-cut were conducted and showed that the origin of these chert by replacement. The suspected siliceous organic matters are of low crystallized silica and were dissolved under the influence of increasing temperature and pH. Most of the chert was localized in the limestone and dolomitic limestone of Appollonia Formation (nodular zone) by percolation of silica-rich solution along microfractures and porous/permeability zones. This local porosity and permeability variations, mostly produced mixing of the diffused digenetic fluids. This process produces the nodular form of the cherts in the Appollonia mudstone facies in the nodular zone, while less marked permeability variations could have produced more regular tabular bodies of chert, which were not observed at least in the studied section. The absence of chert nodules in some adjacent rocks and even at higher elevation in the Appollonia stratigraphic section (non-nodular zone), might reflect effective exhaustion of the silica supply, fewer microfractures condition and perhaps dilution by the marine water of highly reduced silica-rich solution.

1. Introduction

There were superb outcrops of tertiary carbonate rocks along Al Hmmeda road – cut, among them, some yellowish cream limestone with chert nodules. These chert nodules in Appollonia Formation have been reported by some references (Pietersz, 1968; Benerjee, 1980; Muftah *et al*., 2015), but their physical properties, occurrences and origin are largely unknown. The examined outcrop section in the study area (Fig. 1) is characterized by selected limited dimensions of about 300m width and of 280m height at the first escarpment of Al Hmmeda road-cut. The objective of this paper is to describe, characterize and graphically document natural chert occurrence in the Appollonia Formation exposed in Al Hmmeda road-cut, east of Tansulukh Village.

2. Methodology

a) Fieldwork

The present study includes the analysis of chert nodules samples, which are brought from the Appollonia carbonate sites of Al Hmmeda road-cut, Al Jabal Al Akhdar. First, completed the field observation and macroscopic examination of seven samples, took into account the visible physical properties of the chert nodules such as color, shape, size, compactness, spacing and their orientation relative to bedding planes (Table 1). Also paid close attention to other properties like, texture, fragility and sample weight that were determined through simple observation. Field photographs were taken with SONY 12.1 Megapixels camera in which we controlled the coloration of the photographs with auto-reference color scale.

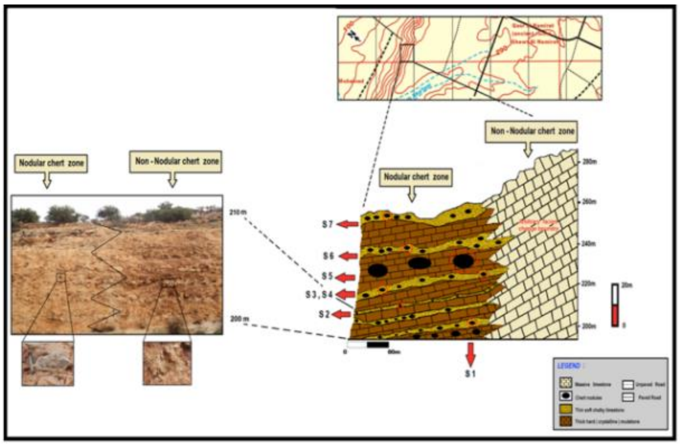

Fig. 1. Location Map and General Outcrop Section of the Study Area, Al Hmmeda Road-Cut, Al Jabal AL Akhdar, NE Libya.

b) Laboratory work

A selection of seven samples was analyzed using a polarized microscope for petrographic examination. Other selected samples (S1, S3, S6) were also examined using XRD techniques for elemental analysis.

 ISSN 2663-1407; National Library of Libya, Legal number: 390/2018

3. Chert nodules description in hand specimens

A composite columnar section (Fig. 2) was constructed and composed of thin soft chalky limestone with dense chert nodules at the base to alternating thick, hard crystalline mudstone with scattered chert nodules, and topped by thick, hard, fossiliferous mudstone with no chert nodules. Several forms of crystalline silica occur locally in Appollonia Formation. Elliptical chert nodules is volumetrically significant (>10%) but relatively sparse in the dolomitic limestone and chalky limestone of the lower section of Appollonia Formation (nodular chert zone), while it could be volumetrically insignificant (<2%) in the mudstone–wackestone facies of the upper part of Appollonia Formation (non–nodular chert zone). These nodules are medium–brown to light black, micro–cryptocrystals texture and generally between (5–30 cm). Upon closer examination of hand specimen, the matrix or (groundmass) is seen to have numerous small (0.2–0.5 mm) dark colored spots (dolomite) crystals and light colored foraminifera fragments.

Chert nodules distribution can be seen in (Fig. 3) in which chert density is concentrated in the lower part of the nodular zone where it decreases and may be absent in some adjacent rocks at higher elevation (non-nodular zone) in the Appollonia stratigraphic section.

Table 1

Field Observation and physical properties of Chert Nodules in Appollonia Formation, Al Hmmeda Road- cut

Sample No.	Elevation (m)	Color	Shape	Size (cm)	Spacing (cm)	Orientation to bedding plane	Texture	Facies	Fragility	Weight	Photo
S7	255	Gray	Sub-elliptical	13	20-25	Parallel	Irregular	Chalky limestone	unfragile	Light	
S6	240	Gray	Sub-elliptical	5	20-25	Parallel	Spotty	Chalky limestone	unfragile	Light	
S5	230	Bluish gray	Elliptical	27-30	90-120	Parallel	Spotty	Mudstone (dense)	unfragile	Light	
S4	225	Gray	Lens	18	25-28	Parallel	Spotty	Chalky limestone	unfragile	Light	
S3	220	Bluish gray	Elliptical	7	25-28	Parallel	Irregular	Chalky limestone	unfragile	Light	
S2	210	Gray	Spherical	3-5	25-30	Parallel	Irregular	Chalky limestone	unfragile	Light	
S1	200	Gray	Semi-spherical	5-7	20-25	Parallel	With cavity	Chalky limestone	unfragile	Light	

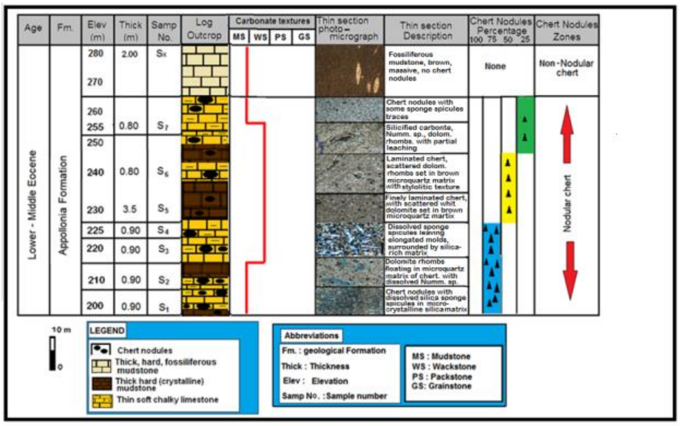

Fig. 2. Composite columnar section of the studied Appollonia Formation, Al Hmmeda Road- cut, AlJabal Al Akhdar, NE Libya

4. Thin section study

Selected thin sections were studied petrographically, in these thin sections, the Appollonian Formation chert nodules at Al Hmmeda road-cut are of light to medium brown translucent, finely laminated chert (Fig. 4), consisting of very fine grained equidimensional micro quartz and chalcedonic quartz with scattered white dolomite rhombs set in brown micro-quartz matrix, fine branched dissolved sponge spicules are also present. Occasionally with minor amounts of carbonate minerals (dolomite rhombs and other undetermined opaque granules or pellets), with some stylolite structures, (Fig. 5).

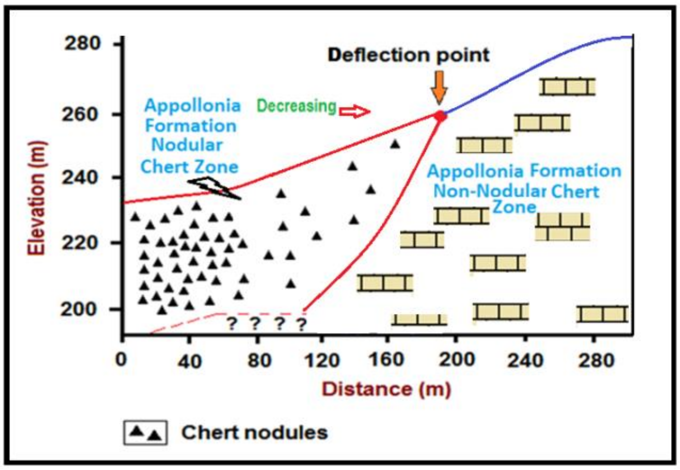

Fig. 3. Chert nodules density graph showing their general distribution in the studied area.

Abundant foraminiferal pseudomorphs are scattered (Fig. 6) where the foraminiferal shells consist occasionally of cryptocrystalline and microcrystalline quartz, which are indistinguishable from the surrounding cement material forming a structure-like ghost. Although the foraminiferal tests are partially or totally replaced and their cavities are filled with silica (Fig. 7). The forms of these microfossils seem to be well preserved in the microquartz matrix of chert. The material filling the foraminiferal pore spaces is mostly fine to medium grained, colorless chalcedonic quartz. Dissolved siliceous sponge spicules are also present in the chert as aggregates or branched forms of blue elongated areas occur as traces of sponge spicule particles showing scattered moldic porosity (Fig. 8).

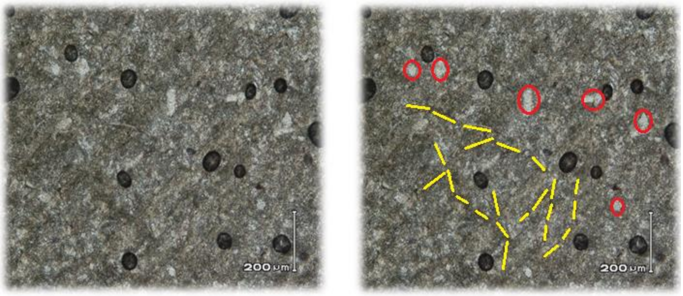

Fig. 4. Thin section photomicrograph of finely laminated chert showing scattered white dolomite rhombs (circles) set in brown micro-quartz matrix, fine branched dissolved sponge spicules (dashed) can be seen.

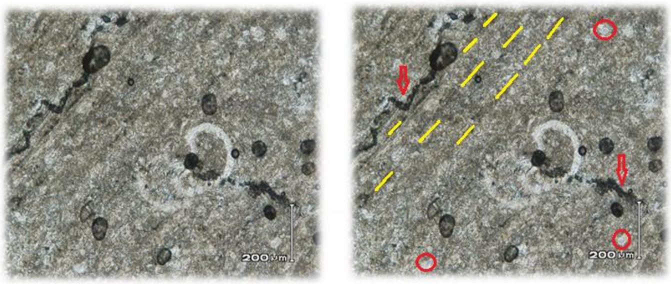

Fig. 5. Thin section photomicrograph of laminated chert (dashed) showing scattered dark –grey dolomite rhombs (circles) set in brown micro-quartz-matrix with stylolitic structures (arrows), dark colored stylolite's boundaries are probably organic origin.

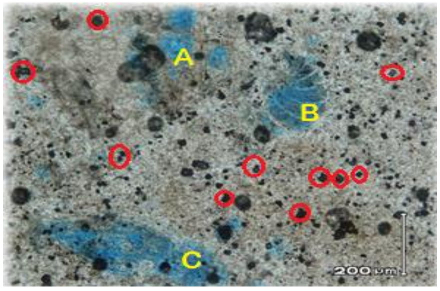

Fig. 6. Thin section photomicrograph of crystalline matrix of chert, showing dolomite rhombs floating in micro-quartz (circles) and dissolved nummulite structures (A, B and C).

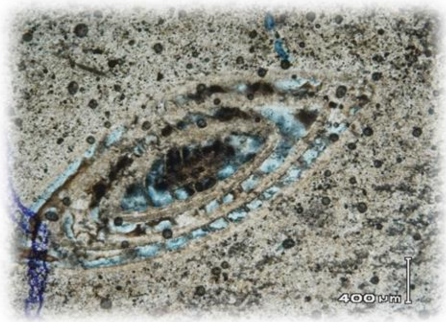

Fig. 7. Thin section photomicrograph showing partially silicified Nummulites *sp.*, with partial leaching intragranular porosity.

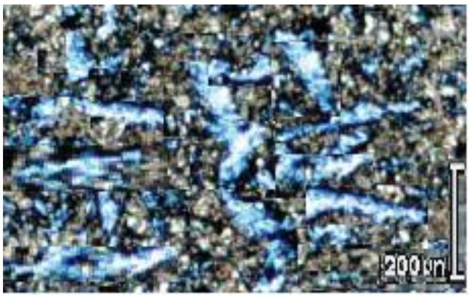

Fig. 8. Thin section photomicrograph showing sponge spicules have been dissolved leaving molds (blue elongated areas) and the surrounding matrix has been mostly replaced by silica (dark grey areas).

5. Interpretation of thin sections

The Appollonia Formation is limestone to dolomitic limestone, the matrix is a calcitic microspar in which the chert nodules which formed by replacement micro-quartz are consistently equicrystalline, suggesting that nucleation sites for replacement (calcite–silica) were evenly distributed under high-level silica supersaturated digenetic fluid (Gregg and Sibley, 1987). The recovered dolomite rhombs are best explained as left- behind phase pre-existing the silicified matrix around. The floating dolomite rhombs and other carbonate pellets may suggest that the replacement of the carbonate matrix was on a micro-volume basis.

The good preservation of carbonate microfossils in micro-quartz matrix may be suggested that foraminiferal test did not dissolve until silica precipitated in their cavities and in cementing groundmass and that the replacement of carbonate by silica prograded gradually in favorable acidic condition. Horizontal stylolites with amplitudes up to 10 cm occur in laminated chert sample (Fig. 5) suggesting that stylolization in a given lithology was progressive during intermediate and deep burial (Duggan, 2004). The dark-colored stylolite's boundaries are probably organic origin. The very early dissolution of sponge –silica spicules may suggest their local moldic preservation as microfractures and permeability increased which effect chert nodules formation . However, the presence of bluish-gray chert nodules in some horizons and are commonly associated with imprints of dissolved sponge spicules may suggest a local biogenic source for much of the silica.

6. X-Ray powder diffraction

Two selected rock samples were crushed to powder and examined under X-Ray diffractometer, type (PW 3050/60) for bulk rock (minerals) examination, where the examined chert samples consisted almost entirely of quartz (98%), with minor amount (2%) of carbonate minerals (calcite/dolomite) (Table 2). These results are not contradictory to those of the petrographic study. In Fig. 9, prominent quartz peak (@ 2Theta 26.60°), other minor quartz peaks (@ 2Theta 21°& 50°) can be seen with some minor calcite peak (@ 2Theta 29.46°). Possible minor dolomite peaks (@ 2Theta 40°& 46°) can also be seen. The absence of distinct patterns of dolomite mineral in X-Ray diffraction analyses in the case of quartz–rich chert samples may be due to the interface between quartz peak and calcite peak, which can cause a serious underestimation of dolomite proportion in the examined samples.

Table 2

Minerals detected in chert nodules of Appollonia formation, using XRD method.

Item No.	Mineral name	Chemical formula	Index name	Quantity (%)	Rel. intensity (%)	d-spacing	2° Theta
1	Quartz	SiO_2	Silicon	98	100.00	3.353	26.60°, 50°
2	Calcite	$CaCO_3$	oxide	2	1.25	3.031	29.46°

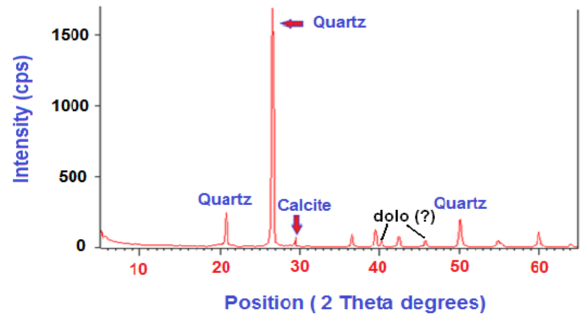

Fig. 9. XRD chart of chert nodules in Appollonia Formation.

7. Conclusions

The study of the characteristics of physical, petrographic and bulk elements of the Appollonia chert nodules in Al Hmmeda area is documenting its origin by replacement; the source of the silica, however, remains speculative. There are, however, minute dissolved sponge spicules in this chert. The suspected siliceous sponge spicules composed of low crystallized silica were buried and dissolved with increasing temperature and pH in the solution trapped in the sediments. Most of the chert was localized in the limestone and dolomitic limestone of Appollonia Formation (nodular zone) by percolation of silica-rich solution along microfractures and porous/permeability zones. This local porosity and permeability variations, mostly produced mixing of the diffused digenetic fluids (Mcbride *et al.*, 1999). This process produces the nodular form of the cherts in the Appollonia mudstone facies in the nodular zone, while less marked permeability variations could have produced more regular tabular bodies of chert, which were not observed at least in the studied section. The absence of chert nodules in some adjacent rocks and even at higher elevation in the Appollonia stratigraphic section (non-nodular zone), might reflect effective exhaustion of the silica supply, fewer microfractures condition and perhaps dilution by the marine water of highly reduced silica-rich solution.

8. Recommendation

Because of the fact that the origin of the chert nodules of Appollonia Formation is still debatable; SEM study for these chert nodules is very needed to ensure the presence of sponge spicules and to define their fragmental morphology and texture. Also suggested oxygen isotope analysis and signature for the chert nodules and their comparison in the studied sections (nodular and non-nodular zones) is highly recommended.

References

Ahmed M. Muftah, Mohamed S. Al-Faitouri and Salah S. El-EKhfifi. (2015) Utilization of the observed geological features in differentiating the exposed rock units in Al Jabal al Akhdar, Libya, In: The First International Conference on Basic Sciences & their Applications, Abstract-Talk, November -29- to December -1 - 2015, Al-Bayda City, NE Libya. p. 171-178.

Banerjee, S., (1980) Stratigraphic lexicon of Libya. *Industrial Research Center*, Tripoli, *S. P. L. A. J.*, 39, pp. 40

Duggan, J, P., (2004) Burial dolomites at Swan Hills Simonette Reef, West Central Alberta Basin (Abstract), In: Article Jan. (2004), Research Gate, 2017-2018.

Gregg, J. M. and Sibley, D.F., (1987) 'Classification of dolomite rock textures', *Journal of sedimentary, paleontology*, 57(6), pp. 967-975.

Mcbride Earle F., Abdel-Wahab Antar Ali, El-Younsy, Ahmed Reda M. (1999) 'Origin of spheroidal chert nodules, Drunka Formation (Lower Eocene), Egypt Article', *Sedimentology*, 46(4), pp. 733-755·

Pietersz, C. R., (1968) Proposed nomenclature for rock units in Northern Cyrenaica. In: F. T. Barr (Ed.) Geology and Archaeology of Northern Cyrenaica, Libya. Petrol Explore. Soc. Libya, Tripoli, pp. 125-130.

Libyan Journal of Science & Technology 9:1 (2019) 102–107
The 2nd International Conference on Geosciences of Libya-GeoLibya 2 (2017), 14-16 October 2017, Benghazi-Libya

Faculty of Science - University of Benghazi
Libyan Journal of Science & Technology
journal home page: www.sc.uob.edu.ly/pages/page/77

دراسة وضعية المياه الجوفية لأبار المياه بعمق 500 متر في المنطقة الممتدة من قيرة إلى آقار بوادي الشاطئ، شمال حوض مرزق

محسن أبو القاسم محمد، يوسف عباس عبد الله، عبد السلام البغدادي الشارف، عماد الدين خليفة محمد

قسم علوم الأرض، كلية العلوم، جامعة سبها

نقاط هامة

- خزانات صخور تكوينات عوينات ونين لبعض الآبار في منطقتي القيرة وآقار بوادي الشاطئ تتميز بمسامية جيدة.
- المياه المستغلة من بعض الآبار تعتبر عذبة جيدة صالحة للشرب، الى عسرة في أماكن آبار أخرى.
- خزانات صخور تكوينات العصر الديفوني العميقة غنية بالحديد قد يستفاد منها في الصناعة.
- المياه في منطقة الدراسة قد تتأثر بعوامل عدة تساهم في زيادة عملية التآكل.

بيانات المقالة

تاريخ المقالة:

استلمت في	01	فبراير	2018
روجعت في	14	أبريل	2018
قبلت في	21	ديسمبر	2018
نشرت عبر الإنترنت	31	مارس	2019

الكلمات الدالة:
وادي الشاطئ، حوض مرزق، خزانات الكمبروأردوفيشي، عوينات ونين، معدل الهبوط، مياه عسرة.

*المؤلف المراسل:
محسن أبو القاسم

ملخص

تقع منطقة وادي الشاطئ في الطرف الشمالي لحوض مرزق، وتعد المياه الجوفية المصدر الرئيسي في المنطقة، تركزت هذه الدراسة على أربعة أبار عميقة في المنطقة من خزان الكمبروأوردوفيشي حيث ان اغلب الابار المستغلة في المنطقة تنتمي لصخور تكوينات عوينات ونين من اعصر الديفوني الغنية بالحديد. تم قياس المناسيب الثابتة في الآبار المدروسة لمعرفة التغيرات في مناسيب المياه، حيث وجد أن معدل الهبوط لم يتجاوز الأربعة أمتار، وكان اتجاه حركة المياه الجوفية من الشمال الغربي إلى الجنوب الشرقي، وقد تميز هذا الخزان بمسامية جيدة وكانت نسبة الطين في صخور الخزان قليلة نسبيا، أجريت بعض التحاليل الكيميائية وتمت مقارنتها بالتحاليل المعمولة اثناء الحفر، وقد بينت هذه التحاليل الكيميائية لهذه الآبار أن هذه المياه عذبة صالحة للشرب بالنسبة للبئرين المستغلين و تعدت الحدود المقبولة للبئرين الغير مستغلين، وبهذا صنفت مياه البئرين الغير مستغلين على انها مياه عسرة الى عسرة جداً، وقد كانت نسبة الصوديوم والكلور مرتفعة، كما تم مقارنة نسبة الحديد في هذه الآبار العميقة بالحديد في مياه الآبار الأقل عمق التي تستغل خزانات العصر الديفوني الغني بالحديد، وكانت صلاحية المياه للزراعة من جيدة الى مشكوك في صلاحيتها، و من ناحية أخرى و في مجال الصناعة فإنها تصلح للعديد من الصناعات مثل صناعة الاسمنت والتعليب والمشروبات.

1. المقدمة

الماء أهم المصادر الطبيعية للإنسان، حيث تُعد المياه الجوفية مصدراً رئيسياً للمياه العذبة على مستوى العالم، وغالباً غير متجددة في المناطق الجافة، وتُعد ليبيا من المناطق التي تعاني نقصا حاد في الموارد المائية لتغطية الاحتياجات المختلفة، ويعتبر السحب الجائر للماء من أهم العوامل التي أدت الى تدهور المخزون المائي كماً ونوعاً، وأغلب الجهود البحثية في الوقت الحاضر تحولت لدراسة مشاكل نوعية المياه أكثر من دراسة كمية المياه (الشاعر، 1984).

2. الهدف من الدراسة

أجريت هذه الدراسة لمجموعة أبار في منطقة وادي الشاطئ (قيرة، براك، الزوية، أقار) في الجنوب الغربي لليبيا. ويتمثل موضوع هذه الدراسة التفصيلية والشاملة في تفسير معلومات سبر الآبار من خلال التقارير الفنية لحفر الآبار والتي أعدتها الشركات الحافرة لهذه الآبار وهي شركات (السبعة، الإتقان، المعول) خلال الفترة 2010/2009 ف، حيث تم الحصول على هذه التقارير من الهيئة العامة للمياه فرع المنطقة الجنوبية. وكذلك، محاولة فهم التغيرات التي طرأت على وضعية مناسيب المياه الجوفية في الآبار المدروسة ومقارنتها بفترة حفر هذه الآبار، بالإضافة إلى عملية المضاهاة بين القطاعات الطبقية وتحديد الطبقات الجافة التي لا تحتوي على المياه والطبقات المستغلة منها المياه، وأيضا دراسة المسامية للطبقات الخازنة للمياه المستغلة وغير المستغلة. وتشتمل أيضا على حساب نسبة الطين في القطاعات الطبقية لكل بئر. كما اشتملت الدراسة على جانب أساسي وهو دراسة الخصائص الكيميائية للمياه الجوفية في الآبار المدروسة وعمل التحاليل الكيميائية ومقارنة النتائج الحالية بالنتائج السابقة وذلك لمعرفة الوضع الكيميائي لها ومقدار التغير الذي قد طرأ عليها منذ حفر هذه الآبار حتى الدراسة الحالية، وخاصة دراسة التغير في تركيز الحديد ومقارنته بالحديد في مياه الخزانات الغير مستغلة (الديفوني) باعتباره سبب حفر هذه الآبار العميقة. وتضمنت الدراسة تصنيف المياه الجوفية لهذه الآبار من حيث صلاحيتها لأغراض الشرب والزراعة والصناعة، وأيضا شملت الدراسة على تعريف التآكل وأسبابه وأثاره

3. الموقع الجغرافي لمنطقة الدراسة

تقع منطقة الدراسة في جنوب غرب ليبيا، شمال مدينة سبها وتبعد عنها بمسافة حوالي 80 كم، ما بين خطي عرض (27.30، 27.35 درجة) شمالاً، وخطي طول (14.7، 14.25 درجة) شرقا (شكل 1)، ويسود في منطقة فزان طبيعة المناخ الصحراوي الجاف مرتفع الحرارة حيث تختلف في المدى الحراري الى درجة كبيرة ليلا – نهارا، صيفا – شتاءً مع ندرة الأمطار وانخفاض معدلاتها في حالة سقوطها كما تشتد حركة الرياح بالمنطقة في بعض فصول السنة وتأخذ اتجاهات مختلفة خاصة في فصل الربيع (الشاعر، 1984).

4. الوضع الجيولوجي للمنطقة

تقع المنطقة في الجزء الجنوبي من مرتفع قرقاف أي الجزء الشمالي لحوض مرزق، والصخور المتكشفة الأساسية هي رسوبيات الباليوزويك الرف القاري الباليوزوية لمنطقة وادي الشاطئ، ورسوبيات حوض مرزق الجوراسية-الطباشيرية السفلية ورسوبيات الثلاثي – الرباعي القارية، كما تتواجد في الجزء الشرقي رسوبيات البحر الضحل المتناثرة والصخور البازلتية في الجزء الشمالي (الشاعر، 1984)، أنظر شكل 2.

التكوينات الطبقية المتكشفة في منطقة الدراسة

الحساونة: هو أقدم وحدة صخرية متكشفة على السطح ويتكون من الأحجار الرملية الكوارتزية والكورتيزيتية ذات التطابق المتخالف غالبا، بها بعض التداخلات الأحجار الغرينية (Seidl and Rohlich, 1984).

بئر القصر: يقابل الدور الأول من تكوينات عوينات ونين، ويتموضع بعدم توافق زاوي مع تكوين الحساونة وأحيانا على تكوين الميمونيات، ويتكون من الأحجار الطينية والأحجار الغرينية وأنواع مختلفة من الأحجار الرملية (Collomb,1962).

إدري: وصف مقطعه النموذجي في لوحة إدري ومكوناته الأساسية أحجار رملية كوارتيزية بها تدرج طبقي مع تواجد الأحجار الغرينية والأحجار الطينية في الجزء الغربي من اللوحة فقط (Seidl and Rohlich, 1984).

قطة: وصف مقطعه النموذجي من مكان يبعد 3 كم شمال شرقي قطة يبدأ في القاعدة بالأحجار الطينية والأحجار الطينية الغرينية التي تحتوي على تداخلات رفيعة من

 ISSN 2663-1407; National Library of Libya, Legal number: 390/2018

الكوارتيزايت دقيق الحبيبات يوجد به أثار حفرية "بيفونجيت فزان" Seidl and Rohlich, 1984).

دبدب: يقابل التكوين السفلي الحامل لخامات الحديد وذلك حسب فريق الدراسات الفرنسي، (Watark and Aldgre and Bnerjee, 1980, 1972) وصف مقطعه النموذجي من مكان يبعد 3.5 كم شمال دبداب حيث أغلب مكوناته أحجار طينية غرينية المحتوية على تداخلات من الأحجار الرملية والأحجار الغرينية Seidl and Rohlich, 1984).

تاروت: يقابل التكوين العلوي الحامل لخامات الحديد، ويشمل الأحجار الطينية الخضراء أو الرمادية والمستوى (A) الحامل للخامات المعدنية (Seidl and Rohlich, 1984).

أشكدة: وصف مقطعه النموذجي من مكان يبعد 4 كم غرب أشكدة في الجهة الغربية من وادي دبداب، ويتميز بتكرار لطبقات الحديد، حيث يتكون غالبا من أحجار رملية دقيقة الحبيبات وأحجار غرينية وأحجار طينية تتناوب في نسب مختلفة Seidl and Rohlich, 1984).

إمرار: يبدأ في أسفله بالأحجار الطينية المسماة (بطبقات السقف) ويحوي بقية الطبقات الكربونية المنكشفة في لوحة سبها، حدوده السفلية توافقية مع تكوين أشكدة ويتميز بوجود أثار الحفريات (بيفونجيت فزان) بالإضافة إلى التغيرات الليثولوجية. يتشكل التكوين غالبا من تناوب الأحجار الطينية والأحجار الغرينية والدولوميت المحتوي على الستروماتوليت طبقات متداخلة في الجزء العلوي من التكوين Seidl and Rohlich, 1984).

محروقة: تطلق هذه التسمية على وحدة كربوناتية في الغالب تتشكل من الرواسب القارية (الثلاثية- الرباعية) وصف مقطعها النموذجي من مكان يبعد 7 كم شرقي محروقة حيث تتكون من الدولوميت الرملي المحتوى على تداخلات طينية متجمعة في شكل شبه كروي ومن الأحجار الجيرية المبيضة. وفي قاعدته يتواجد أحيانا كونجلوميرات جيري، سمك التكوين الظاهر 12 متر(Seidl and Rohlich, 1984).

شكل 1. خريطة ليبيا وصورة فضائية لموقع الدراسة المصدر من برنامج(Google Earth) .

5. الوضع المائي للمنطقة

ساعدت الميزات الرسوبية الليثولوجيا (حجم وشكل وكيفية ترابط الحبيبات ببعضها)، بالإضافة إلى الفواصل والصدوع والتراكيب والتكوينات الجيولوجية حفظ كميات كبيرة من المياه (الشاعر، 1984).

وحسب الدراسات التي اجريت على حوض مرزق و التي نشر جزء منها كما ورد عن (Dubay; Pallas,1980 and 1980، الشاعر، 1984).اتضح ان المياه الجوفية القابلة و الصالحة للاستغلال تتواجد في ثلاث خزانات رئيسية هي:-
الخزانات الجوفية المائية بطبقات دهر الحياة القديمة، الخزانات الجوفية المائية بطبقات دهر الحياة المتوسطة (العلوية)، الخزانات الجوفية المائية بطبقات دهر الحياة المتوسطة(السفلية)(شكل3).

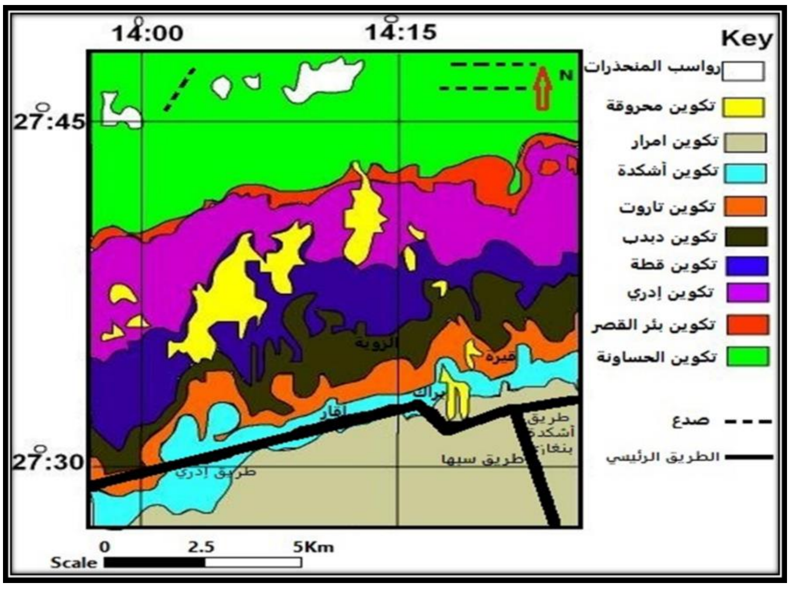

شكل 2. يوضح الخريطة الجيولوجية لمنطقة الدراسة

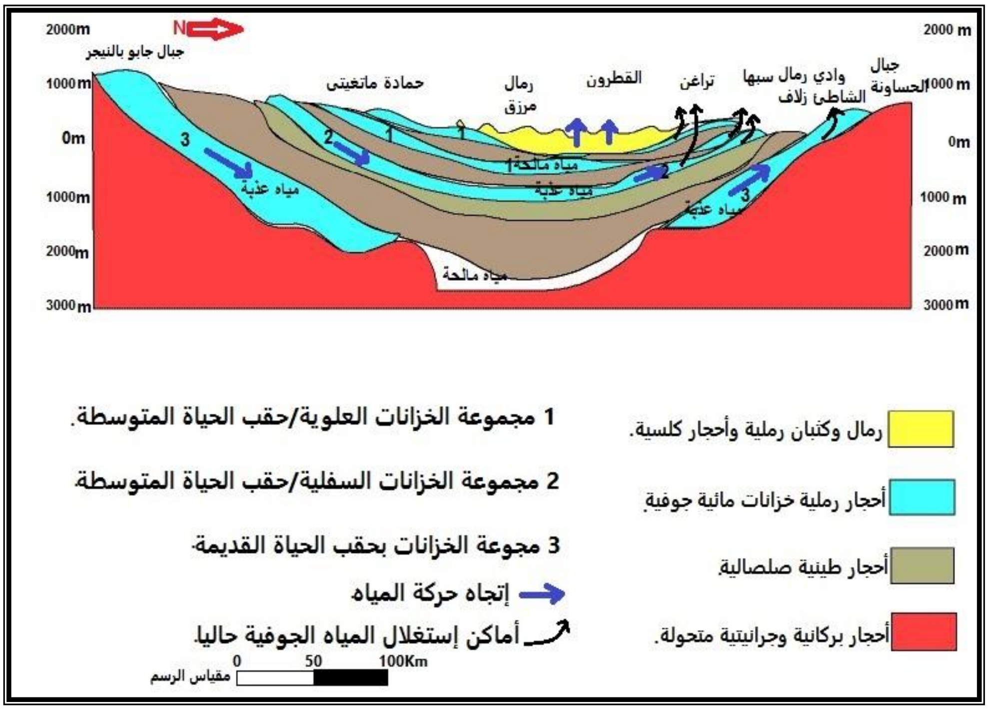

شكل(3) يوضح الخزانات الجوفية في حوض مرزق (الشاعر، 1987)

6. طرق الدراسة

اعتمدت الدراسة على مراجعة التقارير الفنية للآبار الموجودة في الهيئة العامة للمياه وتفسير معلومات سبر الآبار المتمثلة في كل من أشعة جاما والمقاومة "16 والمقاومة "64 المرفقة مع التقارير الفنية. وتم استخلاص معلومات شاملة عن الوصف الصخري وعمل المضاهاة بين القطاعات الصخرية و دراسة بعض الخصائص الصخرية لتحديد مسامية الصخور و حساب نسبة الطين ، وأيضا دراسة الوضع المائي للمياه الجوفية في منطقة الدراسة؛ وقد جمعت العينات المائية في قنينات بلاستكية بسعة (1.5 لتر) بعد تنظيفها بشكل جيد للإجراء بعض التحاليل الكيميائية لتحديد وقياس كل من الأس الهيدروجيني (pH) و مجموع الأملاح الذائبة (TDS) و التوصيل الكهربائي (EC) ودرجة حرارة الماء T(C°) و العكارة، حيث استخدم جهاز (pH -meter) لقياس EC - TDS - pH والملوحة (Salinity)، بالنسبة للعكارة فقد تم قياسها باستخدام جهاز (Turbedmetar)، وتم قياس أيونا الصوديوم والبوتاسيوم بوساطة جهاز قياس ضوء اللهب (Flame Photometer). وقد قدرت نسبة الكالسيوم والماغنيسيوم والكلوريد وكلا من القاعدية الكلية والحامضية الكلية والعسر الكلي والبيكربونات و النترات و المنجنيز و الزئبق فتم بطريقة المعايرات الحجمية باستعمال محلول (EDTA).
اما الكبريتات والحديد والفوسفات فقد حددت بجهاز طيف الأشعة فوق البنفسجية Ultraviolet Spectrophotometer (UV)، والكادميوم والرصاص والنحاس والنيكل والكوبلت بجهاز الامتصاص الذري Atomic Absorption Spectrophotometer.

7. النتائج والمناقشة

تم دراسة وضعية المياه الجوفية في الآبار المدروسة بمنطقة وادي الشاطئ عن طريق دراسة قطاعات جيولوجية تحت سطحية مُستنتجة من بعض الحسابات الجيوفيزيائية (جاما، المقاومية 16-64) الموجودة في تقارير الآبار بالإضافة إلى دراسة الخواص الكيميائية للمياه الجوفية في الآبار المدروسة؛ و لقد أجريت أثناء هذه الدراسة بعض القياسات لمناسيب المياه الجوفية في الآبار المدروسة وذلك من خلال قياس المنسوب الثابت في الآبار المدروسة حيث كانت تتراوح بين (16 و 40) متر و تم استخدامها في معرفة التغيرات في مناسيب المياه و وجد أن معدل الهبوط في الآبار الأربعة يتراوح بين (0.29 و 0.57) متر/سنة (جدول 1).

جدول 1.

ارتفاع المناسيب أثناء حفر الآبار وخلال الدراسة الحالية ويوضح معدل التغير في المنسوب بين الفترتين

الآبار	عمق المناسيب في فترة حفر الآبار2009/2010ف (m)	عمق المناسيب في الدراسة الحالية 2016ف (m)	معدل التغير في منسوب المياه (متر/سنة)
قيرة	36	40	0.57
الزاوية	21	24	0.43
الزويه	33	36	0.5
أقار	14	16	0.29

كما استخدمت قياسات المناسيب الثابتة للمياه الجوفية في فترة حفر الآبار لمعرفة اتجاه حركة المياه الجوفية في تلك الفترة ورسم خريطة كنتورية لهذه المناسيب ووجد أن اتجاه سريان المياه الجوفية في ذلك الوقت من الشمال الغربي إلى الجنوب شرق (شكل 4). تم إجراء عملية مضاهاة للقطاعات الطبقية للآبار المدروسة (Asquith, & Gibson, 1982) (شكل 5).

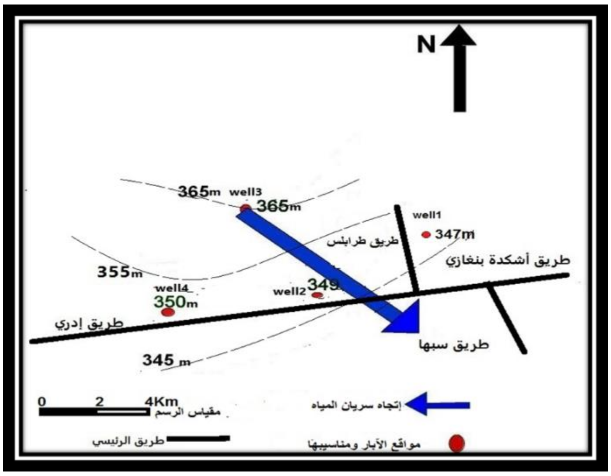

شكل 4. اتجاه سريان المياه وارتفاع مناسيبها عن مستوى سطح البحر.

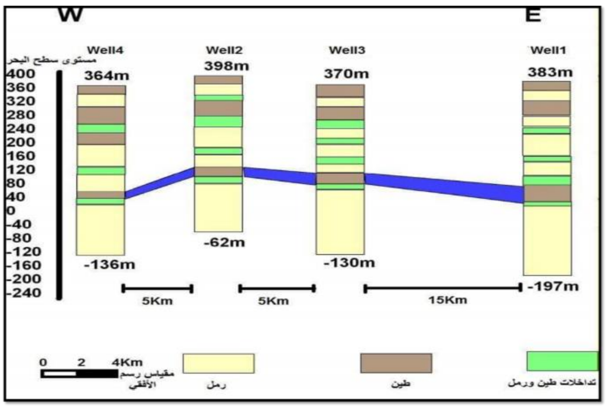

شكل 5. يوضح المضاهاة بين القطاعات الجيولوجية (الهيدرولوجية) للآبار بمنطقة الدراسة

وقد اتضح من الدراسة أن الآبار قائمة على تكوين الحساونة من الكامبري تغطيها رواسب الرابع بسمك غير كبير، والخزان الجوفي المستغل هو خزان الحساونة.

كما تم حساب المسامية للخزانات المستغلة (السفلية) وأيضا للخزانات الغير مستغلة (العلوية) (جدول 2) من خلال الاطلاع على معلومات سبر الآبار في التقارير الفنية لحفر الآبار أمكن تحديد المسامية في بعض الطبقات الصخرية بالاستعانة ببعض المعطيات والتعويض بالمعادلة 1:

معادلة تحديد المسامية

$$\Phi = \left(\frac{aRmf}{Rxo}\right)^{\frac{1}{m}} \qquad (1)$$

جدول 2.

متوسط قيم المسامية في طبقات الأحجار الرملية الخازنة للمياه المستغلة وغير المستغلة.

الآبار	متوسط المسامية في الطبقات غير المستغلة	متوسط المسامية في الطبقات المستغلة
قيره	21%	23%
الزاوية	13%	19%
الزوية	20%	21%
أقار	14%	16%

بالإضافة إلى أنه تم حساب نسبة الطين في القطاعات الطباقية للآبار المدروسة من سجل إشعاع جاما الطبيعي وذلك بأخذ ثلاث قراءات من تذبذبات السجل الشعاعي لجاما كالاتي:

قراءة عند العمق المراد معرفة المحتوى الطيني به وأقصى وأدنى قراءه للتذبذبات في سجل جاما كما هو موضح في المعادلة التالية:

$$IGR = \frac{GR_{read} - GR_{min}}{GR_{max} - GR_{min}} \qquad (2)$$

ثم نعوض عن قيمة IGR في المعادلة التالية

$$V_s = 0.33(2^{2.1IGR} - 1) \qquad (3)$$

Vs=كمية أو نسبة الطين وهذه المعادلة تستخدم في الصخور المتماسكة (شكل 6).

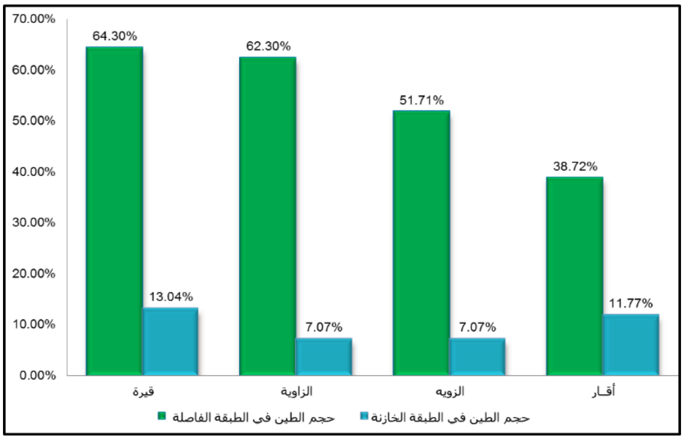

شكل 6. يوضح نسبة حجم الطين في الطبقة الفاصلة وفي الطبقة الخازنة

كما أجريت بعض التحاليل الكيميائية على عينات الآبار الأربعة المدروسة وتم مقارنتها مع التحاليل الكيميائية التي أجريت على المياه الجوفية لهذه الآبار أثناء حفر الآبار (2010/2009) ومن هذه التحاليل الكيميائية:

قياس بعض الخواص الفيزيائية (غاز ثاني أكسيد الكربون، الراسب الكلي، الموصلية الكهربائية، العسر الكلي، الأس الهيدروجيني، العكارة) (جدول 3).

وكذلك قياس نسبة العناصر الأتية (Na,K,Ca,Mg,Fe,Mn,Cl,Cd,Ni,Hg,Pb,Co,Cu) (جدول 3). وتم قياس المجموعات الذرية (CO_3,HCO_3^-,NO_3,SO_4,PO_4^-)(جدول 4).

جدول 3.

المواصفات الليبية القياسية لسنة 1982ونتائج بعض التحليلات الكيميائية أثناء حفر الآبار وخلال الدراسة الحالية وتركيز الحديد من الخزانات العلوية، عمر أسعد أحمد (2009):

العناصر	المواصفات الليبية القياسية لسنة 1982	التحاليل السابقة (mg/l)				التحاليل الحالية لسنة 2016 (mg/l)			
	الحد الأقصى المسموح به mg/l	قيرة	الزاوية	الزويه	أقار	قيرة	الزاوية	الزويه	أقار
كمية الأملاح الذائبة	1500	686	350	691	317	328	1214	426	1081
التوصيل الكهربائي	2500	686	622	1080	634	669	2472	870	2250
درجة الأس الهيدروجيني	9.5	6.66	7.29	6.9	6.25	6.37	6.45	6.52	7.54
العكارة	10 - 1	-	-	-	-	3	0.1	2.6	0.73
الصوديوم	200	66.6	97.2	33.12	61	71.303	64.939	63.727	62.515
البوتاسيوم	40	18	6	12.05	22	9.0650	13.7398	8.0081	7.3577
الكالسيوم	200	20.8	14	36	16	18	38	40	26
المغنيسيوم	150	2.11	4.9	21.6	11.52	54	24	78	58.8
الحديد(+++)	0.3	0	0.14	0.1	0.1535	0.09762	0.8568	0.16269	1.573
الكلوريد	250	153	110	208.7	148.8	166.058	719.584	221.410	608.879
البيكربونات	500	161	12.2	244	126.8	110	3.66	160	90
النترات	45	1.1176	6	0.48	0.0352	7.12	15.61	10.35	5.91
الكبريتات	400	17.6	100	206	48	36.667	51.333	123.583	26.667
الفوسفات	لاشئ	-	-	27.6	-	0.011261	2.984	0.3266	0.1464
العسر الكلي	500	12	55	180	64	270	195	425	310
ثاني أكسيد الكربون	10	-	-	-	-	19.8	29.7	34.65	19.8

جدول 4. تراكيز العناصر الضئيلة الذائبة في المياه الجوفية للآبار المدروسة

البئر	العناصـــر					
	الكادميوم	الرصاص	الزئبق	النحاس	النيكل	الكوبلت
قيرة	0.00631	0.0886	0.00095	0	0	0
الزاوية	0.00767	0.0938	0.00058	0	0	0
الزوية	0.00553	0.0348	0.00068	0	0	0
أقار	0.00713	0.0798	0.00045	0	0	0

وتم في هذه الدراسة تصنيف المياه الجوفية على أساس كمية الأملاح الذائبة الكلية على أنها مياه عذبة في بئر قيرة وبئر الزاوية بينما مالحة في الآبار الراكدة (بدون مضخات) في الزاوية ببراك الشاطئ وأقار حسب (Tood, 1980) (جدول 5).

كما أن المياه الجوفية صُنفت أيضاً على أساس الأيونات الموجبة والأيونات السالبة ويتم وضع النتائج المئوية على مثلث يوضح نوعية المياه حسب موقعها في المثلث :(Ritchard, (1954)).

بالنسبة للأيونات الموجبة فنلاحظ أن المياه الجوفية من خلال التحاليل الكيميائية في الدراسة الحالية يغلب عليها أيونات الصوديوم والكالسيوم والمغنيسيوم (شكل 7). أما بالنسبة للأيونات السالبة نجد أنه في الدراسة الحالية من خلال المثلث المستخدم للتصنيف يغلب عليها أيونات الكلوريد والكبريتات (شكل 8)

جدول 5.

نوعية المياه الجوفية على حسب مجموع الأملاح الذائبة الكلية عن طريق(TOOD,1980) أثناء حفر الآبار والدراسة الحالية:

الراسب الكلي (mg/l)	نوعية المياه	الراسب الكلي في مياه (mg/l) الآبار أثناء فترة الحفر	الراسب الكلي (mg/l) في مياه الآبار أثناء الدراسة الحالية
600-0	مياه عذبة	الزاوية، أقار	قيرة، الزويه
1000-600	مياه مستساغة	قيرة، أقار	
10000-1000	مياه موبلحة		الزاوية، أقار
-10000 100000	مياه مالحة		
>100000	مياه شديدة الملوحة		

كما تم تصنيف المياه في الآبار المدروسة على أساس درجة العسر فكانت المياه في آبار قيرة والزاوية عسرة بينما في آبار الزويه وأقار كانت مياه عسره جداً (جدول 6) (TOOD,1980).

جدول 6.

تصنيف المياه الجوفية حسب درجة العسر الكلي وذلك تبعا لطريقة James (1979).

درجة العسر بالمليجرام/لتر (عسر المياه)	نوعية المياه	عسر مياه الآبار المدروسة: درجة العسر لكل بئر أثناء الحفر	عسر مياه الآبار المدروسة: درجة العسر لكل بئر للدراسة الحالية
75-0	يسرة	قيرة، الزاوية، أقار	
150-75	متوسطة		
300-150	عسرة	الزويه	قيرة، الزاوية
300<	عسرة جدا		الزويه، أقار

كما أن المياه الجوفية صُنفت أيضاً على أساس الأيونات الموجبة والأيونات السالبة ويتم وضع النتائج المئوية على مثلث يوضح نوعية المياه حسب موقعها في المثلث (Ritchard, (1954)):

بالنسبة للأيونات الموجبة فنلاحظ أن المياه الجوفية من خلال التحاليل الكيميائية في الدراسة الحالية يغلب عليها أيونات الصوديوم والكالسيوم والمغنيسيوم (شكل 7). أما بالنسبة للأيونات السالبة نجد أنه في الدراسة الحالية من خلال المثلث المستخدم للتصنيف يغلب عليها أيونات الكلوريد والكبريتات (شكل 8)

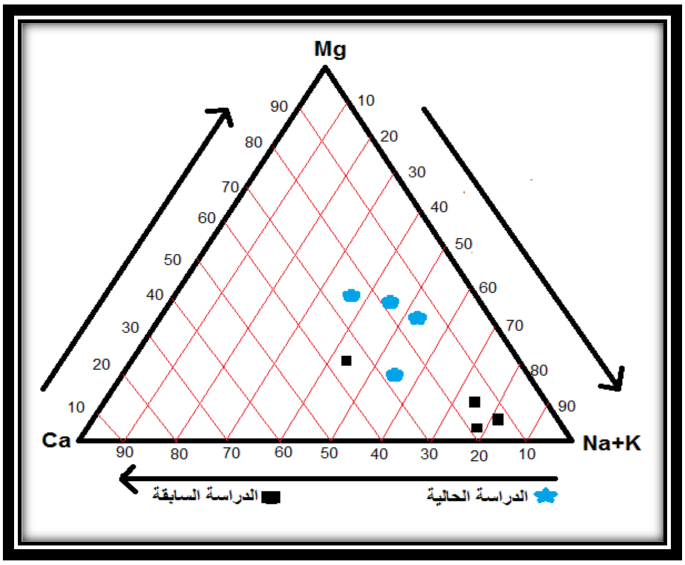

الشكل 7. يوضح تصنيف المياه المثلثي على حسب الايونات الموجبة

و قد تم تصنيف مياه الآبار من حيث صلاحيتها للشرب حيث أثبتت التحاليل الكيميائية أن مياه الآبار المدروسة صالحة للشرب ، حيث تنعدم في مياه الشرب الرائحة و اللون و الطعم و لا تكون عالقة بها مواد و يجب أن تكون مياه الشرب معتدلة غير حامضية أو قاعدية وذلك حسب ما أصدرته منظمة الصحة العالمية بجنيف لسنة 1971م و أيضا حسب المواصفات القياسية الليبية لسنة 1982م الذي يعطي الحد الأقصى و المسموح به لبعض العناصر و المركبات الكيميائية (بالملي جرام/لتر) في مياه الشرب و من خلال مقارنة هذه التركيزات بنتائج التحاليل لمياه الآبار المدروسة نجد أن تركيز بعض العناصر الكيميائية في الآبار الغير مستغلة (الزاوية و أقار) أعلى من المواصفات العالمية و المواصفات القياسية الليبية لمياه الشرب مثل عناصر الحديد و الكلوريد و الأملاح الذائبة الكلية و الموصلية الكهربائية.

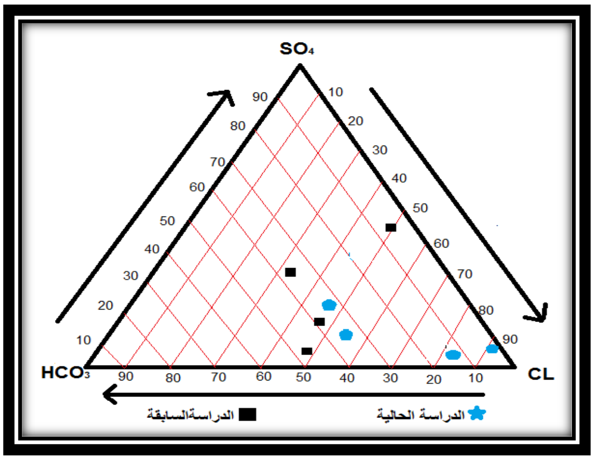

الشكل 8. يوضح تصنيف المياه المثلثي على حسب الايونات السالبة

و تم أيضا تصنيف مياه الآبار المدروسة من حيث صلاحيتها لأغراض الزراعة (شكل 9)، ويمكن تحديدها عادة عن طريق التوصيل الكهربائي و الراسب الكلي و النسبة المئوية للصوديوم الذائب الماء و معدل إدمصاص الصوديوم، و أتضح أن مياه الآبار المدروسة صالحة لأغراض الزراعة من ناحية التوصيل الكهربائي نظراً لأنه لم يتجاوز الحد المسموح به (Wilcox, 1966).

تم حساب النسبة المئوية للصوديوم الذائب في الماء لجميع العينات التي تم دراستها والتي اجريت تحاليلها أثناء فترة حفر الآبار وخلال الدراسة الحالية ذلك حسب المعادلة الاتية:

$$\mathrm{Na\%} = \mathrm{Na} + \frac{\mathrm{k}}{\mathrm{Na}} + \mathrm{k} + \mathrm{Ca} + \mathrm{Mg} \times \frac{100\mathrm{mlq}}{\mathrm{L}} \qquad (4)$$

وتم تصنيف أيضا مياه الآبار المدروسة من حيث صلاحيتها في أغراض الصناعة ؛ حيث تتحكم نوعية المياه في الصناعات المختلفة، وباستعمال المياه لأغراض الصناعية المختلفة يراعى فيها درجة الحرارة و العسر الكلي و الراسب الكلي و يشتمل كذلك على تركيز بعض العناصر الكيميائية مثل الماغنيسيوم و الكالسيوم و الكبريت و الحديد و ثاني أكسيد الكربون من خلال التحاليل الكيميائية للدراسة الحالية نلاحظ أن ثاني أكسيد الكربون يتراوح بين (19.8-34.65 ملليجرام/لتر) و بذلك فإن ثاني أكسيد الكربون يشكل خطر على المعدات كالمضخات والأنابيب حيث يعرضها إلى التآكل خاصة مع ارتفاع درجة الحرارة؛ من ناحية أخرى اتضح أن مياه بعض الآبار المدروسة صالحة لأغراض بعض الصناعات الأخرى مثل صناعة الإسمنت و صناعة الجلود فإن أبار (قيرة والزاويه) تعتبر مياهها صالحة لهذه الصناعات (جدول 7)حسب (Hem,1989).

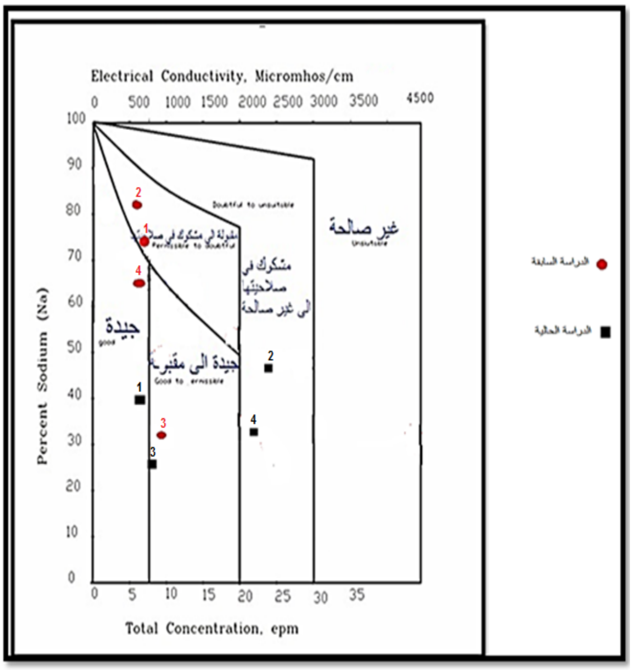

شكل 9. تصنيف على أساس النسبة المئوية للصوديوم الذائب والتركيز الكلي للأملاح والموصلية الكهربية حسب (Wilcox, 1969).

الجدول 7.

نوعية المياه المستخدمة لبعض الصناعات والحدود العليا المسموح بها لكل صناعة حسب (Hem, 1989).

العنصر	صناعة الاسمنت	صناعة الجلود	صناعة التعليب والمشروبات	الفواكه المعلبة والمجمدة	المنتوجات النفطية	صناعة البلاستيك	صناعة النسيج	صناعة الورق	صناعة الأقمشة
Ca	---	---	100	---	75	80	100	20	0
Mg	---	---	---	---	30	36	50	12	0
Cl	250	250	500	250	300	---	500	200	0
HCO3	---	---	---	---	---	---	250	---	0
SO4	250	250	500	250	---	---	100	---	0
NO3	---	---	---	10	---	---	5	---	0
T.H	---	Soft	---	250	350	350	900	100	25
T.D.S	600	---	---	500	1000	---	1000	---	100
pH	8.5-6.5	8-6	---	8.5-6.5	9-6	8.3-6.5	8-6.5	10-6	10.5-2.5
T(F°)	---	---	---	---	---	---	---	---	---
النماذج المقاسة في الدراسة الحالية	قيرة، الزويه فقط نماذج مناسبه	قيرة، الزويه فقط نماذج مناسبه	الآبار الأربعة نماذج مناسبه	الآبار الأربعة نماذج غير مناسبه	الآبار الأربعة نماذج غير مناسبه	الزاوية يعتبر نموذج مناسب	الآبار الأربعة نماذج غير مناسبه	الآبار الأربعة نماذج غير مناسبه	الآبار الأربعة نماذج غير مناسبه

- **التآكل**: هو الناتج عن سلسلة من التفاعلات ما بين المياه وأسطح المواد والمعادن التي تنقل من خلالها أو تختزن فيها.

- العوامل التي تلعب دور مهم في التآكل:

نسبة غاز ثاني أكسيد الكربون، درجة الأس الهيدروجيني، عسر الكربونات، الكلور، تركيز الحديد، كمية الأملاح الذائبة في الماء، درجة حرارة الماء.

- الآثار الصحية للمياه الآكلة :

1- الحد من فعالية مسخنات المياه .

2- تآكل نظام التوزيع المائي .

3- الطعم المر للمياه مما يجعلها غير مستساغة وضارة صحياً .

4- تشكل الصبغات والصدأ على الأحواض والأواني مثل اللون الأحمر والأخضر .

5- إن تآكل بعض المواد السامة مثل (الرصاص، نحاس، كروم، زنك) قد يؤدي إلى أمراض خطيرة.

8. الخلاصة

وقد لخصت هذه الدراسة على إن المسامية في الخزانات المستغلة جيدة؛ حيث تتراوح نسبتها بين (16% - 23%)، وأن مناسيب المياه للآبار المدروسة تتراوح بين (16 - 40) متر، ومعدل الهبوط يتراوح بين (2- 4) متر، وتبين أن اتجاه سريان المياه الجوفية في الآبار المدروسة من الشمال الغربي إلى الجنوب الشرقي.

في الآبار الراكدة (غير المستغلة) كانت قيمة الموصلية والأملاح الذائبة عالية جداً مقارنة بقيمتهاأثناء الحفر.

إن تركيز الحديد يزداد في المياه الجوفية للآبار المدروسة من قيرة إلى أقار حيث تراوح بين (1.573-0.098)، بينما كان تركيزه أكبر في الخزانات غير المستغلة (الخزانات العلوية) التي وجدت تتراوح بين (5.76-0.45).

اتضح أن طبقة الطين (الطبقة الفاصلة بين الخزان المستغل وغير المستغل) يقل سمكها في بئر أقار بينما يزداد سمكها شرقاً في بئر قيرة، وتم تقدير نسبة حجم الطين من سجل جاما لكل قطاع طباقي.

صنفت المياه في منطقة الدراسة على أنها مياه صالحة للشرب، وفي الأغراض الزراعية من جيدة إلى مشكوك فيها، وصالحة لبعض الأغراض الصناعية.

المياه في منطقة الدراسة مع مرور الزمن قد تكون مياه آكلة، وذلك لأن ثاني أكسيد الكربون يتفاعل بزيادة درجة الحرارة، وأيضاً الكلوريد والحديد من العوامل المساهمة في التآكل.

9. التوصيات

أولاً: ضرورة تزويد الآبار الراكدة في براك (الزاوية) وأقار بمضخات، وعند تنمية الآبار أخذ عينات مائية وإجراء التحاليل الكيميائية لها.

ثانياً: في حالة حفر أبار جديدة وقريبة من الآبار المدروسة نوصي بالتركيز على دراسة العينات الصخرية تحت سطحية.

ثالثاً: إجراء تحاليل دورية لكل الآبار المنتجة في فترات متساوية ومتقاربة وذلك لمراقبة جودة مياه الشرب، وتعتبر هذه التحاليل هامة جداً.

رابعاً: إجراء دراسة للمياه الجوفية في منطقة الدراسة من الناحية الكمية لمعرفة كمية المياه المسحوبة والاحتياطي المتبقي واعداد موازنة بينهما للاستفادة منها لأطول فترة ممكنة.

خامساً: الاستغلال الأمثل للحديد الطبيعي الموجود في طبقات الأرض لأنه يؤثر في المياه الجوفية المخزونة في باطنها.

المراجع

الشاعر محمد محمد (1984) الخواص الهيدروجيولوجية والهيدروكيميائية والتركيب الاليزوتي (النظائري) للمياه الجوفية بمنطقة حوض مرزق بفزان، رسالة الدكتوراه، جامعة توبجن ألمانيا الغربية.

الشاعر محمد (1987)، المياه الجوفية بحوض مرزق ومصادر تكونها بحث مقدم إلى المؤتمر العلمي الأول حول المجتمعات الصحراوية (مرزق).

الشاعر محمد (1992)، مجلة الدراسات الصحراوية (المياه المالحة بحوض مرزق).

الهيئة العامة للمياه فرع المنطقة الجنوبية (2009/2010)، التقارير الفنية للآبار المدروسة التي حفرت بواسطة شركات (السبعة، المعول، الإتقان).

عمر أسعد أحمد (2009)، دراسة خصائص المياه الجوفية في منطقة وادي الشاطئ وتقييم التأثيرات لتدهور نوعيتها، كلية العلوم الهندسية والتقنية- جامعة سبها.

Asquith, G., & Gibson, C. (1982) Basic well Log analysis for geologists, Am. Assoc Petro Geologists, Tulsa, Oklahoma

Hem, J. D., (1989). Study and interpretation of the chemical characteristics of Natural Water, 2nd Addition U.S.G.S. Water Supply, Washington, D. C.

James, A. (1979) Biological Indictors of Water, pp. 11-16.

Ritchard, L. A., (1954) Diagnosis and Improvement of Saline and Alkali S. Doils, Agri Handbook 60, U.S. dep. Agric., Washington D.C.

Seidl, K. and Rohlich, P. (1984) Sheet Sabha (NS 33-2,) Geological Map of Libya, scale 1:250,000, Explanatory Booklet, industrial Research Centre, Tripoli.

Tood, D. K. (1980) Groud Water Hydrology Second Edition, By John Wiley & Sons.

Wilcox, L.V.(1966) Salinity Laboratory. USA

Libyan Journal of Science & Technology 9:1 (2019) 108–115
The 2nd International Conference on Geosciences of Libya-GeoLibya 2 (2017), 14-16 October 2017, Benghazi-Libya

Faculty of Science - University of Benghazi
Libyan Journal of Science & Technology
journal home page: www.sc.uob.edu.ly/pages/page/77

حوض مرزق بين الاستهلاك والاستدامة

منار صالح البغدادي[a] *، يوسف عباس عبدالله[b]، الشارف عبدالسلام البغدادي[b]

[a] قسم الجغرافيا، جامعة سبها

[b] قسم علوم الأرض، كلية العلوم، جامعة سبها

نقاط هامة

- **دراسة جيولوجية حوض مرزق ونوعية مياهه.**
- **استنزاف مياه حوض مرزق إلى سنة2013م، والمؤشر الخطير الناتج بسبب الاستنزاف.**
- **أساليب استهلاك حوض مرزق وتأثير الاستهلاك على هبوط المنسوب.**
- **تحقيق تنمية مستدامة لمورد المياه، بأن يكون موضوع المياه من أولويات اهتمام الجهات المسؤولة.**

بيانات المقالة

تاريخ المقالة:

استلمت في	01	فبراير	2018
روجعت في	14	أبريل	2018
قبلت في	21	ديسمبر	2018
نشرت عبر الإنترنت	31	مارس	2019

الكلمات الدالة:

حوض مرزق، الاستهلاك، الاستدامة، المياه الجوفية، الخزان الجوفي، هبوط المنسوب.

*المؤلف المراسل:
منار صالح البغدادي
Email: man.albaghdadi@sebhau.edu.ly

ملخص

إن المياه الجوفية في ليبيا تشكل حوالي 98% من الموارد المائية، فهي بهذا تعد المصدر الرئيسي للمياه؛ لذا فإن الاستقرار واستدامة النمو في ليبيا تتطلب سياسة مائية تنبع من تقييم موضوعي لهذا الوضع المائي.

حوض مرزق الواقع في الجنوب الغربي الليبي هو أكبر أحواض المياه الجوفية في ليبيا ويقع في قلب الصحراء الكبرى حيث ندرة الأمطار ودرجة الحرارة العالية، ومع تزايد النمو السكاني والتطور التكنولوجي تزايدت كمية السحب من المياه غير المقنن، مما نتج عنه هبوط تدريجي للمنسوب، وكذلك تغيّر في الخصائص الفيزوكيميائية للمياه وأصبحت أغلب الآبار في شمال غرب الحوض ذات ملوحة عالية، إذ بلغت ما بين 150-450 ملجم/لتر في طبقات الحياة القديمة، وزاد مكافئ كلوريد الصوديوم 10000 جزئي/مليون.

ولقد حاولنا في هذه الدراسة رصد تغيرات مناسيب مياه ستٍ وعشرون بئرا متفرقة على هذا الحوض بغرض الوقوف على معدل الهبوط وزيادة نسبة الملوحة الناجم عن استنزاف مياه الحوض؛ وذلك في السنوات: 2005، و2010، و2013 ومقارنة بمستوى منسوب مياه الخزان.

وبعد إجراء مقارنات حول معدلات الهبوط في المناطق التي تقع فيها الآبار تبين أن كمية السحب كانت كبيرة حتى وصل الهبوط في خزان حقبة الحياة المتوسطة إلى 72متقريباً، وخزان الديفونيإلى حوالي 56م، وهذا يعد مؤشرا خطيرا يستدعي تعميق الدراسة ووضع استراتيجية لاستهلاك المياه بما يضمن الاستقرار والتنمية المستدامة في هذه المنطقة المهمة من البلاد.

1. تمهيد

اهتم الجغرافيون والجيولوجيين بالماء بما له من خواص فيزيائية وكيميائية، وكذلك للتفاعل بينه وبين المخلوقات الحية وبيئاتها في النظام الأيكولوجي، فالأخير أهم مركب على الأرض لا حياة عليها بدونه، قال تعالى:﴿وجعلنا من الماء كل شيء حي أفلا يؤمنون﴾ (الأنبياء 30).

ندرة المياه الصالحة للاستعمال مشكلة بيئية عالمية بعد أن كانت مشكلة محلية واقليمية، بسبب التزايد السريع للسكان والتوسع في الصناعة والزراعة، وسوء استخدامها أدى إلى استنزاف المياه بشكل ملحوظ، فنصف مساحة الكرة الأرضية تتصف بعدم كفاية مواردها المائية أو انعدامها بشكل عام والمياه العذبة بشكل خاص، ووسط القارة الأفريقية أكثر تهديدا بانعدام المياه خلال العقود القادمة إذا لمتتم المحافظة عليها.

ليبيا من الدول التي أولت اهتماماً كبيراً لمشكلة المياه، وحاولت إيجاد السبل الكفيلة للحد من استنزافه، حيث أجريت العديد من البحوث والدراسات لاستغلال المياه العذبة المخزونة في جوف الأرض، التي تعد المصدر الأساسي للمياه في ليبيا، إذ تشكل 98% من مصادر المياه المتاحة، ولا يوجد بها مصدر أخرى، فالاعتماد عليها بشكل كلي في مختلف الأنشطة بالإضافة إلى ارتفاع عدد السكان وتداعياته من التوسع الزراعي والعمراني، وزيادة تركز السكان في مدن الساحل الليبي، زادت الحاجة للماء مما أدى إلى نقص في المياه الجوفية العذبة في تلك المناطق، وهذا أدى بدوره إلى الاتجاه نحو الجنوب وخاصة أقليم فزان الذي يمتلك خزانات عذبة من المياه الجوفية، فتم سحب المياه من الجنوب إلى الشمال عن طريق مشروع النهر الصناعي، وبذلك أصبح منسوب مخزون المياه في خزانات حوض مرزق في تناقص كبير، ولا يوجد ما يعوض الفاقد نتيجة لوقوع منطقة الدراسة ضمن الإقليم الصحراوي، حيث الحرارة العالية، وندرة الأمطار بمعدل سنوي 20ملم، وتزايد كميات الفاقد بفعل التبخّر، وتعرّض المنطقة لفترات جفاف، فالنظام البيئي في هذا النطاق هش وحساس. إن المنطقة قادمة على التصحّر في الفترات القريبة، والملوحة المتزايد للمياه العذبة تعد مؤشرا سلبيا على مستقبل المنطقة، وهذا يضعف الأنشطة القائمة على الموارد المائية، وخاصة في غياب الاستغلال غير المرشد للمياه.

1.1 الموقع

يقع الحوض جنوب غرب ليبيا، ويحده شمالا منحدر الحماده الحمراء الجنوبي، والحافة الجنوبية لجبل الحساونة، وجبال السوداء وهذا يتفق مع خط عرض 28 شمالاً، وشرقا يحده تكوينات الدهر الثالث لحوض سرت، وحافة جنوب غرب جبل الهروج الأسود، وهو بخط طول 16 شرقاً تقريباً، ويحده جنوبا كل من النيجر وتشاد، وغربا الجزائر. كما في الشكل 1.

 ISSN 2663-1407; National Library of Libya, Legal number: 390/2018

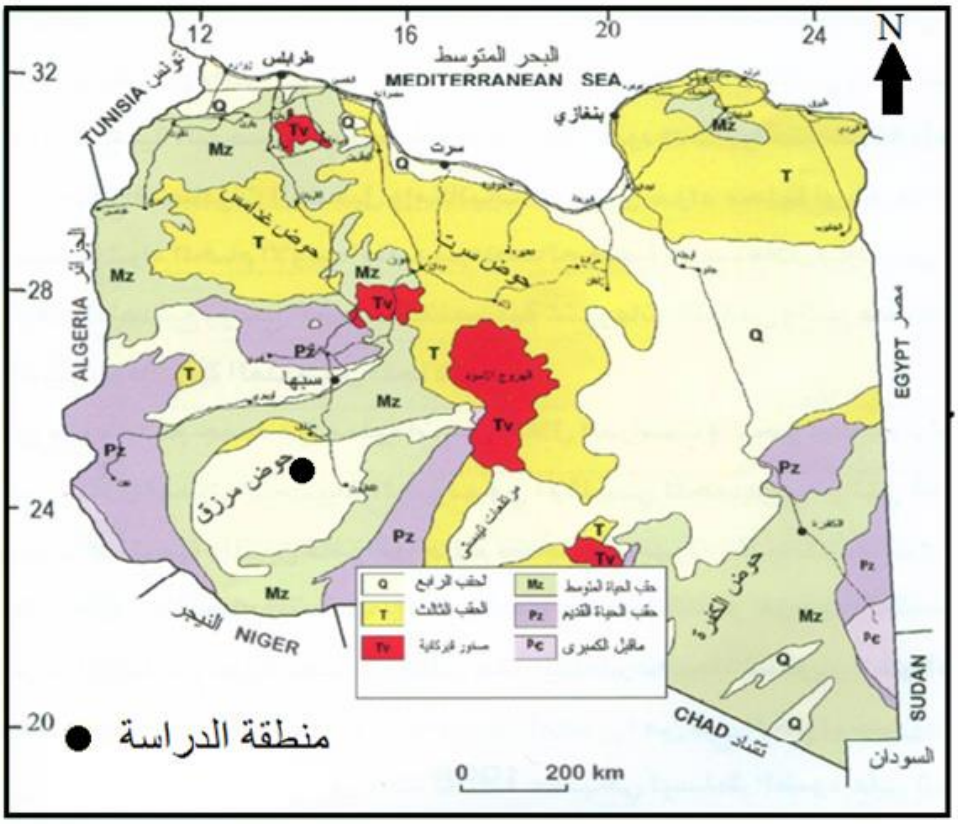

شكل 1. الموقع الجغرافي وجيولوجية منطقة الدراسة

مورفولوجيا حوض مرزق سهلا تحيط به مرتفعات جبلية غير متصلة من تكوينات الدهر الأول (الكمبري والاردوفيشي)، جبال أكاكاس في الغرب وجبل الحساونة في الشمال وجبل بن غنيمة في الشرق. وأبرز معالمه مسطحات رملية (أدهان مرزق وأدهان أوباري)، إذ تبلغ الأولى 70.000كم^2 والثانية مع امتدادها الشرقي لرمال زلاف مساحتها 80.000كم^2. وباقي الحوض يتكون من سهول صحراوية مغطاة بالحصى، ومنخفضات على شكل أودية مثل وادي تنازوفت أو شبه أودية مثل: وادي الشاطئ، ووادي الحياة، ووادي عتبة، ووادي أروان. وتنتهي أودية الحوض بالمرتفعات المحيطة: الحماده الحمراء، وجبل الحساونة، وجبل بن غنيمة بالإضافة إلى وادي تنازوفت الذي يجري غرب الحوض، وتفصله عن حوض مرزق الداخلي سلسلة جبال أكاكوس، كما في الشكل 1.

2. جيولوجية حوض مرزق

يعد حوض مرزق من الاحواض الرسوبية ضمن الرسخ ويقع على مسطح شمالا فريقيا في الجنوب الغربي من ليبيا ويمتد داخلا للنيجر، يحده من الشمال مرتفع القرقاف ومن الغرب مرتفع تهمبوكا ومن الشرق مرتفع تبستي ويغطي الحوض مساحة تقدر بـ 350,000 كيلو متر مربع (Echikh and Sola, 2000). وتشكّل الحوض بسبب العديد من الأحداث التكتونية التي بدأت خلال زمن ما قبل الكامبري، وشكّلت بعض الصدوع الرأسية باتجاهات شمال-جنوب مترافقة مع صدوع باتجاهات شمال شرق-جنوب غرب (Bellini and Massa, 1980) كما هو موضّح في الشكل 2، واتبعت الحركات الأفريقية البانية للجبال في زمن ما قبل الكامبري بعدة حركات تكتونية والتي من اهمها الحركات الكالدونية اثناء حقبة الحياة القديمة المبكر والحركات الهرسينية خلال حقبة الحياة المتأخرة وبداية حقبة الحياة المتوسطة. هذه الحركات تسببت في الطي والتصدع (Bellini and Massa, 1980). وخلال عصر الجوراسي من حقبة الحياة القديمة تعرض الجزء الشرقي من الحوض للرفع وتشكل جبال دور القصة (Yahia *et al.*, 2000).

يحوي الحوض فوق صخور القاعدة قطاع من الصخور الرسوبية بسمك 3500م في مركزه يعود لحقبة الحياة القديمة والمتوسطة Echikh and Sola, (2000). وقد حدد اقصى عمق في مركز الحوض إلى صخور ما قبل الكامبري بـ 3500 متر (Aziz, 2000). والتتابع الطبقي الرسوبي لحوض مرزق يتميز بوجود الأحجار الرملية والطينية. وتتكون صخور العصر الكامبري والاوردفيشي من صخور رملية تعود لتكوين الحساونة من عصر الكامبري، متمثلة في كونجلوميرات (الزلط) واحجار رملية متوسطة الى خشنة الحبيبات تكونت في بيئة نهرية في جزئه السفلي الى بحرية ضحلة في جزئه العلوي. ويعلو تكوين الحساونة بسطح عدم توافق تكوين حوا زمن العصر الاوردفيشي وهو أيضا يتألف من احجار رملية متوسطة وخشنة في حجم الحبيبات، بالإضافة الى الأحجار الغرينية والطينية تشكل في بيئة مروحة دلتاوية (Vos, 1981)، وفي الجنوب الغربي من الحوض يتغير تكوين حوازجانبيا الى تكوين الشبيات ذي الطبيعة الرملية أيضا، ويعلوتكويني حواز والشبيات تكوين ملزشقران الذي يتكون من احجار طينية تكونت في بيئة بحرية ، ويعلو تكوين ملزشقران تكوين الميمونيات الذي يعد الخزان الرئيسي للبترول في حوض مرزق، ويتألف تكوين الميمونيات من احجار رملية جيدة الفروز في مجمله. وترسب تكوين الميمونيات بالإضافة الى تكوين ملزشقران اثناء العصر الجليدي في الاردوفيشي (Davidson *et al.*, 2000).

خلال العصر السلوري ترسبت الصخور الطينية لتكوين تانزوفت الذي ترسب بسبب تقدم البحر بسطح عدم توافق فوق تكوين الميمونيات، ويعد تكوين تانزوفت هو صخر المصدر الرئيسي للبترول في حوض مرزق وهو غني بالخطيات. ويعلو هذا التكوين تكوين اكاكوس والذي تكون اثناء العصر السلوري الاوسط والعلوي في بيئة بحرية ضحلة. ويتوضع تكوين التادرات بسطح عدم توافق فوق تكوين اكاوكوس وهي عبارة عن احجار رملية خشنة الحجم. وفي مركز الحوض، تعلو تكوين اكاكوس احجار رملية غنية بالحديد من العصر الديفوني الاوسط والعلوي تعرف بتكوين عوينات ونين، ترسبت في بيئات ساحلية الى بحر ضحل (*et al.*, 2000 Davidson).

وكذلك تميزت صخور العصر الكربوني بتقدم بحري حيث ترسب تكوين مرار فوق تكوين عوينات ونين ويعلوه تكوين اسد جيفار وهما يتألفان من احجار طينية وغرينية ورملية بدورات رسوبية تكونت في بيئة هادئة في بحر ضحل. تكوين دمبابة من العصر الكربوني الاوسط يتألف من احجار جيرية ورملية واحجار طينية تشكلت في بيئة بحرية. اما العصر الكربوني العلوي فهو متمثل في حجر طيني بحيري احمر اللون يعود لتكوين تيقونتورين الذي يكون غالبا مفقود في بعض اجزاء الحوض بسبب عدم الترسيب او التعرية بسبب الحركات الهرسينية. اما صخور عصر البرمي فهي غير موجودة في الحوص غالبا بسبب عدم ترسيبها.

وخلال العصر الترياسي الى الكريتاسي السفلي ترسبت الصخور في بيئات قارية حيث توضع تكوين زرزاتين وتوراتين من الترياسي الى الجوراسي في بيئة نهرية وهما احجار رملية نهرية وطينية حمراء اللون، واثناء الجوراسي والكريتاسي المبكرترسب تكوين مساك الذي يتألف من كونجلوميرات (الزلط) واحجار رملية نهرية وطينية، ويمثل سمك ترسيبات صخور حقبة الحياة المتوسطة حوالي 1700 متر (Davidson *et al.*, 2000)

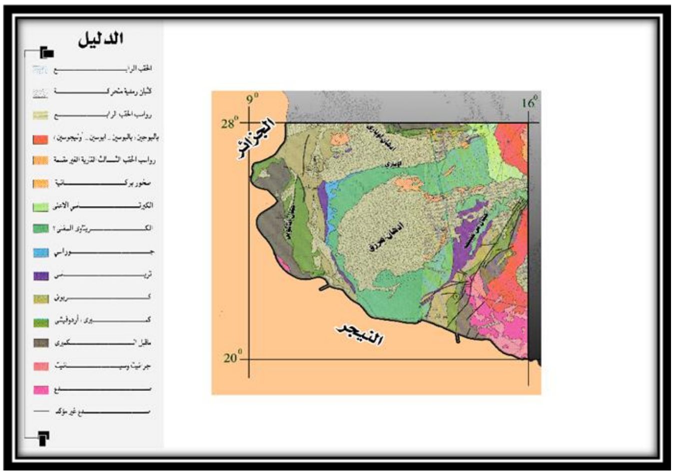

شكل 2. يوضح جيولوجية حوض مرزق (Bellini and Massa, 1980)

3. نوعية المياه

يقصد بنوعية المياه الجوفية مدى ملاءمتها للاستعمال في الأغراض العامة (الشرب-الزراعة-الصناعة) وفقاً للمواصفات القياسية العالمية والمحلية. المياه الجوفية في حوض مرزق تتواجد على أعماق مختلفة بأغلب الأحجار الرسوبية ولقد أشارت الدراسات السابقة الي أن هذه المياه الجوفية تتواجد في ثلاثة مستويات رئيسيه كما في الشكل 3 وهي:

1-المياه الجوفية بطبقات حقبة الحياة القديمة.
2- المياه الجوفية بطبقات حقبة الحياة المتوسطة.
3- المياه الجوفية بطبقات حقبة الحياة الحديثة.

ولقد تم تقسيم الطبقات الحاملة للمياه الجوفية عن طريق (Pallas, 1980) إلى قسمين هما:

أ- الخزان الجوفي السفلي: ويتمثل في الأحجار الرملية التابعة لحقبة الحياة القديمة.
ب- الخزان الجوفي العلوي: ويتمثل في الأحجار الرملية التابعة لحقبة الحياة المتوسطة، ويفصل بين هذين الخزانين طبقات للأحجار الطينية والكربونية.

1- المياه الجوفية بطبقات حقبة الحياة القديمة

المياه الجوفية بحقبة المياه القديمة تتواجد بالأحجار الرملية (الكمبري، والاوردفيشي والسيلوري والديفوني) وتكون عادة صلبه ومتماسكه ورقيقه الي متوسطة الحبيبات ويتم استغلال مياهها العذبة بوادي الشاطئ ووادي ألاريل بالطرف الشمالي لحوض مرزق وبمنطقة وادي تنازوفت والعوينات بالطرف الجنوب الغربي لحوض مرزق ومن خلال نتائج حفر الآبار لغرض التنقيب عن النفط وجد أن المياه الجوفية بالطبقات الرسوبية مرتفعة الملوحة وغير صالحة للاستعمال في وسط حوض مرزق (وادي الآجال ومرزق).

2- المياه الجوفية بطبقات حقبة الحياة المتوسطة

المياه الجوفية بطبقة المياه المتوسطة تتواجد بالأحجار الرملية (الترياسي، الجوراسي، والطباشيري الأسفل) وتتكون من: أحجار رملية مع تبادلات طبقيه من أحجار طينية وغرينيه ذات سمك مختلف من مكان الي أخر. ولقد تم تقسيم المياه الجوفية بحقبة المياه المتوسطة الي مجموعتين رئيسيتين حسب (الشاعر، 1984 و1991):

أ- خزانات المجموعة الاولي (مجموعة الخزانات العلوية): وتتمثل في المياه الجوفية المخزونة بالأحجار الرملية التابعة للدور الجوراسي الأعلى والطباشيري الأسفل، ويلاحظ أن مياه هذه الخزانات تعرضت للتلوث وأصبحت مياهها مالحة.
ب- خزانات المجموعة الثانية (مجموعة الخزانات السفلية): وتتمثل في المياه الجوفية المخزونة بالأحجار الرملية التابعة للدور الترياسي والجوراسي الاسفل ومياه هذه الخزانات مياه عذبة.

3- المياه الجوفية بطبقات تابعة لحقبة المياه الحديثة

تكوينات حقبة المياه الحديثة تتشكل على هيئة خليط من الحصى والطين والأحجار الجيرية والرمال والكثبان الرملية وتتواجد بالوديان والمنخفضات هذه التكوينات تحتوي على مياه تتفاوت عادة في نوعيتها من صالحة للاستعمال الي مالحة ومرتفعة الملوحة.

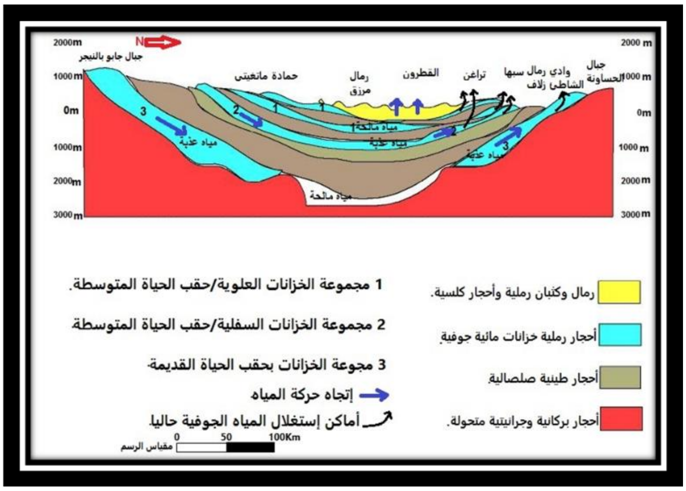

شكل 3. قطاع هيدرولوجي يبين الخزانات المائية بحوض مرزق (Pallas, 1980)

4. حوض مرزق بين الاستهلاك والاستدامة

إن الطلب على الماء يتعاظم مع زيادة معدل النمو السكاني، ومع ارتفاع معدلات الاستهلاك الفردي منه، فكمية الماء الذي يستهلكها الانسان لا تتوقف على احتياجاتهم الأساسية وفق مقدار الماء المتاح فقط، بل توجهها مستويات التحضر والتطور الاقتصادي، كما يزداد سحب الماء من أجل متطلبات كافة أنماط الاستهلاك كالزراعة المروية والصناعة والاحتياجات المنزلية. ففي سنة 2000 كان الفرد في الشاطئ يستهلك ما يصل إلى 1010 لتر في اليوم، و947 لتر في اليوم يستهلكه فرد واحد في وادي الحياة، ويستهلك الفرد في مرزق ما يعادل حوالي 629 لتر في اليوم، وبالنسبة لسبها فيستهلك الفرد فيها 507 لتر في اليوم (الطلحي، 2003). وهذا يدل على أن هناك سوء استعمال للمياه من قبل الفرد، إذا إنه من المفترض أن يكون المتوسط العام للاستهلاك هو 200 لتر في اليوم للفرد، وهذه الكمية تلبي الاحتياجات في حدود مريحة مع المحافظة على الماء.

استنزاف المياه الجوفية مشكلة خطيرة، إن استنزاف المياه الجوفية، ونضوب هذا المورد وتدهور نوعيته بحيث لا يمكن الاستفادة منه يمثّل مشكلة خطيرة، ففي شمال البلاد هي مشكلة قائمة، وفي الجنوب آتية لا محالة. إذ إنه كما سبقت الإشارة تعتمد ليبيا كلياً على سد احتياجاتها وتنمية مواردها على المياه الجوفية بنسبة 98%، ففي سنة 2003 كانت كمية المياه المتاحة 4305.4 مليون م3/سنة، والكمية المستهلكة 2736.6 مليون م3/سنة، (الطلحي، 2003).

وفي حوض مرزق كان الاستهلاك عام 1998حوالي (810.76 مليون م^3) بعد أن كان 715 سنة 1978 (الطلحي، 2003) أما في سنة 2006 فقد وصل مقدار الاستهلاك إلى (2199 مليون م^3) (الهيئة العامة للمياه – سبها، الوضع المائي في ليبيا 2006) وتقدر كميات المياه المستغلة من الحوض سنة 2006 ف بحوالي 2199 مليون متر مكعب، أي أن هناك عجزا مائيا مقداره 199 مليون متر مكعب على أساس أن الكمية المتاحة سنويا تقدر بحوالي 2000 مليون متر مكعب، ويستحوذ النشاط الزراعي على أغلب الاستهلاك بنسبة 97% من إجمالي المياه المستغلة باستثناء ما يتم سحبه من خلال النهر الصناعي (عطية، 2009)، ومن تقرير 2006 للوضع المائي أن النهر الصناعي يسحب ما يقارب 195 مليون م^3 سنويا، وهذا يعادل 9% تقريباً من المياه المستهلكة من حوض مرزق، وذكر الجنابي، (2009) أنه يجري نقل 913 مليون م3 سنويا من الخزانات الجنوبية لتخفيف حجم الاستنزاف الحاصل في خزانات المنطقة الشمالية. هذا السحب قد يكلّف غالياً، فالسحب المستمر من خزانات حقبة الحياة القديمة ووقوعها في النطاق الصحراوي مع كمية أمطار ضئيلة جدا وزيادة نسبة التبخر لا يعوض الفاقد من الخزان، وبذلك ستكون مشكلة المياه أكبر مع الهبوط المتسارع للمنسوب، وخلال العقود القريبة القادمة سينضب مخزون المياه إذا لم تتخذ تشريعات خاصة تقنن الاستهلاك والمحافظة على المياه من الاستنزاف. وهذا خلافه ما ذكره الطلحي، (2003): إن نقل المياه من الأحواض الجنوبية إلى الشمال بواسطة النهر الصناعي أفضل حل لقلة المياه في المناطق الشمالية فهو أقل تكلفة من تحلية مياه البحر أو استيراد مياه من الخارج. وكان لوادي الحياة النصيب الأكبر في الاستهلاك بنسبة 31% من كامل الحوض والجدول 1 يوضح كمية المياه المستهلكة من حوض مرزق سنة 2006 (عطية، 2009).

جدول 1

كمية المياه المستهلكة من حوض مرزق سنة 2006

المنطقة	الاستهلاك (مليون م^3/السنة)	النسبة المئوية
سبها	572	%26
وادي الشاطئ	360	%16.3
وادي الحياة	684	%31
مرزق	388	%16.6
النهر الصناعي	195	%8.8
المجموع	2199	100

إن أجمالي استهلاك المياه بمنطقة **وادي الشاطئ** يصل إلي حوالي 360 مليون متر مكعب في السنة، وتقدر كمية المياه المستغلة في منطقة وادي الشاطئ بحوالي 50 مليون متر مكعب من المياه موزعة علي 64 بئرا وتستهلك المزارع الخاصة حوالي 270 مليون متر مكعب من المياه سنويا، أما المياه المستغلة للأغراض الحضرية بمنطقة وادي الشاطئ فتبلغ حوالي 8 مليون متر مكعب في السنة ويبلغ عدد الآبار المحفورة لهذا الغرض 44 بئرا يستغل أغلبها الطبقة السطحية وهي ذات ملوحة عالية وغير ملائمة للشرب الأمر الذي يستوجب حفر أبار عميقة كما تقدر كميات المياه المفقودة نتيجة تآكل رؤوس الآبار الارتوازية بحوالي 20 مليون متر مكعب سنويا. أما في منطقة سبها فتقدر نسبة استهلاكها من الحوض 26% وكمية المياه المستغلة بالمزارع الخاصة بحوالي 250 مليون متر مكعب/سنة المياه للري موزعة علي77 بئرا. ويبلغ عدد الآبار المحفورة للأغراض الحضرية بمدينة سبها 64 بئرا، وبئران مستغلان للشرب بمنطقة غدوة و 20 بئرا للأغراض الصناعية وعليه فإن أجمالي الإنتاج للأغراض الحضرية والصناعية يقدر بحوالي 22 مليون مكعب/سنة. أما منطقة مرزق فتقدّر نسبة المياه المستغلة بحوالي 16.6% من مياه الحوض فالمشاريع الزراعية تستنزف حوالي 63 مليون متر مكعب في السنة موزعة على 8 آبار ويبلغ عدد الآبار المحفورة للأغراض الحضرية 44 بئرا بإنتاجية تقدر بحوالي 8 مليون متر مكعب في السنة مع العلم بأن أغلب الآبار الحالية تستغل الطبقة السطحية وهي ذات ملوحة عالية وغير ملائمة للشرب وتحتاج المنطقة إلى حفر أبار عميقة تصل إلى حوالي 750 متراً تقدر كمية المياه المستغلة بالمزارع الخاصة بحوالي 317 متر مكعب في السنة (الوضع المائي في ليبيا 2006).

1.4 أساليب الاستهلاك

يتمثل سوء استعمال الموارد المائية في ممارسة أساليب الري التقليدية القديمة مما يؤدي الى فاقد كبير يتراوح ما بين 30-60% من حجم المياه المستعملة (السعيدي، 2012)، وكذلك إهمال شبكات الصرف في مشاريع الري. إن متوسط الاحتياجات المائية للهكتار في الإقليم يفوق المعدل الطبيعي بحوالي مرة ونصف، نظرا للظروف المناخية السائدة، والإفراط في استعمال المياه مما يزيد من هدر المياه وتملّح التربة. وكذلك الضخ الزائد يؤدي الى استنزاف المخزون الجوفي من المياه، فالتغذية قليلة جداً لظروف المنطقة الصحراوية، ومعدل الأمطار السنوي القليل، وكميات الفاقد بفعل التبخر كبيرة، تحت هذه الظروف لا يمكن تعويض النقص الحاصل.

وقد ظهرت مؤشرات سوء الاستخدام والزيادة في الاستهلاك واضحة كما ونوعا منذ عدة عقود في المنطقة الجنوبية نتيجة للنمو السكاني والحضري والزراعي وخاصة في المناطق حول الواحات حيث الاستثمارات الزراعية فأدى السحب الجائر إلى انخفاض منسوب المياه بشكل كبير وجفاف الخزان السطحي في بعض المناطق فتدهورت نوعية المياه بشكل ملحوظ. فحسب الشاعر (1991) بلغت الملوحة ما بين 150-450 ملجم/لتر في طبقات الحياة القديمة، حيث زاد مكافئ كلوريد الصوديوم 10000 جزئي/مليون. وقد ساهم هذا في تدهور التنوع الحيوي والبيئة المحيطة خصوصا في المناطق الصحراوية الحرجة.

إن انخفاض إنتاجية الآبار المحفورة لاستغلال بعض الخزانات الجوفية كان سببا في تدني معدلات الإنتاج الزراعي في المناطق المتضررة. وهذا الهبوط الحاد أدي بدوره إلى استمرار المزارعين في تعميق أبارهم أو حفر أبار بديله وزيادة عمق المضخة المستعملة وتغيير قوتها بما يتناسب مع عمق المياه المتغير باستمرار، فتعرضت بعض الخزانات الجوفية إلى هبوط حاد في مناسيب المياه أدي إلى جفاف الطبقات السطحية الحاملة للمياه (السعيدي، 2012).

2.4 تأثير الاستهلاك على هبوط المنسوب

تمت دراسة تغيرات مناسيب المياه لستة وعشرون بئرا متوزعة على حوض مرزق كما في الشكل 4. وذلك لتوضيح معدل الهبوط كما في الملحق 1. ومن أهمها Tmessa و Idri وAril و Maknussa وIrawan و Semnu و Godwa و Barjuj و Hummero، وبمقارنة معدل الهبوط لها في سنة 2005 و 2010 و2013م على حسب الخزان كما هو موضح في الملاحق 2 و 3 و 4.

وبعد مقارنة معدل الهبوط لخزان حقبة الحياة المتوسطة كما في الشكل 5 والملحق (4)، نستنتج أن معدل هبوط الخزان كبير، وهذا يدل على استنزافه الكبير، فقد وصل حتى 72.18م في Barjuj سنة 2013م، ومشروع Maknussa يعد استهلاكه معتدلاً، فقد وصل معدل هبوطه بين 37.35م خلال السنوات الثلاث. أما البئر (4115) بمشروع Irawan هو الأقل استنزافاً للمياه نتيجة توقف هذا المشروع عن العمل سنة 2010م، فكان معدله 13.1م، وكذلك بئر (4079) Godwa فقد وصل إلى 12.4م في سنة 2005م، ولم يستهلك كثيراً سنة 2013، فقد تكون مشاريع توقفت أو أراضي جفت بسبب قلة المياه.

أما فيما يخص خزان الديفوني فكان البئران 4099 و4100 Quttah و Wanzarik على التوالي هما الأقل سحباً منه فقد وصل معدل الهبوط في 2010 إلى (1.8م) في Quttah، وبمعدل (2.9م) سنة 2005 للبئر (4100)، أما منطقة Tarut للبئر رقم 4098 هي الأكثر سحبا لهذا الخزان (2005-2013)، فمعدل هبوطه وصل خلال الثلاث سنوات بمتوسط حتى (56.4م) (الهيئة العامة للمياه) كما في الشكل 6.

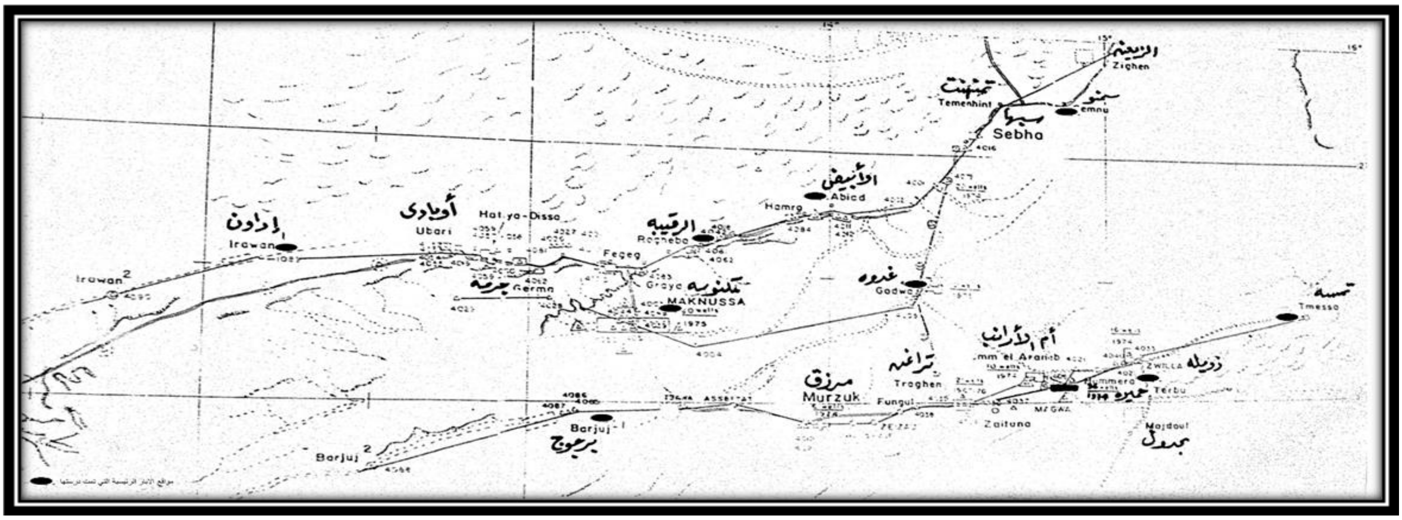

شكل 4. يوضح خريطة المواقع البيزومترية والمشاريع المستهلكة للمياه في حوض مرزق من عمل الباحثين (الهيأة العامة للمياه-سبها، 1972-2000)

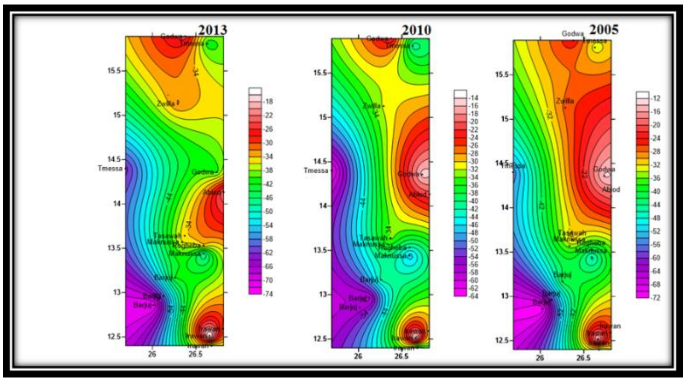

شكل 5. يوضح خرائط بيزومترية لمعدل هبوط الماء خزان حقبة الحياة المتوسطة من عمل الباحثين: استنادا من الهيئة العامة للمياه، حوض مرزق، (الهيئة العامة للمياه-سبها، 2005-2013)

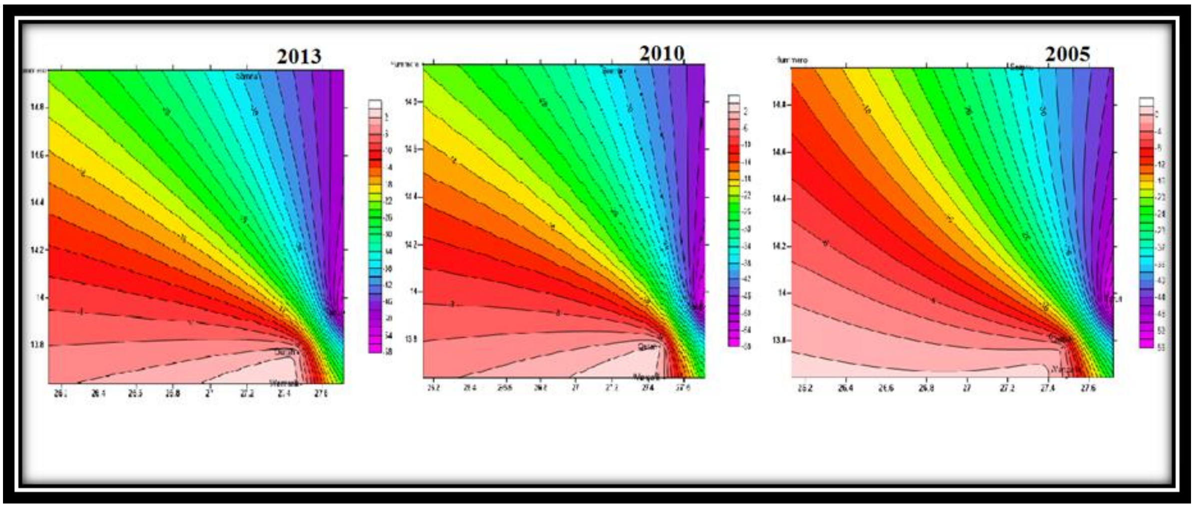

شكل 6. يوضح خرائط بيزومترية لمعدل هبوط الماء خزان حقبة الديفوني من عمل الباحثين: استنادا من الهيئة العامة للمياه، حوض مرزق، (الهيئة العامة للمياه-سبها، 2005-2013).

أما خزان حقبة الكمبري والاردوفيشي فلم يكن السحب كبيرا في 2005 ولم تأخذ بعض القراءات في 2005-2010 لصعوبة فتح غطاء البئر Idri وTahala، وفي 2010 و 2013 كان البئر (4123) لمشروع Aril هو الأكثر استهلاكا لهذا الخزان حتى وصل معدل الهبوط (25م)، أما سنة 2013 فكانت منطقة Idri هي الأقل استنزافا لمياه هذا الخزان بمعدل (0.65م) كما في الشكل 7.

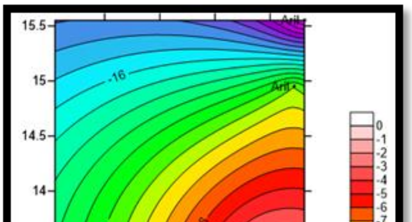

شكل 7. خريطة بيزومترية لمعدل هبوط الماء خزان حقبة الكمبري والاردوفيشي سنة2013م من عمل الباحثين: استنادا من الهيئة العامة للمياه، حوض مرزق، (الهيئة العامة للمياه-سبها، 2005-2013).

ومن قراءات بعض آبار الدراسة لسنوات مختلفة وجد أن خزان الحياة المتوسطة خلال 27 سنة (1972-2000) كان الاستنزاف قليلاً بمعدل (4.2م) في Abiod ففي سنة 1972م كان معدل الهبوط حوالي 10م تقريبا وخلال سنة واحدة (1999-2000) كان مشروع Barjuj للبئر 4115 هو الأكثر سحبا للخزان، فقد كان متوسط معدل الهبوط حتى 70.72م (الهيئة العامة للمياه)، بمقارنة هذا المشروع للسنوات من 1999 -2013 كان هو الأكثر استنزافا لمياه خزان الحياة المتوسطة، ويحتاج ارشاد مستخدميه الى الخطورة المتوقعة إذا استمر استنزافه بهذا الشكل.

أما خزان الديفوني فكان بئر (4099) Quttah استنزافه الأقل من 1978-2013، فخلال 22 سنة من 1978- 2000 كان معدل الهبوط 9.28م فمن سنة 2000بمعدل 2.4م الى 2013بمعدل 2.9م، أما البئر الأكثر استنزافا لهذا الخزان هو Tarut للبئر 4098 من سنة 1979 -2013 ففي سنة 1979وصل معدل الهبوط إلى 47.8م تقريبا وفي سنة 2000 وصل معدل الهبوط حتى 54.5م وعام 2013 ازداد الهبوط حتى وصل المعدل إلى 56.9م تقريبا، وهذا استنزاف كبيرا جدا وأصبحت ملوحته ونسبة الحديد في ازدياد وبعد فترة قصيرة لن يعد البئر صالحا للشرب.

بالنسبة لخزان الكمبري والاردوفيشي فخلال 21 سنة كان مشروع Aril هو الأكثر سحباً من البئر (4123) فوصل معدل الهبوط حتى (9.26م) من سنة 1979- 2000، ففي سنة 2000 وحدها ارتفع الهبوط إلى 25م تقريبا، وبالمقابل كان مشروع Tahala الأقل استهلاكاً خاصة البئر (4073) ففي سنة 1999 و 2000 لم يتعدى معدل الهبوط 1.2م فقط وفي 2005 وصل معدل الهبوط حتى 9.9تقريباً ولم يرتفع كثيرا في 2013 فالمعدل وصل إلى حوالي 13م تقريباً.

نتيجة للاستغلال المفرط للمياه الجوفية الذي تعدي بكثير التغذية الطبيعية للخزانات الجوفية المتجددة أو السريان الطبيعي للمياه بالخزانات الجوفية غير المتجددة حدث اختلال في الميزان الطبيعي المائي في بعض المناطق، سبب في حدوث ظاهرتين علي مستوى كبير من الخطورة هما الهبوط الحاد في مناسيب المياه ببعض الخزانات الجوفية، وتدهورت نوعية المياه بسبب زحف المياه المالحة لتعويض الفاقد من المياه الجوفية العذبة، نتج عنهما تأثيرات وانعكاسات سلبية على البيئة والصحة والنشاط الاقتصادي والزراعي والعمراني، حيث إن استمرار السحب الجائر للمياه الجوفية أدى إلي اختلال الميزان المائي ببعض المناطق نتج عنه استمرار الهبوط في مناسيب المياه وتدهور ملحوظ في نوعيتها سبب عدة مشاكل ترتب عليها بعض الآثار البيئية والاقتصادية والصحية، مثل: جفاف الطبقات السطحية الحاملة للمياه و نضوب وجفاف بعض العيون والآبار الضحلة في بعض المناطق . ويؤدى هذا السحب إلى خروج مساحات كبيرة من النظام الزراعي إما بشكل مؤقت

أو مستمر، والسحب من هذه المياه يؤدي إلى نفاذها إلى الأبد بعد سلسلة طويلة من تدهور نوعية المياه وتملحها لأنها غير متجددة.

إن سوء استخدامات المياه له أثار بيئية سلبية مالم تؤخذ بعين الاعتبار الجوانب البيئية وتدهور النظم البيئية المحلية وعادة ما يصاحب استغلال المياه في الزراعة أثار بيئية تلحق جميع مكونات النظام البيئي كتلوث المياه، ومشكلة مياه الصرف. ونتيجة لزيادة عدد السكان والتوسع في الأنشطة الزراعية فإنه يتم الاعتماد على الاستخدام المتزايد للمبيدات الكيميائية في مكافحة أفات النباتات لأجل تحقيق زيادة في القدرة الانتاجية، الا ان هذه الزيادة ونتيجة للاستخدام المفرط للمبيدات الضارة بالبيئة فإنها تؤدي الى الحاق الأذى والضرر بالبيئة وبالتالي تدهور التربة وتلوث المياه.

5. التوصيات

إن تحقيق تنمية مستدامة بالإمكانيات المتاحة في ليبيا بصفة عامة ومناطق الجنوب بصفة خاصة يتطلب المحافظة على الموارد المائية وتنميتها وفق المقترحات التالية:

1. تفعيل القوانين الخاصة بعدم استنزاف المياه الجوفية، والحد من حفر الآبار لغرض الزراعة، وصيانةالمستعمل منها، واستعمال المياه في الزراعة بالقدر اللازم والاقتصادي فقط، ويجب أتباع الأنظمة الزراعية من ناحية نوعية المزروعات وطرق الري وتحديد مواعيد للري لتجنب الفترات التي ترتفع فيها معدلات البخر، بما يكفل أقل استعمال للمياه وأكبر عائد للإنتاج.
2. دراسة الآبار على الحوض بشكل أدق ودوري بتقدير كمية ونوعية المياه الموجودة في الحوض وتحديد معدل الهبوط ووضع سقف للاستهلاك سنويا بحيث لا يجب تعديه لتقليل الاستنزاف، وتحديد الأسلوب الأكثر ملائمة لاستخراجها.
3. معرفة حدود الخزان الجوفي وتركيبه وتكوينه الجيولوجي، وخواصه الطبيعية.
4. حصر مصادر التلوث التي تؤثر على نوعية المياه وإيجاد الأسلوب الملائم للتقليل منها.
5. قياس معدل الأمطار ودرجة الحرارة ونسبة التبخر لمنطقة الخزان ومناطق تغذيته.
6. معالجة مياه الصرف الصحي وتجهيزها لغرض الاستعمال المباشر للري، أو إعادة ضخها تحت سطح الأرض لتغذية الخزانات الجوفية.
7. متابعة التقنيات الحديثة في مجال إزالة ملوحة مياه البحر، ومحاولة الاستفادة من المصادر الحديثة للطاقة في خفض التكلفة الاقتصادية لتحلية مياه البحر، وهو الحل المناسب لمشكلة المياه في ليبيا، وهو ما ورد في تقرير لجنة الموارد المائية في سبعينيات القرن الماضي.
8. الاتجاه للطاقة الشمسية، المصدر الوحيد المتجدد والمتوفر والأكثر منطقية فيها، فبمتابعة التطورات التقنية لاستغلالها، يتحتم على الجهات المسؤولة عن موضوع المياه أن تكون من أولويات اهتمامهم، فتحلية المياه المالحة بواسطة الطاقة الشمسية هو الحل الأكثر جدوى لتوفير المياه الصالحة للشرب للمناطق التي لا يوجد بها مصدر للمياه.

المراجع

جاد الله عزوز الطلحي (2003) حتى لا نموت عطشاً، الدار الجماهيرية للنشر والتوزيع والإعلان، ط1، يناير، 2003.

حسن كشاش الجنابي (2009) (تحليل جغرافي لإمكانية تحقيق الأمن المائي في ليبيا) مجلة ديالى/ 2009 العدد الحادي والأربعون، كلية التربية والعلوم الإنسانية – جامعة الأنبار.

محمد علي السعيدي (2012) وعائشة رمضان محمد (التغيرات الكمية والنوعية في خصائص مياه حوض مرزق واثارها على الانظمة البيئية المحيطة) Libyan Agriculture Research Center Journal international 3 (S2)1335-1350, 2012، قسم علوم البيئة - كلية العلوم الهندسية والتقنية/جامعة سبها الهيئة الوطنية للبحث العلمي.

محمد محمد الشاعر (1987) المياه الجوفية بحوض مرزق ومصادر تكونها، بحث مقدم إلى المؤتمر العلمي الأول حول المجتمعات الصحراوية (مرزق).

محمد محمد الشاعر (2006) المياه الجوفية المالحة بحوض مرزق، مجلة الدراسات الصحراوية المجلد الأول، المركز العربي لأبحاث الصحراء وتنمية المجتمعات الصحراوية مرزق.

الهيئة العامة للمياه – سبها (1972-2000) الوضع المائي في ليبيا 2006.

الهيئة العامة للمياه، سبها (2005-2013) جداول القراءات التي أخذت لآبار المراقبة بحوض مرزق، 2005-2010-2013.

الهيئة العامة للمياه، سبها (2008-2009) معدلات الهبوط في آبار الشبكة البيزومترية لحوض مرزق 1972-2000.

وفاء محمد عطية (2008-2009) "الهجرة الداخلية في إقليم فزان، دراسة في جغرافية السكان"، (رسالة ماجستير غير منشورة، قسم الجغرافيا، كلية الآداب، جامعة سبها.

References

Aziz, A. (2000) Stratigraphy and hydrocarbon potential of the lower Palaeozoic succession of license NC 115, Murzuq Basin, S.W. Libya, in M. A. Sola and D. Worsley (eds.), Symposium on Geological Exploration in Murzuq Basin: Elsevier, Amsterdam, p. 349-368.

Bellini, E., Massa, D. (1980) A stratigraphic contribution to the palaeozoic of the southern basins of Libya, in M.J. Salem and M.T. Busrewil (eds.), The Geology of Libya: Academic Press, London, p. 3-56.

Davidson, L., S. Beswetherick., J. Craig., M. Eales., A. Fisher., A. Himmali., J. Jho., B. Mejrab and J. Smart 2000. The structure, stratigraphy and petroleum geology of the Murzuq Basin, southwest Libya. In, Sola, M.A. and D. Worsley (Eds.), Geological Exploration of the Murzuq Basin. Elsevier, Amsterdam, p. 295-320.

Echikh, K., Sola, M.A., 2000. Geology and hydrocarbon occurrences in the Murzuq Basin, S.W. Libya. Symposium on Geological Exploration in Murzuq Basin, M.A. Sola and D. Worsley ed. Elsevier, Amsterdam, pp. 175-222.

Pallas, P. 1980 Water resources of the Socialist People's Libyan Arab Jamahariya The Geology of Libyavol 2, ed M J Salem and M T Busrewil (London: Academic) pp. 539–94.

VOS, R.G. (1981) ‘Sedimentology of an Ordovician fan complex, western Libya’, Sediment. Geol., 29, pp. 153-170.

الملاحق مدرجه في الصفحات التالية

الملاحق

ملحق 1. معدلات الهبوط في آبار الشبكة البيزومترية لأبار حوض مرزق (الهيئة العامة للمياه-سبها، 2008-2009).

الخزان	رقم البئر	اسم البئر	العمق/متر	التاريخ	مستوى الماء	التاريخ	مستوى الماء	معدل الهبوط/م	عدد السنوات
الحياة المتوسطة	4116	Barjuj	304	1999/6	−38.71	2000/5	−38.98	−0.27	خلال سنة
الحياة المتوسطة	4002	Abiod	139.6	1972/4	−10.6	2005/5	−14.8	4.2	خلال 27
الحياة المتوسطة	4085	Irawan	273.8	1999/9	−27.81	2000/5	−29.77	−1.96	خلال سنة
الحياة المتوسطة	4103	Irawan	304.6	1999/6	−34.68	2000/5	−39.0	−4.32	خلال سنة
الحياة المتوسطة	4132	Irawan	95	1996/6	−13.61	2005/5	−13.63	−0.02	خلال سنة
الحياة المتوسطة	4041	Zwilla	160	1996/6	−20.98	2005/5	−21.45	−0.47	خلال سنة
الحياة المتوسطة	4126	Tmeassa	313	1996/6	−29.5	2005/5	−29.63	−0.13	خلال سنة
الحياة المتوسطة	4137	Tasawah	395	1996/6	−26.23	2005/5	−25.85	0.38	خلال سنة
الحياة المتوسطة	4062	Rogheba	263	1999/7	−26.93	2005/5	−30.81	−1.88	خلال سنة
الحياة المتوسطة	4144	Maknussa	404	1999/6	−46.05	2000/5	−45.45	0.6	خلال سنة
الحياة المتوسطة	4115	Barjuj	312	1999/6	−70.95	2005/5	−71.5	0.1	خلال سنة
الحياة المتوسطة	4118	Barjuj	78	1999\6	−58.13	2000\5	−58.23	-0.1	خلال سنة
الحياة المتوسطة	4079	Godwa	460	1999\6	−8.67	2000\5	−12.09	3.42	خلال سنة
الحياة المتوسطة	4154	Tmessa	77	1979\7	−23.7	2000\5	−23.8	0.1	خلال 21
الحياة المتوسطة	4151	Godwa	346.5	1999\6	−26.23	2000\5	−25.85	0.38	خلال سنة
الديفوني	4098	Tarut	128	1991\10	−47.85	2000\6	−54.59	6.74	خلال 9 سنوات
الديفوني	4099	Quttah	89	1979\1	11.68	2000\6	2.4	9.28	خلال 21
الديفوني	4100	Wanzarik	123	1978\3	5.34	2000\6	−1.65	6.99	خلال 22
الديفوني	4139	Hummero	528.5	1979\3	−19.47	2000\5	−19.33	0.14	خلال 21
الديفوني	4010	Semnu	372	1999\7	−14.92	2000\5	−28.46	13.54	خلال سنة
الكمبري واردفيشي	4008	Idri	606	1972\8	12.2	2000\6	1.5	10.7	خلال 28
الكمبري واردفيشي	4122	Aril	356	1973\3	5.72	2000\6	−8.68	14.4	خلال 27
الكمبري واردفيشي	4123	Aril	552	1979\6	−15.94	2000\6	−25.2	9.26	خلال 21
الكمبري واردفيشي	4068	Tahala	500	1979\8	−16.43	2000\5	−16.77	−0.34	خلال 21
الكمبري واردقيشي	4073	Tahala	300	1999\8	1.2	2000\5	1.2	0	خلال سنة

ملحق 2. معدلات الهبوط في آبار الشبكة البيزومترية لأبار حوض مرزق سنة 2005 (الهيئة العامة للمياه-سبها، 2005-2013).

الخزان	WT	E	N	رقم البئر	
الحياة المتوسطة	40.9	13.17	26.26	4116	Barjuj
الحياة التوسطة	_	14.13	26.82	4002	Abiod
الحياة المتوسطة	27.18	12.59	26.81	4085	Irawan
الحياة المتوسطة	36.35	12.4	26.68	4130	Irawan
الحياة المتوسطة	13.67	12.51	26.66	4132	Irawan
الحياة المتوسطة	27.22	15.13	26.29	4041	Zwilla
الحياة المتوسطة	33.35	15.81	26.63	4126	Tmessa
الحياة المتوسطة	31.28	13.64	26.37	4137	Tasawah
الحياة المتوسطة	_	13.53	26.59	4062	Rogheba
الحياة المتوسطة	47	13.44	26.59	4144	Maknussa
الحياة المتوسطة	35	13.57	26.34	4145	Maknussa
الحياة المتوسطة	71.6	12.86	26.02	4115	Barjuj
الحياة المتوسطة	58.6	12.96	26.13	4118	Barjuj
الحياة المتوسطة	13.48	14.36	26.74	4079	Godwa
الحياة المتوسطة	55.2	14.4	25.69	4154	Tmessa
الحياة المتوسطة	24.17	15.89	26.38	4151	Godwa
الديفوني	55.8	13.94	27.72	4098	Tarut
الديفوني	2.5	13.77	27.47	4099	Quttah
الديفوني	2.9	13.64	27.49	4100	Wanzarik
الديفوني	12.5	14.96	26.13	4139	Hummero
الديفوني	_	14.93	27.27	4010	Semnu
الكمبري واردفيشي	_	13.24	27.49	4008	Idri
الكمبري واردفيشي	-13.8	14.95	27.72	4122	Aril
الكمبري واردفيشي	_	15.55	27.81	4123	Aril
الكمبري واردفيشي	14.7	10.63	25.55	4068	Tahala
الكمبري واردقيشي	9.9	10.55	25.57	4073	Tahala

ملحق 3. معدلات الهبوط في آبار الشبكة البيزومترية لأبار حوض مرزق سنة 2010 (الهيئة العامة للمياه-سبها، 2005-2013).

	رقم البئر	N	E	WT	الخزان
Barjuj	4116	26.26	13.17	41.25	الحياة المتوسطة
Abiod	4002	26.82	14.13	-	الحياة المتوسطة
Irawan	4085	26.81	12.59	29.95	الحياة المتوسطة
Irawan	4130	26.68	12.4	39.6	الحياة المتوسطة
Irawan	4132	26.66	12.51	13.13	الحياة المتوسطة
Zwilla	4041	26.29	15.13	31.55	الحياة المتوسطة
Tmessa	4126	26.63	15.81	41.36	الحياة المتوسطة
Tasawah	4137	26.37	13.64	33.4	الحياة المتوسطة
Rogheba	4062	26.59	13.53	-	الحياة المتوسطة
Maknussa	4144	26.59	13.44	47.4	الحياة المتوسطة
Maknussa	4145	26.34	13.57	35.65	الحياة المتوسطة
Barjuj	4115	26.02	12.86	-	الحياة المتوسطة
Barjuj	4118	26.13	12.96	58.75	الحياة المتوسطة
Godwa	4079	26.74	14.36	14.8	الحياة المتوسطة
Tmessa	4154	25.69	14.4	62.65	الحياة المتوسطة
Godwa	4151	26.38	15.89	21.95	الحياة المتوسطة
Tarut	4098	27.72	13.94	56.5	الديفوني
Quttah	4099	27.47	13.77	1.8	الديفوني
Wanzarik	4100	27.49	13.64	-4.2	الديفوني
Hummero	4139	26.13	14.96	22.27	الديفوني
Semnu	4010	27.27	14.93	-	الديفوني
Idri	4008	27.49	13.24	-	الكمبري واردفيشي
Aril	4122	27.72	14.95	10.3	الكمبري واردفيشي
Aril	4123	27.81	15.55	25.2	الكمبري واردفيشي
Tahala	4068	25.55	10.63	20.55	الكمبري واردفيشي
Tahala	4073	25.57	10.55	-	الكمبري واردفيشي

ملحق 4. معدلات الهبوط في آبار الشبكة البيزومترية لأبار حوض مرزق سنة 2013 (الهيئة العامة للمياه-سبها، 2005-2013).

	رقم البئر	N	E	WT	الخزان
Barjuj	4116	26.26	13.17	41.77	الحياة المتوسطة
Abiod	4002	26.82	14.13	22.2	الحياة المتوسطة
Irawan	4085	26.81	12.59	31.1	الحياة المتوسطة
Irawan	4130	26.68	12.4	39.9	الحياة المتوسطة
Irawan	4132	26.66	12.51	13.3	الحياة المتوسطة
Zwilla	4041	26.29	15.13	31.85	الحياة المتوسطة
Tmessa	4126	26.63	15.81	41.22	الحياة المتوسطة
Tasawah	4137	26.37	13.64	34.7	الحياة المتوسطة
Rogheba	4062	26.59	13.53	33.95	الحياة المتوسطة
Maknussa	4144	26.59	13.44	48.2	الحياة المتوسطة
Maknussa	4145	26.34	13.57	35.9	الحياة المتوسطة
Barjuj	4115	26.02	12.86	72.18	الحياة المتوسطة
Barjuj	4118	26.13	12.96	59.12	الحياة المتوسطة
Godwa	4079	26.74	14.36	40.79	الحياة المتوسطة
Tmessa	4154	25.69	14.4	62.97	الحياة المتوسطة
Godwa	4151	26.38	15.89	24.7	الحياة المتوسطة
Tarut	4098	27.72	13.94	56.95	الديفوني
Quttah	4099	27.47	13.77	2.9	الديفوني
Wanzarik	4100	27.49	13.64	3.1	الديفوني
Hummero	4139	26.13	14.96	22.6	الديفوني
Semnu	4010	27.27	14.93	40.1	الديفوني
Idri	4008	27.49	13.24	0.65	الكمبري واردفيشي
Aril	4122	27.72	14.95	10	الكمبري واردفيشي
Aril	4123	27.81	15.55	25	الكمبري واردفيشي
Tahala	4068	25.55	10.63	20.8	الكمبري واردفيشي
Tahala	4073	25.57	10.55	13.2	الكمبري واردفيشي

Libyan Journal of Science & Technology 9:1 (2019) 116–121
The 2nd International Conference on Geosciences of Libya-GeoLibya 2 (2017), 14-16 October 2017, Benghazi-Libya

Faculty of Science - University of Benghazi
Libyan Journal of Science & Technology
journal home page: www.sc.uob.edu.ly/pages/page/77

تقييم الخواص الفيزيائية والميكانيكية لأسطح الشقوق والفواصل لمكاشف تكوين سيدي الصيد (السينوماني-الكريتاسي العلوي) واستقرارها على منحدرات الطريق الجبلي جادو (شمال غرب ليبيا).

أبو القاسم عبد الفتاح الاخضر[a,*]، عبد الفتاح مفتاح المزوغي[b]، احمد علي العربي[b]

[a] قسم الهندسة الجيولوجية- كلية الهندسة (جادو)-جامعة الجبل الغربي

[b] قسم الهندسة الجيولوجية- كلية هندسة النفط والغاز-جامعة الزاوية.

نقاط هامة

- **تعد التجوية الميكانيكية العامل الأبرز في تغيير الخواص الهندسية للكتل والمكاشف الصخرية لتكوين سيدي الصيد، الطريق الجبلي جادو- شمال غرب ليبيا.**
- **عمليات شق الطريق الجبلي في منطقة الدراسة تعد العامل المهم في تحديد نوع الحركة على أسطح المنحدرات.**
- **أبرز حركات الكتل الصخرية حدوثاً على منحدرات منطقة الدراسة هي من نوع السقوط الصخري تحت تأثير التغيرات في الخواص الفيزيائية والميكانيكية مدعوما بتغير زاوية الاستقرار.**

بيانات المقالة

تاريخ المقالة:

استلمت في	01	فبراير	2018
روجعت في	14	أبريل	2018
قبلت في	21	ديسمبر	2018
نشرت عبر الإنترنت	31	مارس	2019

الكلمات الدالة:

زاوية الاستقرار، المحفزات، الخواص الفيزيائية، الخواص الميكانيكية، السقوط الصخري، التجوية الميكانيكية

*المؤلف المراسل:

أبو القاسم الأخضر
ba_w2007@hotmail.com

ملخص

أوضحت الدراسة الميدانية للمنحدرات المتاخمة للمنطقة محل الدراسة الطريق الجبلي جادو (الشليوني) ومقارنتها بالمعايير العلمية العالمية حدوث تغير في الخواص الفيزيائية والميكانيكية لأسطح الشقوق والفواصل للكتل الصخرية والتي ترجع لتكوين سيدي الصيد، ويتبع هذا التكوين فترة السينوماني ويمثل أقدم وحدة صخرية للكريتاسي العلوي وبسمك يصل حوالي 100 متر وبتركيب صخري مميز (حجر صخري دولوميتي) لعضو عين طبي. كان هناك تباين في النتائج المتحصل عليها مع التغير في الارتفاع ويعد ذلك التباين والتغير في الخواص كنتاجٍ لأعمال الحفريات التي استخدمت لشق الطريق الجبلي، فكانت السبب الأبرز في تكشف صخور التكوين وبالتالي كانت اكثر عرضة لعوامل التعرية والتجوية وبخاصة التجوية الميكانيكية وأهمها التأثير الحراري، وكان تأثير التجوية الكيميائية على نطاق ضيق في حفر ترسب فيها معدن الكالسيت ($CaCo_3$) وكذلك ترسيب ثانوي للمعدن في المناطق التي تمر بها الأودية الفصلية والقاطعة للطريق الجبلي او بمحاذاته، وتعد الأمطار الفصلية عاملا محفزا للتحرك الكتلي وسبباً في الإخلال بعملية التوازن وتغيير زاوية الاستقرار للكتل وأجزاء منها على أسطح المنحدرات ويعد الجزء الأكبر من المكاشف الصخرية للتكوين ثابتة ميكانيكيا رغم حدوث تغير في الخواص الميكانيكية لوصولها لحالة اتزان ولعدم وجود محفزات الحركة بينما في بعض أجزاء الكتل أدي التغير في الخواص الفيزيائية والميكانيكية مدعوما بتغير زاوية الاستقرار تحت تأثير محفزات التحرك الكتلي الي حدوث حركة لأجزاء من الكتل، فمن خلال الدراسة الحقلية اتضح ان ابرز حركات المواد حدوثاً على منحدرات منطقة الدراسة هي من نوع السقوط الصخري او الكتلي الناجم عن انفصال الكتل او أجزاء من الكتل.

1. مقدمة

تعد المنحدرات من المظاهر الجيومورفولوجية المتواجدة على سطح الأرض، وتختلف بإختلاف أماكن وأسباب وظروف تكونها كما تختلف من حيث درجة الانحدار وطبيعة المواد المكونة لها، فبعض المنحدرات مكونة من كتل صلبة أو من حطام صخري من نفس نوع التكوين المكون للمنحدر او منقولة من مواضع أخرى، وقد تكون المواد المكونة لأسطح المنحدرات متماسكة أو غير متماسكة، حيث ان المواد غير المتماسكة أقل استقرارا على المنحدرات (Bloom, A. L., 1998). ان ما يميز الكتل الصخرية والمواد المكونة لها والمستقرة على المنحدرات أنها تحافظ على استقرارها بزاوية تسمي زاوية الاستقرار (السكون) وهي أقصي زاوية ميل للمنحدر تضمن بقاء المواد والكتل دون حركة وتتغير هذه الزاوية بوجود محفزات التحرك, وتبقى الكتل الصخرية في حالة اتزان في موقعها ما لم يحدث عليها تغير في الخواص الهندسية، إذ توجد بعض المحفزات التي تسبب تغيرا في زاوية الاستقرار للكتلة ككل او لأجزاء منها، ومن ناحية أخرى قد يحدث تغير في الخواص الهندسية للكتل الصخرية كنتاج لأعمال الحفريات المستخدمة لشق الطرق الجبلية او التفجيرات المفتعلة من قبل الانسان (Chatziangelou, M. & Christaras, B., 2013)، وتعد المنحدرات المتاخمة للطريق الجبلي جادو مثالا مهما لحركة وسقوط الكتل الصخرية، لذلك وجب تقييم تلك الخواص.

1.1. الموقع الجغرافي لمنطقة الدراسة (جادو)

منطقة الدراسة تقع في منتصف الجبل الغربي وتبعد عن العاصمة طرابلس 170 كم تقريبا شكل 1.

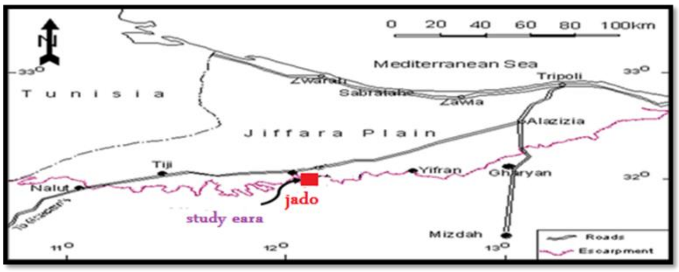

شكل 1. موقع منطقة الدراسة من الجبل الغربي (Hammuda *et al.*, 2000)

2.1. جيولوجية منطقة الدراسة

منطقة الدراسة جزء لا يتجزأ من التتابع الطبقي العام المتكشف ضمن سلسلة جبل نفوسة والتي تقع في الشمال الغربي لليبيا يفصلها من الناحية الشمالية عن البحر الأبيض المتوسط سهل الجفارة وتمتد السلسلة لتلتقي بالبحر في منطقة الخمس شرقا ومن الناحية الجنوبية حوض غدامس (الحمادة الحمراء) كما تمتد سلسلة جبل نفوسة لتدخل الى الحدود التونسية غربا، وتتنوع الصخور في جبل نفوسة بتنوع بيئة الترسيب حيث مرت بعدة دورات من تقدم للبحر وتراجعه لترسب جميع أنواع الصخور الرسوبية من صخور قارية الى بحرية ضحله وعميقة وصخور ترسبت في بيئة انتقالية مابين القارية والبحرية, كما يتواجد بعض التداخلات المنتشرة لأجسام نارية مثل البازلت والفونولايت. (-El

 ISSN 2663-1407; National Library of Libya, Legal number: 390/2018

(Bakai *et al.*, 1997 بدء العمر الجيولوجي للتتابع الطبقي مع بداية حقب الحياة الأوسط (الترياسي السفلي) بتكوين كرش واستمر إلى بداية حقب الحياة الحديث (الثلاثي) بتكوين زمام حيث في منطقة الدراســة (جناون) ينتهي التتابع الطبقي بتكوين نالوت بعمر الكريتاسي العلوي التتابع الطبقي لمنطقة جادو، شكل 2.

3.1. تكوين سيدي الصيد

أعطي هذا الاســم للتكوين لأول مرة بواســطة (El Hinnawy & Cheshited 1975) حيث يتكون من تتابع طبقي للصـخور الكربونية المترسـبة بسـمك 100 متر على مستوي سطح عدم توافق في بيئة بحرية ضحلة في منطقة غريان بحيث يكون فوق تكوين ككلة في المنطقة الغربية وفوق تكوين ابوشيبة في المنطقـــة الشرقية ويتألف التكوين من عضـــوين العلوي عضـــو يفرن المتكون أســاســا من الأحجار الجيرية الطينية (المارل) والدولوميتية مع تداخلات من حجر الطين والجبس، أما الســفلي فهو عضـــو عين طبي المتكون أساسا من أحجار الدولوميت الذي يتفاوت في حجم بلوراته بين الدقيقة والخشنة ذات لون أصــفر الى رصــاصي مع تداخلات طبقات رقيقة من المارل ويتواجد به وفرة من الأحافير التي تدل على عمر الطباشيري المتأخر (السينوماني).(EL-Bakai, 1997)

4.1. مشكلة الدراسة

ان مـايميز المنحـدرات إنهـا دائمـا في حالـة اتـزان طبيعيـة ولهـا زاويـة تعـرف بزاويـة الاســتقرار فبحــدوث أي خلــل في زاويــة الاتــزان بفعــل محفــزات الحركــة كالميــاه والحركـات الأرضـية وإزالـة الغطـاء النبـاتي، سـيؤدي الي حـدوث حركـة عـلى أسـطح المنحـدرات المتاخمـة للطـرق الجبليـة والـتي سـتعمل بـدورها عـلى إعطـاب الطريـق وعرقلـــة الحركـــة عليهـــا وإغـــلاق مجـــاري تصريـــف الميـــاه، والإضرار بالمنشـــآت والمركبـات الآليـة، فمـع الاسـتمرار في عـدم فهـم العلاقـة بـين الظـروف المسـاهمة في إحـداث تلـك الحركات للرواسـب والكتـل الصـخرية سـيؤدي إلى حـدوث أحـد أنـواع الحركـات والـتي بـدورها تـؤدي إلى إحـداث ضرر بـالطرق الجبليـة وعـلى مسـتخدميها، وبمـا ان تكـوين سـيدي الصـيد يمثـل الجـزء الأكـبر للمكاشـف المتاخمـة للطريـق الجبلي جادو عليه وجب دراسة مقدار التغير في الخواص الهندسية.

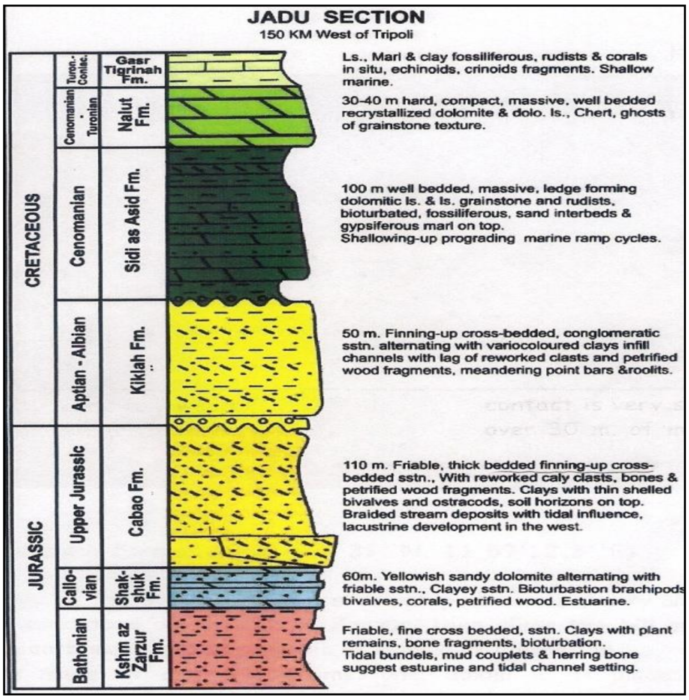

شكل 2. التتابع الطبقي لمنطقة جادو(Sbeta *et al.*, 2005)

5.1. أهمية الدراسة

تعد هذه الدراســة جزء من أبحاث ســابقة اهتمت بدراســة الخواص الفيزيائية والميكانيكية للكتل الصـخرية اجريت على الطرق الجبلية (جناون، الطريق الجبلي الزنتان) وهي المرحلة الأولي والمســتهدف في المرحلة الثانية إجراء دراســات معملية على عينات صـخرية لتكون المرحلة الثالثة دراسـات معملية تهدف لتصـنيع مادة لاحمة مناسـبة يتم رشها أو حقنها بحيث تتماشي مع نوعية التكوين وطبيعة الشقوق وتصنيفها للحد والتقليل من أضرار حدوث حركة على أسطح المكاشف استكمالا لكلا المرحلتين.

2. العوامل المؤثرة في حركـــة المواد والكتـل الصخرية

تحدث حركة المواد على أســطح المنحدرات مع الجاذبية عندما تفقد الصــخور توازنها فتسـقط أو تنحدر وقد تنزلق لأسـباب مختلفة كعوامل التجوية والتعرية وتدخل الإنســان الغير مدروس في البيئة الطبيعية النجم عن اســتخدام الأراضي وقد تصــنف الحركات بأنها ضـحلة والمؤثر في حركاتها الأمطار الغزيرة (Persichillo *et al.* 2016) وتختلف الحركات فيما بينها فزحف التربة أو زحف الصــخور يحدث ببطء شــديد، أما عمليات الانزلاق الأرضي فإنها تحدث بسرعة شـديدة دون أن ترى مثل الحركات الناجمة عن فعل الزلازل، (Newmark, 1965) وتـــــعد عمليات تساقط الصخور من اخطر الحركات كونها تحدث بسرعـــة وفـــجأة، (Andriani & Walsh, 2007) وتبـــرز أهمية الظروف المناخية كعوامل ومحفزات التحرك الكتلي على المنحدرات ولعل أبرزها التأثير الحراري والأمطار، ويعد الماء بشـتى صـوره من محفزات التحرك الكتلي (Bajzelj *et al.*, 1992) إذ تتأثر المنـحدرات الجبـلية بسقوط الأمطار وبالتالي تزيد من عمليات تساقط الصخور أو انزلاقها وبخاصة إذا كانت تلك المنحدرات تفتقر للغطاء النباتي والذي يساعد على جعل المنحدرات والتربة الغير مغطاة أكثر عرضة لحركة المواد على أسطحها (Xu *et al.*, 2012) ويعد التماسك الداخلي للكتلة الصخرية مهما إذ يضعُف التماسك مع الوقت تدريجـــــيا نتيـــجة عوامل منها تأثير التجوية بنوعيها الكيميائية والميكانيكية ويعمل التغير في التماســـك الداخلي وبخاصـــة إذا اختلف التركيب المعدني والكيميائي للصـــخور على إحداث تراكيب مثل الفواصـــل والشـــقوق وهي من التراكيب الثانوية في الصـخور الرسـوبية (Noffke *et al.*, 2001). إن التغير في زاوية الاتزان للكتل الصـخرية والتي تقدر ما بين °70-°90 مع المستوي الأفقي ينجم عنه حركـــة للكتل الصخرية إلى ما تحت أقدامها تعرف هذه الحالة باســم تســاقط الصــخور او تســاقط التربة او تســاقط المفتتات (Dorren, 2003) ان مجموع العمليات التي تسـبب تفتت الصـخور ميكانيكيًا أو تحللها كيميائيًا تســـمي عوامل التجوية الميكانيكية والكيميائية،(Hack, 2016) ولدراسة الكــتل الصخرية تــم الاعتمــاد على دراســـة الــخواص الهندســـية لأسطــح الشــقوق.

1.2. التجوية الكيميائية:

هي نـاتج لتفاعــل غــازات الجــو مثــل الأكســجين وثــاني اكســيد الكربــون وبخــار المــاء مــع العنــاصر المكونــة لمعــادن الصــخور، ويتــأثر الحجــر الجــيري بشــكل كبــير بالميـاه ونوعيتهـا ومـن أهـم العمليـات الـتي تحـدث لـه عمليـة الإذابـة للمعـادن القابلـة للإذابـة او قـد تحـدث عمليـة تكـربن عنـدما يتحـد غـاز (CO_2) مـع ميـاه الأمطـار ليكـون حمــض الكربونيــك الــذي يــؤثر عــلى الصــخور بخاصــة الصــخور الجيريــة ($CaCO_3$) القابلـة للـذوبان ويحولهـا إلى بيكربونـات الكالسـيوم (Hack, 2012)، و قـد لـوحظ في منطقــة الدراســة وجــود ترســيب ثــانوي لمعــدن الكالســيت في انطــق ضــيقة جــدا كدليل على تأثير التجوية الكيميائية

2.2. التجوية الميكانيكية

تعرف عملية التجوية الميكانيكية بأنها عملية تحطم الصخور وتفتيتها دون إحداث أي تغير في خصائصها الأصلية وتحدث في المناطق الحارة الجافة وشبه الجافة فتأثير التباين في درجة حرارة النهار والليل تحدث تمددا وانكماشا للمعادن الداخلة في تكوين الصخر، خاصة إذا اختلف معدل تمدد تلك المعادن أو انكماش كل معدن منها مما يؤدى إلى تفكك الصخر إلى جزيئات أصغر حجما ومن مظاهرها التفكك الكتلي إذ تنكسر أجزاء الصخر وكتل على طول خطوط المفاصل وسطوح الانفصال بالكتل الصخرية (Huisman *et al.*, 2006).

3. الخــواص الهندسـية لأسطـح الشقوق والفواصـل

1.3. الخواص الفيزيائية

أ. التمــوج: يقصد بها شكل سطح الشق ويعتمد الوصـف على أصل تكون السطح ومنها ثلاث أنواع أصلية: أسطـح نـاعم، أسطـح خشنـة، أسطـــح بيـــن ناعمـــة وخشنة وتفرعت منها مقاييس أخرى تصف شكل سطح الشق جدول 1. فكلما كانت الأســطح خشــنة قلت الحركة على الســطح بينما في الأســطح الناعمة لا يكون هناك تماسك فتكون الحركة أكثر حدوثـــا وخاصـــة بوجود محفـز للحـركة كالمياه.

ب. المواصـلة: يقصــد بهـا تعمق الشق في الكتـلة الصخريـة فزيـادة عمق الشق تضعف الكتلة.

ت. المسـافات بين الشقـوق: ويقصد بها المسافـة بالسنتيمتـر بين الشـق والشق المجاور له وما تم ملاحظته في مكاشـف منطقة الدراسـة انه كلما قلت المسـافة بين الشقوق فإن ذلك يعد دليلا على ضعف الكتلة.

ث. عــدد مجمـــوعات الشقـــوق: كلما زاد عدد الشقوق ضعفت الكتلة الصخرية، وبغض النظر ان كانت الشــقوق منظمة او عشــوائية فإنها تســهم في إضـــعاف الكتل.

ج. الانفصـــال: ويقصد بها مقدار انفـصال الكتلة أو أجزاء منها عن الكتلة الأصلية، ويتم تقييم القياســات الحقلية المتحصــل عليها من التصــنيف التي وضــعته الجمعية الجيولوجية لندن (1977) جدول 2.

ح. المـــواد بين الفراغات: ويقصـد بها المواد الموجودة بين الشـقوق والفواصـل، وتعمل المواد الموجودة أحد أمرين فإما ان تســهم في ثبات الكتل الصــخرية او يكون لها دور في الحركة وفي كلا الأمرين فإن مقدار الثبات او الحركة يعتمد على نوع المواد والمفتتات وحجمها، جدول 3.

جدول 1.

تصنيف أشكال سطح الشق (Boyer, 1971)

TERM	DESCRIPTION
Very rough	Near vertical steps and ridges occur with interlocking effect on the joint surface.
Rough	Some ridge and side-angle steps are evident; asperities are clearly visible; discontinuity surface feels very abrasive (Like sandpaper grade approx.< 30)
Slightly rough	Asperities on the discontinuity surfaces are distinguishable and can be felt.
Smooth	(Like sandpaper grade approx. 30 - 300).
Polished	Surface appear smooth and feels so to the touch. (Smoother than sandpaper grade approx. 300).
Slicken sided	Visual evidence of polishing exists, or very smooth surface as is often seen in coatings of chlorite and specially talc.

جدول 2.

تصنيف الانفصال بناء على قياسه (Fanti *et al.* 2013)

Aperture	Term
>200 mm	Wide
60 – 200 mm	Moderately wide
20 – 60 mm	Moderately narrow
6 – 20 mm	Narrow
2 – 6 mm	Very narrow
0 – 2 mm	Extremely narrow
< 2 mm	Tight

جدول 3.

المواد بين الفراغات وخصائصها (Habibi and Gharibreza 2015)

TYPE OF FILLING	PROPERTIES
Chlorite, talc,	Graphite Very low friction materials, in particular when wet.
Inactive clay materials	Weak, cohesion materials with low friction properties
Swelling clay	Exhibits a very low friction and loss of strength together with high swelling pressure
Calcite.	May dissolve, particularly when being porous or flaky.
Gypsum	May dissolve
Sandy or silty	Materials Cohesion less, friction materials
Epidote, quartz	May cause healing or welding of the joint

2.3. الخواص الميكانيكية

الشـــقوق والفواصـــل في الكتل الصـــخرية هي ظاهرة طبيعة وتعد من اكثر التراكيب الثانوية حدوثا نتيجة لعوامل طبيعية وهي تفتقر إلى أي حركة مرئية على الرغم من أنها يمكن أن تحدث منفردة فإنها غالبا ما تحدث كمجموعات وأنظمة مشـــتركة ويمكن قياســـها من خلال دراســـة الخصـــائص الفيزيائية والميكانيكية (Dafalla and Malik, 2015) ويمكن ان تقـاس الخواص الميكانيكيـة للكتـل الصـــخرية في الحقل او في المعمل وفي هذا البحث تم الاعتماد على القياســـات الحقلية لدراســـة الخواص الميكانيكية وكون العمل الميداني اكثر محاكاة لواقع ميكانيكا الصخور فقد تم الاعتماد على قياس الخواص الميكانيكية وبخاصة قياس قوة الصخر (RQD) كمرحلة أولى فكانت الخواص التي اهتم البحث بدراستها على النحو التالي:

أ- خاصية نظام الشقوق (Joint System= Js)

يوصف نظـــام الشـــــقوق (Joint System) بعد قيـــــاس المسافة بين الشـــقوق المنتظمة على طول خط المسح تبعا لمواصفات الجمعية الجيولوجية في لندن حـــــيث (JS) = المسافة بين الشقوق/عدد العينات بينهم. أي المسافة بين الشـــقوق المنتظمة والتي اعتمد عليها في اخذ القياســـات الحقلية على طول خط المسح، جدول 4.

جدول 4.

يوضح نظام تصنيف الشقوق بالاعتماد على المسافة بين الشقوق (Palmström *et al.* 2001)

Intervals (cm)	Symbols	Description
>200	F1	Extremely wide spaced
200-60	F2	Widely spaced
60-20	F3	Moderately wide spaced
20-6	F4	Closely spaced
6-2	F5	Very closely spaced
<2	F6	Extremely closed spaced

ب- تعيين جودة صخرة (Rock Quality Determination=RQD): تسمية او تعيين نوعية الصخور هو مؤشر يستخدم عادة لوصف الكتلة الصخرية وتحديد قوتها، جدول 5، ويمكن تحديد قوة كتلة الصـــخور في المعمل على العينات الصـــخرية او الحقل على الكتل الصـــخرية المحتوية على شـــقوق وفواصـــل، وتســـتخدم المعادلة التالية لقياســـها بالاعتماد على حجم الشقوق في المتر المكعب الواحد. RQD= 115-3.3(JV)

جدول 5.

نظام التصنيف بخاصية جودة تركيب الصخر(Palmstrom, 2005)

Descriptive Term	RQD %	Symbols
Very Good	90 – 100	R1
Good	75 – 90	R2
Fair	50 – 75	R3
Poor	25 – 50	R4
Very Poor	<25	R5

4. الدراسة الميدانية

اعتمدت الدراســـة الميدانية على القياس المباشر على طول خط المســـح أي ذلك الخط الوهمي الذي تم اخذ القراءات والقياسـات عليه، فقد بلغ إجمالي طول خط المسح 22.44 متر وزعت على ثلاثة ارتفاعات مختلفة لتقييم الخواص الفيزيائية والميكانيكية للكتل الصخرية. فقد تم اختيـــار المكاشف الواضحة والأقـــرب إلي الطريق الجبلـــي وتم تجميـــع المعلومـات المتعلقـــة بدراسة الخواص الهندسية (الفيزيائية والميكانيكية). وفيما يلي عرض للدراســـة الميدانية والنتائج المنبثقة عنها حيث تم اختيار رمز لموقع الدراســـة (L-Ja-17). إذ يرمز L إلي الموقع (location) وترمز Ja إلي (Jado) 17 ســـنـة إجراء الدراسة 2017 ويبن الجدول 6 والشكل 3. الدراسة الميدانية والنتائج المتحصل عليها في الموقع الأول (L1-Ja-17) ويبن الجدول 7 والشـــكل 4. الدراســـة الميدانية والنتائج المتحصـــل عليها في الموقع الأول (L2-Ja-17). ويبن الجدول 8 والشـــكل 5. الدراســـة الميدانية والنتائج المتحصل عليها في الموقع الأول (L3-Ja-17)

1.4. الدراسة الميدانية للكتلة الصخرية (L1-Ja-17)

يبين جدول 6 البيانات والقياسات المتحصل عليها من الدراسة الميدانية للكتلة الصخرية ويمثل الشكل 3. جزء من تكوين سيدي الصيد وهو نتاج اعمال الحفريات التي استخدمت لشق الطريق الجبلي وكان من المتوقع ان نجد تأثير للتجوية الكيميائية بموقع الدراسة على اعتبارات عدة منها ان الصخور الجيرية تتأثر بشكل مباشر بالمياه إذ تعمل على إحداث عملية الإذابة وترسيب معدن الكالسيت فكانت النتائج عكس ذلك والسبب يرجع الى ان زاوية الميل تراوحت بين (85-90) والشقوق الأفقية والرأسية متصلة فهي لا تسمح باستقرار المياه بين الشقوق والفواصل الا في انطقة ضيقة والتي لوحظ فيها نمو بلورات الكالسيت التي تتراوح ألوانها بين الأبيض والشفاف وما تم ملاحظته ان اغلب *الشقوق الرئيسية* تمر بها مجاري مائية منحدرة من اعلى شكل(G, G1-3).

وأسهمت في عملية تعرية المواد بين الشقوق فكانت تلك المناطق أكثر ضعفا وهذا على عكس مناطق أخرى كانت فيها نواتج عملية التعرية مســـتقرة لتشـــكل أشكال مخروطية شكل (A, A1-3). لذلك كانت اكثر ثباتا ولا تحوى شقوقا رئيسة منتظمة شكل (F, D1, D-3) فكانت الكتل المتساقطة بحجم اكبر شكل(E-3) في المناطق الواقعة بين المجاري المائية ولوحظ ان أسـطح الشـقوق والفواصـل في تلك المناطق ذات أسطح ناعمة شكل (D,D1 -3) ومن النتائج التي تحصلنا عليها من التحليل الرياضي من خلال اخذ متوسط نظام الشقوق(Joint System = Js) والتي تمثل مقدار تباعد أجزاء الكتلة المنفصـــلة تبين أنها متباعدة على نطاق واسع بمقدار(Js =168.25 cm Widely spaced) وهذا يعد دليلا على ان الكتل في حال حركتها سـتكون كبيرة وكان متوسـط الانفصال أي مقدار اتساع كل شـق

من الشقوق الرئيسة الخمسة على طول خط المسح (Moderately 64.8 mm) wide متوسط الاتساع وبالنسبة لجودة الكتلة بالاعتماد على عدد الشقوق في المتر المكعب (11) 3.3 – RQD =115 فإن متانة الكتلة صنفت R2 (Good)

2.4. الدراسة الميدانية للكتلة الصخرية (L2-Ja-17)

في الكتلة (L2-Ja-17) يبلغ طول خط المســـح حوالي 9.00 متر ورغم طول خط المسح فلم تتواجد الا ثلاث شقوق منتظمة جدول 7 وتجتمع في الكتلة التي يظهر جزءا منها بالشكل 4 تأثير عوامل التجوية الكيميائية فكان واضحا الترسيب الثانوي لمعدن الكالســـيت بلون شـــفاف في حفر الإذابة وكانت هذه الظاهرة اكثر انتشارا إذا ما قورنت بالمواقع الأخرى فكانت تلك الحفر غير متصلة بشقوق مما سمح للمياه بان تقوم بعملها في إذابة وإعادة ترسيب الكالسيت، والتأثير الأبرز كان موجودا للتجوية الميكانيكية إذ تظهر الألوان الفاتحة على أسطح الكتلة شكل (4- D) كدليل على التأثير الحراري وحدوث عملية تقشير لسطح الكتلة، ومن مظاهر التجوية الميكانيكية نمو النباتات بين الشقوق ،والتي أسهمت في تعبئة الفراغات بين الشقوق بالمفتتات شكل (4- C).

.

جدول 6.

البيانات والقياسات المتحصل عليها من الدراسات الميدانية للكتلة (L1-Ja-17).

E12º.00.26'					N31º56.4'					Location Astronomer
526m										Height
(Length of scan line) 7.05 *Height 5.4 = 38.07 m²										Section area
Carbonate										Type Rock
Rough										Type Roughness
40cm		60cm		15cm		40cm		cm56		Continuity
Carbonate and mud										Infilling materials
140cm			163cm		160cm		210cm			Joint System cm
Rocky debris (Carbonate)										Type sediment beside blocks
0.8	0.6	3	1	1.7	2.4	0.5	1.5	1	0.2	Joint Set No // cm
1	9	0.3	5	1	3	3.3	1.6	0.5	0.9	

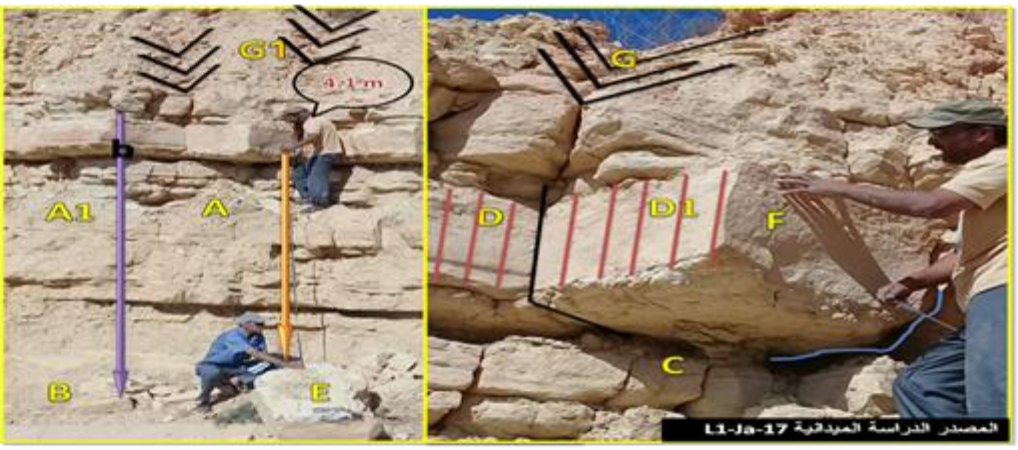

شكل 3. الكتلة بالموقع L1-Ja-17

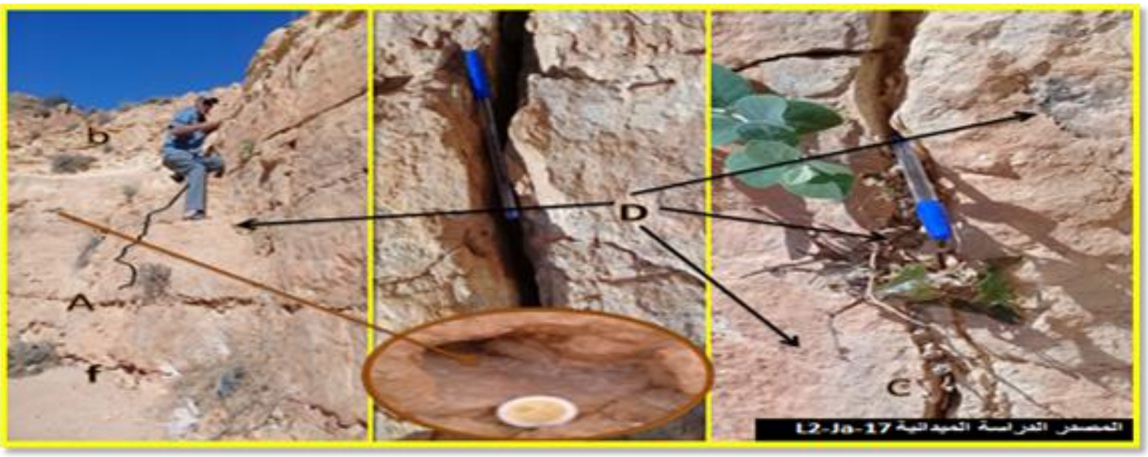

شكل 4. الكتلة الموقع (L2-Ja-17)

جدول 7.

البيانات والقياسات المتحصل عليها من الدراسة الميدانية للكتلة (L2-Ja-17)

E12º.00.27'					N31º57.00'				Location Astronomer
519m									Height
(Length of scan line) 9.865 * Height 2.40 = 23.676 m²									Section area
Carbonate									Type Rock
Rough									Type Roughness
10cm			26.5cm		20cm				Continuity
Carbonate									Infilling materials
740cm					240cm				Joint System cm
Rocky debris (Carbonate)								Type sediment beside blocks	
1.1	2.7	1.3	1.1	0.6	1.4	1.1	1	1	Joint Set No // cm
					0.7	5	1.4	0.6	

من الجدول (7) يعد امتداد الشقوق داخليا بسيط بمتوسط بلغ 19 سم تقريبا فهو يزيد من ثبات الكتلة وهذا ما أكدته نتائج التحليل الرياضي إذ وصفت جودة الصخر (R2) very Good بجيده جدا وبقيمة وصلت RQD = 98.9 % جدول (5) كنتيجة لقلة الشقوق في المتر المكعب إذ بلغ عدد الشقوق في الكتلة ككل سواء كانت الشقوق العشوائية او المنتظمة (16 شق) ورغم وصف نضام الشقوق بأنها متسعة للغاية، فالنتيجة متوقعة كنتيجة لطول خط المسح وقلة الشقوق المنتظمة بالمكشف الصخري, وبالنسبة للانفصال فإنه متوسط الضيق إذ وصلت قيمته (21.6mm) وعلى ما ذكر فإن المكشف في حالة ثبات، ولان زاوية الاستقرار تصل الى 90 ففي حالة حدوث حركة فستكون سقوط الصخري.

3.4. الدراسات الميدانية للكتلة الصخرية (L3-Ja-17)

يبين الجدول (8) البيانات القياسية للمكشف الصخري (L3-Ja-17) المبين بالشكل(5) على ارتفاع 519 متر، مثل تكوين سيدي الصيد المتكشف بفعل عوامل التعرية المائية وبما ان التكوين يقطعه وادي فصلي، فلم يتبين وجود أي ترسيب ثانوي لمعدن الكالسيت الا في مناطق ضيقة جدا، لان الصخور في هذا التكوين من نوع دولومايت والذي يمتاز بصلابته لارتفاع نسبة الماغنسيوم، ويمكن ملاحظة الكتل الصخرية بأحجام كبيرة ومنفصلة عن التكوين الأصلي بشقوق راسية شكل (A, A1-5) وأخري أفقية تسهم في إحداث حالة ضعف بالمكشف.

جدول 8.

البيانات والقياسات المتحصل عليها من الدراسات الميدانية للكتلة (L3-Ja-17)

E12º.00.39'				N31º57.15'					Location Astronomer
484m									Height
(Length of scan line) 5.527*Height 2.10 = 11.6067 m²									Section area
Carbonate									Type Rock
Rough									Type Roughness
180 cm		65 cm		30 cm			110 cm		Continuity
Carbonate and mud									Infilling materials
140 cm		310 cm			90 cm				Joint System cm
Rocky debris (Carbonate)									Type sediment beside blocks
6	1	1.5	0.3	0.5	0.5	1.5	0.2	0.2	Joint Set No // cm
	0.5	0.5	2.5	0.5	3	0.5	0.5	1.2	

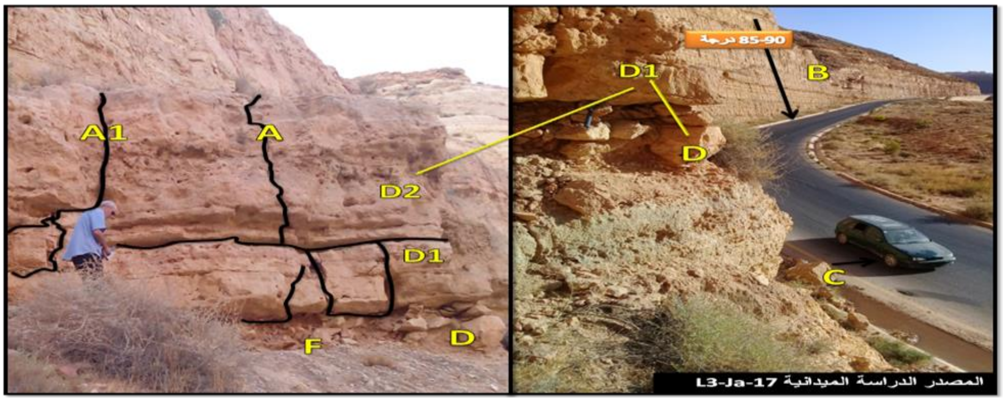

شكل 5. الكتلة بالموقع (L3-Ja-17)

ان الكتلتين في الشكل (D1,D2-5) في حالة اتزان مالم يحدث حركة في الموقع شكل (5-D) والذي يتكون من حطام صخري وكتل صغيرة فإن إمكانية الحركة موجودة في حالة حدوث محفز او إزاحة للرواسب في الموقع (D) ليؤول حال الكتل ككل السقوط الصخري كون زاوية المنحدر°90 حالهم حال الكتلة شكل (C-5) والتي تم إزاحتها من الطريق الرئيسي لتستقر في مجري تصريف المياه الموازية للطريق، وبالنسبة للخواص الميكانيكية

وصفت جودة الكتلة بجيدة جدا وبنسبة بلغت (% 98.9)، جدول 5 والمسافة بين الشقوق وصفت من جدول(4) بأنها متسعة للغاية وكانت قيمة متوسط نظام الشقوق (Js= 490 cm) كدليل على ان أجزاء الكتل المنفصلة ذات حجم كبير، وبلغت قيمة الانفصال 21.6 mm بتصنيف متوسط الضيق وتعد الخواص الميكانيكية متغيرة

والكتلة ثابتة ميكانيكيا أي أنها متزنة , ويجب العمل على تفتيها كون ما يحدد اتزانها حطام صخري.

5. العلاقة بين الخواص الفيزيائية والميكانيكية لأسطح الشقوق والفواصل والارتفاع.

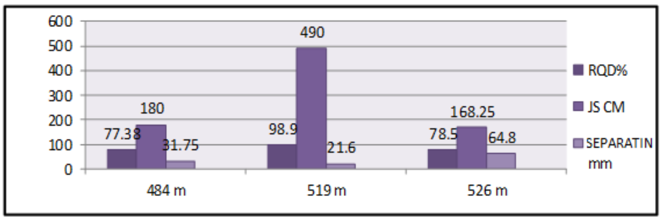

شكل 6. العلاقة بين الارتفاع والخواص الهندسية في الموقع (L-Ja-17).

رغم اختلاف الأرقام بالنسبة لنظام الشقوق (Joint System =Js) فقد كان التصنيف ما بين شقوق متسعة وأخرى متسعة للغاية وكان المتوسط العام لمنطقة الدراسة (279 mm) بتصنيف شقوق متسعة للغاية وكان المتوسط العام RQD (84.9 %) بتصنيف جيد (Good) أي ان تصنيف الكتل من حيث القوة والجودة جيدة وكان متوسط الانفصال للكتل (39.4 mm) تباعد أجزاء الكتل بتصنيف متوسطة الضيق.

6. الخاتمة

يوجد تغير واضح في الخواص الميكانيكية والفيزيائية للكتل الصخرية، مما أسهم في إحداث حالة من الضعف للكتل الصخرية، وتعد التجوية الميكانيكية العامل الأبرز في تغيير الخواص الهندسية للكتل والمكاشف الصخرية، كما أسهمت اعمال شق الطريق الجبلي في عملية ظهور المكاشف صخرية، وسببت أيضا في جعلها أكثر عرضة لعوامل المناخ وبخاصة مياه الأمطار والتي تعد العامل الأبرز للتحرك الكتلي. ويطغى تكوين سيدي الصيد على مكاشف المنحدرات المتاخمة للطريق الجبلي أسهم هذا التكوين بثاب المكاشف كون نوع صخوره من الدولومايت والذي يتكون من والماغنيسيوم بشكل أساسي, بهذا التركيب اتصف بالصلابة فانعكس ذلك على الخواص الهندسية فجعل الكتل اكثر استقرارا على المنحدرات) فبالتالي الكتل تعد ثابتة ميكانيكيا أي لا توجد حركة رغم ان التغير موجود في الخواص الهندسية الكيميائية والميكانيكية , ان عمليات شق الطريق الجبلي تعد العامل المهم في تحديد نوع الحركة على أسطح المنحدرات فأغلب زوايا التكوين تتراوح بين 70°-95° لتكون نوع الحركة (FALL).

7. التوصيات

1- مراقبة الكتل الصخرية من وقت لأخر وعلى فترات منتظمة.

2- تحطيم بعض الكتل والتي تشكل خطراً في حال انهيارها.

المراجع

Andriani, G.F. and Walsh, N., 2007. Rocky coast geomorphology and erosional processes: a case study along the Murgia coastline South of Bari, Apulia—SE Italy. Geomorphology, 87(3), pp.224-238

Bajzelj, U., Likar, J., Zigman, F., Subelj, A. and Spek, S., 1992. Geotechnical analyses of the mining method using long cable bolts. In Rock support in mining and underground construction, proc. int. symp. on rock support (pp. 393-402).

Bloom, A.L., 1998. Geomorphology: a systematic analysis of late Cenozoic landforms (No. 551.79 BLO).p.164.

Boyer, R.E., 1971. Field Guide to Rock Weathering. Earth Science Curriculum Project Pamphlet Series PS-1 PP 5-35.

Chatziangelou, M. and Christaras, B., 2013. Rock mass blastability dependence on rock mass quality. Bulletin of the Geological Society of Greece, 47(13). PP.2-13.

Dafalla, D. S., & Malik, I. A. G. (2015). Evaluation of Structural Geology of Jabal Omar. Evaluation, 11(01), p.71

Dorren, L.K., 2003. A review of rockfall mechanics and modelling approaches. Progress in Physical Geography, 27(1), pp.69-87.

El-Bakai, M., Idris, M. and Sghair, A., 1997. Petrography, geochemistry and stable isotopes constraints on the origin of the Cretaceous dolomite (Ain Tobi Member) in NW Libya

El-Bakai, M.T., 1997. Petrography and palaeoenvironment of the Sidi as Sid Formation in Northwest Libya. Petroleum Research Journal, 9, pp.9-26.

Fanti, R., Gigli, G., Lombardi, L., Tapete, D., & Canuti, P. (2013). Terrestrial laser scanning for rockfall stability analysis in the cultural heritage site of Pitigliano (Italy). Landslides, 10(4), 409-420

Habibi, A., & Gharibreza, M. (2015). Estimation of the relative active tectonics in Shahriary basin (Central Iran) using geomorphic and seismicity indices. Natural Environment Change, 1(1), 71-83.

Hack, H.R.G.K., 2016, Weathering, rock mass classification (SSPC), and remote sensing with a link to levee stability: Presented in Fall 2016 graduate and undergraduate UMD civil engineering seminar series, University of Minnesota Duluth, United States of America, 23 September 2016, p. s1-s63 (https://research.utwente.nl/en/publications/p.s1-s63).

Hack, H.R.G.K., 2012. Weathering influence on engineering structures:In Lunch lectures, ESA, ITC, University of Twente, 30 October 2012. pp. s1-s38, (http://www.itc.nl/library/papers_2012/pres/hack_wea_ppt.pdf)

Hammuda, O.S., Sbeta, A.M. and Worsley, D., 2000. Field guide to the Mesozoic succession of Jabal Nefusah. In NW Libya: Sedimentary basins of Libya-second symposium: Geology of Northwest Libya p. 50

Huisman, M., Hack, H.R.G.K. and Nieuwenhuis, J.D., 2006. Predicting rock mass decay in engineering lifetimes: the influence of slope aspect and climate. Environmental & Engineering Geoscience, 12(1), pp.39-51

Newmark, N.M., 1965. Effects of earthquakes on dams and embankments. Geotechnique, 15(2), pp.139-160.

Noffke, N., Gerdes, G., Klenke, T. and Krumbein, W.E., 2001. Microbially Induced Sedimentary Structures--A New Category within the Classification of Primary Sedimentary Structures: PERSPECTIVES. Journal of Sedimentary Research, 71(5), pp.649-656.

Palmstrom, A., 2005. Measurements of and correlations between block size and rock quality designation (RQD). Tunnelling and Underground Space Technology, 20(4),.362-377, p 11

Palmström, A., Sharma, V.I. and Saxena, K., 2001. In-situ characterization of rocks. BALKEMA Publ, p.31.

Persichillo, M.G., Bordoni, M., Meisina, C., Bartelletti, C., Giannecchini, R., D'Amato Avanzi, G., Galanti, Y., Cevasco, A., Brandolini, P., Galve, J.P. and Barsanti, M., 2016. Shallow landslide susceptibility analysis in relation to land use scenarios. Landslides and engineered slopes. Experience, theory and practice, 3, pp.1605-1612.

Sbeta, A., El-Hawat, A. and Salem, M., 2005. A Field guide book to the geology of Jabal Nafusah. NW Libya.

Xu, Q., Liu, S., Wan, X., Jiang, C., Song, X. and Wang, J., 2012. Effects of rainfall on soil moisture and water movement in a subalpine dark coniferous forest in southwestern China. Hydrological Processes, 26(25), pp.3800-3809.